

# World Journal of *Gastroenterology*

*World J Gastroenterol* 2022 October 7; 28(37): 5383-5514



**STANDARD AND CONSENSUS**

- 5383 Baishideng's *Reference Citation Analysis* database announces the first *Journal Article Influence Index* of 101 core journals and a list of high-quality academic journals in gastroenterology and hepatology  
*Wang JL, Ma YJ, Ma L, Ma N, Guo DM, Ma LS*

**OPINION REVIEW**

- 5395 Milestones in the discovery of hepatitis C  
*Campollo O, Amaya G, McCormick PA*

**REVIEW**

- 5403 Immunotherapy-based novel nanoparticles in the treatment of gastrointestinal cancer: Trends and challenges  
*Ding YN, Xue M, Tang QS, Wang LJ, Ding HY, Li H, Gao CC, Yu WP*

**ORIGINAL ARTICLE****Basic Study**

- 5420 Lentivirus-mediated short hairpin RNA interference of CENPK inhibits growth of colorectal cancer cells with overexpression of Cullin 4A  
*Li X, Han YR, Xuefeng X, Ma YX, Xing GS, Yang ZW, Zhang Z, Shi L, Wu XL*

**Retrospective Cohort Study**

- 5444 Prognostic performance of an index based on lactic dehydrogenase and transaminases for patients with liver steatosis and COVID-19  
*Macías-Rodríguez RU, Solís-Ortega AA, Ornelas-Arroyo VJ, Ruiz-Margáin A, González-Huezo MS, Urdiales-Morán NA, Román-Calleja BM, Mayorquin-Aguilar JM, González-Regueiro JA, Campos-Murguía A, Toledo-Coronado IV, Chapa-Ibargüengoitia M, Valencia-Peña B, Martínez-Cabrera CF, Flores-García NC*

**Retrospective Study**

- 5457 Efficacy of endoscopic ultrasound in the evaluation of small gastrointestinal stromal tumors  
*Ge QC, Wu YF, Liu ZM, Wang Z, Wang S, Liu X, Ge N, Guo JT, Sun SY*
- 5469 Online calculator for predicting the risk of malignancy in patients with pancreatic cystic neoplasms: A multicenter, retrospective study  
*Jiang D, Chen ZX, Ma FX, Gong YY, Pu T, Chen JM, Liu XQ, Zhao YJ, Xie K, Hou H, Wang C, Geng XP, Liu FB*

**Observational Study**

- 5483 Application of an artificial intelligence system for endoscopic diagnosis of superficial esophageal squamous cell carcinoma  
*Meng QQ, Gao Y, Lin H, Wang TJ, Zhang YR, Feng J, Li ZS, Xin L, Wang LW*

- 5494** Insights into hepatitis E virus epidemiology in Croatia

*Jelicic P, Ferenc T, Mrzljak A, Jemersic L, Janev-Holcer N, Milosevic M, Bogdanic M, Barbic L, Kolaric B, Stevanovic V, Vujica M, Jurekovic Z, Pavicic Saric J, Vilibic M, Vilibic-Cavlek T*

**CASE REPORT**

- 5506** Massive bleeding from gastric submucosal arterial collaterals secondary to splenic artery thrombosis: A case report

*Martino A, Di Serafino M, Zito FP, Maglione F, Bennato R, Orsini L, Iacobelli A, Niola R, Romano L, Lombardi G*

**ABOUT COVER**

Editorial Board Member of *World Journal of Gastroenterology*, Masahiro Iizuka, MD, PhD, Director, Akita Health Care Center, Akita Red Cross Hospital, 3-4-23 Nakadori, Akita-shi, Akita 010-0001, Japan.  
maiizuka@woody.ocn.ne.jp

**AIMS AND SCOPE**

The primary aim of *World Journal of Gastroenterology* (WJG, *World J Gastroenterol*) is to provide scholars and readers from various fields of gastroenterology and hepatology with a platform to publish high-quality basic and clinical research articles and communicate their research findings online. WJG mainly publishes articles reporting research results and findings obtained in the field of gastroenterology and hepatology and covering a wide range of topics including gastroenterology, hepatology, gastrointestinal endoscopy, gastrointestinal surgery, gastrointestinal oncology, and pediatric gastroenterology.

**INDEXING/ABSTRACTING**

The WJG is now abstracted and indexed in Science Citation Index Expanded (SCIE, also known as SciSearch®), Current Contents/Clinical Medicine, Journal Citation Reports, Index Medicus, MEDLINE, PubMed, PubMed Central, Scopus, Reference Citation Analysis, China National Knowledge Infrastructure, China Science and Technology Journal Database, and Superstar Journals Database. The 2022 edition of Journal Citation Reports® cites the 2021 impact factor (IF) for WJG as 5.374; IF without journal self cites: 5.187; 5-year IF: 5.715; Journal Citation Indicator: 0.84; Ranking: 31 among 93 journals in gastroenterology and hepatology; and Quartile category: Q2. The WJG's CiteScore for 2021 is 8.1 and Scopus CiteScore rank 2021: Gastroenterology is 18/149.

**RESPONSIBLE EDITORS FOR THIS ISSUE**

Production Editor: *Ying-Yi Yuan*; Production Department Director: *Xiang Li*; Editorial Office Director: *Jia-Ru Fan*.

**NAME OF JOURNAL**

*World Journal of Gastroenterology*

**ISSN**

ISSN 1007-9327 (print) ISSN 2219-2840 (online)

**LAUNCH DATE**

October 1, 1995

**FREQUENCY**

Weekly

**EDITORS-IN-CHIEF**

Andrzej S Tarnawski

**EDITORIAL BOARD MEMBERS**

<http://www.wjgnet.com/1007-9327/editorialboard.htm>

**PUBLICATION DATE**

October 7, 2022

**COPYRIGHT**

© 2022 Baishideng Publishing Group Inc

**INSTRUCTIONS TO AUTHORS**

<https://www.wjgnet.com/bpg/gerinfo/204>

**GUIDELINES FOR ETHICS DOCUMENTS**

<https://www.wjgnet.com/bpg/GerInfo/287>

**GUIDELINES FOR NON-NATIVE SPEAKERS OF ENGLISH**

<https://www.wjgnet.com/bpg/gerinfo/240>

**PUBLICATION ETHICS**

<https://www.wjgnet.com/bpg/GerInfo/288>

**PUBLICATION MISCONDUCT**

<https://www.wjgnet.com/bpg/gerinfo/208>

**ARTICLE PROCESSING CHARGE**

<https://www.wjgnet.com/bpg/gerinfo/242>

**STEPS FOR SUBMITTING MANUSCRIPTS**

<https://www.wjgnet.com/bpg/GerInfo/239>

**ONLINE SUBMISSION**

<https://www.f6publishing.com>

## Baishideng's Reference Citation Analysis database announces the first Journal Article Influence Index of 101 core journals and a list of high-quality academic journals in gastroenterology and hepatology

Jin-Lei Wang, Yu-Jie Ma, Li Ma, Na Ma, Diao-Mei Guo, Lian-Sheng Ma

**Specialty type:** Gastroenterology and hepatology

**Provenance and peer review:** Unsolicited article; Externally peer reviewed.

**Peer-review model:** Single blind

**Peer-review report's scientific quality classification**

Grade A (Excellent): 0  
Grade B (Very good): B  
Grade C (Good): 0  
Grade D (Fair): 0  
Grade E (Poor): 0

**P-Reviewer:** Morozov S, Russia

**Received:** August 16, 2022

**Peer-review started:** August 16, 2022

**First decision:** August 25, 2022

**Revised:** September 6, 2022

**Accepted:** September 21, 2022

**Article in press:** September 21, 2022

**Published online:** October 7, 2022



**Jin-Lei Wang, Yu-Jie Ma, Li Ma, Na Ma, Diao-Mei Guo, Lian-Sheng Ma**, Baishideng Publishing Group Inc, Pleasanton, CA 94566, United States

**Corresponding author:** Lian-Sheng Ma, Doctor, Founder and CEO, Baishideng Publishing Group Inc, 7041 Koll Center Parkway, Suite 160, Pleasanton, CA 94566, United States. [l.s.ma@baishideng.com](mailto:l.s.ma@baishideng.com)

### Abstract

After three rounds of rigorous evaluation of core journals in gastroenterology and hepatology conducted by the *Reference Citation Analysis (RCA)* editorial team of Baishideng Publishing Group (Baishideng), the *RCA* database of Baishideng officially released the 2022 *Journal Article Influence Index (2022 JAI)* of 101 core journals in gastroenterology and hepatology, for the first time. The list of 101 core journals can be found at: <https://www.referencecitationanalysis.com/Search-Journal>. Among them, the highest 2022 *JAI* is 48.014 and the lowest is 3.900. This article highlights the top 20 journals, describes the calculation method for the 2022 *JAI*, the evaluation process, and the inclusion principles for journals in the *RCA*. These steps are the underpinning of the *RCA*'s empirical journal academic evaluation service by which the digital platform addresses the needs of authors to select reliable journals for submission, readers to select high-quality literature for reading, and editors to track their own journal citation performance. As such, the *RCA* core journal list will serve as a useful Find-a-Journal tool. Any interested party is welcome to use this journal list and recommend it to their peers.

**Key Words:** *Reference Citation Analysis*; *Journal Article Influence Index*; Gastroenterology and hepatology; Journal list; Find a journal; Announcement

©The Author(s) 2022. Published by Baishideng Publishing Group Inc. All rights reserved.

**Core Tip:** The *Reference Citation Analysis (RCA)* database of Baishideng Publishing Group officially released the 2022 *Journal Article Influence Index (2022 JAI)* of 101 core journals in gastroenterology and hepatology, for the first time. This article highlights the top 20 journals, describes the calculation method for the 2022 *JAI*, evaluation process and inclusion principles. The *RCA* journal academic evaluation service platform addresses the needs of authors to select reliable journals for submission, readers to select high-quality literature for reading, and editors to track their own journal citation performance, effectively serving as a useful Find-a-Journal tool. You are welcome to use this journal list and recommend it to your peers.

**Citation:** Wang JL, Ma YJ, Ma L, Ma N, Guo DM, Ma LS. Baishideng's *Reference Citation Analysis* database announces the first *Journal Article Influence Index* of 101 core journals and a list of high-quality academic journals in gastroenterology and hepatology. *World J Gastroenterol* 2022; 28(37): 5383-5394

**URL:** <https://www.wjgnet.com/1007-9327/full/v28/i37/5383.htm>

**DOI:** <https://dx.doi.org/10.3748/wjg.v28.i37.5383>

## INTRODUCTION

We are very pleased to announce that the *Reference Citation Analysis (RCA)* database of Baishideng Publishing Group (Baishideng) has, for the first time, officially released the 2022 *Journal Article Influence Index (2022 JAI)* of 101 core journals in the field of gastroenterology and hepatology on August 8, 2022. A total of 101 core journals in gastroenterology and hepatology can be found at: <https://www.referencecitationanalysis.com/SearchJournal>.

*RCA* is an artificial intelligence technology-based open multidisciplinary citation analysis database. It was carefully designed to lead the development of wisdom, knowledge innovation, and emerging disciplines[1]. As such, the functions of *RCA* include: Find an Article (54753299), Find a Category (254), Find a Journal (14087), Find a Scholar (631), and Find an Academic Assistant (15). *RCA* updates its list of journals daily, according to relevant data including total number of articles, total citations, and the *JAI*. *RCA* acquires newly released abstracts and references from Crossref and adds them to the *RCA* database weekly. *RCA* also acquires abstracts and references released within the calendar year from Crossref and adds them to the *RCA* database monthly, and then updates the total number of articles, citations, and *JAI* accordingly. Herein, we introduce the top 20 2022 *JAI* from the total 101 core journals in the field of gastroenterology and hepatology included in *RCA*, the calculation method for the 2022 *JAI*, and the evaluation process and the inclusion principles of *RCA* journals.

## TOP 20 2022 JAI JOURNALS IN THE FIELD OF GASTROENTEROLOGY AND HEPATOLOGY INCLUDED IN THE RCA

The *RCA* classifies academic journals with a *JAI* of 20.0 or above as high quality academic journals, which will be highly recommended to authors and readers. There are 101 core journals in the field of gastroenterology and hepatology in the *RCA*, of which 20 were identified to be high quality academic journals, accounting for 19.8%. These 20 journals are listed below.

### 2022 JAI and rankings of Seminars in Liver Disease

In the *RCA* database, the 2022 *JAI* for *Seminars in Liver Disease* is 48.014, ranking 1<sup>st</sup> among 101 core journals in the field of gastroenterology and hepatology included in the *RCA*, with a total of 83641 citations (28/101) and a total of 1742 articles (50/101) (Figure 1). For more information on *Seminars in Liver Disease*, please visit: <https://www.referencecitationanalysis.com/SearchJournal>.

### 2022 JAI and rankings of Hepatology

In the *RCA* database, the 2022 *JAI* for *Hepatology* is 43.054, ranking 2<sup>nd</sup> among 101 core journals in the field of gastroenterology and hepatology included in the *RCA*, with a total of 1169100 citations (2/101) and a total of 27154 articles (2/101) (Figure 2). For more information on *Hepatology*, please visit: <https://www.referencecitationanalysis.com/SearchJournal>.

### 2022 JAI and rankings of Gastroenterology

In the *RCA* database, the 2022 *JAI* for *Gastroenterology* is 37.170, ranking 3<sup>rd</sup> among 101 core journals in the field of gastroenterology and hepatology included in the *RCA*, with a total of 1711173 citations (1/101) and a total of 46037 articles (1/101) (Figure 3). For more information on *Gastroenterology*, please



**Figure 1 2022 Journal Article Influence Index and rankings of Seminars in Liver Disease.** The image of the journal cover is originally from the home page of the journal: <https://www.thieme.in/seminars-in-liver-disease>.

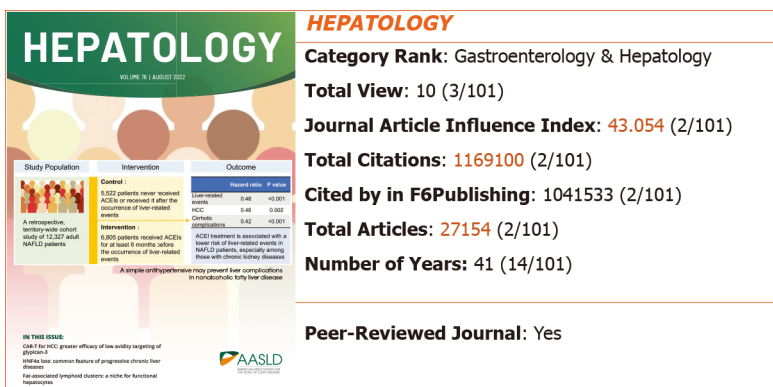


**Figure 2 2022 Journal Article Influence Index and rankings of Hepatology.** The image of the journal cover is originally from the home page of the journal: <https://aasldpubs.onlinelibrary.wiley.com/journal/15273350>.



**Figure 3 2022 Journal Article Influence Index and rankings of Gastroenterology.** The image of the journal cover is originally from the home page of the journal: <https://www.gastrojournal.org/>.

visit: <https://www.referencecitationanalysis.com/SearchJournal>.

**2022 JAIJ and rankings of Gut**

In the RCA database, the 2022 JAIJ for Gut is 36.751, ranking 4<sup>th</sup> among 101 core journals in the field of gastroenterology and hepatology included in the RCA, with a total of 914769 citations (3/101) and a total of 24891 articles (3/101) (Figure 4). For more information on Gut, please visit: <https://www.referencecitationanalysis.com/SearchJournal>.

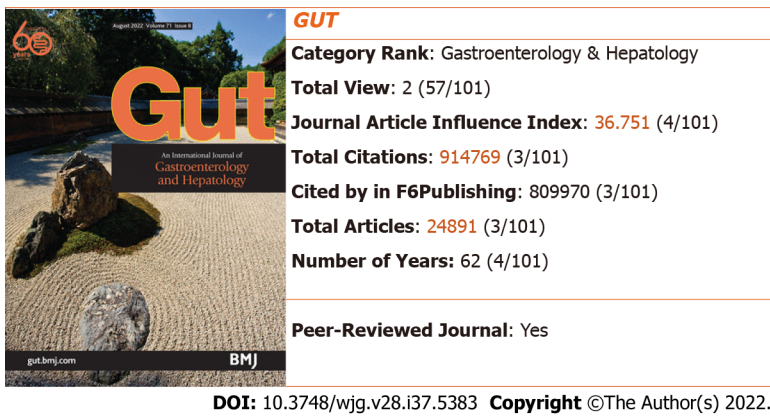


**Figure 4** 2022 *Journal Article Influence Index* and rankings of *Gut*. The image of the journal cover is originally from the home page of the journal: <http://gut.bmj.com/>.

### 2022 JAll and rankings of *Nature Reviews Gastroenterology & Hepatology*

In the RCA database, the 2022 JAll for *Nature Reviews Gastroenterology & Hepatology* is 35.473, ranking 5<sup>th</sup> among 101 core journals in the field of gastroenterology and hepatology included in the RCA, with a total of 100601 citations (24/101) and a total of 2836 articles (40/101) (Figure 5). For more information on *Nature Reviews Gastroenterology & Hepatology*, please visit: <https://www.referencecitationanalysis.com/SearchJournal>.

### 2022 JAll and rankings of *Gut Microbes*

In the RCA database, the 2022 JAll for *Gut Microbes* is 31.557, ranking 6<sup>th</sup> among 101 core journals in the field of gastroenterology and hepatology included in the RCA, with a total of 38720 citations (41/101) and a total of 1227 articles (64/101) (Figure 6). For more information on *Gut Microbes*, please visit: <https://www.referencecitationanalysis.com/SearchJournal>.

### 2022 JAll and rankings of *Alimentary Pharmacology & Therapeutics*

In the RCA database, the 2022 JAll for *Alimentary Pharmacology & Therapeutics* is 28.725, ranking 7<sup>th</sup> among 101 core journals in the field of gastroenterology and hepatology included in the RCA, with a total of 323707 citations (10/101) and a total of 11269 articles (13/101) (Figure 7). For more information on *Alimentary Pharmacology & Therapeutics*, please visit: <https://www.referencecitationanalysis.com/SearchJournal>.

### 2022 JAll and rankings of *Journal of Hepatology*

In the RCA database, the 2022 JAll for *Journal of Hepatology* is 28.725, ranking 8<sup>th</sup> among 101 core journals in the field of gastroenterology and hepatology included in the RCA, with a total of 556699 citations (4/101) and a total of 19575 articles (7/101) (Figure 8). For more information on *Journal of Hepatology*, please visit: <https://www.referencecitationanalysis.com/SearchJournal>.

### 2022 JAll and rankings of *Best Practice & Research Clinical Gastroenterology*

In the RCA database, the 2022 JAll for *Best Practice & Research Clinical Gastroenterology* is 28.428, ranking 9<sup>th</sup> among 101 core journals in the field of gastroenterology and hepatology included in the RCA, with a total of 44917 citations (36/101) and a total of 1580 articles (54/101) (Figure 9). For more information on *Best Practice & Research Clinical Gastroenterology*, please visit: <https://www.referencecitationanalysis.com/SearchJournal>.

### 2022 JAll and rankings of *Diseases of the Colon & Rectum*

In the RCA database, the 2022 JAll for *Diseases of the Colon & Rectum* is 26.946, ranking 10<sup>th</sup> among 101 core journals in the field of gastroenterology and hepatology included in the RCA, with a total of 344714 citations (9/101) and a total of 12793 articles (10/101) (Figure 10). For more information on *Diseases of the Colon & Rectum*, please visit: <https://www.referencecitationanalysis.com/SearchJournal>.

### 2022 JAll and rankings of *Liver Transplantation*

In the RCA database, the 2022 JAll for *Liver Transplantation* is 26.872, ranking 11<sup>th</sup> among 101 core journals in the field of gastroenterology and hepatology included in the RCA, with a total of 159891 citations (18/101) and a total of 5950 articles (25/101) (Figure 11). For more information on *Liver Transplantation*, please visit: <https://www.referencecitationanalysis.com/SearchJournal>.



DOI: 10.3748/wjg.v28.i37.5383 Copyright ©The Author(s) 2022.

**Figure 5 2022 Journal Article Influence Index and rankings of Nature Reviews Gastroenterology & Hepatology.** The image of the journal cover is originally from the home page of the journal: <https://www.nature.com/nrgastro/>.



DOI: 10.3748/wjg.v28.i37.5383 Copyright ©The Author(s) 2022.

**Figure 6 2022 Journal Article Influence Index and rankings of Gut Microbes.** The image of the journal cover is originally from the home page of the journal: <http://www.tandfonline.com/kgmi>.



DOI: 10.3748/wjg.v28.i37.5383 Copyright ©The Author(s) 2022.

**Figure 7 2022 Journal Article Influence Index and rankings of Alimentary Pharmacology & Therapeutics.** The image of the journal cover is originally from the home page of the journal: <https://onlinelibrary.wiley.com/journal/13652036>.

**2022 JAI and rankings of Gastric Cancer**

In the RCA database, the 2022 JAI for Gastric Cancer is 24.105, ranking 12<sup>th</sup> among 101 core journals in the field of gastroenterology and hepatology included in the RCA, with a total of 45558 citations (35/101) and a total of 1890 articles (49/101) (Figure 12). For more information on Gastric Cancer, please visit: <https://www.referencecitationanalysis.com/SearchJournal>.



**Figure 8 2022 Journal Article Influence Index and rankings of Journal of Hepatology.** The image of the journal cover is originally from the home page of the journal: <https://www.sciencedirect.com/journal/journal-of-hepatology>.



**Figure 9 2022 Journal Article Influence Index and rankings of Best Practice & Research Clinical Gastroenterology.** The image of the journal cover is originally from the home page of the journal: <http://www.sciencedirect.com/science/journal/15216918>.

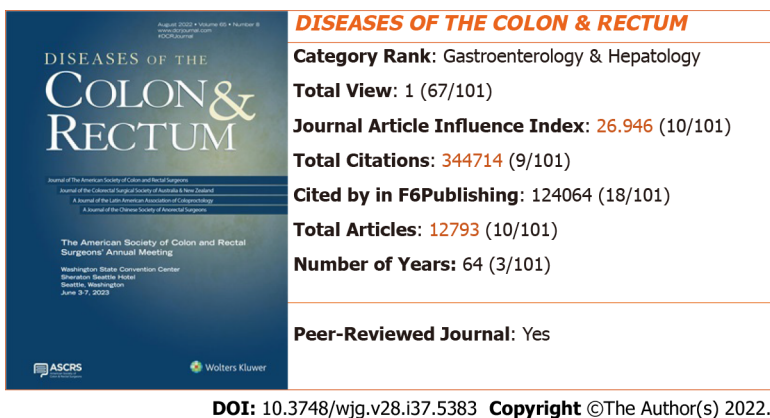


**Figure 10 2022 Journal Article Influence Index and rankings of Diseases of the Colon & Rectum.** The image of the journal cover is originally from the home page of the journal: <https://journals.lww.com/dcrjournal/pages/default.aspx>.

**2022 JAI and rankings of The American Journal of Gastroenterology**

In the RCA database, the 2022 JAI for *The American Journal of Gastroenterology* is 23.563, ranking 13<sup>th</sup> among 101 core journals in the field of gastroenterology and hepatology included in the RCA, with a total of 476726 citations (5/101) and a total of 20232 articles (6/101) (Figure 13). For more information on *The American Journal of Gastroenterology*, please visit: <https://www.referencecitationanalysis.com/SearchJournal>.



DOI: 10.3748/wjg.v28.i37.5383 Copyright ©The Author(s) 2022.

**Figure 11 2022 Journal Article Influence Index and rankings of Liver Transplantation.** The image of the journal cover is originally from the home page of the journal: <https://aasldpubs.onlinelibrary.wiley.com/journal/15276473>.



DOI: 10.3748/wjg.v28.i37.5383 Copyright ©The Author(s) 2022.

**Figure 12 2022 Journal Article Influence Index and rankings of Gastric Cancer.** The image of the journal cover is originally from the home page of the journal: <https://link.springer.com/journal/10120>.



DOI: 10.3748/wjg.v28.i37.5383 Copyright ©The Author(s) 2022.

**Figure 13 2022 Journal Article Influence Index and rankings of the American Journal of Gastroenterology.** The image of the journal cover is originally from the home page of the journal: <https://journals.lww.com/ajg/pages/default.aspx>.

### 2022 JAll and rankings of Lancet Gastroenterology & Hepatology

In the RCA database, the 2022 JAll for *Lancet Gastroenterology & Hepatology* is 23.470, ranking 14<sup>th</sup> among 101 core journals in the field of gastroenterology and hepatology included in the RCA, with a total of 30276 citations (48/101) and a total of 1290 articles (63/101) (Figure 14). For more information on *Lancet Gastroenterology & Hepatology*, please visit: <https://www.referencecitationanalysis.com/SearchJournal>.



**Figure 14 2022 Journal Article Influence Index and rankings of Lancet Gastroenterology & Hepatology.** The image of the journal cover is originally from the home page of the journal: <https://www.thelancet.com/journals/langas/home>.

### 2022 JAI and rankings of Journal of Gastroenterology

In the RCA database, the 2022 JAI for *Journal of Gastroenterology* is 22.837, ranking 15<sup>th</sup> among 101 core journals in the field of gastroenterology and hepatology included in the RCA, with a total of 110941 citations (22/101) and a total of 4858 articles (28/101) (Figure 15). For more information on *Journal of Gastroenterology*, please visit: <https://www.referencecitationanalysis.com/SearchJournal>.

### 2022 JAI and rankings of Neurogastroenterology and Motility

In the RCA database, the 2022 JAI for *Neurogastroenterology and Motility* is 22.335, ranking 16<sup>th</sup> among 101 core journals in the field of gastroenterology and hepatology included in the RCA, with a total of 93695 citations (26/101) and a total of 4195 articles (30/101) (Figure 16). For more information on *Neurogastroenterology and Motility*, please visit: <https://www.referencecitationanalysis.com/SearchJournal>.

### 2022 JAI and rankings of Clinical Gastroenterology and Hepatology

In the RCA database, the 2022 JAI for *Clinical Gastroenterology and Hepatology* is 22.295, ranking 17<sup>th</sup> among 101 core journals in the field of gastroenterology and hepatology included in the RCA, with a total of 223108 citations (13/101) and a total of 10007 articles (17/101) (Figure 17). For more information on *Clinical Gastroenterology and Hepatology*, please visit: <https://www.referencecitationanalysis.com/SearchJournal>.

### 2022 JAI and rankings of World Journal of Gastroenterology

In the RCA database, the 2022 JAI for *World Journal of Gastroenterology* is 21.914, ranking 18<sup>th</sup> among 101 core journals in the field of gastroenterology and hepatology included in the RCA, with a total of 471463 citations (4/101) and a total of 21514 articles (5/101) (Figure 18). For more information on *World Journal of Gastroenterology*, please visit: <https://www.referencecitationanalysis.com/00000009>.

### 2022 JAI and rankings of American Journal of Physiology-Gastrointestinal and Liver Physiology

In the RCA database, the 2022 JAI for *American Journal of Physiology-Gastrointestinal and Liver Physiology* is 21.406, ranking 19<sup>th</sup> among 101 core journals in the field of gastroenterology and hepatology included in the RCA, with a total of 230179 citations (11/101) and a total of 10753 articles (14/101) (Figure 19). For more information on *American Journal of Physiology-Gastrointestinal and Liver Physiology*, please visit: <https://www.referencecitationanalysis.com/SearchJournal>.

### 2022 JAI and rankings of Journal of Gastrointestinal Surgery

In the RCA database, the 2022 JAI for *Journal of Gastrointestinal Surgery* is 20.714, ranking 20<sup>th</sup> among 101 core journals in the field of gastroenterology and hepatology included in the RCA, with a total of 138742 citations (20/101) and a total of 6698 articles (22/101) (Figure 20). For more information on *Journal of Gastrointestinal Surgery*, please visit: <https://www.referencecitationanalysis.com/SearchJournal>.

---

## RCA'S MISSION

The mission of RCA is to provide a high quality academic article evaluation service platform for various categories. At present, there are many evaluation methods for academic articles, but their calculation methods are complicated. The RCA is a new method of evaluating the quality of academic articles,



DOI: 10.3748/wjg.v28.i37.5383 Copyright ©The Author(s) 2022.

**Figure 15 2022 Journal Article Influence Index and rankings of Journal of Gastroenterology.** The image of the journal cover is originally from the home page of the journal: <https://link.springer.com/journal/535>.



DOI: 10.3748/wjg.v28.i37.5383 Copyright ©The Author(s) 2022.

**Figure 16 2022 Journal Article Influence Index and rankings of Neurogastroenterology and Motility.** The image of the journal cover is originally from the home page of the journal: <https://onlinelibrary.wiley.com/journal/13652982>.



DOI: 10.3748/wjg.v28.i37.5383 Copyright ©The Author(s) 2022.

**Figure 17 2022 Journal Article Influence Index and rankings of Clinical Gastroenterology and Hepatology.** The image of the journal cover is originally from the home page of the journal: <http://www.sciencedirect.com/science/journal/15423565>.

which allows academic evaluation of journals, scholars, institutions, drugs, medical devices, and publishers based on the *JAI* of each article in the citation analysis database, thus greatly enriching the academic evaluation systems across different disciplines and guiding the healthy development of the academic community[2].



DOI: 10.3748/wjg.v28.i37.5383 Copyright ©The Author(s) 2022.

Figure 18 2022 Journal Article Influence Index and rankings of World Journal of Gastroenterology. The image of the journal cover is originally from the home page of the journal: <http://www.wjgnet.com/1007-9327/index.htm>.



DOI: 10.3748/wjg.v28.i37.5383 Copyright ©The Author(s) 2022.

Figure 19 2022 Journal Article Influence Index and rankings of American Journal of Physiology-Gastrointestinal and Liver Physiology. The image of the journal cover is originally from the home page of the journal: <https://journals.physiology.org/journal/ajpgi>.



DOI: 10.3748/wjg.v28.i37.5383 Copyright ©The Author(s) 2022.

Figure 20 2022 Journal Article Influence Index and rankings of Journal of Gastrointestinal Surgery. The image of the journal cover is originally from the home page of the journal: <https://link.springer.com/journal/11605>.

## OPENNESS AND TRANSPARENCY OF RCA EVALUATION

RCA is unique in its objective, impartial, fair, and transparent release of citation analysis data of important academic journals to authors and readers, including evaluation data, evaluation indices, evaluation methods, and evaluation results, in order to ensure the reliability of academic evaluation[2].

---

## CALCULATION METHOD FOR 2022 *JAI*

---

The 2022 *JAI*, calculated as Total citations/Total articles, is not a 2-year or 5-year average of citations, but is an average of citations for all articles since the journal was assigned its DOI number. Article types are not only limited to original articles and review articles, but for all types of articles. In this way, it is a more objective, fair, and transparent calculation of the academic influence index of an academic journal. Furthermore, the journal list itself is evaluated dynamically, its bibliographic metrics being updated daily, including total number of articles, total citations, and *JAI*[2].

---

## EVALUATION PROCESS OF RCA JOURNALS

---

The journals included in the RCA core journal list need to undergo three rounds of strict evaluation. The evaluation process is as follows[2]:

**First-round evaluation:** Verify the basic information on the journal, including Journal Name, Abbreviated Title, Print ISSN, Online ISSN, Language, Category, Peer-Reviewed Journal, Ownership, Publisher, Journal Website, Editorial Board Members, Submit a Manuscript, and Indexed by.

**Second-round evaluation:** Verify the activity of the journal, including Total Articles, Total Citations, Cited by in F6Publishing, and the *JAI*.

**Third-round evaluation:** Based on the reliability of journal information, the activity of publication data, whether the journal is a peer-reviewed journal or not, and *JAI*, the editorial team evaluates every journal, makes the decision to accept or reject the journal, and creates a list of core journals by discipline. The function of the list of core academic journals is to classify journals according to categories and rank them according to various bibliometrics, including Total Views, *JAI*, Total Citations, Cited by in F6Publishing, Total Articles, and Number of Years.

---

## INCLUSION PRINCIPLES OF RCA JOURNAL

---

The RCA editorial team of Baishideng conducted three rounds of rigorous evaluation on core journals in gastroenterology and hepatology. The resultant RCA core journal list for the field of gastroenterology and hepatology includes a total of 101 journals, among which the highest 2022 *JAI* is 48.014 and the lowest *JAI* is 3.900, the highest total number of citations is 1711173 and the lowest is 698, and the highest total number of articles is 46037 and the lowest is 133. The RCA core journal list does not include any journals with a *JAI* lower than 3.0. We implement dynamic evaluation inclusively for the RCA core journal list. Evaluation is initiated once an RCA-nonincluded journal receives a *JAI* over 3.0. Similarly, if a journal included in the RCA core journal list receives a *JAI* lower than 3.0, it will be excluded[2]. The RCA core journal list is designed by publishers, scientific editors, and engineers for use by readers, authors, and editorial offices, and is free-of-charge to users.

Upon completion of the three rounds of rigorous evaluation on core journals in gastroenterology and hepatology by the RCA editorial team, all data in each journal are organized for public consumption according to category rank, including the 2022 *JAI*, total citations, cited by in F6Publishing, total articles, and the 2021 Journal Impact Factor™. All information in each journal, including Journal Name, Print ISSN, Online ISSN, Language, Free Access, Peer-Reviewed Journal, Ownership, Publisher, Journal Website, Editorial Board Members, Submit a Manuscript, and Indexed by are made available in RCA. Moreover, the citations of each journal can be then ranked in RCA by the *Impact Index Per Article*, Cited by in Crossref, and Cited by in F6Publishing parameters. Results analysis available for each journal includes Year Published Analysis, Article Type Analysis, Journal Title Analysis, and Category Analysis. The references of each journal are also refined by Year Published and Article Type. Each reference's citation information is displayed, including PMID, DOI, Cited by in Crossref, *Impact Index Per Article*, RCA, and Track Full Text[2].

---

## CONCLUSION

---

The ultimate purpose of RCA is to provide an open, objective, fair, and reliable academic evaluation service platform for readers, authors, and journal editors. The RCA journal academic evaluation service platform is designed and actively maintained to address the needs of authors to select reliable journals for submission, readers to select high-quality literature for reading, and editors to track their own journal citation performance. The RCA core journal list itself will serve as a useful Find-a-Journal tool. Any interested party is welcome to use this journal list and recommend it to their peers.

---

## FOOTNOTES

---

**Author contributions:** Wang JL analyzed the data and drafted the manuscript; Ma YJ participated in the data collection; Ma LS revised the manuscript for important intellectual content; and all authors participated in manuscript revision.

**Conflict-of-interest statement:** The authors are employees of the Baishideng Publishing Group Inc, and declare that they have no other real or potential conflicts of interest to disclose.

**Open-Access:** This article is an open-access article that was selected by an in-house editor and fully peer-reviewed by external reviewers. It is distributed in accordance with the Creative Commons Attribution NonCommercial (CC BY-NC 4.0) license, which permits others to distribute, remix, adapt, build upon this work non-commercially, and license their derivative works on different terms, provided the original work is properly cited and the use is non-commercial. See: <https://creativecommons.org/licenses/by-nc/4.0/>

**Country/Territory of origin:** United States

**ORCID number:** Jin-Lei Wang [0000-0002-5197-3051](https://orcid.org/0000-0002-5197-3051); Lian-Sheng Ma [0000-0002-1430-4844](https://orcid.org/0000-0002-1430-4844).

**S-Editor:** Wang JJ

**L-Editor:** Webster JR

**P-Editor:** Wang JJ

---

## REFERENCES

---

- 1 **Baishideng Publishing Group Inc.** Welcome to the Reference Citation Analysis. Available from: <https://www.referencecitationanalysis.com>
- 2 **Baishideng Publishing Group Inc.** Reference Citation Analysis's evaluation process for inclusion of academic journals. Available from: <https://www.wjgnet.com/bpg/GerInfo/303>

## Milestones in the discovery of hepatitis C

Octavio Campollo, Gerardo Amaya, P Aiden McCormick

**Specialty type:** Gastroenterology and hepatology

**Provenance and peer review:** Invited article; Externally peer reviewed.

**Peer-review model:** Single blind

**Peer-review report's scientific quality classification**

Grade A (Excellent): A  
Grade B (Very good): B, B, B  
Grade C (Good): 0  
Grade D (Fair): D  
Grade E (Poor): 0

**P-Reviewer:** Ballestín SS, Spain; Lo SY, Taiwan; Villela-Nogueira CA, Brazil; Yu ML, Taiwan

**Received:** March 4, 2022

**Peer-review started:** March 4, 2022

**First decision:** March 27, 2022

**Revised:** April 11, 2022

**Accepted:** August 16, 2022

**Article in press:** August 16, 2022

**Published online:** October 7, 2022



**Octavio Campollo**, Center of Studies on Alcohol and Addictions, Antiguo Hospital Civil de Guadalajara, Department of Medical Clinics, Universidad de Guadalajara, Guadalajara 44280, Jalisco, Mexico

**Gerardo Amaya**, Medical Clinics, CUCS, Universidad de Guadalajara, Guadalajara 44280, Jalisco, Mexico

**P Aiden McCormick**, Department of Hepatology, Saint Vincent's University Hospital, National Liver Transplant Unit, Dublin D04, Ireland

**Corresponding author:** Octavio Campollo, MD, PhD, Full Professor, Center of Studies on Alcohol and Addictions, Antiguo Hospital Civil de Guadalajara, Department of Medical Clinics, Universidad de Guadalajara, Calle Hospital 278, Col. El Retiro, Guadalajara 44280, Jalisco, Mexico. [renaceboy@hotmail.com](mailto:renaceboy@hotmail.com)

### Abstract

The discovery of hepatitis C has been a landmark in public health as it brought the opportunity to save millions of lives through the diagnosis, prevention and cure of the disease. The combined work of three researchers, Alter H, Houghton M and Rice C, which set the basis for the diagnosis, treatment and prevention of hepatitis C apart from laying the ground work for a new approach to study infections in general and developing new antiviral agents. This is a story of a transfusion-associated infection. A series of clinical studies demonstrated the existence of an infectious agent associated with hepatitis. That was followed by the identification of what was later known to be the hepatitis C virus (HCV) and the development of diagnostic tests. It all preceded the full molecular identification and demonstration of a causal effect. Finally it ended up with the development and discovery of a new class of therapeutic drugs, the direct acting antivirals, which are now used not only to cure the disease but most probably, to eliminate the problem. This work started with Dr Alter H who demonstrated that a new virus was responsible for the majority of post-transfusion hepatitis followed by Houghton M who cloned the virus and developed the blood test to identify those cases that carried the virus. Finally, the work of Rice C demonstrated that a cloned HCV produced after applying molecular biology techniques could cause long-standing infection and cause the same disease as the one observed in humans.

**Key Words:** Hepatitis C; Nobel prize; Discovery; Diagnosis; Treatment; Elimination; World Health Organization initiative

**Core Tip:** The discovery of hepatitis C has been a landmark in public health as it brought the opportunity to save millions of lives through the diagnosis, prevention and cure of a disease that was perhaps noticed 5000 years ago. It was through the combined work of three researchers, Alter H, Houghton M and Rice C, which set the basis for the diagnosis, treatment and prevention of hepatitis C apart from laying the ground work for a new approach to study infections in general and developing new antiviral agents.

**Citation:** Campollo O, Amaya G, McCormick PA. Milestones in the discovery of hepatitis C. *World J Gastroenterol* 2022; 28(37): 5395-5402

**URL:** <https://www.wjgnet.com/1007-9327/full/v28/i37/5395.htm>

**DOI:** <https://dx.doi.org/10.3748/wjg.v28.i37.5395>

## INTRODUCTION

*“The methodological studies of transfusion-associated hepatitis by Harvey J. Alter demonstrated that an unknown virus was a common cause of chronic hepatitis. Michael Houghton used an untested strategy to isolate the genome of the new virus that was named Hepatitis C virus. Charles M. Rice provided the final evidence showing that Hepatitis C virus alone could cause hepatitis.” Nobel Prize assembly, 2020[1].*

## THE DISCOVERY OF HEPATITIS C VIRUS WAS A LANDMARK IN PUBLIC HEALTH

The prolonged campaign to discover and treat the various causes of viral hepatitis is a major medical success story as it brought about the opportunity to save thousands of lives through the diagnosis, prevention and cure of the disease, sparing lives that would be lost to chronic hepatitis C and its complications. It was through the combined work of three researchers starting with Dr Alter H working at National Institutes of Health (NIH) who demonstrated that a new virus was responsible for the majority of post-transfusion hepatitis. That was followed by Houghton M who cloned the virus and developed the blood test to identify those cases that carried the virus. And finally, Rice C demonstrated that a cloned hepatitis C virus (HCV), produced after applying molecular biology techniques (a virion), could cause long-standing infection and cause the same disease as the one observed in humans[2]. These scientific breakthroughs enabled the World Health Organization (WHO) to set the, once unthinkable, goal for HCV elimination by 2030[3]. The implications of this work are not limited to hepatitis C as the new diagnostic techniques and methods of drug development may be applicable to other viral pathogens. Furthermore, the complete new approach to treatment based on the study and new knowledge of the HCV genetics and lifecycle together with the molecular biology approach attacking many targets directly (in the HCV lifecycle) *i.e.*, protease inhibitors, polymerase inhibitors and NS5A inhibitors[4-6], the former being the most successful prodrug developed and currently used in the WHO policy for world elimination of hepatitis C aimed at either[6,7], virion processing, RNA replication and virion assembly in the liver cell[6,8].

For those of us who grew up in the hepatology field when non-A non-B hepatitis (what a strange name!) was a common topic of discussion in the clinic and the laboratory, the award of the Nobel prize for the discovery of HCV in 2020 marked a fitting end to a long saga. This is the second Nobel prize awarded to investigators in viral hepatitis recognizing the major advances in this field of clinical and laboratory research [the first Nobel prize was awarded to Blumberg B in 1976 for the discovery of hepatitis B virus (HBV)][9]. Initially viral hepatitis was regarded as an epidemic disease which was a major problem in congregated settings such as residential schools and military establishments. It became a major issue in time of war when epidemics reduced the effectiveness of armies in the field. Much important early research was funded by the military. Only later did it become apparent that chronic viral hepatitis could lead to cirrhosis and hepatocellular carcinoma (HCC). Many millions of people were infected making it one of the leading causes of morbidity and mortality in some parts of the world. In the early 2000's it was estimated that chronic viral hepatitis was responsible for over one million deaths annually[10]. The development of vaccines for hepatitis B and effective anti-viral therapy for hepatitis B and C have been dramatically effective and offer the prospect of banishing these diseases to the sidelines of human history.

## BRIEF HISTORY OF HEPATITIS

The hepatitis problem was perhaps noticed 5000 years ago when epidemics of jaundice were attributed to a devil called “Ahhazu” by the Sumerians[11] and many years later were described by Hippocrates in the 5<sup>th</sup> century BC in his book “Epidemics”. They were particularly noted in armies during time of war, hence the term “campaign jaundice”. The cause of jaundice was not understood and up till the outbreak of the second world war many clinicians accepted Virchow’s theory that a mucous plug at the mouth of the common bile duct caused “catarrhal jaundice”[12]. The large number of hepatitis cases and the impact it had on battle readiness acted as a major stimulus to understanding hepatitis. Most of the subsequent advances in knowledge were described in the British and American literature. Up until D-day in 1944 the British army was mainly engaged in fighting in the Mediterranean theatre. Hepatitis, with malaria and venereal disease were the three most important medical conditions afflicting the troops there[13]. On the other side of the Atlantic ocean, 28585 United States servicemen developed jaundice after receiving the yellow fever vaccine[14]. Clinical, epidemiological and transmission studies established that there were two distinct forms of hepatitis, characterized as infectious or serum hepatitis. Infectious hepatitis was transmitted by the fecal-oral route whereas serum hepatitis was transmitted by injection or blood products[15].

Stokes and Neff of the United States Army Medical Corps had been using concentrated gamma globulin to prevent or attenuate measles infection. Despite several thousand treatments they recorded no cases of hepatitis[16]. They reasoned that there may be neutralizing antibodies in gamma globulin prepared from large pools of adult plasma and suggested that gamma globulin could be useful in the treatment of viral hepatitis. The hypothesis was tested when there was a large epidemic of hepatitis in a summer camp for boys and girls in September 1944. There was sufficient gamma globulin to treat 45 children, who were compared to 246 controls. Hepatitis was subsequently documented in 16% (7/45) treated compared to (70%) 172/246 controls. None of those treated developed clinical jaundice thus demonstrating that gamma globulin could prevent or attenuate infectious hepatitis[17]. Many of the subsequent transmission studies on viral hepatitis of questionable procedures were performed in the Willowbrook State School in New York for children with mental disorders which had a major problem with endemic infectious hepatitis[15]. The investigators clearly demonstrated two types of hepatitis, with different incubation periods and no cross-immunity, subsequently proven to be hepatitis A and hepatitis B. The ethics of that program have since been questioned[18].

The problem of hepatitis continued up until modern times when many cases of un-explained jaundice continued to puzzle clinicians until some 51 years ago when Holland, Schmidt, Purcell, Walsh and Alter began to study what was called “Transfusion-associated hepatitis” in 1969[19]. It would take some 20 years more until the infectious agent, HCV, was discovered[20]. Those of us who grew up in the hepatology field when non-A non-B hepatitis was a common topic for discussion in clinical meetings and on the wards remember the cases of unexplained post-transfusion hepatitis. In addition there were many cases of “nosocomial” hepatitis[21] and cryptogenic hepatitis and a lack of diagnostic tests. The journey to unravel this problem took another 39 years, 14 years from the identification of non-A non-B hepatitis to the discovery of the HCV and 25 years from the discovery of HCV in 1989 to the approval of one of the most prescribed direct acting antiviral agents (DAA) Sofosbuvir in 2013 for the treatment of hepatitis C[22]. In all, those 39 years don’t seem too bad now when we look at the progress made from those early clinical and epidemiologic studies by Alter and others up to the incredibly creative and imaginative pharmacological approach to therapy involving the design of DAA that inhibit HCV infection by blocking viral assembly and replication at the present time[22].

Currently, it is estimated, that there are more than 71 million people around the world infected with HCV. Complications of end-stage liver disease due to hepatitis C make it one of the world’s most important causes of death with 400000 cases a year[23]. It is well-known that HCV can cause chronic hepatitis C, a silent but progressive condition which may progress to cirrhosis and HCC over decades. Hepatitis C is transmitted by the parenteral route. As blood products for transfusion have become increasingly safe due to effective viral testing, the main route of transmission in most countries is through intravenous drug use. Eradication of hepatitis C requires effective harm reduction strategies for intravenous drug use in addition to antiviral therapy[7,20].

Interest in this problem (now known as hepatitis C) was renewed almost 70 years ago when there was a high incidence of chronic hepatitis after blood transfusions or use of blood products. At that time it was impossible to know who of the donors carried the disease. In 1960, Alter[24] started his search for the “source” of post-transfusion hepatitis having previously worked with Blumberg B with whom he had observed a “precipitin line ... that stained intensely red” in a reaction between blood from a patient with hemophilia and blood from an Australian aborigine which they called initially the “Australia antigen”. That was later identified as the surface protein of the HBV (HBsAg). Blumberg continued his research on the Australia antigen to establish the link with HBV for which he won the Nobel prize in Medicine in 1976[11]. In his studies, Alter[19] found that even if hepatitis B contaminated blood was excluded from use most post-transfusional hepatitis remained. He tested the blood supplies for the presence of suspected known viruses and followed up patients who developed hepatitis after receiving a blood transfusion and found that an incredible high number of cases could not be explained. Alter[19] and other researchers suspected there was another infectious agent. In 1978, Alter[24] demonstrated that

plasma from those patients with post-transfusion hepatitis could infect chimpanzees who developed clinical and laboratory signs of hepatitis suggesting that the cause of that liver inflammation was infectious. Further studies by Alter[24] showed that the causative agent had characteristics of a virus. The next goal was the search for the virus which took lots of effort and time *i.e.*, years! Nevertheless Alter[19] had learnt from Blumberg to work with tenacity and perseverance to carry on with his work. Robert Purcell and Steve Feinstone at the NIH[19] and Alfred Prince in New York noted that most cases of post-transfusion hepatitis were HBsAg negative and hepatitis A virus negative[11]. At that time they started calling it non-A non-B hepatitis (NANBH)[11]. Another important step was the observation that infectivity titers in chimps studied by Purcell were almost identical to the genomic titers in a patient with severe acute NANBH studied by Alter[19]. Alter[19] worked with the assumption that genetic material would be present in pools of DNA sequences isolated from those animals infected with hepatitis, and on the other hand that serum from humans with this form of hepatitis would have specific antibodies against that virus that would bind to some proteins or viral particles and could then be used to identify those samples with the virus. Together with Purcell he attempted every serological approach known at the time to identify the virus without success.

In 1989, Houghton[25] at Chiron Laboratories in California (now part of Novartis) tried a combination of molecular biology and immunology methods. They extracted nucleic acid from plasma and cloned it in an expression vector (GT11) creating a phage expression library. This technique enabled them to identify the first epitope characteristic of the HCV envelope in 1989[11]. They later named it HCV. Houghton rapidly came up with the idea of developing immunoassays to detect antibodies to protein products of those clones establishing a blood test for HCV which he evaluated using Alter's blood samples' collection at NIH[26]. They correctly identified all samples which were thought to be infected with the virus as well as all negative controls. This was a major milestone for medicine and public health. It allowed blood banks to screen all blood supplies resulting in an immediate and dramatic drop in the incidence of post-transfusion hepatitis.

At this point there was another crucial question, that is whether this virus could reproduce infection if inoculated into an experimental model, hence probing that the now called HCV was the causative agent of the formerly known NANBH. Rice C a researcher at the University of Washington who had been working with molecular virology of *Flavivirus*[22] focused on dissecting HCV gene expression using blood from infected chimpanzees to introduce DNA fragments into bacteria to express individual protein fragments. Those products were then screened with the antiviral antibodies until they could isolate one positive clone. The positive clone encoded a sequence that was very similar to sequences of the virus family of flaviviruses. Next, Rice started investigating what was needed for the molecularly cloned HCV to be reproduced *in vitro*. In 1996, he and his group identified the conserved 3'-terminal region of the HCV genomic RNA which was previously unknown[27], and was crucial for recovery of infectious HCV cDNA clones. However, initially they could not produce infection when injected into the liver of animals speculating that there could be some inactivating random mutations in the genome produced during the replication of the virus[28]. That meant that some individual clones may be defective. He sequenced many clones and compared them with each other and found that some of these clones contained potentially inactivating mutations which he thought could be removed with genetic engineering[29]. He later combined that repaired viral genome with the 3'-end of the genomic RNA hoping he would obtain a functional virus. When he injected this genome into the liver of chimpanzees clinical signs of hepatitis ensued and there was virus present in the blood producing now the evidence that the clone of the HCV could produce the disease associated with hepatitis infection[22,30]. That was a very important advance because the development of HCV replicons provided a live HCV system in the laboratory where viral replication, pathogenesis and evolution in culture could be studied in a viable *in vitro* replication system[22]. Later on newer constructs were obtained with higher replicative ability *in vitro*[22]. This was another milestone. Within 1 year of the cloning of HCV the nucleotide sequence of the entire viral genome was determined and the agent was characterized as a single-stranded positive-sense RNA virus of about 9600 nucleotides in length[2,31]. The advent of functional replicons also enabled the assay development for antiviral drug development which made the search for effective anti-viral drugs much easier[22]. Another collaborator of Rice, Ralf Bartenschlager, a molecular biologist who had previously worked with HBV, successfully replicated HCV genomic RNA in a human hepatoma cell line Huh7[32]. Confirmatory reports from various groups worldwide all corroborated that replicons were robust *in vitro* replication (subgenomic HCV replication system) systems that set the basis for production of infectious virus particles in cell cultures[22,32]. That improved the HCV RNA replicon system model was used in collaboration with Michael Sofia to design the new DAA[22]. One of those developed, DAA PSI-7797 (Sofosbuvir), had a very effective antiviral effect with broader genotype coverage and fewer side effects on a shorter duration treatment[11,22]. This prodrug enters the hepatocyte readily where it is metabolized to produce a triphosphate derivative which is a potent viral replication inhibitor[20,22]. It has just recently been announced that it can cure up to 95% of patients infected with HCV[33]. Different prodrugs were tested in genotype-specific cell lines that have been used in preclinical studies to select and validate novel targets for HCV. Those included NS3-4A protease inhibitors, nucleoside analogue viral polymerase inhibitors, non-nucleoside inhibitors of the viral RNA polymerase, NS5A inhibitors, host targeted agents (HTA), cyclophilin inhibitors and a cellular miRNA antagonist[4]. The discovery of over 30 new DAAs and HTAs revolutionized the treatment of chronic

HCV[8]. The swift development of interferon-free protocols using DAA monotherapy or the combined administration of two or three DAAs or HTAs, administered for 8-12 and up to 24 wk, led to sustained virological response (SVR) rates between 90% and 100%[8,33,34].

With the widespread use of DAAs many countries are now reporting a reduction in mortality associated with chronic hepatitis C and its complications such as liver cirrhosis and HCC[3]. A strategy of “treatment as prevention” has been proposed with the aim of reducing the population prevalence, interrupting the chain of viral transmission and ultimately leading to elimination of HCV infection[11, 20], although patients with HCV infection with cirrhosis or decompensated liver disease present special challenges such as post-SVR complications including HCV reinfection, HCC risk, residual HCC which should be addressed by early detection and treatment, combination and multiple DAA therapy avoiding the use of protease inhibitors and risk reduction counseling[7,34]. As epidemiologists, infectious diseases and liver specialists analyze the natural history, epidemiology and public health figures, world experts have proposed a rationale towards hepatitis C elimination based on infection control and disease elimination and eradication[7,20].

---

## ELIMINATION OF HEPATITIS C

---

Viral hepatitis is a global health burden affecting 325 million people globally of which 71 million have hepatitis C with 1.5 million infections occurring per year and 542316 global HCV related deaths[3,20]. In 2016, the WHO set the Global health sector strategy for viral hepatitis proposing to eliminate viral hepatitis as a public health problem by 2030[3]. That is a 90% reduction in incidence and a 65% reduction in mortality by 2030 and a new guidance was released in June 2021[35]. These targets are achievable with the tools now at our disposal as demonstrated for hepatitis B in Taiwan[36] and hepatitis C in Egypt[37]. The main global strategies are to increase HCV testing, improve clinical education of providers, utilize simple models for HCV care and provide universal access to antiviral treatment at affordable cost. While there have been technical, geographic and policy limitations such as limited funding, lack of transparency and high in-country process, fragmented procurement, HCV diagnostics inefficiencies[3] and most recently the severe acute respiratory syndrome coronavirus 2 pandemic to mention a few there have been many examples around the globe showing that the goals are feasible[35]. In Egypt the cost of hepatitis C antiviral therapy fell from \$1650 to \$85 United States dollars between 2015 and 2018. A nationwide screening and treatment program identified 1.15 million infected individuals. By September 2019 over 1.05 million had commenced treatment with sustained virological clearance rates of 98.8%[37]. In spite of those challenges mentioned above, the future of mankind looks promising as millions of people will have the chance of a life free of hepatitis virus.

---

## CONCLUSION

---

We have summarized the contributions of several groups of medical researchers starting with Dr Alter H who demonstrated that a new virus was responsible for the majority of post-transfusion hepatitis followed by Houghton M who cloned the virus and developed the blood test to identify those cases that carried the virus. That was continued with the work of Rice C that demonstrated that a cloned HCV produced after applying molecular biology techniques could produce long-standing infection and cause the same disease in animals as the one observed in humans[2] (Figure 1). That is a milestone not only in the diagnosis, treatment and prevention of hepatitis C, but in the approach to study infections in general apart from contributing to the understanding of the role genetic and environmental factors play in the development of this infection. In all, that set the basis for the production of new antivirals which are central for hepatitis C control and elimination. Of note, the cloning of HCV in 1989 was a remarkable accomplishment that has not only saved a large number of human lives but also demonstrated the power of molecular biology in unearthing new infectious agents. The discovery of HCV, the first virus ever discovered by molecular cloning technology, with its accompanying development of new methodologies such as new generation sequencing and new generation diagnostic automated systems[38], is also a landmark in public health. The discovery of HCV provides the opportunity to save thousands of lives through prevention and now, cure of the disease, which would otherwise be lost to chronic hepatitis C and its complications.

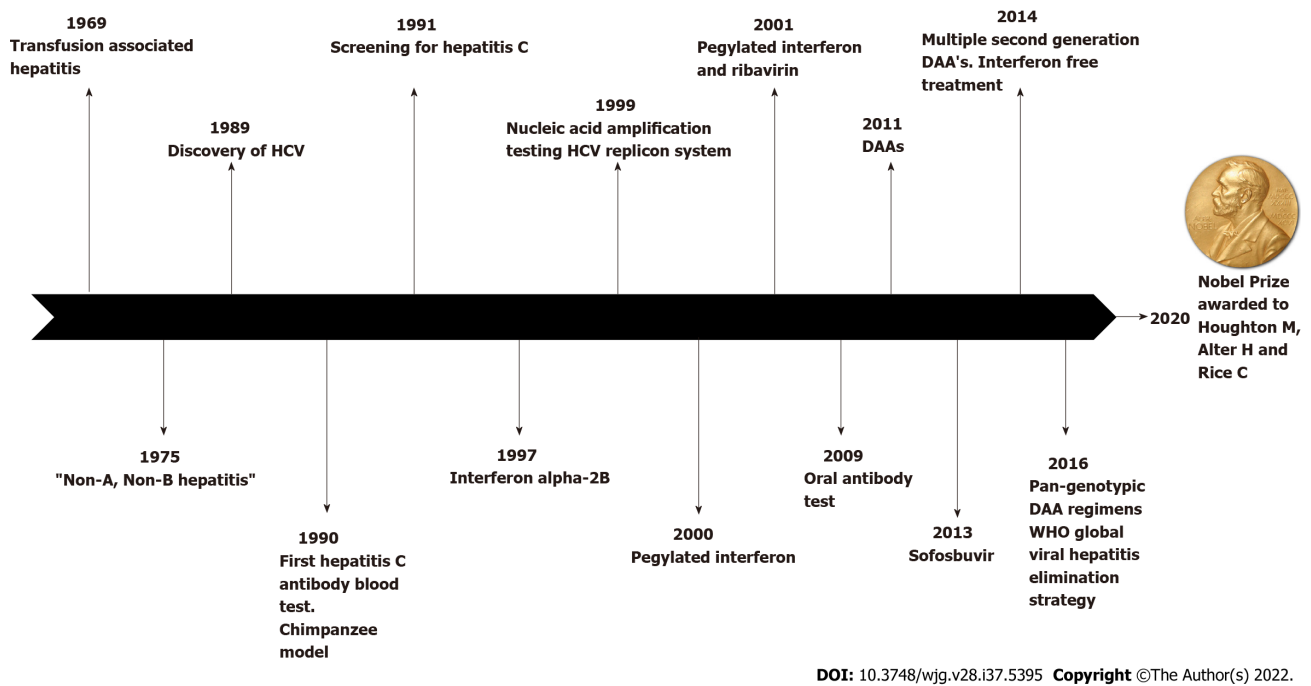


**Figure 1** Timeline of the events leading and following the discovery of the hepatitis C virus. DAAs: Direct-acting antivirals; HCV: Hepatitis C virus; WHO: World Health Organization.

## ACKNOWLEDGEMENTS

We thank Octavio Guadalupe Campollo for the art work.

## FOOTNOTES

**Author contributions:** Campollo O conceived the idea of the article, discussed and collaborated with the authors, answered the reviewers comments and reviewed the final version; Amaya G reviewed the literature and updated the references, made contributions to the manuscript, reviewed and corrected the drafts, and answered the reviewers comments; McCormick PA wrote several sections of earlier and final versions of the manuscript, reviewed and corrected the final draft, and, reviewed the English language.

**Conflict-of-interest statement:** All the authors report no relevant conflicts of interest for this article.

**Open-Access:** This article is an open-access article that was selected by an in-house editor and fully peer-reviewed by external reviewers. It is distributed in accordance with the Creative Commons Attribution NonCommercial (CC BY-NC 4.0) license, which permits others to distribute, remix, adapt, build upon this work non-commercially, and license their derivative works on different terms, provided the original work is properly cited and the use is non-commercial. See: <https://creativecommons.org/licenses/by-nc/4.0/>

**Country/Territory of origin:** Mexico

**ORCID number:** Octavio Campollo 0000-0003-1812-4207; Gerardo Amaya 0000-0002-6747-1881; P Aiden McCormick 0000-0002-5994-6023.

**S-Editor:** Wang JJ

**L-Editor:** Webster JR

**P-Editor:** Wang JJ

## REFERENCES

- Masaccio MG, Hedestam GK. The discovery of Hepatitis C virus. The Nobel assembly at Karolinska Institutet. [cited 12 February 2022]. Available from: <https://www.nobelprize.org/prizes/medicine/2020/advanced-information/>
- Farci P, Choo QL, Kuo G, Weiner AJ, Overby LR, Bradley DW, Houghton M. Isolation of a cDNA clone derived from a blood-borne non-A, non-B viral hepatitis genome [Science 1989; 244: 359-362]. *J Hepatol* 2002; **36**: 582-585 [PMID:

- 11983439 DOI: [10.1016/s0168-8278\(02\)00051-X](https://doi.org/10.1016/s0168-8278(02)00051-X)]
- 3 **World Health Organization.** Global health sector strategy on viral hepatitis 2016-2021. Towards ending viral hepatitis. [cited 15 February 2022]. Available from: <https://www.who.int/publications/i/item/WHO-HIV-2016.06>
  - 4 **Johnson KA,** Dangerfield T. Mechanisms of inhibition of viral RNA replication by nucleotide analogs. *Enzymes* 2021; **49**: 39-62 [PMID: [34696838](https://pubmed.ncbi.nlm.nih.gov/34696838/) DOI: [10.1016/bs.enz.2021.07.001](https://doi.org/10.1016/bs.enz.2021.07.001)]
  - 5 **European Association for the Study of the Liver.** Clinical Practice Guidelines Panel: Chair:: EASL Governing Board representative:: Panel members:. EASL recommendations on treatment of hepatitis C: Final update of the series<sup>☆</sup>. *J Hepatol* 2020; **73**: 1170-1218 [PMID: [32956768](https://pubmed.ncbi.nlm.nih.gov/32956768/) DOI: [10.1016/j.jhep.2020.08.018](https://doi.org/10.1016/j.jhep.2020.08.018)]
  - 6 **Manns MP,** Buti M, Gane E, Pawlotsky JM, Razavi H, Terrault N, Younossi Z. Hepatitis C virus infection. *Nat Rev Dis Primers* 2017; **3**: 17006 [PMID: [28252637](https://pubmed.ncbi.nlm.nih.gov/28252637/) DOI: [10.1038/nrdp.2017.6](https://doi.org/10.1038/nrdp.2017.6)]
  - 7 **Ghany MG,** Morgan TR; AASLD-IDSAs Hepatitis C Guidance Panel. Hepatitis C Guidance 2019 Update: American Association for the Study of Liver Diseases-Infectious Diseases Society of America Recommendations for Testing, Managing, and Treating Hepatitis C Virus Infection. *Hepatology* 2020; **71**: 686-721 [PMID: [31816111](https://pubmed.ncbi.nlm.nih.gov/31816111/) DOI: [10.1002/hep.31060](https://doi.org/10.1002/hep.31060)]
  - 8 **Webster DP,** Klenerman P, Dusheiko GM. Hepatitis C. *Lancet* 2015; **385**: 1124-1135 [PMID: [25687730](https://pubmed.ncbi.nlm.nih.gov/25687730/) DOI: [10.1016/S0140-6736\(14\)62401-6](https://doi.org/10.1016/S0140-6736(14)62401-6)]
  - 9 **Gerlich WH.** Medical virology of hepatitis B: how it began and where we are now. *Virology* 2013; **10**: 239 [PMID: [23870415](https://pubmed.ncbi.nlm.nih.gov/23870415/) DOI: [10.1186/1743-422X-10-239](https://doi.org/10.1186/1743-422X-10-239)]
  - 10 **Stanaway JD,** Flaxman AD, Naghavi M, Fitzmaurice C, Vos T, Abubakar I, Abu-Raddad LJ, Assadi R, Bhala N, Cowie B, Forouzanfar MH, Groeger J, Hanafiah KM, Jacobsen KH, James SL, MacLachlan J, Malekzadeh R, Martin NK, Mokdad AA, Mokdad AH, Murray CJL, Plass D, Rana S, Rein DB, Richardus JH, Sanabria J, Saylan M, Shahraz S, So S, Vlassov VV, Weiderpass E, Wiersma ST, Younis M, Yu C, El Sayed Zaki M, Cooke GS. The global burden of viral hepatitis from 1990 to 2013: findings from the Global Burden of Disease Study 2013. *Lancet* 2016; **388**: 1081-1088 [PMID: [27394647](https://pubmed.ncbi.nlm.nih.gov/27394647/) DOI: [10.1016/S0140-6736\(16\)30579-7](https://doi.org/10.1016/S0140-6736(16)30579-7)]
  - 11 **Treppo C.** A brief history of hepatitis milestones. *Liver Int* 2014; **34** Suppl 1: 29-37 [PMID: [24373076](https://pubmed.ncbi.nlm.nih.gov/24373076/) DOI: [10.1111/liv.12409](https://doi.org/10.1111/liv.12409)]
  - 12 **MacCallum FO.** 1971 International Symposium on Viral Hepatitis. Historical perspectives. *Can Med Assoc J* 1972; **106** Suppl: 423-Suppl:426 [PMID: [4552628](https://pubmed.ncbi.nlm.nih.gov/4552628/)]
  - 13 **Witts LJ.** Some Problems of Infective Hepatitis. *Br Med J* 1944; **1**: 739-743 [PMID: [20785459](https://pubmed.ncbi.nlm.nih.gov/20785459/) DOI: [10.1136/bmj.1.4352.739](https://doi.org/10.1136/bmj.1.4352.739)]
  - 14 **Reuben A.** The thin red line. *Hepatology* 2002; **36**: 770-773 [PMID: [12198682](https://pubmed.ncbi.nlm.nih.gov/12198682/) DOI: [10.1002/hep.510360341](https://doi.org/10.1002/hep.510360341)]
  - 15 **Krugman S,** Giles JP, Hammond J. Infectious hepatitis. Evidence for two distinctive clinical, epidemiological, and immunological types of infection. *JAMA* 1967; **200**: 365-373 [PMID: [4164595](https://pubmed.ncbi.nlm.nih.gov/4164595/) DOI: [10.1001/jama.1967.03120180053006](https://doi.org/10.1001/jama.1967.03120180053006)]
  - 16 **Stokes J,** Maris EP, Gellis SS. Chemical, clinical, and immunological studies on the products of human plasma fractionation. xi. the use of concentrated normal human serum gamma globulin (human immune serum globulin) in the prophylaxis and treatment of measles. *J Clin Invest* 1944; **23**: 531-540 [PMID: [16695129](https://pubmed.ncbi.nlm.nih.gov/16695129/) DOI: [10.1172/JCI101518](https://doi.org/10.1172/JCI101518)]
  - 17 **Stokes JJ,** Neefe JR. Prevention and attenuation of infectious hepatitis by gamma globulin: preliminary note. *JAMA* 1945; **127**: 144-145 [DOI: [10.1001/jama.1945.02860030016004](https://doi.org/10.1001/jama.1945.02860030016004)]
  - 18 **Rothman DJ.** Were Tuskegee & Willowbrook 'studies in nature'? *Hastings Cent Rep* 1982; **12**: 5-7 [PMID: [7096065](https://pubmed.ncbi.nlm.nih.gov/7096065/) DOI: [10.2307/3561798](https://doi.org/10.2307/3561798)]
  - 19 **Alter HJ.** The road not taken or how I learned to love the liver: a personal perspective on hepatitis history. *Hepatology* 2014; **59**: 4-12 [PMID: [24123147](https://pubmed.ncbi.nlm.nih.gov/24123147/) DOI: [10.1002/hep.26787](https://doi.org/10.1002/hep.26787)]
  - 20 **Ward JW.** Hepatitis C virus: the 25-year journey from discovery to cure. *Hepatology* 2014; **60**: 1479-1482 [PMID: [25131647](https://pubmed.ncbi.nlm.nih.gov/25131647/) DOI: [10.1002/hep.27377](https://doi.org/10.1002/hep.27377)]
  - 21 **Campollo O,** Valencia-Salinas JJ, Berumen-Arellano A, Pérez-Aranda MA, Panduro-Cerda A, Segura-Ortega J. [Epidemiological characteristics of liver cirrhosis at the Hospital Civil of Guadalajara]. *Salud Publica Mex* 1997; **39**: 195-200 [PMID: [9304222](https://pubmed.ncbi.nlm.nih.gov/9304222/) DOI: [10.1590/S0036-36341997000300004](https://doi.org/10.1590/S0036-36341997000300004)]
  - 22 **Zhao Q,** Xia N. The 2016 Lasker-DeBakey Clinical Medical Research Award: Innovative hepatitis C virus (HCV) replicons leading to drug development for hepatitis C cure. *Sci China Life Sci* 2016; **59**: 1198-1201 [PMID: [27785725](https://pubmed.ncbi.nlm.nih.gov/27785725/) DOI: [10.1007/s11427-016-0313-9](https://doi.org/10.1007/s11427-016-0313-9)]
  - 23 **EASL.** EASL Policy Statement on Hepatitis C Elimination. [cited 15 February 2022]. Available from: <https://easl.eu/wp-content/uploads/2019/04/EASL-Policy-Statement-on-Hepatitis-C-Elimination.pdf>
  - 24 **Alter HJ,** Purcell RH, Holland PV, Popper H. Transmissible agent in non-A, non-B hepatitis. *Lancet* 1978; **1**: 459-463 [PMID: [76017](https://pubmed.ncbi.nlm.nih.gov/76017/) DOI: [10.1016/s0140-6736\(78\)90131-9](https://doi.org/10.1016/s0140-6736(78)90131-9)]
  - 25 **Houghton M.** The long and winding road leading to the identification of the hepatitis C virus. *J Hepatol* 2009; **51**: 939-948 [PMID: [19781804](https://pubmed.ncbi.nlm.nih.gov/19781804/) DOI: [10.1016/j.jhep.2009.08.004](https://doi.org/10.1016/j.jhep.2009.08.004)]
  - 26 **Kuo G,** Choo QL, Alter HJ, Gitnick GL, Redeker AG, Purcell RH, Miyamura T, Dienstag JL, Alter MJ, Stevens CE. An assay for circulating antibodies to a major etiologic virus of human non-A, non-B hepatitis. *Science* 1989; **244**: 362-364 [PMID: [2496467](https://pubmed.ncbi.nlm.nih.gov/2496467/) DOI: [10.1126/science.2496467](https://doi.org/10.1126/science.2496467)]
  - 27 **Kolykhalov AA,** Feinstone SM, Rice CM. Identification of a highly conserved sequence element at the 3' terminus of hepatitis C virus genome RNA. *J Virol* 1996; **70**: 3363-3371 [PMID: [8648666](https://pubmed.ncbi.nlm.nih.gov/8648666/) DOI: [10.1128/JVI.70.6.3363-3371.1996](https://doi.org/10.1128/JVI.70.6.3363-3371.1996)]
  - 28 **Harak C,** Meyrath M, Romero-Brey I, Schenk C, Gondeau C, Schult P, Esser-Nobis K, Saeed M, Neddermann P, Schnitzler P, Gotthardt D, Perez-Del-Pulgar S, Neumann-Haefelin C, Thimme R, Meuleman P, Vondran FW, De Francesco R, Rice CM, Bartenschlager R, Lohmann V. Tuning a cellular lipid kinase activity adapts hepatitis C virus to replication in cell culture. *Nat Microbiol* 2016; **2**: 16247 [PMID: [27991882](https://pubmed.ncbi.nlm.nih.gov/27991882/) DOI: [10.1038/nmicrobiol.2016.247](https://doi.org/10.1038/nmicrobiol.2016.247)]
  - 29 **Saeed M,** Andreo U, Chung HY, Espiritu C, Branch AD, Silva JM, Rice CM. SEC14L2 enables pan-genotype HCV replication in cell culture. *Nature* 2015; **524**: 471-475 [PMID: [26266980](https://pubmed.ncbi.nlm.nih.gov/26266980/) DOI: [10.1038/nature14899](https://doi.org/10.1038/nature14899)]
  - 30 **Kolykhalov AA,** Agapov EV, Blight KJ, Mihalik K, Feinstone SM, Rice CM. Transmission of hepatitis C by intrahepatic inoculation with transcribed RNA. *Science* 1997; **277**: 570-574 [PMID: [9228008](https://pubmed.ncbi.nlm.nih.gov/9228008/) DOI: [10.1126/science.277.5325.570](https://doi.org/10.1126/science.277.5325.570)]

- 31 **Choo QL**, Kuo G, Weiner AJ, Overby LR, Bradley DW, Houghton M. Isolation of a cDNA clone derived from a blood-borne non-A, non-B viral hepatitis genome. *Science* 1989; **244**: 359-362 [PMID: [2523562](#) DOI: [10.1126/science.2523562](#)]
- 32 **Lohmann V**, Körner F, Koch J, Herian U, Theilmann L, Bartenschlager R. Replication of subgenomic hepatitis C virus RNAs in a hepatoma cell line. *Science* 1999; **285**: 110-113 [PMID: [10390360](#) DOI: [10.1126/science.285.5424.110](#)]
- 33 **Shouval D**, Friedman SL. Focusing on the past, present, and future of hepatology. *J Hepatol* 2014; **61**: 1196-1198 [PMID: [25195549](#) DOI: [10.1016/j.jhep.2014.08.039](#)]
- 34 **Huang CF**, Yu ML. Unmet needs of chronic hepatitis C in the era of direct-acting antiviral therapy. *Clin Mol Hepatol* 2020; **26**: 251-260 [PMID: [32188235](#) DOI: [10.3350/cmh.2020.0018](#)]
- 35 **World Health Organization**. Interim guidance for country validation of viral hepatitis elimination. [cited 15 February 2022]. Available from: <https://www.who.int/publications/i/item/9789240028395>
- 36 **Chang MH**, You SL, Chen CJ, Liu CJ, Lai MW, Wu TC, Wu SF, Lee CM, Yang SS, Chu HC, Wang TE, Chen BW, Chuang WL, Soon MS, Lin CY, Chiou ST, Kuo HS, Chen DS; Taiwan Hepatoma Study Group. Long-term Effects of Hepatitis B Immunization of Infants in Preventing Liver Cancer. *Gastroenterology* 2016; **151**: 472-480.e1 [PMID: [27269245](#) DOI: [10.1053/j.gastro.2016.05.048](#)]
- 37 **Waked I**, Esmat G, Elsharkawy A, El-Serafy M, Abdel-Razek W, Ghalab R, Elshishiney G, Salah A, Abdel Megid S, Kabil K, El-Sayed MH, Dabbous H, El Shazly Y, Abo Sliman M, Abou Hashem K, Abdel Gawad S, El Nahas N, El Sobky A, El Sonbaty S, El Tabakh H, Emad E, Gemeah H, Hashem A, Hassany M, Hefnawy N, Hemida AN, Khadary A, Labib K, Mahmoud F, Mamoun S, Marei T, Mekky S, Meshref A, Othman A, Ragab O, Ramadan E, Rehan A, Saad T, Saeed R, Sharshar M, Shawky H, Shawky M, Shehata W, Soror H, Taha M, Talha M, Tealaab A, Zein M, Hashish A, Cordie A, Omar Y, Kamal E, Ammar I, AbdAlla M, El Akel W, Doss W, Zaid H. Screening and Treatment Program to Eliminate Hepatitis C in Egypt. *N Engl J Med* 2020; **382**: 1166-1174 [PMID: [32187475](#) DOI: [10.1056/NEJMsr1912628](#)]
- 38 **Panduro A**. Viruses and the Liver 2020: Before COVID-19 and the beginning of a new age in medicine. *Ann Hepatol* 2021; **20**: 100293 [PMID: [33388122](#) DOI: [10.1016/j.aohp.2020.100293](#)]

## Immunotherapy-based novel nanoparticles in the treatment of gastrointestinal cancer: Trends and challenges

Yi-Nan Ding, Ming Xue, Qiu-Sha Tang, Li-Jun Wang, Hui-Yan Ding, Han Li, Cheng-Cheng Gao, Wei-Ping Yu

**Specialty type:** Gastroenterology and hepatology

**Provenance and peer review:** Invited article; Externally peer reviewed.

**Peer-review model:** Single blind

**Peer-review report's scientific quality classification**

Grade A (Excellent): 0  
Grade B (Very good): B  
Grade C (Good): C  
Grade D (Fair): 0  
Grade E (Poor): 0

**P-Reviewer:** Manojlovic N, Serbia; Serban ED, Romania

**Received:** July 21, 2022

**Peer-review started:** July 21, 2022

**First decision:** August 19, 2022

**Revised:** August 27, 2022

**Accepted:** September 15, 2022

**Article in press:** September 15, 2022

**Published online:** October 7, 2022



**Yi-Nan Ding, Qiu-Sha Tang, Li-Jun Wang, Hui-Yan Ding,** Department of Pathophysiology, College of Medicine, Southeast University, Nanjing 210000, Jiangsu Province, China

**Ming Xue,** Department of Critical Care Medicine, Zhongda Hospital, School of Medicine, Southeast University, Nanjing 210000, Jiangsu Province, China

**Han Li,** Department of Tuberculosis, The Second Hospital of Nanjing, Nanjing University of Chinese Medicine, Nanjing 210000, Jiangsu Province, China

**Cheng-Cheng Gao,** Department of Radiology, Affiliated Hangzhou First People's Hospital, Zhejiang University School of Medicine, Hangzhou 310000, Zhejiang Province, China

**Wei-Ping Yu,** Medical School, Southeast University, Nanjing 210009, Jiangsu Province, China

**Corresponding author:** Wei-Ping Yu, MD, PhD, Doctor, Professor, Medical School, Southeast University, No. 87 Dingjiaqiao, Nanjing 210009, Jiangsu Province, China.

[wpylg@hotmail.com](mailto:wpylg@hotmail.com)

### Abstract

Gastrointestinal cancer (GIC) is the most common cancer with a poor prognosis. Currently, surgery is the main treatment for GIC. However, the high rate of postoperative recurrence leads to a low five-year survival rate. In recent years, immunotherapy has received much attention. As the only immunotherapy drugs approved by the Food and Drug Administration (FDA), immune checkpoint blockade (ICB) drugs have great potential in cancer therapy. Nevertheless, the efficacy of ICB treatment is greatly limited by the low immunogenicity and immunosuppressive microenvironment of GIC. Therefore, the targets of immunotherapy have expanded from ICB to increasing tumor immunogenicity, increasing the recruitment and maturation of immune cells and reducing the proportion of inhibitory immune cells, such as M2-like macrophages, regulatory T cells and myeloid-derived suppressor cells. Moreover, with the development of nanotechnology, a variety of nanoparticles have been approved by the FDA for clinical therapy, so novel nanodrug delivery systems have become a research focus for anticancer therapy. In this review, we summarize recent advances in the application of immunotherapy-based nanoparticles in GICs, such as gastric cancer, hepatocellular carcinoma, colorectal cancer and pancreatic cancer, and described the existing challenges and future trends.

**Key Words:** Gastrointestinal cancer; Gastric cancer; Hepatocellular carcinoma; Colorectal cancer; Pancreatic cancer; Immunotherapy-based novel nanoparticles

©The Author(s) 2022. Published by Baishideng Publishing Group Inc. All rights reserved.

**Core Tip:** Recently, immunotherapy has received substantial attention. Although there are several Food and Drug Administration-approved immune checkpoint blockade (ICB) drugs, the efficacy remains limited, and the response rate is less than 20%. Because gastrointestinal cancer (GIC) is a group of immunosuppressive cancers, the efficacy of ICB treatment is also limited. Therefore, enhancing the immunogenicity of GIC or reversing the immunosuppressive microenvironment of GIC have become potential approaches for GIC immunotherapy. There are many studies on nanoparticle-based cancer therapy. However, there are only a few studies on immunotherapy-based nanoparticles in GIC. Here, we summarize recent advances in the application of immunotherapy-based nanoparticles in GIC and present our thoughts about this topic.

**Citation:** Ding YN, Xue M, Tang QS, Wang LJ, Ding HY, Li H, Gao CC, Yu WP. Immunotherapy-based novel nanoparticles in the treatment of gastrointestinal cancer: Trends and challenges. *World J Gastroenterol* 2022; 28(37): 5403-5419

**URL:** <https://www.wjgnet.com/1007-9327/full/v28/i37/5403.htm>

**DOI:** <https://dx.doi.org/10.3748/wjg.v28.i37.5403>

## INTRODUCTION

Gastrointestinal cancer (GIC) has been among the most commonly diagnosed cancers in recent decades [1-3]. In recent reports, the incidence and mortality rates have gradually decreased for gastric cancer (GC), hepatocellular carcinoma (HCC) and esophageal cancer in China; in contrast, the rates for colorectal cancer (CRC) have increased[4]. Regardless of the changes in the incidence and mortality rates of GIC, the disease has greatly affected the quality of life of many individuals.

Similar to other types of cancer, GIC has several therapies available. As the most conventional means of cancer treatment, surgery, chemotherapy and radiotherapy play important roles. Although traditional therapies effectively prolong survival for patients with GIC, there are still many drawbacks that cannot be ignored[5]. Surgery, especially minimally invasive surgery and radiotherapy, can effectively shrink the tumor and even make the local tumor disappear; chemotherapy can be administered systematically to kill cancer cells[6-8]. However, these treatments cannot prevent recurrence. Moreover, for GICs, the side effects of radiotherapy and chemotherapy on the digestive system seriously affect the quality of life of patients and cannot be ignored[9-11]. To improve the therapeutic effect and reduce the occurrence of adverse reactions, clinicians often try a variety of therapeutic combinations to achieve complementary advantages[12,13].

With progress in the concept of cancer treatment and the development of diagnosis and treatment technology, various precision treatment methods, such as targeted therapy, photodynamic therapy (PDT), photothermal therapy (PTT) and immunotherapy, have emerged as new sources of hope for patients[14-19]. Some scholars believe that the characteristics of the GIC immune microenvironment are related to the high mortality of patients with GIC; therefore, treatments that target the GIC immune microenvironment are gradually being recognized[20]. As one of the therapeutic methods that targets the cancer immune microenvironment, immune checkpoint blockade (ICB) treatment has achieved great success in clinical practice, laying a good foundation for the development of cancer immunotherapy[21].

Recently, a variety of nanobased drugs (such as Eligard[22], Marqibo[23], Onivyde[24], Doxil[25], Abraxane[26], Ontak[27] and Nanotherm[28]) have been widely used in clinical practice due to several characteristics, including their low toxicity, long circulation and passive targeting ability[29,30]. However, most of the nanobased drugs mentioned above are liposomes. In addition to liposomes, there are also other types of nanoparticles that possess the same potential for clinical translation. Similar to liposomes, small extracellular vesicles and cell membrane vesicles also have lipid bilayers, and they have better biocompatibility than liposomes due to their origin[31-34]. Furthermore, due to their simple production process and high drug loading efficiency, polymersomes are also considered candidate nanoparticles for clinical translation[35-37]. There are also many kinds of novel nanoparticles, such as gold nanoparticles, manganese dioxide nanoparticles, upconversion nanoparticles (UCNPs), metal organic framework nanoparticles and mesoporous silica nanoparticles (MSNPs), which can also play important roles in different diseases or cancers through their own characteristics[38-42]. Here, among the GICs, we focus on GC, HCC, CRC and pancreatic cancer and summarize the application trends of immunotherapy-based novel nanoparticles in these cancers as well as the challenges and opportunities

in the future.

## IMMUNOTHERAPY-BASED NOVEL NANOPARTICLES IN GC

GC remains one of the most common causes of cancer-related death globally. Although a variety of treatments have been developed, the main treatment for GC is still surgery or endoscopic resection. The probability of patients experiencing recurrence after surgery is approximately 60% [43]. Currently, the median overall survival time with fluoropyrimidine-based combination chemotherapy is less than one year. In general, the overall clinical therapeutic effect of GC is not satisfactory [44,45]. In addition, immunotherapy for GC will become an important treatment option in the future, and nanoparticles, as highly efficient drug carriers, have played an important role in clinical practice [46-48]. Whether the combination of immunotherapy and nanoparticles can produce improved therapeutic effects is also worth examining.

Immune checkpoint inhibitors (ICIs), such as anti-programmed death receptor-1 (anti-PD-1) antibody and anti-programmed death receptor-ligand 1 (anti-PD-L1) antibody, can effectively block the PD-1/PD-L1 pathway and enhance the anticancer immune response [49]. Based on ICI treatment, Xu *et al* [50] prepared a novel nanoparticle named docetaxel (DOC)-PEG-PCL-monoconal antibody (mAb) NP, which contained DOC as the chemotherapeutic drug and conjugated PD-L1 mAb on the surface of the nanoparticle. This nanodrug delivery system (NDDS) can effectively improve drug delivery efficiency and the solubility of hydrophobic drugs such as DOC. In addition, the system can target PD-L1-positive GC cells, exhibiting clinical translation potential. Recently, scientists found that a gradually acquired heritable *de novo* methylation program inhibited T-cell proliferation and clonal diversity during PD-1 blockade therapy [51]. Inspired by this study, Hu *et al* [52] designed copolymers loaded with the epigenetic agent 5-Aza-20-deoxycytidine (DAC), and an anti-PD-1 antibody was conjugated to the surface of the nanoparticles. The nanoparticles increased the stability of DAC and improved the therapeutic effect of ICI treatment *in vivo*.

Due to the characteristics of the cancer immune microenvironment, T-cell infiltration in GC patients is insufficient, which limits the effect of ICB treatment in GC [53]. Guo *et al* [54] constructed an NDDS named HMON<sup>®</sup>IR820/Pt-NPs, which coencapsulated platinum nanoparticles (chemo-prodrugs) and IR820 (photosensitizer) into hollow mesoporous organosilica nanoparticles. IR820-mediated PDT can lead to the release of oxidative mitochondrial DNA (mitoDNA). In addition, this oxidative process can oxidize Pt(0) to cytotoxic Pt(II), which can lead to the dysfunction of nuclear DNA (nDNA). The dual damage of mitoDNA and nDNA can activate the c-GAS/stimulator of interferon genes (STING) pathway, which can directly stimulate innate immunity and increase the infiltration of CD8<sup>+</sup> T cells, thus improving the efficacy of immunotherapy for GC.

Multiple studies have confirmed that tumor-associated macrophages (TAMs) are also involved in the composition of the tumor immune microenvironment. Moreover, M2-like macrophages can inhibit tumor immunity and promote tumor immune escape [55,56]. Zhang *et al* [57]'s group designed a novel human serum albumin (HSA)-Au(III) thiosemicarbazone agent nanoparticle delivery system for chemotherapy and immunotherapy in GC. This NDDS can simultaneously directly kill GC cells and polarize TAMs into M1-like macrophages, providing a new immunotherapy strategy for clinical translation.

The majority of cancer patients are often unable to activate adequate levels of anticancer immunity, whereas therapeutic tumor vaccines can help patients proactively generate adequate anticancer immune responses against tumor-specific antigens (TSAs) and tumor-associated antigens [58]. Among the different types of tumor vaccines, dendritic cell (DC)-based tumor vaccines have been explored in clinical experiments [59,60]. Kohnepoushi *et al* [61] prepared poly(lactic-co-glycolic) acid nanoparticles to protect the human gastric tumor antigen against proteolytic enzymes. In addition, nanoparticles that contain human gastric tumor antigen can facilitate DC maturation and further enhance the efficacy of DC vaccines in clinical practice.

In addition to ICB treatment and other therapies that can improve the cancer immune microenvironment, immunoadjuvants can act as a potential adjunctive therapy to stimulate anticancer immunity [62,63]. Zhang *et al* [64] developed a gold nanoshell-based NDDS that can convert near-infrared (NIR) light into thermal energy, enabling PTT. Moreover, high temperature can also break thiol bonds to release gene therapy agents and oligonucleotides that contain cytosine-guanine (CpG) motifs (which are also known as immunoadjuvants). This study designed a novel NDDS combined with hyperthermia, gene therapy and immunotherapy, which exhibited encouraging anticancer efficacy against GC *in vitro* and *in vivo* (Table 1).

## IMMUNOTHERAPY-BASED NOVEL NANOPARTICLES IN HCC

Primary liver cancer is among the most commonly diagnosed cancers, most of which are HCC [65,66]. Due to the high infection rate of hepatitis B virus, the incidence of HCC in China remains high [67].

**Table 1 Overview of immunotherapy-based novel nanoparticles in the treatment of gastric cancer [PubMed Search (immunotherapy) AND (nanoparticle) AND (gastric cancer)]**

Type of nanoparticle	Treatment strategy	Drugs or active substance involved	The main involvement of immune cells	Ref.
Copolymers	ICIs, chemotherapy	DOC, PD-L1 mAb	T cells	Xu <i>et al</i> [50]
Copolymers	ICIs, epigenetic treatment	DAC, nivolumab	PD1 <sup>+</sup> CD8 <sup>+</sup> TILs	Hu <i>et al</i> [52]
Hollow mesoporous organosilica nanoparticles	Dual-damage to nDNA and mitoDNA activates the c-GAS/STING pathway to stimulate innate immunity	Platinum, IR820	CD8 <sup>+</sup> T cells, DCs	Guo <i>et al</i> [54]
HSA nanoparticles	Targeted chemotherapy and immunotherapy	Au(III) thiosemicarbazone agent	TAMs	Zhang <i>et al</i> [57]
Polymers	DC vaccine	Human gastric tumor antigens	DCs	Kohnepoushi <i>et al</i> [61]
Gold nanoshell	Gene therapy, hyperthermia and immunoadjuvants therapy	HER-2 targeted siRNA, gold, CpG	DCs, T cells	Zhang <i>et al</i> [64]

ICIs: Immune checkpoint inhibitors; DOC: Docetaxel; PD-L1: Programmed cell death ligand 1; mAb: Monoclonal antibody; DAC: 5-Aza-20-deoxycytidine; TILs: Tumor-infiltrating T cells; DCs: Dendritic cells; HSA: Human serum albumin; TAMs: Tumor-associated macrophages; HER-2: Human epidermal growth factor receptor-2; CpG: Cytosine-guanine.

Surgical resection of the liver is the main treatment for HCC. However, the prognosis after surgery is still poor. Recently, the development of molecular targeted therapy and immunotherapy for HCC has gained recognition in clinical studies[68]. Moreover, NDDSs can improve the efficiency of drug delivery into the tumor area and reduce side effects[69-71]. At present, a large number of studies using immunotherapy-based NDDSs have shown great potential for clinical translation.

ICB treatment has also emerged as a new option for advanced HCC[72]. However, ICB treatment alone has limited efficacy against HCC. Therefore, how to combine other kinds of therapies to improve the efficiency of ICB treatment has become a new academic topic. For example, Food and Drug Administration (FDA)-approved sorafenib-experienced patients used ipilimumab (anti-CTLA-4) combined with nivolumab (anti-PD-1) in March 2020[73]. In the last two decades, scientists have found that chemotherapeutic drugs, radiotherapy, PDT and some other treatments can induce immunogenic cell death (ICD), which can lead to the release of TSAs and increase tumor antigenicity[74]. Hence, ICD can improve the efficacy of ICB treatment by increasing tumor immunogenicity. According to the therapeutic strategies mentioned above, Xu *et al*[75] designed a cyclic arginine-glycine-aspartic acid peptide-modified self-assembling polymer-based NDDS. Cancer cells were damaged by PDT and chemotherapy, while induced ICD and enhanced tumor immunogenicity provided a suitable immune microenvironment for ICB treatment. Previous studies found that a lack of the p53 tumor suppressor gene leads to tumorigenesis and drug resistance[76-78]. With the development of research on the p53 tumor suppressor gene, an increasing body of evidence indicates that the p53 protein plays an important role in anticancer immunity by regulating the cancer immune microenvironment[79-81]. Furthermore, a recent study suggested that ICD induced by cytotoxic agents, such as chemotherapy drugs, may be involved in the activation of the p53 pathway[82]. Xiao *et al*[83] developed a novel lipid-polymer hybrid nanopatform for mRNA delivery that can induce the expression of p53, effectively reprogramming the immune microenvironment of HCC. Moreover, combination with anti-PD-1 therapy can reverse the inhibitory immune microenvironment of HCC. To solve the problem of HCC recurrence after surgery, Li *et al*[84] designed a bionic NDDS consisting of MSNPs loaded with anti-PD-L1 and sorafenib and coated with platelet membranes at the surface of the MSNPs. This NDDS can target wounds and generate potent anti-HCC immunity, providing a new therapeutic idea for preventing recurrence in postsurgery HCC patients.

As we mentioned before, chemotherapy-based ICD can cause cancer cells to be more easily recognized by the immune system. However, the effect of single-drug-mediated ICD is very limited. Some studies have attempted to enhance the effect of ICD by combining two different ICD inducers to solve this problem. Yu *et al*[85] evaluated the potential of icaritin as an ICD inducer and utilized NDDS to deliver low doses of icaritin and doxorubicin simultaneously to the tumor area. This NDDS can reprogram the immune microenvironment and induce satisfactory anti-HCC effects. Furthermore, NDDS can lower the dose of chemotherapy to reduce the side effects.

TAMs play a major role in the immunosuppressive microenvironment of HCC[86]. Wang *et al*[87] screened chemokine C-C motif ligand (CCL)2 and CCL5 as two major chemokines responsible for the polarization of M2-like macrophages and designed a CCL2 and CCL5 dual-target lipid nanoparticle system. The combination of TAMs targeting lipid nanoparticles with ICB treatment achieved long-term survival in HCC mice. Similarly, as a common feature of the tumor microenvironment, hypoxia is also

common in HCC. Hypoxia can lead to radioresistance and the formation of an immunosuppressive microenvironment, including the accumulation of TAMs and depletion of effector T cells, which are closely related to the occurrence and development of cancer[88-90]. Dai *et al*[91] synthesized polydopamine-nanoparticle-stabilized oxygen microcapsules that can deliver oxygen to the tumor region and rapidly increase the concentration of oxygen. In this study, oxygen microcapsules increased HCC sensitivity to radiotherapy and polarized M2-like macrophages into M1-like macrophages, consequently activating anti-HCC immunity. In addition to conventional immune cells, liver sinusoidal endothelial cells (LSECs) can also play a significant role in immunosuppressive regulation[92]. Yu *et al*[93] designed a simvastatin-loaded NDDS to target LSECs in HCC patients. This NDDS can reduce the capillarization of LSECs to improve the stromal microenvironment and recruit natural killer T cells to inhibit tumor progression.

Cationic lipid nanoparticles have been suggested to be suitable delivery vectors for RNA, and several messenger RNA vaccines are based on lipid nanotechnology that was approved by the FDA during the severe acute respiratory syndrome coronavirus 2 (SARS-CoV-2) pandemic[94-97]. Zhang *et al*[98] developed a total HCC-derived RNA-loaded lipid nanoparticle vaccine to target DCs and activate anticancer immunity (Figure 1 and Table 2).

## IMMUNOTHERAPY-BASED NOVEL NANOPARTICLES IN CRC

CRC is the third leading cause of cancer-related deaths globally[99]. CRC is the only cancer that can be reduced by screening. Most CRC patients can be screened by flexible sigmoidoscopy or guaiac-based fecal occult blood tests[100]. However, approximately 25% of CRC patients are at stage 4, and the 5-year survival rate is only 11%[101,102]. To improve the survival rate of advanced CRC patients, immunotherapy and nanoparticle-based drug delivery systems have become the focus of basic and clinical research for the past few years[103-105].

Similar to GC and HCC, ICB treatment is more widely used in CRC patients, but its curative effect is extremely limited, especially for mismatch repair-proficient/microsatellite stability/microsatellite instability-low CRC patients[106]. As we reported earlier, ICB treatment combined with ICD can achieve a "1 + 1 > 2" effect. A similar treatment strategy has also been applied in CRC research. For example, Yuan *et al*[107] utilized the ability of PDT to induce ICD and developed a photosensitive NDDS combined with ICB treatment that can enhance the response rate of anti-PD-L1 therapy in CRC. Zhu *et al*[108] also designed an oxaliplatin prodrug-conjugated photosensitive NDDS that can be stimulated by the NIR-II window (1000-1700 nm) for PTT, which is a proven to induce ICD. Moreover, oxaliplatin, a chemotherapy drug, is also known as an ICD inducer. This novel NDDS can induce ICD through both PTT and chemotherapy, which may provide a promising immunotherapy strategy for advanced CRC treatment. Shikonin (SK), a major active ingredient isolated from traditional Chinese medicine, has also been proven to induce ICD. Li *et al*[109] designed a versatile nanoparticle that can deliver knockdown siRNA for both the ICD inducer SK and PD-L1, which presents potential for CRC immunotherapy. Recently, ferroptosis was discovered as a nonapoptotic form of regulated cell death [110]. In addition, Duan *et al*[111]'s group proved that dihydroartemisinin (DHA), as a reactive oxygen species (ROS)-producing drug and ferroptosis inducer, can also induce ICD to potentiate anticancer immunity. Therefore, the same research group developed a Zn-pyrophosphate core-shell NDDS codeliver DHA and pyropheophorbide-iron (pyro-Fe). Glutathione and other thiol-based reductants in cancer cells can reduce Pyro-Fe<sup>III</sup> to Pyro-Fe<sup>I</sup>, which can catalyze the decomposition of DHA to induce ICD and ferroptosis. This novel NDDS overcame the deficiency of iron in solid tumors, enhanced the ability of DHA to induce ferroptosis and ICD, and increased the infiltration of CD8<sup>+</sup> T cells in CRC.

In addition to actively increasing the immunogenicity of CRC, stimulating immune cells can also activate anti-CRC immunity. Immune cells can be activated by stimulating toll-like receptors (TLRs), such as DCs and macrophages. Several TLR agonists have been approved by the FDA. However, none are currently approved for CRC treatment. The major problem for TLR agonists is the small size of the drugs, which allows the drugs to spread rapidly from the administration site and cause severe systemic side effects (Figure 2)[112]. Fortunately, nanoparticle-based delivery systems can solve this problem. Bahmani *et al*[113] prepared a platelet membrane-coated nanoparticle loaded with the TLR7 agonist R848. This biomimetic NDDS enhanced the retention of the drug in the tumor and effectively stimulated the maturation of DCs, resulting in complete tumor eradication in a murine model of CRC.

Notably, long noncoding RNAs (lncRNAs) have recently been reported to be involved in the formation of the immunosuppressive cancer microenvironment and have become a potential immunotherapy target[114-116]. Liu *et al*[117] designed a bioscaffold loaded with a lncRNA-targeting biomimetic NDDS that modulated the cancer immune microenvironment against CRC recurrence after surgery. The biomimetic NDDS coated with a CRC membrane, which provides NDDS with a tumor-homing capacity and carries TSAs into the tumor area, promotes the maturation of DCs. Moreover, a plasmid-encoding short hairpin RNA against Pvt1 was encapsulated inside the NDDS to enhance ICD and ameliorate granulocytic-myeloid-derived suppressor cell (G-MDSC)-mediated immunosuppression. This work provides a new perspective for NDDS-based lncRNA-targeted immunotherapy.

**Table 2 Overview of Immunotherapy-based novel nanoparticles in the treatment of hepatocellular carcinoma [PubMed Search (immunotherapy) AND (nanoparticle) AND (hepatocellular carcinoma)]**

Type of nanoparticle	Treatment strategy	Drugs or active substance involved	The main involvement of immune cells	Ref.
Nano-micelles	ICD, chemotherapy, PDT	PTX, TPABDIO	CTLs, MDSCs, Tregs, DCs	Xu <i>et al</i> [75]
Polymers	p53 gene reprograms the immune microenvironment	p53 mRNA	T cells, NK cells	Xiao <i>et al</i> [83]
MSNPs	Anti-angiogenic drugs, ICI	Sorafenib, PD-L1 antibody	T cells	Li <i>et al</i> [84]
Copolymers	ICD, chemotherapy	Icaritin, DOX	T cells, DCs	Yu <i>et al</i> [85]
Lipid nanoparticle	CCL2 and CCL5 dual-target	BisCCL2/5i mRNA	TAMs	Wang <i>et al</i> [87]
Microcapsules	Improving hypoxia	Oxygen	TAMs	Dai <i>et al</i> [91]
Copolymers	Mitigates LSEC capillarization	Simvastatin	NKT cells	Yu <i>et al</i> [93]
LNPs	Antigen specific vaccine	Tumor-derived RNA	T cells, DCs	Zhang <i>et al</i> [98]

ICD: Immunogenic cell death; PDT: Photodynamic therapy; CTLs: Cytotoxic T lymphocytes; PTX: Paclitaxel; MDSCs: Myeloid-derived suppressor cells; DCs: Dendritic cells; CCL2: Chemokine C-C motif ligand 2; CCL5: Chemokine C-C motif ligand 5; DOX: Doxorubicin; PD-L1: Programmed cell death ligand 1; NK cells: Natural killer cells; TAMs: Tumor-associated macrophages; Tregs: Regulatory T lymphocytes; MSNPs: Mesoporous silica nanoparticles; LSEC: Liver sinusoidal endothelial cells; LNPs: Lipid nanoparticles; NKT: Natural killer T.

In recent years, as an important component of the immunosuppressive cancer microenvironment, MDSCs have also been identified as potential targets for cancer immunotherapy. Additionally, recent studies reported that MDSCs could be selectively enlarged because of the enrichment of *Fusobacterium nucleatum* (Fn) in CRC tissue, resulting in a cancer immunosuppressive microenvironment[118-121]. Dong *et al*[122] proposed a phage-based antibacterial system that used the broad-spectrum antibacterial effect of silver nanoparticles (AgNPs) for antibacterial activity and then transported phage M13 into the tumor and utilized the recognition mechanism of phages to selectively kill Fn, thus preventing the recruitment of MDSCs. In addition, phages are highly immunogenic and can directly stimulate the maturation of DCs and promote the activation of M1-like macrophages, significantly enhancing the anti-CRC immune response.

Over the years, CRC vaccines have been a focus of scientific research. Zhang *et al*[123] designed an *in situ* cancer vaccine. They reported a supramolecular assembled programmable immune activation nanomedicine (PIAN) that can produce strong and durable anticancer immunity *in situ*. PIAN entered the tumor area through enhanced permeability and retention (EPR) after tail vein injection and was then disassembled by the high ROS within the tumor tissue. The release of poly-[(N-2-hydroxyethyl)-aspartamide]-Pt(IV)/beta-cyclodextrin simultaneously mediated tumor cell death and antigen release. In addition, CpG/polyamidoamine (CpG/PAMAM) captured the released antigen and entered the tumor draining lymph node to stimulate DC maturation, thus activating anti-CRC-specific immunity. This excellent work provides a new idea for designing nanomedicine-based programmable *in situ* cancer vaccines for cancer immunotherapy (Table 3).

## IMMUNOTHERAPY-BASED NOVEL NANOPARTICLES IN PANCREATIC CANCER

As one of the most aggressive and fatal cancers, pancreatic cancer has been the leading cause of cancer-related deaths worldwide in the last few decades[124,125]. Most patients experience no obvious symptoms during the development of the disease. Therefore, it is difficult to diagnose the disease in the early stage, and patients often miss the optimal treatment time after they have been diagnosed with pancreatic cancer. Moreover, the majority of patients eventually relapse, even if they receive potentially radical treatment[126]. In contrast to other malignant tumors, stromal hyperplasia is the main feature of the pancreatic cancer microenvironment[127]. As a result, pancreatic cancer does not have a sufficient blood supply, so antiangiogenic drugs are not suitable for pancreatic cancer[128]. In addition, the tumor stroma of pancreatic cancer acts as a natural physical barrier between the tumor tissue and the body's immune system, which also limits the application of immunotherapy[129,130]. Until now, most phase I and II clinical trials of immunotherapy in pancreatic cancer have failed. Interestingly, ICB treatment combined with chemotherapy and/or radiotherapy has shown encouraging clinical efficacy[131]. In recent years, with the continuous development of nanotechnology, scientists have proposed a variety of nanodelivery systems aimed at the unique pathological characteristics of pancreatic cancer. They attempted to utilize NDDSs to achieve synergistic therapy and improve the tumor microenvironment to reverse the current situation of pancreatic cancer[132].

**Table 3 Overview of Immunotherapy-based novel nanoparticles in the treatment of colorectal cancer [PubMed Search (immunotherapy) AND (nanoparticle) AND (colorectal cancer)]**

Type of nanoparticle	Treatment strategy	Drugs or active substance involved	The main involvement of immune cells	Ref.
Copolymers	PDT induces HIF-1 $\alpha$ expression, leading to the upregulation of PD-L1 expression, ICIs	Photosensitizer, PD-L1 antibody	DCs, CD8 <sup>+</sup> T cells, memory T cells	Yuan <i>et al</i> [107]
Polymeric nanoparticle	PTT, chemotherapy, ICD	PBOXA, donor-spacer-acceptor-spacer-donor type fluorophore	DCs, T cells, CTLs	Zhu <i>et al</i> [108]
Copolymers	ICD, ICIs	SK, PD-L1 knockdown siRNA	DCs, TAMs, Tregs, T cells	Li <i>et al</i> [109]
Polymers	ICD, ferroptosis	DHA	DCs, T cells	Duan <i>et al</i> [111]
Platelet membrane-coated nanoparticle	TLR7 treatment	R848	DCs	Bahmani <i>et al</i> [113]
Liposomes with cell membrane	ICD, chemotherapy, lncRNA-targeting therapy	Oxaliplatin, shPvt1	DCs, MDSCs, CD8 <sup>+</sup> T cells	Liu <i>et al</i> [117]
Silver nanoparticles	Anti-Fn	Phage M13	MDSCs, DCs, TAMs	Dong <i>et al</i> [122]
Supramolecular assembled programmable immune activation nanomedicine	<i>In-situ</i> cancer vaccine, ICD	PPCD, CpG/PAMAM	DCs, CD8 <sup>+</sup> T cells	Zhang <i>et al</i> [123]

ICIs: Immune checkpoint inhibitors; HIF-1 $\alpha$ : Hypoxia-inducible factor 1 $\alpha$ ; PDT: Photodynamic therapy; PTT: Photothermal therapy; ICD: Immunogenic cell death; PD-L1: Programmed cell death ligand 1; PBOXA: Oxaliplatin prodrug; SK: Shikonin, DHA: Dihydroartemisinin; TLR: Toll-like receptor; shPvt1: Short hair-pinned RNA against Pvt1; Fn: *Fusobacterium nucleatum*; PPCD: Poly-[(N-2-hydroxyethyl)-aspartamide]-Pt(IV)/beta-cyclodextrin; PAMAM: Polyamidoamine; MDSCs: Myeloid-derived suppressor cells; DCs: Dendritic cells; CTLs: Cytotoxic T lymphocytes; TAMs: Tumor-associated macrophages; Tregs: Regulatory T lymphocytes; MDSCs: Myeloid-derived suppressor cells.

As we mentioned above, the tumor stroma of pancreatic cancer limits the efficacy of immunotherapy. Wang *et al*[133] reported a pH-responsive clustered nanoparticle (iCluster) loaded with both siPD-L1 and transforming growth factor- $\beta$  (TGF- $\beta$ ) receptor inhibitors (LY2157299). iCluster can deliver siPD-L1 and LY2157299 to tumor blood vessels and then release small PAMAM at acidic tumor extracellular pH (pH<sub>e</sub>). Therefore, siPD-L1 can penetrate into tumor tissue as deeply as possible to activate anticancer immunity, and a TGF- $\beta$  receptor inhibitor can reduce the barrier function of the tumor stroma to help more drugs penetrate into the tumor tissue, further promoting the activation of anticancer immunity. Similarly, Yu *et al*[134] designed a size-adjustable nanoparticle consisting of IR780 containing the thermosensitive ICB drug (BMS-202) conjugated to HSA-BMS. Under mild hyperthermia therapy, this novel nanoparticle releases the small HSA-BMS into the tumor site and relieves the immunosuppressive environment to normalize immunity. In recent years, some studies have reported that RNA interference (RNAi) has emerged as a better agent for inducing anticancer immunity than antibodies or small molecules *in vivo*[135]. PLGA polymers have been proven to be a potentially excellent siRNA delivery vector exhibiting low toxicity, sustained release and the EPR effect[136,137]. Jung *et al*[138] developed a poly(lactic-co-glycolic) acid (PLGA)-based siRNA nanoparticle named siPD-L1@PLGA. siPD-L1@PLGA increased the infiltration of CD8<sup>+</sup>T cells and significantly inhibited tumor growth.

The poor immunogenicity and excessive immunosuppressive cancer microenvironment of pancreatic cancer result in a lack of adequate antigen-presenting cells in the tumor microenvironment. Lorkowski *et al*[139] reported a dual-immunostimulatory nanoparticle that was simultaneously loaded with a STING agonist and TLR4 agonist. These dual-immunostimulatory nanoparticles can be taken up by DCs in the tumor site to significantly increase the number of mature DCs and activate anticancer immunity in pancreatic cancer. Theoretically, cancer immunosuppressive cells mainly include TAMs, MDSCs and regulatory T cells (Tregs). Recent studies have shown that MDSCs are the major inhibitory immune cells in the immunosuppressive microenvironment of pancreatic cancer[140]. A previous study found that low-molecular-weight heparin-D- $\alpha$ -tocopheryl (LMWH) could significantly inhibit G-MDSC recruitment[141]. Therefore, Lu *et al*[142] designed a paclitaxel-loaded 3-aminophenylboronic acid-modified LMWH-based nanoparticle. This novel LMWH-based nanoparticle can inhibit the recruitment of MDSCs and weaken the immunosuppressive state.

Pyroptosis is a mode of programmed cell death[143]. Recent studies have shown that pyroptosis can induce powerful anticancer immunity[144-146]. However, pyroptosis is usually induced by chemotherapeutic drugs, which limits the applications of pyroptosis in drug-resistant tumors[147]. Ding *et al* [148] designed biodegradable K3ZrF7:Yb/Er UCNPs (ZrNPs) as self-therapeutic agents and pyroptosis

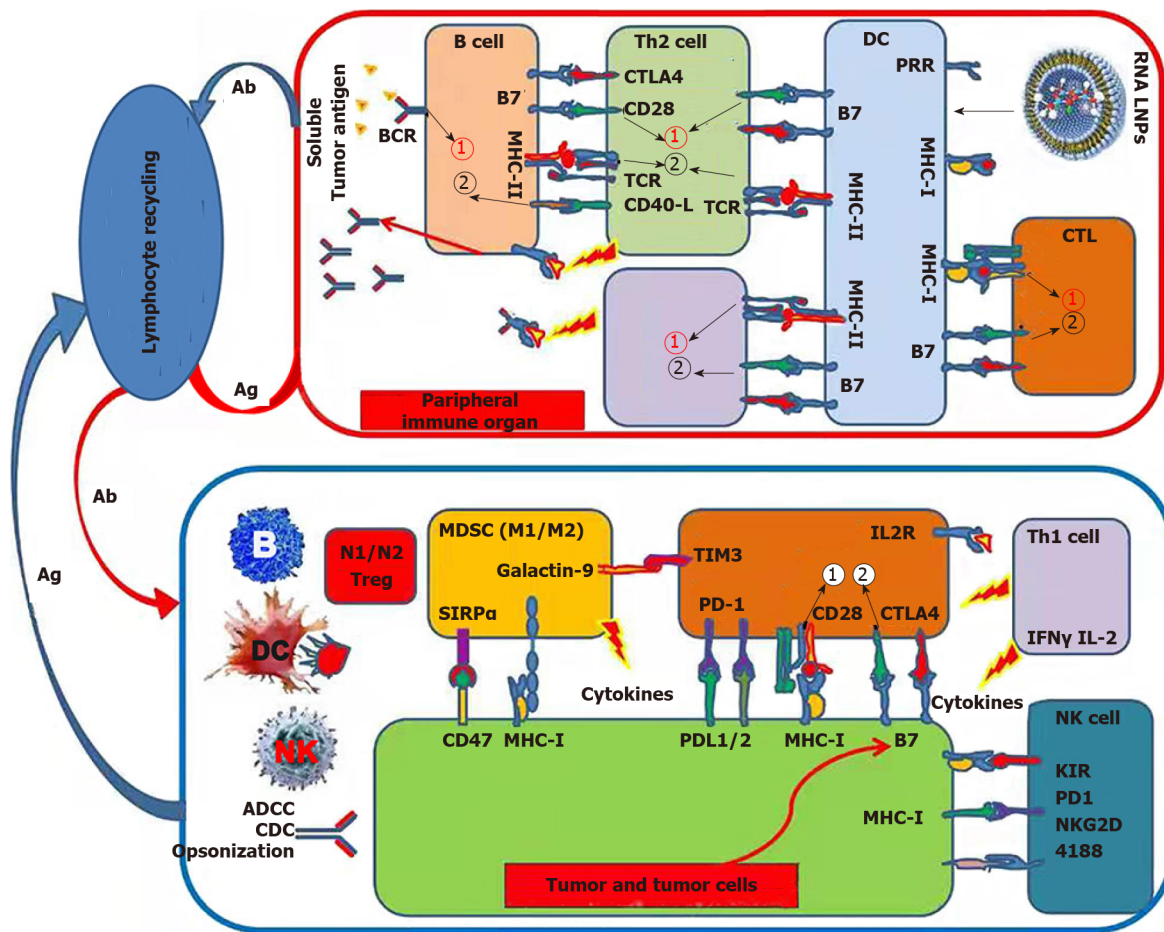


**Figure 1 Tumor vaccine and tumor immunotherapy.** Total tumor RNA was extracted and mixed with an immune adjuvant to formulate tumor vaccine. Tumor antigen was expressed and presented or cross-presented to Th and Tc cells by antigen presenting cells in lymph node to generate specific anti-tumor response. Citation: Zhang Y, Xie F, Yin Y, Zhang Q, Jin H, Wu Y, Pang L, Li J, Gao J. Immunotherapy of Tumor RNA-Loaded Lipid Nanoparticles Against Hepatocellular Carcinoma. *Int J Nanomedicine* 2021; 16: 1553-1564. Copyright ©The Authors 2011. Published by Dove Medical Press. The authors have obtained the permission for figure using from the Dove Medical Press Publishing Group (Supplementary material). Ab: Antibody; Ag: Antigen; BCR: B cell receptor; TCR: T-cell receptor; MHC: Major histocompatibility complex; PRR: Pattern recognition receptors; Th1/2: T helper type 1/2; CTL: Cytotoxic T-lymphocyte; CTLA4: Cytotoxic T-lymphocyte-associated protein 4; Treg: Regulatory T cell; DC: Dendritic cell; NK: Natural killer cell; MDSC: Mmyeloid-derived suppressor cell; ADCC: Antibody-dependent cellular cytotoxicity; CDC: Complement-dependent cytotoxicity; SIRPα: Signal regulatory protein α; LILRB1: Leukocyte immunoglobulin like receptor B1; TIM-3: T-cell immunoglobulin and mucin domain-3; PD1: Programmed cell death protein 1; PD-L1: Programmed death-ligand 1; IL-2: Interleukin-2; IFNγ: Interferon γ; KIR: Killer cell immunoglobulin-like receptor; NKG2D: Natural killer group 2 member D.

inducers for the first time. ZrNP can lead to osmotic pressure disorder and further result in an increase in ROS, the activation of caspase-1 protein, the cleavage of gasdermin, the maturation of interleukin-1β, and ultimately cytolysis. ZrNP-induced pyroptosis can lead to DC maturation and activate effector memory T cells, as well as inhibit tumor growth and metastasis.

Gemcitabine is among the most effective FDA-approved chemotherapy drugs to prolong survival in patients with pancreatic cancer. However, the immunosuppressive cancer microenvironment, especially the presence of TAMs, significantly weakens the efficacy of gemcitabine. It has even been reported that gemcitabine can induce an increase in TAMs and promote the establishment of a tumor-suppressive immune microenvironment, which further increases gemcitabine drug resistance[149]. Furthermore, gemcitabine can even induce an increase in TAMs and promote the establishment of an immunosuppressive tumor microenvironment, which further leads to gemcitabine drug resistance[150]. Thus, Wang *et al*[151] developed a biomimetic nanoparticle named PG<sup>®</sup>KMCM consisting of gemcitabine-loaded PLGA nanoparticles coated with stable M2-like macrophage targeting peptides (M2pep). Pancreatic cancer cell membranes can deliver PG<sup>®</sup>KMCM to pancreatic cancer and target M2-like macrophages by M2pep to reprogram TAMs and reverse gemcitabine drug resistance. Cao *et al*[152] also considered TAMs to be a therapeutic target and reported a reduction-responsive RNAi NDDS to regulate the function of TAMs and reprogram tumor lipid metabolism. On the one hand, this novel NDDS can block the activity of monoacylglycerol lipase (MGLL) by MGLL siRNA to reduce the production of free fatty acids and thus cut off the tumor's nutrition supply. On the other hand, MGLL blockade may lead to the accumulation of 2-arachidonoylglycerol, which can be secreted into the cancer microenvironment and activate the endocannabinoid receptor-2 (CB-2), which can transform TAMs into M2-like macrophages.

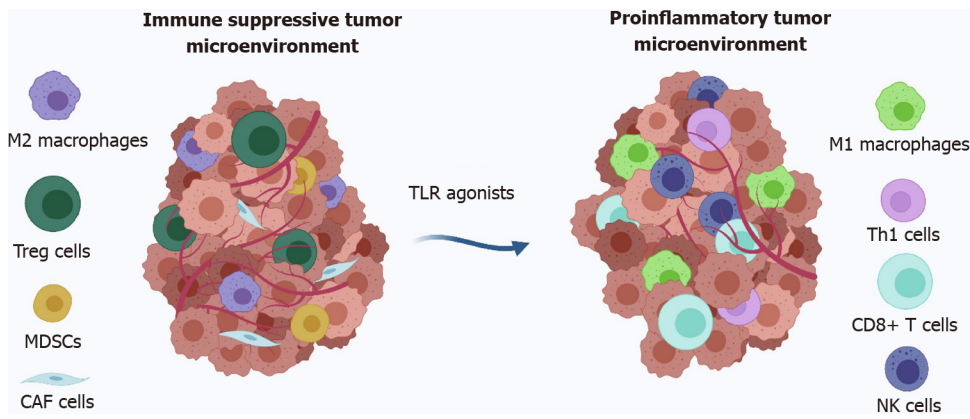


**Figure 2** Altering an immunosuppressive tumor microenvironment into a pro-inflammatory microenvironment with the use of toll-like receptor agonists. Citation: Haegebaert RMS, Kempers M, Ceelen W, Lentacker I, Remaut K. Nanoparticle mediated targeting of toll-like receptors to treat colorectal cancer. *Eur J Pharm Biopharm* 2022; 172: 16-30. Copyright ©The Authors 2022. Published by Elsevier. The authors have obtained the permission for figure using from the Elsevier Publishing Group (Supplementary material). Treg: T regulatory cell; MDSCs: Myeloid-derived suppressor cells; CAF: Cancer-associated fibroblast; Th1: T-helper 1; CD8<sup>+</sup> T cells: Cytotoxic T cells; NK: Natural killer; TLR: Toll-like receptor.

Therefore, they prepared CB-2 siRNA to block CB-2 expression, preventing the transition of M2-like macrophages. The dual-RNAi NDDS developed in this research shows significant enhancement of the immunological environment in pancreatic cancer.

PTT has achieved satisfactory results in animal experiments, but it is difficult to apply widely in the clinic. The main reason is poor light penetration. It is harder to achieve the desired therapeutic effect for pancreatic cancer due to the depth of pancreatic cancer and the presence of the tumor stroma. To solve this conundrum, Wang *et al*[153] proposed magnetic resonance imaging (MRI)-guided interventional PTT (IPTT). They designed an iron oxide-based nanoparticle loaded with indocyanine green for PTT and imiquimod (IMQ) as an immunostimulant. IPTT can induce *in situ* cancer vaccination, which can be amplified by IMQ. In addition, iron oxide is a widely used MRI contrast agent. A recent study reported that iron oxide can modulate the cancer microenvironment by transforming M2-like macrophages into M1-like macrophages[154]. Overall, these novel iron oxide-based nanoparticles can improve therapeutic effects by directly killing cancer cells and activating the long-lasting immune effect by *in situ* vaccination and regulation of the immune microenvironment (Table 4).

## FUTURE DIRECTIONS

In recent years, the increased development of immunotherapy has provided hope to patients with advanced cancer. Several ICB drugs have been approved by the FDA for clinical application in cancer treatment. However, due to the immunosuppressive microenvironment, only approximately 20% of patients can benefit from ICB treatment. In addition to ICB treatment, some conventional therapies, such as chemotherapy and radiotherapy, are also closely related to the immunosuppressive tumor microenvironment. The facts we mentioned above also exist in GIC. Therefore, we believe that in addition to ICB treatment, we should focus on reversing the immunosuppressive microenvironment in the future. Moreover, advances in nanotechnology have made drug delivery more efficient, allowing us to deliver drugs at specific times and locations based on the characteristics of the cancer and the drugs. We wondered whether the combination of nanotechnology and immunotherapy could achieve satisfactory therapeutic efficacy in GIC. Here, we summarize recent advances in immunotherapy-based novel nanoparticles in the treatment of GIC.

Since GC, HCC and CRC share similar tumor immune microenvironments, we will discuss the application of immunotherapy-based nanoparticles in these three kinds of GICs in the following paragraphs. Due to the limited monotherapy effect of ICB treatment, nanoparticles, as drug delivery vehicles, cannot significantly improve the therapeutic effect of ICB treatment. Thus, basically all ICB-based nanoparticles are combined with other therapeutic strategies. ICB treatment can reverse tumor immune escape from T cells. However, the low immunogenicity of the tumor results in insufficient T-cell infiltration in the tumor tissue. Hence, most studies have attempted to promote the therapeutic effect of ICB-based nanoparticles by inducing ICD.

ICD can increase tumor immunogenicity, but similar to ICB treatment, the immune-stimulating effect of ICD is limited. To amplify the ICD effect, some studies utilized the drug-loading capacity of nanoparticles and adopted a combination of multiple ICD inducers to enhance the immune response. Even so, we still do not recommend the combination of multiple ICD inducers to promote anticancer immunity. On the one hand, this strategy does not solve the problem of insufficient T-cell infiltration; on

**Table 4 Overview of Immunotherapy-based novel nanoparticles in the treatment of pancreatic cancer [PubMed Search (immunotherapy) AND (nanoparticle) AND (pancreatic cancer)]**

Type of nanoparticle	Treatment strategy	Drugs or active substance involved	The main involvement of immune cells	Ref.
Clustered nanoparticle	ICIs, TGF- $\beta$ receptor inhibitors	LY2157299, siPD-L1	T cells	Wang <i>et al</i> [133]
HAS-Liposomes	ICD, ICIs, PTT	BMS-202, IR780	DCs, CTLs, T cells	Yu <i>et al</i> [134]
Copolymers	ICIs	siPD-L1	CD8 <sup>+</sup> T cells, NK cells	Jung <i>et al</i> [138]
LNPs	STING and TLR4 therapy	STING agonist, R4 agonist	DCs, Tregs, TAMs	Lorkowski <i>et al</i> [139]
Micellar nanoparticle	Inhibit G-MDSCs recruitment, chemotherapy	LMWH, PTX	G-MDSC, CD8 <sup>+</sup> T cells, CD4 <sup>+</sup> T cells	Lu <i>et al</i> [142]
UCNPs	Pyroptosis	K3ZrF7:Yb/Er UCNPs	DCs, memory T cells	Ding <i>et al</i> [148]
Cancer cell membrane with copolymers	ICIs, M2-macrophages targeting	M2pep, TAAs, PD-L1 antibody	TAMs, CD8 <sup>+</sup> T cells	Wang <i>et al</i> [151]
PDSA-based nanoplatform	Suppression of FFAs, repolarization of TAMs	siMGLL, siCB-2	TAMs	Cao <i>et al</i> [152]
Copolymers	PTT, immunotherapy	ICG, IMQ, IONs	TAMs, CD8 <sup>+</sup> T cells, CD4 <sup>+</sup> T cells, CD4 <sup>+</sup> T cells	Wang <i>et al</i> [153]
IONs	Repolarization of TAMs	Ferumoxytol	TAMs	Zanganeh <i>et al</i> [154]

ICIs: Immune checkpoint inhibitors; PD-L1: Programmed cell death ligand 1; TGF- $\beta$ : Transforming growth factor- $\beta$ ; ICD: Immunogenic cell death; DCs: Dendritic cells; STING: Stimulator of interferon genes; LMWH: Low molecular weight heparin; MDSCs: Myeloid-derived suppressor cells; G-MDSCs: Granulocytic myeloid-derived suppressor cells; UCNPs: Upconversion nanoparticles; M2pep: Peptides targeting M2-like macrophages; TAAs: Tumor-associated antigens; PDSA: Poly (disulfide amide); FFAs: Free fatty acids; siMGLL: MGLL siRNA; siCB-2: CB-2 siRNA; ICG Indocyanine green; IMQ: Imiquimod; IONs: Iron oxide nanoparticles; PTX: Paclitaxel; PTT: Photothermal therapy; TAMs: Tumor-associated macrophages; Tregs: Regulatory T lymphocytes; TLR: Toll-like receptor.

the other hand, ICD inducers themselves can directly kill tumor cells. It is difficult to determine whether tumor inhibition is due to cytotoxicity or ICD-induced anticancer immunity.

Compared with ICD and ICB treatment, we believe that reprogramming the immunosuppressive tumor microenvironment by targeting inhibitory immune cells (*e.g.*, TAMs, Tregs and MDSCs) will be a revolutionary breakthrough in cancer immunotherapy in the future. Recently, many studies have attempted to successfully reprogram the tumor immune microenvironment by polarizing M2-like macrophages into M1-like macrophages. However, few reports have designed NDDSs to target Tregs and MDSCs in the tumor microenvironment. Therefore, it is of great significance to develop NDDSs for Tregs and MDSCs. In addition, the relationship between the intestinal flora and the immunosuppressive microenvironment of CRC also deserves future attention.

TLR agonists have also emerged as a promising treatment for cancer immunotherapy. However, due to the lack of targeting of TLR agonists, free TLR agonists often lead to serious systemic side effects. Therefore, it is necessary to deliver TLR agonists by nanoparticles. Numerous TLR agonists have been proven to be effective in stimulating anticancer immunity. In addition, combination therapies of TLR agonists with other immunotherapies are also anticipated. However, how to deliver TLR agonists to the tumor site stably and accurately and reduce serious systemic side effects are still problems that need prompt solutions.

With the successful large-scale clinical application of SARS-CoV-2 mRNA vaccines, research on cancer vaccines is also imminent. Due to the high heterogeneity of cancer, RNA vaccines are the best option. However, RNA is highly unstable. Liposomes, as mature NDDSs, can prepare cancer vaccines by encapsulating RNA. In addition, to improve the vaccine effect, NDDSs can be encapsulated with immune adjuvants to promote immune activation. RNA-based cancer vaccines, as a personalized cancer treatment strategy, can effectively improve anticancer immunity.

Next, we will discuss the application of immunotherapy-based nanoparticles in pancreatic cancer. Pancreatic cancer has several characteristics that are not found in other kinds of GICs, including the following: (1) Pancreatic cancer is surrounded by a tumor stroma, resulting in a physical barrier that isolates pancreatic cancer from the surrounding immune microenvironment; (2) Due to the anatomic position of the pancreas, pancreatic cancer is located deep in the abdominal cavity and therefore is not sensitive to PDT and PTT; and (3) Unlike other GICs, pancreatic cancer lacks blood supply and can adapt to nutrient deficiency and in a long-term hypoxic state.

To pass through the physical barrier of pancreatic cancer, size-adjusted NDDSs are the best option. Due to the deep location of pancreatic cancer, PTT has limited efficacy. Inspired by a previous study, we believe that IPTT and interventional PDT can be widely applied in the treatment of pancreatic cancer.

Additionally, interventional light-mediated therapy can be extended to GC, esophageal cancer and CRC, as well as HCC.

Compared with GC, HCC and CRC, pancreatic cancer has a similar immunosuppressive microenvironment, and the immunosuppressive situation is even worse. Most of the treatment strategies mentioned in GC, HCC and CRC can also be applied in pancreatic cancer. In previous reports, immunotherapy-based nanoparticles mainly used liposomes and copolymer nanoparticles, which are chemical synthesis products. Therefore, the nanoparticles can be designed according to demand. To increase biocompatibility and deliver tumor antigens, some literature has used tumor cell membranes to prepare biomimetic NDDSs, which have also achieved good results. In addition to the abovementioned nanoparticles, we particularly recommend small extracellular vesicles (also known as exosomes) as immunotherapy-based nanoparticles. First, exosomes are naturally nanosized. Second, similar to cell membrane vesicles, exosomes derived from tumor cells can carry tumor antigens. Third, exosomes can use surface modification to achieve biological functions, such as targeting. Last, exosomes have a certain drug delivery capacity. Thus, exosomes are potential immunotherapy-based nanoparticles for GIC that have not been reported in previous studies.

---

## CONCLUSION

GIC is a common tumor worldwide. The immune microenvironments of GC, HCC, CRC and pancreatic cancer have similarities and differences. There are still many mechanisms of immune escape in GIC that are not well understood. Therefore, we need an in-depth understanding of the characteristics of each kind of GIC to take advantage of its characteristics and design immunotherapy-based nanoparticles.

---

## FOOTNOTES

**Author contributions:** Ding YN and Ding HY wrote the paper; Ding YN, Li H, Gao CC and Wang LJ carried out reference searching; Yu WP and Tang QS made review and final editing; and all authors have read and agree to the published version of the manuscript.

**Supported by** the National Natural Science Foundation of China, No. 82102303; and Natural Science Foundation of Jiangsu Province, China, No. BK20210231.

**Conflict-of-interest statement:** All the authors report no relevant conflicts of interest for this article.

**Open-Access:** This article is an open-access article that was selected by an in-house editor and fully peer-reviewed by external reviewers. It is distributed in accordance with the Creative Commons Attribution NonCommercial (CC BY-NC 4.0) license, which permits others to distribute, remix, adapt, build upon this work non-commercially, and license their derivative works on different terms, provided the original work is properly cited and the use is non-commercial. See: <https://creativecommons.org/licenses/by-nc/4.0/>

**Country/Territory of origin:** China

**ORCID number:** Yi-Nan Ding 0000-0002-1010-2874; Ming Xue 0000-0002-5178-6424; Qiu-Sha Tang 0000-0001-5701-0996; Li-Jun Wang 0000-0002-0208-0273; Hui-Yan Ding 0000-0002-5850-8080; Han Li 0000-0003-4174-8480; Cheng-Cheng Gao 0000-0002-9482-9535; Wei-Ping Yu 0000-0003-3968-3104.

**S-Editor:** Wang JJ

**L-Editor:** A

**P-Editor:** Wang JJ

---

## REFERENCES

- Huang F, Wang BR, Wu YQ, Wang FC, Zhang J, Wang YG. Oncolytic viruses against cancer stem cells: A promising approach for gastrointestinal cancer. *World J Gastroenterol* 2016; **22**: 7999-8009 [PMID: 27672294 DOI: 10.3748/wjg.v22.i35.7999]
- Siegel RL, Miller KD, Fuchs HE, Jemal A. Cancer statistics, 2022. *CA Cancer J Clin* 2022; **72**: 7-33 [PMID: 35020204 DOI: 10.3322/caac.21708]
- Ferlay J, Colombet M, Soerjomataram I, Parkin DM, Piñeros M, Znaor A, Bray F. Cancer statistics for the year 2020: An overview. *Int J Cancer* 2021 [PMID: 33818764 DOI: 10.1002/ijc.33588]
- Xia C, Dong X, Li H, Cao M, Sun D, He S, Yang F, Yan X, Zhang S, Li N, Chen W. Cancer statistics in China and United States, 2022: profiles, trends, and determinants. *Chin Med J (Engl)* 2022; **135**: 584-590 [PMID: 35143424 DOI: 10.1097/CM9.0000000000002108]

- 5 **Neumann PA**, Berlet MW, Friess H. Surgical oncology in the age of multimodality therapy for cancer of the upper and lower gastrointestinal tract. *Expert Rev Anticancer Ther* 2021; **21**: 511-522 [PMID: 33355020 DOI: 10.1080/14737140.2021.1868991]
- 6 **Hamed OH**, Gusani NJ, Kimchi ET, Kavic SM. Minimally invasive surgery in gastrointestinal cancer: benefits, challenges, and solutions for underutilization. *JSLs* 2014; **18** [PMID: 25489209 DOI: 10.4293/JSLs.2014.00134]
- 7 **Pofahl WE**, Pories WJ. Current status and future directions of geriatric general surgery. *J Am Geriatr Soc* 2003; **51**: S351-S354 [PMID: 12823667 DOI: 10.1046/j.1365-2389.2003.51347.x]
- 8 **Ciabatti S**, Cammelli S, Frakulli R, Arcelli A, Macchia G, Deodato F, Cilla S, Giaccherini L, Buwenge M, Morganti AG. Radiotherapy of pancreatic cancer in older patients: A systematic review. *J Geriatr Oncol* 2019; **10**: 534-539 [PMID: 30270196 DOI: 10.1016/j.jgo.2018.09.007]
- 9 **Grabebauer GG**, Holger G. Management of radiation and chemotherapy related acute toxicity in gastrointestinal cancer. *Best Pract Res Clin Gastroenterol* 2016; **30**: 655-664 [PMID: 27644912 DOI: 10.1016/j.bpg.2016.06.001]
- 10 **Sipaviciute A**, Sileika E, Burneckis A, Dulskas A. Late gastrointestinal toxicity after radiotherapy for rectal cancer: a systematic review. *Int J Colorectal Dis* 2020; **35**: 977-983 [PMID: 32296933 DOI: 10.1007/s00384-020-03595-x]
- 11 **Marin JJ**, Romero MR, Blazquez AG, Herraiz E, Keck E, Briz O. Importance and limitations of chemotherapy among the available treatments for gastrointestinal tumours. *Anticancer Agents Med Chem* 2009; **9**: 162-184 [PMID: 19199863 DOI: 10.2174/187152009787313828]
- 12 **Kelly RJ**. Emerging Multimodality Approaches to Treat Localized Esophageal Cancer. *J Natl Compr Canc Netw* 2019; **17**: 1009-1014 [PMID: 31390584 DOI: 10.6004/jnccn.2019.7337]
- 13 **Metzger R**, Bollschweiler E, Hölscher AH, Warnecke-Eberz U. ERCC1: impact in multimodality treatment of upper gastrointestinal cancer. *Future Oncol* 2010; **6**: 1735-1749 [PMID: 21142660 DOI: 10.2217/fon.10.140]
- 14 **Tazawa H**, Kagawa S, Fujiwara T. MicroRNAs as potential target gene in cancer gene therapy of gastrointestinal tumors. *Expert Opin Biol Ther* 2011; **11**: 145-155 [PMID: 21219233 DOI: 10.1517/14712598.2011.542749]
- 15 **Rosenbaum MW**, Gonzalez RS. Targeted therapy for upper gastrointestinal tract cancer: current and future prospects. *Histopathology* 2021; **78**: 148-161 [PMID: 33382497 DOI: 10.1111/his.14244]
- 16 **Yano T**, Wang KK. Photodynamic Therapy for Gastrointestinal Cancer. *Photochem Photobiol* 2020; **96**: 517-523 [PMID: 31886891 DOI: 10.1111/php.13206]
- 17 **Hao M**, Kong C, Jiang C, Hou R, Zhao X, Li J, Wang Y, Gao Y, Zhang H, Yang B, Jiang J. Polydopamine-coated Au-Ag nanoparticle-guided photothermal colorectal cancer therapy through multiple cell death pathways. *Acta Biomater* 2019; **83**: 414-424 [PMID: 30366131 DOI: 10.1016/j.actbio.2018.10.032]
- 18 **Lee SY**, Shieh MJ. Platinum(II) Drug-Loaded Gold Nanoshells for Chemo-Photothermal Therapy in Colorectal Cancer. *ACS Appl Mater Interfaces* 2020; **12**: 4254-4264 [PMID: 31927943 DOI: 10.1021/acsami.9b18855]
- 19 **Ding Y**, Yang R, Yu W, Hu C, Zhang Z, Liu D, An Y, Wang X, He C, Liu P, Tang Q, Chen D. Chitosan oligosaccharide decorated liposomes combined with TH302 for photodynamic therapy in triple negative breast cancer. *J Nanobiotechnology* 2021; **19**: 147 [PMID: 34011362 DOI: 10.1186/s12951-021-00891-8]
- 20 **Zhang Y**, Xu J, Zhang N, Chen M, Wang H, Zhu D. Targeting the tumour immune microenvironment for cancer therapy in human gastrointestinal malignancies. *Cancer Lett* 2019; **458**: 123-135 [PMID: 31121212 DOI: 10.1016/j.canlet.2019.05.017]
- 21 **He M**, Yang T, Wang Y, Wang M, Chen X, Ding D, Zheng Y, Chen H. Immune Checkpoint Inhibitor-Based Strategies for Synergistic Cancer Therapy. *Adv Healthc Mater* 2021; **10**: e2002104 [PMID: 33709564 DOI: 10.1002/adhm.202002104]
- 22 **Sartor O**. Eligard: leuprolide acetate in a novel sustained-release delivery system. *Urology* 2003; **61**: 25-31 [PMID: 12667884 DOI: 10.1016/s0090-4295(02)02396-8]
- 23 FDA approves liposomal vincristine (Marqibo) for rare leukemia. *Oncology (Williston Park)* 2012; **26**: 841 [PMID: 23061340]
- 24 **Frampton JE**. Liposomal Irinotecan: A Review in Metastatic Pancreatic Adenocarcinoma. *Drugs* 2020; **80**: 1007-1018 [PMID: 32557396 DOI: 10.1007/s40265-020-01336-6]
- 25 **Safra T**, Muggia F, Jeffers S, Tsao-Wei DD, Groshen S, Lyass O, Henderson R, Berry G, Gabizon A. Pegylated liposomal doxorubicin (doxil): reduced clinical cardiotoxicity in patients reaching or exceeding cumulative doses of 500 mg/m<sup>2</sup>. *Ann Oncol* 2000; **11**: 1029-1033 [PMID: 11038041 DOI: 10.1023/a:1008365716693]
- 26 **Yardley DA**. nab-Paclitaxel mechanisms of action and delivery. *J Control Release* 2013; **170**: 365-372 [PMID: 23770008 DOI: 10.1016/j.jconrel.2013.05.041]
- 27 **Duvic M**, Talpur R. Optimizing denileukin diftitox (Ontak) therapy. *Future Oncol* 2008; **4**: 457-469 [PMID: 18684057 DOI: 10.2217/14796694.4.4.457]
- 28 **Rivera Gil P**, Hühn D, del Mercato LL, Sasse D, Parak WJ. Nanopharmacy: Inorganic nanoscale devices as vectors and active compounds. *Pharmacol Res* 2010; **62**: 115-125 [PMID: 20097288 DOI: 10.1016/j.phrs.2010.01.009]
- 29 **Ding Y**, Wang L, Li H, Miao F, Zhang Z, Hu C, Yu W, Tang Q, Shao G. Application of lipid nanovesicle drug delivery system in cancer immunotherapy. *J Nanobiotechnology* 2022; **20**: 214 [PMID: 35524277 DOI: 10.1186/s12951-022-01429-2]
- 30 DaunoXome approved. *AIDS Patient Care STDS* 1996; **10**: 263 [PMID: 11361607]
- 31 **Bost JP**, Barriga H, Holme MN, Gallud A, Maugeri M, Gupta D, Lehto T, Valadi H, Esbjörner EK, Stevens MM, El-Andaloussi S. Delivery of Oligonucleotide Therapeutics: Chemical Modifications, Lipid Nanoparticles, and Extracellular Vesicles. *ACS Nano* 2021; **15**: 13993-14021 [PMID: 34505766 DOI: 10.1021/acsnano.1c05099]
- 32 **Zou S**, Wang B, Wang C, Wang Q, Zhang L. Cell membrane-coated nanoparticles: research advances. *Nanomedicine (Lond)* 2020; **15**: 625-641 [PMID: 32098564 DOI: 10.2217/nnm-2019-0388]
- 33 **Huang R**, Cai GQ, Li J, Li XS, Liu HT, Shang XL, Zhou JD, Nie XM, Gui R. Platelet membrane-camouflaged silver metal-organic framework drug system against infections caused by methicillin-resistant *Staphylococcus aureus*. *J Nanobiotechnology* 2021; **19**: 229 [PMID: 34348721 DOI: 10.1186/s12951-021-00978-2]

- 34 **Jing B**, Qian R, Jiang D, Gai Y, Liu Z, Guo F, Ren S, Gao Y, Lan X, An R. Extracellular vesicles-based pre-targeting strategy enables multi-modal imaging of orthotopic colon cancer and image-guided surgery. *J Nanobiotechnology* 2021; **19**: 151 [PMID: 34022897 DOI: 10.1186/s12951-021-00888-3]
- 35 **Moulaoum H**, Ghorbanizamani F, Zihnioglu F, Timur S. Surface Biomodification of Liposomes and Polymersomes for Efficient Targeted Drug Delivery. *Bioconj Chem* 2021; **32**: 1491-1502 [PMID: 34283580 DOI: 10.1021/acs.bioconjchem.1c00285]
- 36 **He C**, Ding H, Chen J, Ding Y, Yang R, Hu C, An Y, Liu D, Liu P, Tang Q, Zhang Z. Immunogenic Cell Death Induced by Chemoradiotherapy of Novel pH-Sensitive Cargo-Loaded Polymersomes in Glioblastoma. *Int J Nanomedicine* 2021; **16**: 7123-7135 [PMID: 34712045 DOI: 10.2147/IJN.S333197]
- 37 **He C**, Zhang Z, Ding Y, Xue K, Wang X, Yang R, An Y, Liu D, Hu C, Tang Q. LRP1-mediated pH-sensitive polymersomes facilitate combination therapy of glioblastoma *in vitro* and *in vivo*. *J Nanobiotechnology* 2021; **19**: 29 [PMID: 33482822 DOI: 10.1186/s12951-020-00751-x]
- 38 **Han Y**, An Y, Jia G, Wang X, He C, Ding Y, Tang Q. Facile assembly of upconversion nanoparticle-based micelles for active targeted dual-mode imaging in pancreatic cancer. *J Nanobiotechnology* 2018; **16**: 7 [PMID: 29378593 DOI: 10.1186/s12951-018-0335-4]
- 39 **Xu W**, Qing X, Liu S, Chen Z, Zhang Y. Manganese oxide nanomaterials for bacterial infection detection and therapy. *J Mater Chem B* 2022; **10**: 1343-1358 [PMID: 35129557 DOI: 10.1039/d1tb02646a]
- 40 **Connor DM**, Broome AM. Gold Nanoparticles for the Delivery of Cancer Therapeutics. *Adv Cancer Res* 2018; **139**: 163-184 [PMID: 29941104 DOI: 10.1016/bs.acr.2018.05.001]
- 41 **Zhang X**, Lu Y, Jia D, Qiu W, Ma X, Zhang X, Xu Z, Wen F. Acidic microenvironment responsive polymeric MOF-based nanoparticles induce immunogenic cell death for combined cancer therapy. *J Nanobiotechnology* 2021; **19**: 455 [PMID: 34963499 DOI: 10.1186/s12951-021-01217-4]
- 42 **Iranpour S**, Bahrami AR, Nekooei S, Sh Saljooghi A, Matin MM. Improving anti-cancer drug delivery performance of magnetic mesoporous silica nanocarriers for more efficient colorectal cancer therapy. *J Nanobiotechnology* 2021; **19**: 314 [PMID: 34641857 DOI: 10.1186/s12951-021-01056-3]
- 43 **Smyth EC**, Nilsson M, Grabsch HI, van Grieken NC, Lordick F. Gastric cancer. *Lancet* 2020; **396**: 635-648 [PMID: 32861308 DOI: 10.1016/S0140-6736(20)31288-5]
- 44 **Menges M**, Hoehler T. Current strategies in systemic treatment of gastric cancer and cancer of the gastroesophageal junction. *J Cancer Res Clin Oncol* 2009; **135**: 29-38 [PMID: 18523800 DOI: 10.1007/s00432-008-0425-z]
- 45 **Sasaki Y**, Nishina T, Yasui H, Goto M, Muro K, Tsuji A, Koizumi W, Toh Y, Hara T, Miyata Y. Phase II trial of nanoparticle albumin-bound paclitaxel as second-line chemotherapy for unresectable or recurrent gastric cancer. *Cancer Sci* 2014; **105**: 812-817 [PMID: 24716542 DOI: 10.1111/cas.12419]
- 46 **Avgustinovich AV**, Bakina OV, Afanas'ev SG, Cheremisina OV, Spirina LV, Dobrodeev AY, Buldakov M, Choyznovov EL. Nanoparticles in Gastric Cancer Management. *Curr Pharm Des* 2021; **27**: 2436-2444 [PMID: 33222664 DOI: 10.2174/1381612826666201120155120]
- 47 **Zhao Q**, Cao L, Guan L, Bie L, Wang S, Xie B, Chen X, Shen X, Cao F. Immunotherapy for gastric cancer: dilemmas and prospect. *Brief Funct Genomics* 2019; **18**: 107-112 [PMID: 30388190 DOI: 10.1093/bfpg/ely019]
- 48 **Nakamura M**, Ojima T, Katsuda M, Hayata K, Kitadani J, Nakamori M, Yamaue H. Phase I Study of Combined Chemotherapy of Nab-Paclitaxel, S-1, and Oxaliplatin for Gastric Cancer with Peritoneal Metastasis (NSOX Study). *Oncology* 2021; **99**: 57-61 [PMID: 32877909 DOI: 10.1159/000509396]
- 49 **Han Y**, Liu D, Li L. PD-1/PD-L1 pathway: current researches in cancer. *Am J Cancer Res* 2020; **10**: 727-742 [PMID: 32266087]
- 50 **Xu S**, Cui F, Huang D, Zhang D, Zhu A, Sun X, Cao Y, Ding S, Wang Y, Gao E, Zhang F. PD-L1 monoclonal antibody-conjugated nanoparticles enhance drug delivery level and chemotherapy efficacy in gastric cancer cells. *Int J Nanomedicine* 2019; **14**: 17-32 [PMID: 30587982 DOI: 10.2147/IJN.S175340]
- 51 **Sharma P**, Allison JP. Immune checkpoint targeting in cancer therapy: toward combination strategies with curative potential. *Cell* 2015; **161**: 205-214 [PMID: 25860605 DOI: 10.1016/j.cell.2015.03.030]
- 52 **Hu N**, Li W, Hong Y, Zeng Z, Zhang J, Wu X, Zhou K, Wu F. A PD1 targeted nano-delivery system based on epigenetic alterations of T cell responses in the treatment of gastric cancer. *Mol Ther Oncolytics* 2022; **24**: 148-159 [PMID: 35024441 DOI: 10.1016/j.omto.2021.12.006]
- 53 **Kumagai S**, Togashi Y, Sakai C, Kawazoe A, Kawazu M, Ueno T, Sato E, Kuwata T, Kinoshita T, Yamamoto M, Nomura S, Tsukamoto T, Mano H, Shitara K, Nishikawa H. An Oncogenic Alteration Creates a Microenvironment that Promotes Tumor Progression by Conferring a Metabolic Advantage to Regulatory T Cells. *Immunity* 2020; **53**: 187-203.e8 [PMID: 32640259 DOI: 10.1016/j.immuni.2020.06.016]
- 54 **Guo W**, Chen Z, Li Z, Huang H, Ren Y, Zhao B, Li G, Hu Y. Improved immunotherapy for gastric cancer by nanocomposites with capability of triggering Dual-Damage of Nuclear/Mitochondrial DNA and cGAS/STING-Mediated innate immunity. *Chem Eng J* 2022; **443**: 136428 [DOI: 10.1016/j.cej.2022.136428]
- 55 **Pan Y**, Yu Y, Wang X, Zhang T. Tumor-Associated Macrophages in Tumor Immunity. *Front Immunol* 2020; **11**: 583084 [PMID: 33365025 DOI: 10.3389/fimmu.2020.583084]
- 56 **Cheng N**, Bai X, Shu Y, Ahmad O, Shen P. Targeting tumor-associated macrophages as an antitumor strategy. *Biochem Pharmacol* 2021; **183**: 114354 [PMID: 33279498 DOI: 10.1016/j.bcp.2020.114354]
- 57 **Zhang J**, Jiang M, Li S, Zhang Z, Sun H, Yang F, Liang H. Developing a Novel Anticancer Gold(III) Agent to Integrate Chemotherapy and Immunotherapy. *J Med Chem* 2021; **64**: 6777-6791 [PMID: 34000198 DOI: 10.1021/acs.jmedchem.1c00050]
- 58 **Morse MA**, Gwin WR 3rd, Mitchell DA. Vaccine Therapies for Cancer: Then and Now. *Target Oncol* 2021; **16**: 121-152 [PMID: 33512679 DOI: 10.1007/s11523-020-00788-w]
- 59 **Liu BY**, Chen XH, Gu QL, Li JF, Yin HR, Zhu ZG, Lin YZ. Antitumor effects of vaccine consisting of dendritic cells pulsed with tumor RNA from gastric cancer. *World J Gastroenterol* 2004; **10**: 630-633 [PMID: 14991927 DOI: 10.3748/wjg.v10.i5.630]

- 60 **Wu Y**, Wang L, Zhang Y. Dendritic cells as vectors for immunotherapy of tumor and its application for gastric cancer therapy. *Cell Mol Immunol* 2004; **1**: 351-356 [PMID: 16285894]
- 61 **Kohnepoushi C**, Nejati V, Delirez N, Biparva P. Poly Lactic-co-Glycolic Acid Nanoparticles Containing Human Gastric Tumor Lysates as Antigen Delivery Vehicles for Dendritic Cell-Based Antitumor Immunotherapy. *Immunol Invest* 2019; **48**: 794-808 [PMID: 31094258 DOI: 10.1080/08820139.2019.1610889]
- 62 **Banstola A**, Jeong JH, Yook S. Immunoadjuvants for cancer immunotherapy: A review of recent developments. *Acta Biomater* 2020; **114**: 16-30 [PMID: 32777293 DOI: 10.1016/j.actbio.2020.07.063]
- 63 **Bode C**, Zhao G, Steinhagen F, Kinjo T, Klinman DM. CpG DNA as a vaccine adjuvant. *Expert Rev Vaccines* 2011; **10**: 499-511 [PMID: 21506647 DOI: 10.1586/erv.10.174]
- 64 **Zhang J**, Zhao T, Han F, Hu Y, Li Y. Photothermal and gene therapy combined with immunotherapy to gastric cancer by the gold nanoshell-based system. *J Nanobiotechnology* 2019; **17**: 80 [PMID: 31277667 DOI: 10.1186/s12951-019-0515-x]
- 65 **Xu XF**, Xing H, Han J, Li ZL, Lau WY, Zhou YH, Gu WM, Wang H, Chen TH, Zeng YY, Li C, Wu MC, Shen F, Yang T. Risk Factors, Patterns, and Outcomes of Late Recurrence After Liver Resection for Hepatocellular Carcinoma: A Multicenter Study From China. *JAMA Surg* 2019; **154**: 209-217 [PMID: 30422241 DOI: 10.1001/jamasurg.2018.4334]
- 66 **Wang DX**, Yang X, Lin JZ, Bai Y, Long JY, Yang XB, Seery S, Zhao HT. Efficacy and safety of lenvatinib for patients with advanced hepatocellular carcinoma: A retrospective, real-world study conducted in China. *World J Gastroenterol* 2020; **26**: 4465-4478 [PMID: 32874058 DOI: 10.3748/wjg.v26.i30.4465]
- 67 **Lou T**, Li B, Xiong P, Jin C, Chen Y. External validation of hepatocellular carcinoma risk scores in patients with chronic hepatitis B virus infection in China. *J Viral Hepat* 2021; **28**: 1373-1380 [PMID: 34218498 DOI: 10.1111/jvh.13569]
- 68 **Qing X**, Xu W, Zong J, Du X, Peng H, Zhang Y. Emerging treatment modalities for systemic therapy in hepatocellular carcinoma. *Biomark Res* 2021; **9**: 64 [PMID: 34419152 DOI: 10.1186/s40364-021-00319-3]
- 69 **Kumari P**, Ghosh B, Biswas S. Nanocarriers for cancer-targeted drug delivery. *J Drug Target* 2016; **24**: 179-191 [PMID: 26061298 DOI: 10.3109/1061186X.2015.1051049]
- 70 **Jia G**, Han Y, An Y, Ding Y, He C, Wang X, Tang Q. NRP-1 targeted and cargo-loaded exosomes facilitate simultaneous imaging and therapy of glioma in vitro and in vivo. *Biomaterials* 2018; **178**: 302-316 [PMID: 29982104 DOI: 10.1016/j.biomaterials.2018.06.029]
- 71 **An Y**, Yang R, Wang X, Han Y, Jia G, Hu C, Zhang Z, Liu D, Tang Q. Facile Assembly of Thermosensitive Liposomes for Active Targeting Imaging and Synergetic Chemo-/Magnetic Hyperthermia Therapy. *Front Bioeng Biotechnol* 2021; **9**: 691091 [PMID: 34422777 DOI: 10.3389/fbioe.2021.691091]
- 72 **Lee YH**, Tai D, Yip C, Choo SP, Chew V. Combinational Immunotherapy for Hepatocellular Carcinoma: Radiotherapy, Immune Checkpoint Blockade and Beyond. *Front Immunol* 2020; **11**: 568759 [PMID: 33117354 DOI: 10.3389/fimmu.2020.568759]
- 73 **Yau T**, Kang Y-K, Kim T-Y, El-Khoueiry AB, Santoro A, Sangro B, Melero I, Kudo M, Hou M-M, Matilla A, Tovoli F, Knox JJ, He AR, El-Rayes BF, Acosta-Rivera M, Neely J, Shen Y, Baccan C, Cruz CMD, Hsu C. Nivolumab (NIVO) + ipilimumab (IPI) combination therapy in patients (pts) with advanced hepatocellular carcinoma (aHCC): Results from CheckMate 040. *J Clin Oncol* 2019; **37**: 4012-4012 [DOI: 10.1200/JCO.2019.37.15\_suppl.4012]
- 74 **Galluzzi L**, Vitale I, Warren S, Adjemian S, Agostinis P, Martinez AB, Chan TA, Coukos G, Demaria S, Deutsch E, Draganov D, Edelson RL, Formenti SC, Fucikova J, Gabriele L, Gaipal US, Gameiro SR, Garg AD, Golden E, Han J, Harrington KJ, Hemminki A, Hodge JW, Hossain DMS, Illidge T, Karin M, Kaufman HL, Kepp O, Kroemer G, Lasarte JJ, Loi S, Lotze MT, Manic G, Merghoub T, Melcher AA, Mossman KL, Prosper F, Rekdal Ø, Rescigno M, Riganti C, Sistigu A, Smyth MJ, Spisek R, Stagg J, Strauss BE, Tang D, Tatsuno K, van Gool SW, Vandenabeele P, Yamazaki T, Zamarin D, Zitvogel L, Cesano A, Marincola FM. Consensus guidelines for the definition, detection and interpretation of immunogenic cell death. *J Immunother Cancer* 2020; **8** [PMID: 32209603 DOI: 10.1136/jitc-2019-000337]
- 75 **Xu J**, Zheng Q, Cheng X, Hu S, Zhang C, Zhou X, Sun P, Wang W, Su Z, Zou T, Song Z, Xia Y, Yi X, Gao Y. Chemo-photodynamic therapy with light-triggered disassembly of theranostic nanoplatfrom in combination with checkpoint blockade for immunotherapy of hepatocellular carcinoma. *J Nanobiotechnology* 2021; **19**: 355 [PMID: 34717654 DOI: 10.1186/s12951-021-01101-1]
- 76 **Chang F**, Syrjänen S, Syrjänen K. Implications of the p53 tumor-suppressor gene in clinical oncology. *J Clin Oncol* 1995; **13**: 1009-1022 [PMID: 7707100 DOI: 10.1200/JCO.1995.13.4.1009]
- 77 **Harris CC**. Structure and function of the p53 tumor suppressor gene: clues for rational cancer therapeutic strategies. *J Natl Cancer Inst* 1996; **88**: 1442-1455 [PMID: 8841019 DOI: 10.1093/jnci/88.20.1442]
- 78 **Xu L**, Pirolo KF, Chang EH. Tumor-targeted p53-gene therapy enhances the efficacy of conventional chemo/radiotherapy. *J Control Release* 2001; **74**: 115-128 [PMID: 11489488 DOI: 10.1016/s0168-3659(01)00324-8]
- 79 **Cui Y**, Guo G. Immunomodulatory Function of the Tumor Suppressor p53 in Host Immune Response and the Tumor Microenvironment. *Int J Mol Sci* 2016; **17** [PMID: 27869779 DOI: 10.3390/ijms17111942]
- 80 **Blagih J**, Buck MD, Vouden KH. p53, cancer and the immune response. *J Cell Sci* 2020; **133** [PMID: 32144194 DOI: 10.1242/jcs.237453]
- 81 **Bezzi M**, Seitzer N, Ishikawa T, Reschke M, Chen M, Wang G, Mitchell C, Ng C, Katon J, Lunardi A, Signoretti S, Clohessy JG, Zhang J, Pandolfi PP. Diverse genetic-driven immune landscapes dictate tumor progression through distinct mechanisms. *Nat Med* 2018; **24**: 165-175 [PMID: 29309058 DOI: 10.1038/nm.4463]
- 82 **Guo G**, Yu M, Xiao W, Celis E, Cui Y. Local Activation of p53 in the Tumor Microenvironment Overcomes Immune Suppression and Enhances Antitumor Immunity. *Cancer Res* 2017; **77**: 2292-2305 [PMID: 28280037 DOI: 10.1158/0008-5472.CAN-16-2832]
- 83 **Xiao Y**, Chen J, Zhou H, Zeng X, Ruan Z, Pu Z, Jiang X, Matsui A, Zhu L, Amoozgar Z, Chen DS, Han X, Duda DG, Shi J. Combining p53 mRNA nanotherapy with immune checkpoint blockade reprograms the immune microenvironment for effective cancer therapy. *Nat Commun* 2022; **13**: 758 [PMID: 35140208 DOI: 10.1038/s41467-022-28279-8]
- 84 **Li B**, Zhang X, Wu Z, Chu T, Yang Z, Xu S, Wu S, Qie Y, Lu Z, Qi F, Hu M, Zhao G, Wei J, Zhao Y, Nie G, Meng H, Liu R, Li S. Reducing Postoperative Recurrence of Early-Stage Hepatocellular Carcinoma by a Wound-Targeted

- Nanodrug. *Adv Sci (Weinh)* 2022; **9**: e2200477 [PMID: 35524631 DOI: 10.1002/advs.202200477]
- 85 **Yu Z**, Guo J, Hu M, Gao Y, Huang L. Icaritin Exacerbates Mitophagy and Synergizes with Doxorubicin to Induce Immunogenic Cell Death in Hepatocellular Carcinoma. *ACS Nano* 2020; **14**: 4816-4828 [PMID: 32188241 DOI: 10.1021/acsnano.0c00708]
- 86 **Li Z**, Wu T, Zheng B, Chen L. Individualized precision treatment: Targeting TAM in HCC. *Cancer Lett* 2019; **458**: 86-91 [PMID: 31129147 DOI: 10.1016/j.canlet.2019.05.019]
- 87 **Wang Y**, Tiruthani K, Li S, Hu M, Zhong G, Tang Y, Roy S, Zhang L, Tan J, Liao C, Liu R. mRNA Delivery of a Bispecific Single-Domain Antibody to Polarize Tumor-Associated Macrophages and Synergize Immunotherapy against Liver Malignancies. *Adv Mater* 2021; **33**: e2007603 [PMID: 33945178 DOI: 10.1002/adma.202007603]
- 88 **Kabakov AE**, Yakimova AO. Hypoxia-Induced Cancer Cell Responses Driving Radioresistance of Hypoxic Tumors: Approaches to Targeting and Radiosensitizing. *Cancers (Basel)* 2021; **13** [PMID: 33806538 DOI: 10.3390/cancers13051102]
- 89 **Manoochehri Khoshinani H**, Afshar S, Najafi R. Hypoxia: A Double-Edged Sword in Cancer Therapy. *Cancer Invest* 2016; **34**: 536-545 [PMID: 27824512 DOI: 10.1080/07357907.2016.1245317]
- 90 **Boutillier AJ**, Elsawa SF. Macrophage Polarization States in the Tumor Microenvironment. *Int J Mol Sci* 2021; **22** [PMID: 34209703 DOI: 10.3390/ijms22136995]
- 91 **Dai X**, Ruan J, Guo Y, Sun Z, Liu J, Bao X, Zhang H, Li Q, Ye C, Wang X, Zhao CX, Zhou F, Sheng J, Chen D, Zhao P. Enhanced radiotherapy efficacy and induced anti-tumor immunity in HCC by improving hypoxia microenvironment using oxygen microcapsules. *Chem Eng J* 2021; **422**: 130109 [DOI: 10.1016/j.cej.2021.130109]
- 92 **Yang M**, Zhang C. The role of liver sinusoidal endothelial cells in cancer liver metastasis. *Am J Cancer Res* 2021; **11**: 1845-1860 [PMID: 34094657]
- 93 **Yu Z**, Guo J, Liu Y, Wang M, Liu Z, Gao Y, Huang L. Nano delivery of simvastatin targets liver sinusoidal endothelial cells to remodel tumor microenvironment for hepatocellular carcinoma. *J Nanobiotechnology* 2022; **20**: 9 [PMID: 34983554 DOI: 10.1186/s12951-021-01205-8]
- 94 **Kon E**, Elia U, Peer D. Principles for designing an optimal mRNA lipid nanoparticle vaccine. *Curr Opin Biotechnol* 2022; **73**: 329-336 [PMID: 34715546 DOI: 10.1016/j.copbio.2021.09.016]
- 95 **Gebre MS**, Brito LA, Tostanoski LH, Edwards DK, Carfi A, Barouch DH. Novel approaches for vaccine development. *Cell* 2021; **184**: 1589-1603 [PMID: 33740454 DOI: 10.1016/j.cell.2021.02.030]
- 96 **Huang H**, Zhang C, Yang S, Xiao W, Zheng Q, Song X. The investigation of mRNA vaccines formulated in liposomes administrated in multiple routes against SARS-CoV-2. *J Control Release* 2021; **335**: 449-456 [PMID: 34029632 DOI: 10.1016/j.jconrel.2021.05.024]
- 97 **Szebeni J**, Storm G, Ljubimova JY, Castells M, Phillips EJ, Turjeman K, Barenholz Y, Crommelin DJA, Dobrovolskaia MA. Applying lessons learned from nanomedicines to understand rare hypersensitivity reactions to mRNA-based SARS-CoV-2 vaccines. *Nat Nanotechnol* 2022; **17**: 337-346 [PMID: 35393599 DOI: 10.1038/s41565-022-01071-x]
- 98 **Zhang Y**, Xie F, Yin Y, Zhang Q, Jin H, Wu Y, Pang L, Li J, Gao J. Immunotherapy of Tumor RNA-Loaded Lipid Nanoparticles Against Hepatocellular Carcinoma. *Int J Nanomedicine* 2021; **16**: 1553-1564 [PMID: 33658783 DOI: 10.2147/IJN.S291421]
- 99 **Siegel RL**, Miller KD, Jemal A. Cancer statistics, 2020. *CA Cancer J Clin* 2020; **70**: 7-30 [PMID: 31912902 DOI: 10.3322/caac.21590]
- 100 **Ladabaum U**, Dominitz JA, Kahi C, Schoen RE. Strategies for Colorectal Cancer Screening. *Gastroenterology* 2020; **158**: 418-432 [PMID: 31394083 DOI: 10.1053/j.gastro.2019.06.043]
- 101 **Sagaert X**, Vanstapel A, Verbeek S. Tumor Heterogeneity in Colorectal Cancer: What Do We Know So Far? *Pathobiology* 2018; **85**: 72-84 [PMID: 29414818 DOI: 10.1159/000486721]
- 102 **Siegel RL**, Miller KD, Fedewa SA, Ahnen DJ, Meester RGS, Barzi A, Jemal A. Colorectal cancer statistics, 2017. *CA Cancer J Clin* 2017; **67**: 177-193 [PMID: 28248415 DOI: 10.3322/caac.21395]
- 103 **Bai J**, Chen H, Bai X. Relationship between microsatellite status and immune microenvironment of colorectal cancer and its application to diagnosis and treatment. *J Clin Lab Anal* 2021; **35**: e23810 [PMID: 33938589 DOI: 10.1002/jcla.23810]
- 104 **Krasteva N**, Georgieva M. Promising Therapeutic Strategies for Colorectal Cancer Treatment Based on Nanomaterials. *Pharmaceutics* 2022; **14** [PMID: 35745786 DOI: 10.3390/pharmaceutics14061213]
- 105 **Liu H**, Xu C, Meng M, Li S, Sheng S, Zhang S, Ni W, Tian H, Wang Q. Metal-organic framework-mediated multifunctional nanoparticles for combined chemo-photothermal therapy and enhanced immunotherapy against colorectal cancer. *Acta Biomater* 2022; **144**: 132-141 [PMID: 35307591 DOI: 10.1016/j.actbio.2022.03.023]
- 106 **Wangmo D**, Premsrirut PK, Yuan C, Morris WS, Zhao X, Subramanian S. ACKR4 in Tumor Cells Regulates Dendritic Cell Migration to Tumor-Draining Lymph Nodes and T-Cell Priming. *Cancers (Basel)* 2021; **13** [PMID: 34638505 DOI: 10.3390/cancers13195021]
- 107 **Yuan Z**, Fan G, Wu H, Liu C, Zhan Y, Qiu Y, Shou C, Gao F, Zhang J, Yin P, Xu K. Photodynamic therapy synergizes with PD-L1 checkpoint blockade for immunotherapy of CRC by multifunctional nanoparticles. *Mol Ther* 2021; **29**: 2931-2948 [PMID: 34023507 DOI: 10.1016/j.ymthe.2021.05.017]
- 108 **Zhu Q**, Sun F, Li T, Zhou M, Ye J, Ji A, Wang H, Ding C, Chen H, Xu Z, Yu H. Engineering Oxaliplatin Prodrug Nanoparticles for Second Near-Infrared Fluorescence Imaging-Guided Immunotherapy of Colorectal Cancer. *Small* 2021; **17**: e2007882 [PMID: 33690984 DOI: 10.1002/sml.202007882]
- 109 **Li J**, Zhao M, Sun M, Wu S, Zhang H, Dai Y, Wang D. Multifunctional Nanoparticles Boost Cancer Immunotherapy Based on Modulating the Immunosuppressive Tumor Microenvironment. *ACS Appl Mater Interfaces* 2020; **12**: 50734-50747 [PMID: 33124808 DOI: 10.1021/acsmi.0c14909]
- 110 **Liang C**, Zhang X, Yang M, Dong X. Recent Progress in Ferroptosis Inducers for Cancer Therapy. *Adv Mater* 2019; **31**: e1904197 [PMID: 31595562 DOI: 10.1002/adma.201904197]
- 111 **Duan X**, Chan C, Han W, Guo N, Weichselbaum RR, Lin W. Immunostimulatory nanomedicines synergize with checkpoint blockade immunotherapy to eradicate colorectal tumors. *Nat Commun* 2019; **10**: 1899 [PMID: 31015397 DOI: 10.1038/s41467-019-09221-x]

- 112 **Haegebaert RMS**, Kempers M, Ceelen W, Lentacker I, Remaut K. Nanoparticle mediated targeting of toll-like receptors to treat colorectal cancer. *Eur J Pharm Biopharm* 2022; **172**: 16-30 [PMID: 35074555 DOI: 10.1016/j.ejpb.2022.01.002]
- 113 **Bahmani B**, Gong H, Luk BT, Haushalter KJ, DeTeresa E, Previti M, Zhou J, Gao W, Bui JD, Zhang L, Fang RH, Zhang J. Intratumoral immunotherapy using platelet-cloaked nanoparticles enhances antitumor immunity in solid tumors. *Nat Commun* 2021; **12**: 1999 [PMID: 33790276 DOI: 10.1038/s41467-021-22311-z]
- 114 **Luo Y**, Yang J, Yu J, Liu X, Yu C, Hu J, Shi H, Ma X. Long Non-coding RNAs: Emerging Roles in the Immunosuppressive Tumor Microenvironment. *Front Oncol* 2020; **10**: 48 [PMID: 32083005 DOI: 10.3389/fonc.2020.00048]
- 115 **Huang D**, Chen J, Yang L, Ouyang Q, Li J, Lao L, Zhao J, Liu J, Lu Y, Xing Y, Chen F, Su F, Yao H, Liu Q, Su S, Song E. NKILA lncRNA promotes tumor immune evasion by sensitizing T cells to activation-induced cell death. *Nat Immunol* 2018; **19**: 1112-1125 [PMID: 30224822 DOI: 10.1038/s41590-018-0207-y]
- 116 **Zheng Y**, Tian X, Wang T, Xia X, Cao F, Tian J, Xu P, Ma J, Xu H, Wang S. Long noncoding RNA Pvt1 regulates the immunosuppression activity of granulocytic myeloid-derived suppressor cells in tumor-bearing mice. *Mol Cancer* 2019; **18**: 61 [PMID: 30925926 DOI: 10.1186/s12943-019-0978-2]
- 117 **Liu F**, Dai Z, Cheng Q, Xu L, Huang L, Liu Z, Li X, Wang N, Wang G, Wang L, Wang Z. LncRNA-targeting bio-scaffold mediates triple immune effects for postoperative colorectal cancer immunotherapy. *Biomaterials* 2022; **284**: 121485 [PMID: 35367839 DOI: 10.1016/j.biomaterials.2022.121485]
- 118 **Tilg H**, Adolph TE, Gerner RR, Moschen AR. The Intestinal Microbiota in Colorectal Cancer. *Cancer Cell* 2018; **33**: 954-964 [PMID: 29657127 DOI: 10.1016/j.ccell.2018.03.004]
- 119 **Louis P**, Hold GL, Flint HJ. The gut microbiota, bacterial metabolites and colorectal cancer. *Nat Rev Microbiol* 2014; **12**: 661-672 [PMID: 25198138 DOI: 10.1038/nrmicro3344]
- 120 **Kostic AD**, Chun E, Robertson L, Glickman JN, Gallini CA, Michaud M, Clancy TE, Chung DC, Lochhead P, Hold GL, El-Omar EM, Brenner D, Fuchs CS, Meyerson M, Garrett WS. Fusobacterium nucleatum potentiates intestinal tumorigenesis and modulates the tumor-immune microenvironment. *Cell Host Microbe* 2013; **14**: 207-215 [PMID: 23954159 DOI: 10.1016/j.chom.2013.07.007]
- 121 **Chen T**, Li Q, Wu J, Wu Y, Peng W, Li H, Wang J, Tang X, Peng Y, Fu X. Fusobacterium nucleatum promotes M2 polarization of macrophages in the microenvironment of colorectal tumours via a TLR4-dependent mechanism. *Cancer Immunol Immunother* 2018; **67**: 1635-1646 [PMID: 30121899 DOI: 10.1007/s00262-018-2233-x]
- 122 **Dong X**, Pan P, Zheng DW, Bao P, Zeng X, Zhang XZ. Bioinorganic hybrid bacteriophage for modulation of intestinal microbiota to remodel tumor-immune microenvironment against colorectal cancer. *Sci Adv* 2020; **6**: eaba1590 [PMID: 32440552 DOI: 10.1126/sciadv.aba1590]
- 123 **Zhang Y**, Ma S, Liu X, Xu Y, Zhao J, Si X, Li H, Huang Z, Wang Z, Tang Z, Song W, Chen X. Supramolecular Assembled Programmable Nanomedicine As In Situ Cancer Vaccine for Cancer Immunotherapy. *Adv Mater* 2021; **33**: e2007293 [PMID: 33448050 DOI: 10.1002/adma.202007293]
- 124 **GBD 2017 Pancreatic Cancer Collaborators**. The global, regional, and national burden of pancreatic cancer and its attributable risk factors in 195 countries and territories, 1990-2017: a systematic analysis for the Global Burden of Disease Study 2017. *Lancet Gastroenterol Hepatol* 2019; **4**: 934-947 [PMID: 31648972 DOI: 10.1016/S2468-1253(19)30347-4]
- 125 **Klein AP**. Pancreatic cancer epidemiology: understanding the role of lifestyle and inherited risk factors. *Nat Rev Gastroenterol Hepatol* 2021; **18**: 493-502 [PMID: 34002083 DOI: 10.1038/s41575-021-00457-x]
- 126 **Zhao Z**, Liu W. Pancreatic Cancer: A Review of Risk Factors, Diagnosis, and Treatment. *Technol Cancer Res Treat* 2020; **19**: 1533033820962117 [PMID: 33357065 DOI: 10.1177/1533033820962117]
- 127 **Nishida T**, Yoshitomi H, Takano S, Kagawa S, Shimizu H, Ohtsuka M, Kato A, Furukawa K, Miyazaki M. Low Stromal Area and High Stromal Microvessel Density Predict Poor Prognosis in Pancreatic Cancer. *Pancreas* 2016; **45**: 593-600 [PMID: 26495781 DOI: 10.1097/MPA.0000000000000499]
- 128 **Li S**, Xu HX, Wu CT, Wang WQ, Jin W, Gao HL, Li H, Zhang SR, Xu JZ, Qi ZH, Ni QX, Yu XJ, Liu L. Angiogenesis in pancreatic cancer: current research status and clinical implications. *Angiogenesis* 2019; **22**: 15-36 [PMID: 30168025 DOI: 10.1007/s10456-018-9645-2]
- 129 **Selvanesan BC**, Meena K, Beck A, Meheus L, Lara O, Rooman I, Gravekamp C. Nicotinamide combined with gemcitabine is an immunomodulatory therapy that restrains pancreatic cancer in mice. *J Immunother Cancer* 2020; **8**: [PMID: 33154149 DOI: 10.1136/jitc-2020-001250]
- 130 **Rocha FG**. Landmark Series: Immunotherapy and Targeted Therapy for Pancreatic Cancer. *Ann Surg Oncol* 2021; **28**: 1400-1406 [PMID: 33386541 DOI: 10.1245/s10434-020-09367-9]
- 131 **Schizas D**, Charalampakis N, Kole C, Economopoulou P, Koustas E, Gkotsis E, Ziogas D, Psyrii A, Karamouzis MV. Immunotherapy for pancreatic cancer: A 2020 update. *Cancer Treat Rev* 2020; **86**: 102016 [PMID: 32247999 DOI: 10.1016/j.ctrv.2020.102016]
- 132 **Jia M**, Zhang D, Zhang C, Li C. Nanoparticle-based delivery systems modulate the tumor microenvironment in pancreatic cancer for enhanced therapy. *J Nanobiotechnology* 2021; **19**: 384 [PMID: 34809634 DOI: 10.1186/s12951-021-01134-6]
- 133 **Wang Y**, Gao Z, Du X, Chen S, Zhang W, Wang J, Li H, He X, Cao J. Co-inhibition of the TGF- $\beta$  pathway and the PD-L1 checkpoint by pH-responsive clustered nanoparticles for pancreatic cancer microenvironment regulation and anti-tumor immunotherapy. *Biomater Sci* 2020; **8**: 5121-5132 [PMID: 32820750 DOI: 10.1039/d0bm00916d]
- 134 **Yu Q**, Tang X, Zhao W, Qiu Y, He J, Wan D, Li J, Wang X, He X, Liu Y, Li M, Zhang Z, He Q. Mild hyperthermia promotes immune checkpoint blockade-based immunotherapy against metastatic pancreatic cancer using size-adjustable nanoparticles. *Acta Biomater* 2021; **133**: 244-256 [PMID: 34000465 DOI: 10.1016/j.actbio.2021.05.002]
- 135 **Wang C**, Shi X, Song H, Zhang C, Wang X, Huang P, Dong A, Zhang Y, Kong D, Wang W. Polymer-lipid hybrid nanovesicle-enabled combination of immunogenic chemotherapy and RNAi-mediated PD-L1 knockdown elicits antitumor immunity against melanoma. *Biomaterials* 2021; **268**: 120579 [PMID: 33278683 DOI: 10.1016/j.biomaterials.2020.120579]
- 136 **Danhier F**, Ansorena E, Silva JM, Coco R, Le Breton A, Pr at V. PLGA-based nanoparticles: an overview of biomedical applications. *J Control Release* 2012; **161**: 505-522 [PMID: 22353619 DOI: 10.1016/j.jconrel.2012.01.043]

- 137 **Allavena P**, Palmioli A, Avigni R, Sironi M, La Ferla B, Maeda A. PLGA Based Nanoparticles for the Monocyte-Mediated Anti-Tumor Drug Delivery System. *J Biomed Nanotechnol* 2020; **16**: 212-223 [PMID: 32252882 DOI: 10.1166/jbn.2020.2881]
- 138 **Jung JY**, Ryu HJ, Lee SH, Kim DY, Kim MJ, Lee EJ, Ryu YM, Kim SY, Kim KP, Choi EY, Ahn HJ, Chang S. siRNA Nanoparticle Targeting PD-L1 Activates Tumor Immunity and Abrogates Pancreatic Cancer Growth in Humanized Preclinical Model. *Cells* 2021; **10** [PMID: 34685714 DOI: 10.3390/cells10102734]
- 139 **Lorkowski ME**, Atukorale PU, Bielecki PA, Tong KH, Covarrubias G, Zhang Y, Loutrianakis G, Moon TJ, Santulli AR, Becicka WM, Karathanasis E. Immunostimulatory nanoparticle incorporating two immune agonists for the treatment of pancreatic tumors. *J Control Release* 2021; **330**: 1095-1105 [PMID: 33188827 DOI: 10.1016/j.jconrel.2020.11.014]
- 140 **Porembka MR**, Mitchem JB, Belt BA, Hsieh CS, Lee HM, Herndon J, Gillanders WE, Linehan DC, Goedegebuure P. Pancreatic adenocarcinoma induces bone marrow mobilization of myeloid-derived suppressor cells which promote primary tumor growth. *Cancer Immunol Immunother* 2012; **61**: 1373-1385 [PMID: 22215137 DOI: 10.1007/s00262-011-1178-0]
- 141 **Long Y**, Lu Z, Xu S, Li M, Wang X, Zhang Z, He Q. Self-Delivery Micellar Nanoparticles Prevent Premetastatic Niche Formation by Interfering with the Early Recruitment and Vascular Destruction of Granulocytic Myeloid-Derived Suppressor Cells. *Nano Lett* 2020; **20**: 2219-2229 [PMID: 31823615 DOI: 10.1021/acs.nanolett.9b03883]
- 142 **Lu Z**, Long Y, Wang Y, Wang X, Xia C, Li M, Zhang Z, He Q. Phenylboronic acid modified nanoparticles simultaneously target pancreatic cancer and its metastasis and alleviate immunosuppression. *Eur J Pharm Biopharm* 2021; **165**: 164-173 [PMID: 34020022 DOI: 10.1016/j.ejpb.2021.05.014]
- 143 **Yu P**, Zhang X, Liu N, Tang L, Peng C, Chen X. Pyroptosis: mechanisms and diseases. *Signal Transduct Target Ther* 2021; **6**: 128 [PMID: 33776057 DOI: 10.1038/s41392-021-00507-5]
- 144 **Li J**, Anraku Y, Kataoka K. Self-Boosting Catalytic Nanoreactors Integrated with Triggerable Crosslinking Membrane Networks for Initiation of Immunogenic Cell Death by Pyroptosis. *Angew Chem Int Ed Engl* 2020; **59**: 13526-13530 [PMID: 32383236 DOI: 10.1002/anie.202004180]
- 145 **Liu Y**, Zhen W, Wang Y, Song S, Zhang H. Na<sub>2</sub>S<sub>2</sub>O<sub>8</sub> Nanoparticles Trigger Antitumor Immunotherapy through Reactive Oxygen Species Storm and Surge of Tumor Osmolarity. *J Am Chem Soc* 2020; **142**: 21751-21757 [PMID: 33337859 DOI: 10.1021/jacs.0c09482]
- 146 **Zhao P**, Wang M, Chen M, Chen Z, Peng X, Zhou F, Song J, Qu J. Programming cell pyroptosis with biomimetic nanoparticles for solid tumor immunotherapy. *Biomaterials* 2020; **254**: 120142 [PMID: 32485591 DOI: 10.1016/j.biomaterials.2020.120142]
- 147 **Fan JX**, Deng RH, Wang H, Liu XH, Wang XN, Qin R, Jin X, Lei TR, Zheng D, Zhou PH, Sun Y, Zhang XZ. Epigenetics-Based Tumor Cells Pyroptosis for Enhancing the Immunological Effect of Chemotherapeutic Nanocarriers. *Nano Lett* 2019; **19**: 8049-8058 [PMID: 31558023 DOI: 10.1021/acs.nanolett.9b03245]
- 148 **Ding B**, Sheng J, Zheng P, Li C, Li D, Cheng Z, Ma P, Lin J. Biodegradable Upconversion Nanoparticles Induce Pyroptosis for Cancer Immunotherapy. *Nano Lett* 2021; **21**: 8281-8289 [PMID: 34591494 DOI: 10.1021/acs.nanolett.1c02790]
- 149 **D'Errico G**, Alonso-Nocelo M, Vallespinos M, Hermann PC, Alcalá S, García CP, Martín-Hijano L, Valle S, Earl J, Cassiano C, Lombardia L, Feliu J, Monti MC, Seufferlein T, García-Bermejo L, Martinelli P, Carrato A, Sainz B Jr. Tumor-associated macrophage-secreted 14-3-3ζ signals via AXL to promote pancreatic cancer chemoresistance. *Oncogene* 2019; **38**: 5469-5485 [PMID: 30936462 DOI: 10.1038/s41388-019-0803-9]
- 150 **Bulle A**, Dekervel J, Deschuttere L, Nittner D, Libbrecht L, Janky R, Plaisance S, Topal B, Coosemans A, Lambrechts D, Van Cutsem E, Verslype C, van Pelt J. Gemcitabine Recruits M2-Type Tumor-Associated Macrophages into the Stroma of Pancreatic Cancer. *Transl Oncol* 2020; **13**: 100743 [PMID: 32145636 DOI: 10.1016/j.tranon.2020.01.004]
- 151 **Wang M**, Hu Q, Huang J, Zhao X, Shao S, Zhang F, Yao Z, Ping Y, Liang T. Engineered a dual-targeting biomimetic nanomedicine for pancreatic cancer chemoimmunotherapy. *J Nanobiotechnology* 2022; **20**: 85 [PMID: 35177078 DOI: 10.1186/s12951-022-01282-3]
- 152 **Cao S**, Saw PE, Shen Q, Li R, Liu Y, Xu X. Reduction-responsive RNAi nanoplatfom to reprogram tumor lipid metabolism and repolarize macrophage for combination pancreatic cancer therapy. *Biomaterials* 2022; **280**: 121264 [PMID: 34823884 DOI: 10.1016/j.biomaterials.2021.121264]
- 153 **Wang M**, Li Y, Wang M, Liu K, Hoover AR, Li M, Towner RA, Mukherjee P, Zhou F, Qu J, Chen WR. Synergistic interventional photothermal therapy and immunotherapy using an iron oxide nanoplatfom for the treatment of pancreatic cancer. *Acta Biomater* 2022; **138**: 453-462 [PMID: 34757232 DOI: 10.1016/j.actbio.2021.10.048]
- 154 **Zanganeh S**, Hutter G, Spittler R, Lenkov O, Mahmoudi M, Shaw A, Pajarinen JS, Nejadnik H, Goodman S, Moseley M, Coussens LM, Daldrup-Link HE. Iron oxide nanoparticles inhibit tumour growth by inducing pro-inflammatory macrophage polarization in tumour tissues. *Nat Nanotechnol* 2016; **11**: 986-994 [PMID: 27668795 DOI: 10.1038/nnano.2016.168]

## Basic Study

# Lentivirus-mediated short hairpin RNA interference of CENPK inhibits growth of colorectal cancer cells with overexpression of Cullin 4A

Xian Li, Yi-Ru Han, Xuefeng Xuefeng, Yong-Xiang Ma, Guo-Sheng Xing, Zhi-Wen Yang, Zhen Zhang, Lin Shi, Xin-Lin Wu

**Specialty type:** Gastroenterology and hepatology

**Provenance and peer review:** Unsolicited article; Externally peer reviewed.

**Peer-review model:** Single blind

**Peer-review report's scientific quality classification**

Grade A (Excellent): 0  
Grade B (Very good): B, B  
Grade C (Good): 0  
Grade D (Fair): 0  
Grade E (Poor): 0

**P-Reviewer:** Fouad MA, Egypt; Mohamed SY, Egypt

**Received:** November 22, 2021

**Peer-review started:** November 22, 2021

**First decision:** January 11, 2022

**Revised:** January 24, 2022

**Accepted:** September 12, 2022

**Article in press:** September 12, 2022

**Published online:** October 7, 2022



**Xian Li**, Clinical Medical Research Center, The Affiliated Hospital of Inner Mongolia Medical University, Hohhot 010050, Inner Mongolia Autonomous Region, China

**Yi-Ru Han, Xuefeng Xuefeng, Yong-Xiang Ma, Guo-Sheng Xing, Zhi-Wen Yang, Zhen Zhang, Xin-Lin Wu**, Department of Gastrointestinal Surgery, The Affiliated Hospital of Inner Mongolia Medical University, Hohhot 010050, Inner Mongolia Autonomous Region, China

**Lin Shi**, Department of Pathology, The Affiliated Hospital of Inner Mongolia Medical University, Hohhot 010050, Inner Mongolia Autonomous Region, China

**Corresponding author:** Xin-Lin Wu, Doctor, Chief Doctor, Department of Gastrointestinal Surgery, The Affiliated Hospital of Inner Mongolia Medical University, No. 1 North Street, Hohhot 010050, Inner Mongolia Autonomous Region, China. [wuxinlin@126.com](mailto:wuxinlin@126.com)

## Abstract

### BACKGROUND

Colorectal cancer (CRC) is one of the most common malignant tumors worldwide. The identification of novel diagnostic and prognostic biomarkers for CRC is a key research imperative. Immunohistochemical analysis has revealed high expression of centromere protein K (CENPK) in CRC. However, the role of CENPK in the progression of CRC is not well characterized.

### AIM

To evaluate the effects of knockdown of CENPK and overexpression of Cullin 4A (CUL4A) in RKO and HCT116 cells.

### METHODS

Human colon cancer samples were collected and tested using a human gene expression chip. We identified CENPK as a potential oncogene for CRC based on bioinformatics analysis. *In vitro* experiments verified the function of this gene. We investigated the expression of CENPK in RKO and HCT116 cells using quantitative polymerase chain reaction (qPCR), western blot, and flow cytometry. The effect of short hairpin RNA (shRNA) virus-infected RKO cells on tumor growth was evaluated *in vivo* using quantitative analysis of fluorescence imaging. To evaluate the effects of knockdown of CENPK and overexpression of CUL4A in

RKO and HCT116 cells, we performed a series of *in vitro* experiments, using qPCR, western blot, MTT assay, and flow cytometry.

## RESULTS

We demonstrated overexpression of CENPK in human colon cancer samples. CENPK was an independent risk factor in patients with CRC. The downstream genes FBX32, CUL4A, and Yes-associated protein isoform 1 were examined to evaluate the regulatory action of CENPK in RKO cells. Significantly delayed xenograft tumor emergence, slower growth rate, and lower final tumor weight and volume were observed in the CENPK short hairpin RNA virus infected group compared with the CENPK negative control group. The CENPK gene interference inhibited the proliferation of RKO cells *in vitro* and *in vivo*. The lentivirus-mediated shRNA interference of CENPK inhibited the proliferation of RKO and HCT116 colon cancer cells, with overexpression of the CUL4A.

## CONCLUSION

We indicated a potential role of CENPK in promoting tumor proliferation, and it may be a novel diagnostic and prognostic biomarker for CRC.

**Key Words:** Colorectal cancer; Centromere protein K; Bioinformatics analysis; Lentivirus-mediated short hairpin RNA interference; Cullin 4A

©The Author(s) 2022. Published by Baishideng Publishing Group Inc. All rights reserved.

**Core Tip:** High expression of centromere protein K (CENPK) in colorectal cancer (CRC) was found by immunohistochemistry. We demonstrated overexpression of CENPK in human colon cancer samples. CENPK was an independent risk factor in patients with CRC. Our findings indicate a potential role of CENPK in promoting tumor proliferation. CENPK may serve as a novel diagnostic and prognostic biomarker in patients with CRC.

**Citation:** Li X, Han YR, Xuefeng X, Ma YX, Xing GS, Yang ZW, Zhang Z, Shi L, Wu XL. Lentivirus-mediated short hairpin RNA interference of CENPK inhibits growth of colorectal cancer cells with overexpression of Cullin 4A. *World J Gastroenterol* 2022; 28(37): 5420-5443

**URL:** <https://www.wjgnet.com/1007-9327/full/v28/i37/5420.htm>

**DOI:** <https://dx.doi.org/10.3748/wjg.v28.i37.5420>

## INTRODUCTION

Colorectal cancer (CRC) is the third most common cancer in the Western Hemisphere, and the incidence increases with age. RNA interference has been developed to silence genes of interest. Short hairpin RNA (shRNA) expression vectors are useful in gene silencing[1]. The shRNA-mediated silencing of MASTL expression in colon cancer cells induced cell cycle arrest and apoptosis *in vitro* and xenograft-tumor growth *in vivo*[2]. Emerging studies have suggested that shRNAs play a crucial role in CRC tumorigenesis and progression[3]. Inducible gene knockdown systems based on lentivirus-mediated gene transfer were developed to regulate colon cancer progression[1]. This property of the shRNA system offers unique applications to study gene function in animals that cannot be achieved using knockout technologies[4]. Although lentivirus vectors have been used for several years, the use of Tet-on lentiviral vectors expressing shRNA as a therapeutic tool for CRC has not been clearly explored[5].

The role of centromere protein K (CENPK) in cancer is an emerging research hotspot. CENPK is overexpressed in several tumor types, and it promotes tumor progression. Research on the role of CENPK in the progression of hepatocellular carcinoma (HCC) has shown that CENPK knockdown significantly inhibits proliferation, migration, invasion, and epithelial-mesenchymal transition in HCC cells[6]. The expression of CENPK has been silenced and promoted *via* lentivirus-mediated transfection with shRNA sequences in differentiated thyroid carcinomas, such as two pore channel 1 and FTC-133 cells[7]. CENPK is specifically upregulated in ovarian cancer tissues and cell lines, and its overexpression is associated with a poor prognosis in patients with ovarian cancer[8]. Overexpression of CENPK promotes expression of oncogenic cell cycle regulators[9]. However, there has been little research on the role of CENPK in the progression of CRC.

The ubiquitin ligase Cullin 4A (CUL4A) is highly expressed in CRC. CUL4A promotes proliferation and inhibits apoptosis of CRC cells by regulating the Hippo pathway[10]. CUL4A significantly promotes the migration of CRC cells *in vitro*, which suggests that CUL4A acts as an oncogene in CRC

and may become a potential therapeutic target[11]. Therefore, CUL4A expression positively correlates with the prognosis of CRC[12]. Despite extensive fundamental studies, the role of CUL4A expression and lentivirus-mediated transfection with shRNA for CENPK in CRC is not clear. The present study identified CENPK as a novel proto-oncogene in CRC. Increased CENPK levels were found in CRC specimens and negatively correlated with survival rate. Knockdown of CENPK in RKO and HCT116 CRC cells induced apoptosis and suppressed cell proliferation and xenograft tumor formation. Lentivirus-mediated transfection with shRNA for CENPK and CUL4A overexpression played major regulatory roles in CRC.

## MATERIALS AND METHODS

### **Patient information and immunohistochemistry**

Fourteen patients with CRC were enrolled from 2016 to 2019, and five tumor-adjacent normal tissues were taken from an area > 10 cm away from the primary neoplasm. The median age of the patients was 59 years (range: 49-68 years) at the time of surgery, and the median follow-up was 31 mo postoperatively (range: 25-37 mo). The Ethics Committee of The Affiliated Hospital of Inner Mongolia Medical University approved the study. Written informed consent was obtained from all patients.

The expression and localization of CENPK protein in 14 cancerous and five noncancerous tissue samples were detected using immunohistochemistry. An antibody against CENPK (26208-1-AP, 1:100; SIGMA) was used for analysis. Vulcan Fast Red Chromogen kit 2 staining was performed for 15-20 min to stop the reaction until 3,3-diaminobenzidine staining was performed to obtain a yellow color to complete the reaction. The staining intensity and positive rate of cytosolic and membrane staining of the antibody (0/1+/2+/3+) in the cancer and adjacent tissue (epithelium) were interpreted. The intensity of the staining score was 0 (negative), 1 (weak), 2 (middle), and 3 (strong). The positive rate of staining was as follows: 0 (negative), 1 (1%-25%), 2 (26%-50%), 3 (51%-75%), and 4 (76%-100%).

### **Primeview human gene expression array of PathArray™**

Gene expression in a human colon cancer tissue chip (C06161) was detected. The sample was divided into male (age < 57 years) and female (age > 57 years) groups by T stage, N stage, pathological grade, and clinical stage. For the chip assay, total RNA was extracted from tissue using the TRIzol method and measured using a Nanodrop 2000. Qualified samples were used in the chip experiment. The quality checking standard was  $1.7 < A260/A280 < 2.2$  on Thermo NanoDrop 2000 and RNA integrity number (RIN)  $\geq 7.0$  and  $28S/18S > 0.7$  on the Agilent 2100 Bioanalyzer. The quality check results are shown in Table 1. The human gene expression chip type was GeneChip PrimeView Human (100 format, 902487; Affymetrix). Chip hybridization was performed in a GeneChip Hybridization Oven 645 ChIP, washing and dyeing were performed using a GeneChip Fluidics Station 450, and ChIP scanning was performed using a GeneChip Scanner 3000. The reagent used was a GeneChip Hybridization Wash and Stain Kit.

For the chip detection, gradient dilution of poly-A RNA controls was prepared to synthesize the first-chain cDNA and second-chain cDNA, and then cRNA of synthetic markers was synthesized *via* transcription *in vitro*, which was followed by cRNA purification and quantification to obtain cRNA fragment markers. The expression analysis of the CENPK gene in human colon cancer tissue in the chip (C06161) and clinical data are shown in Table 2. A statistical analysis of CRC tissue chips was performed.

### **Cell culture**

The human CRC cell lines RKO and HCT 116 were cultured in RPMI 1640 medium (Invitrogen) supplemented with 10% fetal bovine serum (FBS) (Corning) and 1% penicillin and streptomycin solution (Corning) at 37 °C with 5% CO<sub>2</sub>[13].

### **Quantitative polymerase chain reaction**

Total RNA was extracted from RKO cells with TRIzol reagent (Thermo Fisher Scientific). A 1-mg RNA sample was reverse transcribed into first-strand cDNA using the Revert Aid First Strand cDNA Synthesis kit (Thermo Fisher Scientific). Quantitative polymerase chain reaction (qPCR) was performed using the Taq-Man Gene Expression assay (Thermo Fisher Scientific) on an Mx3000P real-time PCR system (Agilent Technologies). The primer pairs were designed and synthesized by Sangon Biotech (GAPDH: Forward, TGACTTCAACAGCGACACCCA and reverse, CACCCTGTTGCTGTAGCCAAA; CENPK: Forward, ATGGTACTGTCCACTAAGGAGTC and reverse, TGITCATCCAACCACCGTTGT). The mRNA levels were normalized to the internal reference gene GAPDH, with the mRNA relative expression calculated using the 2<sup>-ΔΔCt</sup> method.

### **Western blot analysis**

After protein extraction from RKO cells, the protein concentrations of different groups were quantified using a commercial BCA kit. Electrophoresis was performed for 2 h at 4 °C and 300 mA, and the protein

Table 1 Quality check results

Order number	Sample number	Sample name	Thermo NanoDrop 2000		2100 result		Results
			Concentration (ng/ $\mu$ L)	A260/A280	RIN	28S/18S	
1	Y9148-1	NC	739.969	1.951	10	2.1	Pass
2	Y9148-2	NC	688.748	1.979	10	2.1	Pass
3	Y9148-3	NC	668.435	1.944	10	1.9	Pass
4	Y9149-1	KD	676.797	1.93	10	1.7	Pass
5	Y9149-2	KD	697.671	1.958	10	1.7	Pass
6	Y9149-3	KD	678.338	1.971	10	1.7	Pass

NC: RKO cells infected with centromere protein K negative control virus; KD: RKO cells with centromere protein K gene short hairpin RNA virus infection.

Table 2 Clustering of clinical data

Number	Variable	Group 1	Group 2
1	Age (yr)	< 57	> 57
2	Sex	Male	Female
3	T stage	T1/2/3	T4
4	N metastasis	N0	N1/2
5	Pathological grade	1/2	3
6	Clinical stage	I/II	III/IV

was transferred to polyvinylidene fluoride (PVDF) membranes (IPVH00010; Millipore) for immunostaining. The PVDF membranes were incubated in TBST solution containing 5% skimmed milk at room temperature for 1 h. The antibodies were diluted in the blocking solution and then incubated with the PVDF membranes for 2 h at room temperature. The antibodies applied in the present study included those against Yes-associated protein isoform 1 (YAP1) (ab52771; Abcam), CENPK (ab13939; Abcam), CUL4A (ab92554; Abcam), F-box protein 32 (FBX32) (ab168372; Abcam), X chromosome-linked inhibitor of apoptosis (XIAP) (ab28151; Abcam), heat shock protein 90 family class A member 1 (HSP90AA1) (4877; Cell Signaling Technology), class III-tubulin (TUBB3) (#5568; Abcam), and mitogen-activated protein kinase kinase kinase 7 (MAP3K7) (ab109526; Abcam). After primary antibody incubation, the membranes were washed three times with TBST (10 min each) and incubated with the secondary antibodies mouse immunoglobulin G (IgG) (1:2000, sc-2005; Santa Cruz Biotechnology) and rabbit IgG (1:2000, sc-2004; Santa Cruz Biotechnology) at room temperature for 2 h. The Pierce ECL Western Blotting Substrate kit (Thermo) was used for X-ray photography.

#### Establishment and examination of a tumor model

The Ethics Committee of The Affiliated Hospital of Inner Mongolia Medical University approved the study. RKO cells with sufficient logarithmic growth were digested with trypsin and suspended in culture medium with the final cell density adjusted to  $2.0 \times 10^7$ /mL. To establish the tumor model,  $4.0 \times 10^6$  cells were subcutaneously injected into mice. The tumor size and animal body weight were measured 5-20 d later. The tumor volume was calculated as  $\pi/6 \times L \times W \times W$ , where L represents the long diameter, and W and W represent the short diameter. Cancer progression was imaged at 10 d after tumor formation (animals were fasted for 1 d in advance to reduce fluorescence interference) with intraperitoneal injection of 10  $\mu$ L/g D-luciferin (Bench Mark 15 mg/mL) into mice. After anesthesia by intraperitoneal injection of 10  $\mu$ L/g pentobarbital solution (BM 7 mg/mL), the mice underwent imaging examination, quantitative analysis, and total fluorescence examination to determine the CENPK function *in vivo*. After imaging, the experimental animals were killed with an overdose of 2% sodium pentobarbital (0.5 mL) and were in a complete coma before removal of the cervical spine to confirm death. Animals were dissected with medical scissors and tweezers to observe the lungs, liver, and other organs and tissues, which were removed for imaging to observe biological changes and measure the fluorescence.

### **Construction and packaging of lentiviral vectors**

293T cells for lentivirus packaging were cultured in Dulbecco's modified Eagle's medium supplemented with 10% FBS. The scramble order for the RNAi negative control was TTCTCCGAACGTGTCACGT. Vector enzyme digestion products were obtained for agarose gel electrophoresis to recover bands of interest. The framework of the viral vector was constructed, and single-strand primers were synthesized. Double-stranded DNA was formed by annealing the primer to the vector. After transformation, the bacterial colonies were assessed by PCR. Identified positive carbendazim transformants were inoculated into Luria-Bertani (LB) liquid medium containing an appropriate amount of antibiotics, and an appropriate amount of bacterial solution was incubated at 37 °C for 12-16 h. The incubated bacterial solution was transferred to 10 mL LB liquid medium containing the corresponding antibiotics for culture at 37 °C overnight. The plasmid was extracted with the small medium-lift kit from Tiangen, and the qualified plasmid was extracted for the following experiments.

### **Lentiviral infection**

The lentivirus-infected HCT116 cells are shown in Table 3. RKO and HCT 116 cells ( $2 \times 10^5$  cell/mL) were cultured in RPMI 1640 medium containing 10% FBS with polybrene in six-well plates. The following experimental groups were used: (1) Cells (RKO or HCT 116 cells) infected with CENPK negative control virus [NC (KD)]; (2) Cells with lentivirus-mediated shRNA interference of CENPK (KD); (3) Cells with overexpression and negative control virus interference [NC (OE)]; (4) Cells virally infected with CUL4A (OE); (5) Cells with shRNA interference of CENPK and overexpression of negative control virus [KD + NC (OE)]; and (6) Cells with lentivirus-mediated shRNA interference of CENPK and CUL4A (KD + OE).

For the lentiviral infection, media for adherent cell inoculation and viral infection were used at a 1:1 ratio in 96-well plates. The culture medium was replaced, and the optimal amount of virus was added for the infection. The most appropriate time point after infection was selected for the replacement of conventional medium and continued culture, 8-12 h after infection. When fluorescently labeled lentiviral infection occurred, the green fluorescent protein reporter signal was observed by fluorescence microscopy 72 h after infection. After infection efficiency reached 80%, 0.5 mL of puromycin was used for cell function experiments. Western blot and qPCR analysis were performed to confirm the knockdown of CENPK.

### **Detection of cell growth**

The proliferation potential of RKO and HCT 116 cells was analyzed by cell growth curve and MTT assay. For the cell growth curve assay, RKO and HCT 116 cells of different groups [shCtrl and shCENPK or NC, NC (KD), NC (OE), OE, KD + NC (OE), and KD + OE] were collected, replated in 24-well plates at 2000 cells/well, and cultured at 37 °C in a 5% CO<sub>2</sub> incubator for 5 d. Beginning on day 2, the optical absorption value of each group was checked once daily and the number of fluorescent cells calculated. A growth curve was drawn to show cell proliferation.

For the MTT assay, RKO and HCT 116 cells were replated in 24-well plates at 2000 cells/well and cultured at 37 °C in a 5% CO<sub>2</sub> incubator for 24 h. Subsequently, 20  $\mu$ L MTT (5 mg/mL) was added to the wells. After incubation for 4 h, reactions were stopped with 100  $\mu$ L DMSO. After shaking for 2-5 min, the OD value at 490/570 nm was determined (M2009PR, Tecan Infinite).

### **Apoptosis detection**

Apoptosis was analyzed by flow cytometry (fluorescence-activated cell sorting; FACS) with a commercial Annexin V-APC kit (88-8007, eBioscience). RKO and HCT 116 cells of each group were collected after washing in  $1 \times$  binding buffer, and centrifuged at 1300 rpm for 3 min. After centrifugation, the cell suspension was prepared by adding 200  $\mu$ L of  $1 \times$  binding buffer. Subsequently, 10  $\mu$ L of Annexin V-APC staining solution was added to the suspension. After incubation in the dark at room temperature for 10-15 min, 400  $\mu$ L of  $1 \times$  binding buffer was added to the cell suspension, and FACS was conducted for apoptosis detection.

### **Caspase 3/7 detection**

Caspases 3/7 were detected in RKO and HCT 116 cells using a commercial Caspase-Glo3/7 detection kit (G8091, Promega). For the preparation of Caspase-Glo reaction solution, 10 mL of caspase-Glo3/7 buffer was added and vortexed until the dissolve of substrates. After collection and counting, the RKO and HCT 116 cells at a final density of  $10^4$  cells/well were replated in 96-well plates, and an empty control group containing culture medium without RKO or HCT 116 cells was established. Next, 100  $\mu$ L of Caspase-Glo reaction solution was added to each well and shaken for 30 min at 500 rpm at room temperature for 2 h. The signal strength was measured using a microplate reader (M2009PR, Tecan Infinite).

### **PathScan® array detection**

RKO cells were incubated with 1 mL of  $1 \times$  cell lysis buffer (Cell Signaling Technology) containing 1 mmol/L PMSF on ice for 2 min. Then, 100  $\mu$ L of blocking solution was added to RKO cells with the cell

Table 3 Lentiviral-infected HCT 116 cells

Virus number	Experimental group	Virus titer	Virus infection dose
psc3741	NC (KD)	2.0E + 08 TU/mL	10.00 $\mu$ L
LVpGCSIL-004PSC45249-1	KD	3.0E + 08 TU/mL	6.67 $\mu$ L
KL9688-21	NC (OE)	4.0E + 8 TU/mL	5.00 $\mu$ L
LVKL6733-2	OE	2.0E + 08 TU/mL	10.00 $\mu$ L
LVpGCSIL-004PSC45249-1+ KL9688-21	KD+NC (OE)	3.0E + 08 + 2E + 8 TU/mL	3.33 + 5.00 $\mu$ L
LVpGCSIL-004PSC45249-1+ LVKL6733-2	KD+OE	3.0E + 08 + 2E + 8 TU/mL	3.33 + 5.00 $\mu$ L

NC: HCT 116 cells infected with centromere protein K negative control virus; KD: HCT 116 cells with centromere protein K gene short hairpin RNA virus infection; OE: HCT 116 cells virally infected with Cullin 4A.

lysate samples shaken at room temperature for 15 min. After incubation at room temperature for 2 h, the cell lysate samples were washed with 1  $\times$  cleaning solution on a horizontal shaker for 5 min. After three washes, 75  $\mu$ L of 1  $\times$  antibody was added to the cell lysate samples and incubated on a horizontal shaker for 1 h. Then, 75  $\mu$ L of 1  $\times$  HRP-linked streptavidin solution was added, followed by incubation on a horizontal shaker for 1 h. 1  $\times$  array cleaning solution was added to the cell lysate samples, which were then washed on a horizontal shaking bed four times (5 min each). The slides were placed in 1  $\times$  cleaning solution and then in exposure liquid (9 mL deionized water + 0.5 mL lumiGlo + 0.5 mL hydrogen peroxide) for 1-2 s, followed by observation with a chemiluminescence imaging system (ChemiScope 5300; Clinx Science Instruments).

### Statistical analysis

Statistical analyses were performed using SPSS version 19.0 (IBM Corp.). Data are presented as the mean  $\pm$  SD. Data comparing two samples were analyzed using student's *t*-test. Comparisons of datasets containing > 3 groups were evaluated by one-way repeated-measures ANOVA followed by the Bonferroni *post hoc* test. Gene expression of cancer and noncancer tissue groups was evaluated by the Mann-Whitney *U* test. *P* < 0.05 was considered to indicate a significant difference.

## RESULTS

### Lentivirus infection for inducing CENPK knockdown

For lentiviral infection marked with antibiotic resistance genes, the antibiotics (such as puromycin) were used to screen cells after 72 h, and the infection efficiency was approximately 80% for fluorescence labeled lentivirus infection (Figure 1A). CENPK knockdown efficiency in RKO cells in the KD group reached 86.1% compared to the NC group (23.4%) (Figure 1B). This analysis revealed the genes related to tumor cell proliferation and invasion. The genes that inhibited tumor cell proliferation or tumor invasion were selected, together with the target genes of concern, to develop a gene relationship network diagram. This analysis suggested that CENPK affected the proliferation and invasion of cells by acting on YWHAZ and BMI1, which affected the performance of downstream genes. The gene interaction network diagram shows a network of interaction relationships between molecules within a determined functional region. Different shapes represent genes, proteins, and chemicals in the network maps (Figure 1C).

### Screening of target genes CENPK by chip detection

The original quality evaluation for the quality control data and the remaining data meeting the filter standards, including significant difference analysis and functional analysis of differential genes, was used to evaluate the tumor occurrence, development, metastasis, and other molecular mechanisms using chip information analysis for target screening and drug design. Figure 2A shows the signal strength distribution of the entire chip probes. Better signal intensity distribution curves of different samples indicated higher reliability of the chip experiment. The average Z score of all samples within one signal strength range was < 2, which supported the reliability of all chip results meeting the continuing analysis criteria. Figure 2B shows the distribution of the relative logarithmic signal strength for all chips. Closer distribution of the relative logarithmic signal strength box diagram indicated better repeatability of the data. The median Z score for all samples was < 2, which indicated good repeatability of the chip experiments in the project that met the continued analysis criteria. The Pearson correlation coefficient distribution diagram shows the level of correlation of the signal strength between all chips, where each lattice represents the degree of correlation between two samples corresponding to the

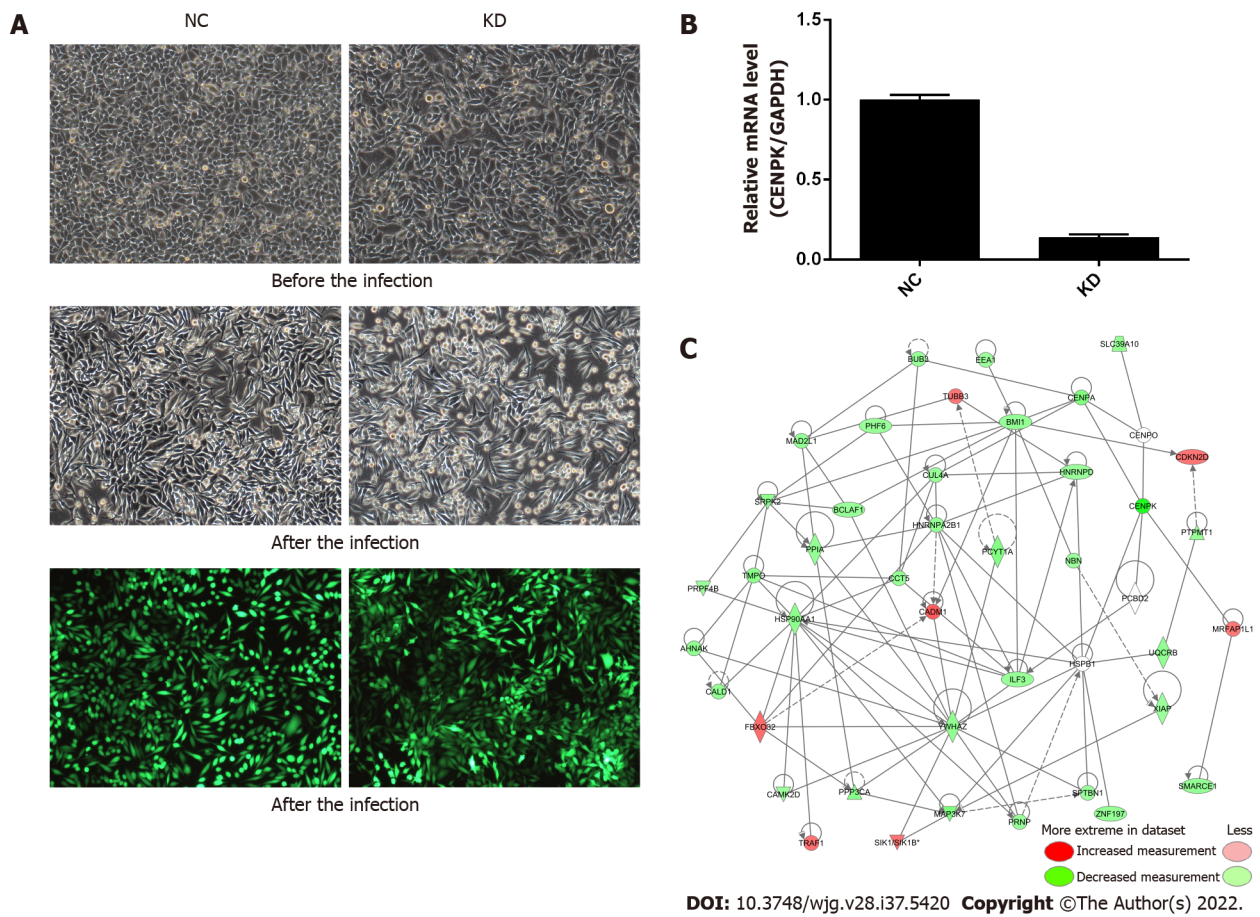
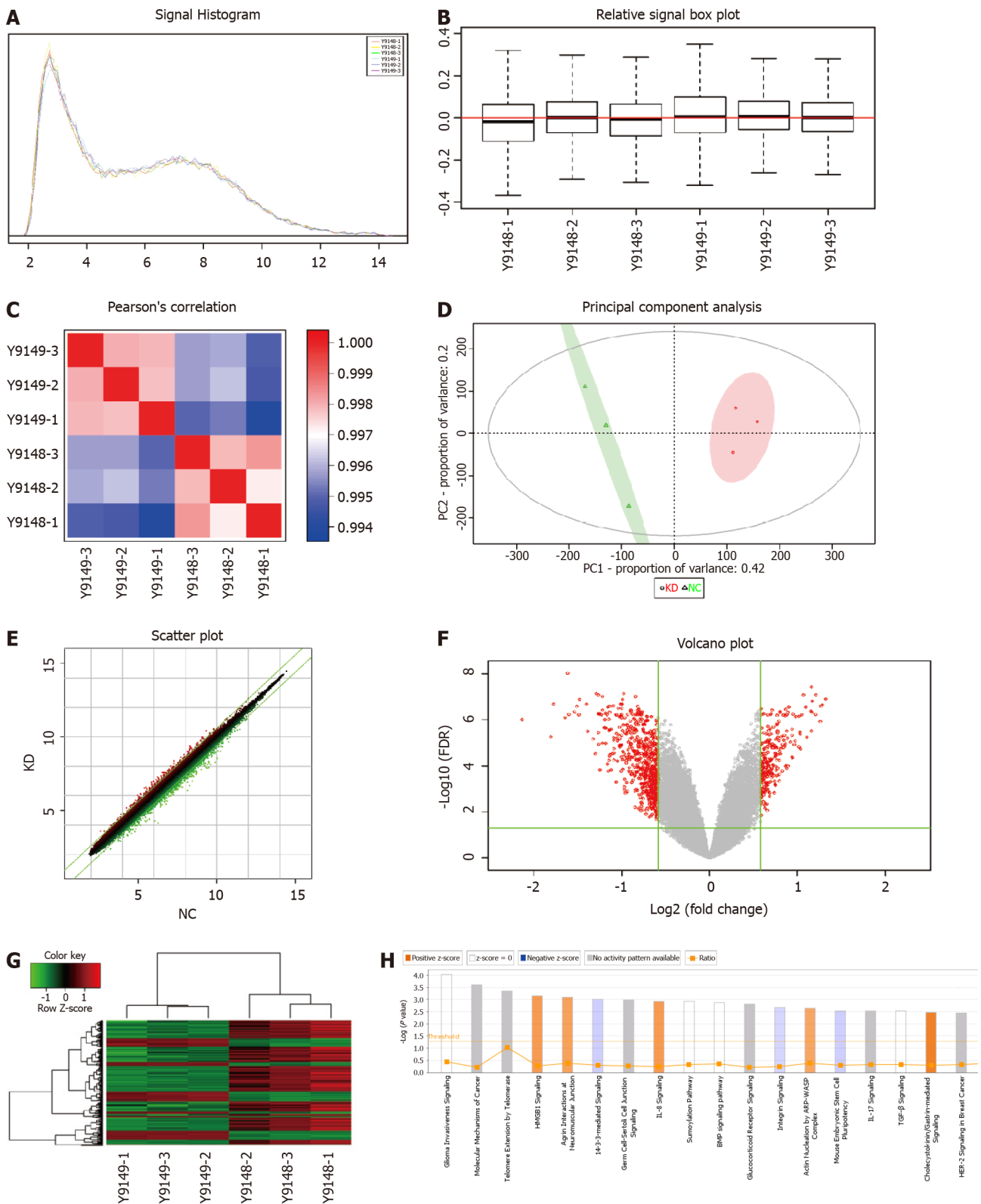


**Figure 1 Centromere protein K affects the proliferation and invasion of colorectal cancer cells by acting on downstream genes.** A: Morphology of RKO cells in NC and KD groups before and after lentivirus infection as well as infection efficiency assessed using fluorescence microscopy ( $\times 100$  magnification); B: Relative expression level of centromere protein K by quantitative polymerase chain reaction in NC and KD groups; C: Gene interaction network diagram. Genes, proteins, and chemicals are represented by different shapes; color labeling of molecules is shown in the illustration. NC: RKO cells infected with centromere protein K negative control virus; KD: RKO cells with lentivirus-mediated short hairpin RNA interference of centromere protein K; CENPK: Centromere protein K.

ordinate and transverse (Figure 2C). The group sample gene expression patterns were typically similar and demonstrated a high correlation coefficient, as shown in red in the correlation coefficient distribution diagram. The gene expression pattern difference between groups demonstrated a low correlation coefficient, which is shown in blue in the correlation coefficient distribution diagram. The correlation coefficient in the KD and NC groups was  $> 0.99$ , which indicated a high similarity of gene expression in the same group. The intergroup correlation coefficient was significantly lower than the group correlation coefficient, which indicated a large difference between groups that met the continuing analysis standard.

From the PCA score chart (Figure 2D), there was an obvious sample aggregation trend in the PC1 and PC2 dimensions in the KD and NC groups and an obvious intergroup separation trend, which indicated similar samples and significant differences between groups that met the standard of the continuing analysis. The cross ordinate of each point in Figure 2E represents the signal strength of a probe group in the NC and KD groups. The parallel green solid line is the reference line difference, and the points in the interval within the reference line represent the probe group without a significant change. The red point outside the interval represents the relatively elevated probe group in the KD group, and the green point represents the relatively elevated probe group in the NC group. A volcano graph was drawn using gene expression differences (fold change) and false discovery rate (FDR) tests between the two samples to show the significant differences between the two samples (Figure 2F). Thermal mapping of KD and NC samples was performed using the differential expression spectrum of genes screened by  $|\text{fold change}| \geq 1.5$  and  $\text{FDR} < 0.05$  (Figure 2G). Figure 2H shows the significant enrichment of differentially expressed genes in the classical pathway. The orange notation indicates an activated pathway ( $Z > 0$ ); the blue label indicates inhibition of the pathway ( $Z < 0$ ); shades of orange and blue (or absolute Z values) represent the degree of activation or inhibition ( $Z \geq 2$  represents a significant activation and standard, and  $Z \leq -2$  denotes significant suppression); and the ratio represents the ratio of the difference of the gene number in this signaling pathway to all genes contained in the pathway. G1/S checkpoint regulation was activated in the cell cycle, and Z was 2.236.



DOI: 10.3748/wjg.v28.i37.5420 Copyright ©The Author(s) 2022.

**Figure 2 Screening of target genes by chip detection.** A: Signal strength distribution curve diagram, with the cross coordinates representing the probe signal strength range and the longitudinal coordinates representing the number of probe sets within the signal strength range; B: Relative line ram of the logarithmic signal strength, with the horizontal coordinate representing the sample name, the vertical coordinate indicating the relative logarithmic signal strength, the red line in the middle representing the average of the relative logarithmic signal strength of all samples, and the upper and lower horizontal lines representing the 90% confidence interval. The upper and lower edges represent the upper and lower quartiles, and the black line in the middle represents the median; C: Distribution diagram of the Pearson correlation coefficient among samples. The correlation coefficient indicates a positive correlation of the expression mode of genes in two subjects, and a negative value indicates an expression mode with a negative correlation. As the absolute value of the correlation coefficient approaches 1.0, the correlation increases; D: Principal component analysis. Red dots represent normal purpose cells with centromere protein K (CENPK) gene short hairpin RNA virus infection (KD) samples, and green dots represent normal purpose cells infected with CENPK negative control virus (NC) samples; E: Scatter diagram. The cross

coordinate represents the NC group, and the vertical coordinate represents the KD group; F: Volcano map, where the cross coordinate is a difference multiple (the logarithmic change in the bottom 2); longitudinal significance false discovery rate (FDR) (of the difference in the bottom 10 Logarithmic change); significantly different genes screened by  $|\text{fold change}| \geq 1.5$  and  $\text{FDR} < 0.05$  in red, and other genes with no significant difference in gray; G: Cluster analysis results. Each column represents a sample, and each row represents a differentially expressed gene; H: Statistics for the classical pathway enrichment analysis. The transverse coordinate is the path name and the longitudinal significance level of enrichment (negative logarithmic transformation in the bottom 10).

G1/S checkpoint regulation was significantly activated. Red represents significant upregulation, and green represents the genes. **Figure 3A** shows the changing trend of gene expression in the pathway, which provided the basis for the study of the molecular mechanisms involved in the changes between sample groups. The upstream regulator network diagram (**Figure 3B**) shows the interaction between upstream regulators and downstream molecules that were directly associated in the dataset. Let-7 significantly suppressed SOX9 mRNA levels, and consistent trends were observed between let-7 and signal sequence receptor 1. **Figure 3C** shows the significant enrichment of differentially expressed genes in disease and function. According to the internal algorithms and standards of IPA,  $Z \geq 2$  denoted significant activation of the disease or function, and  $Z \leq -2$  indicated significant suppression of the disease or function. Significantly activated diseases or functions included morbidity or mortality ( $Z = 4.216$ ) and organismal death ( $Z = 4.164$ ). Significantly suppressed diseases or functions included infection by human immunodeficiency virus 1 ( $Z = -3.335$ ) and viral infection ( $Z = -3.2$ ) (**Figure 3D**). The network contains all the differentially expressed genes associated with the specified disease or function, and demonstrates possible interactions and changes in expression trends between genes based on the ingenuity knowledge base (**Figure 3E**). The top ranked regulatory network in this regulatory effect analysis suggested that the dataset was inhibitory due to the regulator miR-8 in the binding of tumor cell lines and the proliferation of stem cells *via* BMI1, COMMD3-BMI1, HMGB1, and YAP1 (**Figure 3F**). The network of interactions between molecules of a disease or function-related relationship is shown in **Figure 3G**.

Based on the above biological analysis, we speculated that CENPK was more likely to function in CRC by regulating the expression of the above-mentioned genes. Therefore, these genes were selected for western blot validation. Western blot analyses and qPCR showed that expression of FBX32 was upregulated, and CUL4A and YAP1 were downregulated (**Figures 4A-D**). Taken together, these results suggested that CENPK played a role in CRC by regulating FBX32, CUL4A, YAP1, and other genes in RKO cells.

### High expression of CENPK in CRC

The expression of CENPK in CRC tissue was measured using immunohistochemistry to detect target protein expression and localization in tissue cells. Expression of CENPK was higher in cancerous than in paracancerous tissues (**Figure 5A**). Positive expression of CENPK in the cancerous and noncancerous tissues exhibited a differential multiple of 2.61, which was a significant difference (**Figure 5B**). Expression and proportional statistics of the CENPK gene in cancerous and noncancerous tissue are shown in **Table 4**.

CENPK gene expression in cancerous and noncancerous tissues is shown in **Table 5**. The differential expression of CENPK gene in cancerous and noncancerous tissues was analyzed using the Mann-Whitney *U* test. The significantly higher expression of CENPK in cancerous than in noncancerous tissues ( $P < 0.05$ ) supports CENPK as an effective diagnostic marker for CRC. The expression and proportion of CENPK genes in cancerous tissues are shown in **Table 6**. The CENPK gene expression in different types of clinical experiment, including sex, age, T stage, and N metastases, was analyzed to compare its low expression and high expression. Expression of CENPK gene in cancerous tissue differed significantly according to T stage, N stage, and clinical stage, which suggested that CENPK expression was associated with these pathological indicators. The correlation between CENPK expression and clinical data (T stage, N stage, and clinical stage) in cancerous tissues was examined using Spearman's test, and the potential role of these clinical data in the development of CRC was examined (**Table 7**). Expression of the CENPK gene in cancerous tissues was positively correlated with T stage, N stage, and clinical stage, which suggested that low CENPK expression in the early stage of cancer gradually increased with the disease course.

### shRNA lentivirus infects RKO cells and inhibits the growth of tumor cells

RKO cells infected by viruses were subcutaneously injected into nude mice for analysis of tumor growth conditions (**Figure 6**). RKO cells were infected with lentivirus, and there was no significant cell death, especially in the NC group, which was comparable to the control group. In contrast, the infection efficiency reached approximately 80% in the KD group (**Figure 6A**). The infection efficiency in the target screening experiment was  $> 90\%$  in the KD group. Therefore, the good cell conditions and qualified infection efficiency up to 80% were used for downstream testing. Here, RKO cells were injected subcutaneously into the nude mice to analyze the tumor growth conditions and detect the infection efficiency of RKO cells. Based on the PCR results, CENPK gene knockdown efficiency in RKO cells reached 83.2% in the KD group compared to the NC group. The tumor status (the tumor formed and

**Table 4 Expression and proportional statistics of the centromere protein K gene in cancerous and noncancerous tissue by immunohistochemical staining.**

	Case group		P value
	Cancerous tissues	Noncancerous tissue	
Higher expression	4	5	0.008
Lower expression	10	0	

**Table 5 Tissue type group \* gene expression group using the Mann-Whitney U test**

		CENPK gene expression group		Total	P value
		Low expression	High expression		
Tissue type group	Cancerous tissues	146	160	306	0.000
	Noncancerous tissue	27	1	28	
Total		173	161	334	

CENPK: Centromere protein K.

**Table 6 Clinical data \* gene expression group analysis using the Mann-Whitney U test**

		CENPK gene expression group		Total	P value
		Low expression	High expression		
Sex	Male	88	103	191	0.460
	Female	58	57	115	
Total		146	160	306	
Age	< 57	75	82	157	0.983
	> 57	71	78	149	
Total		146	160	306	
T stage	T1/2/3	108	98	206	0.018
	T4	38	62	100	
Total		146	160	306	
N metastasis	N0	117	108	225	0.012
	N1/2	29	52	81	
Total		146	160	306	
Pathological grade	1/2	111	114	225	0.130
	3	29	45	74	
Total		140	159	299	
Clinical stage	I/II	116	108	224	0.019
	III/IV	30	52	82	
Total		146	160	306	

CENPK: Centromere protein K.

size) was good 1 d after subcutaneous injection. Over 20 d, the tumors gradually decreased and even disappeared in the KD group, but they persisted in the NC group (Figure 6C). Tumors in mice were analyzed using live imaging. The total fluorescence expression volume in ten nude mice in the KD and NC groups was measured *via* quantitative analysis of fluorescence (Figures 6D and 6E). Total fluorescence expression in the region was significantly decreased in the KD group compared to the NC



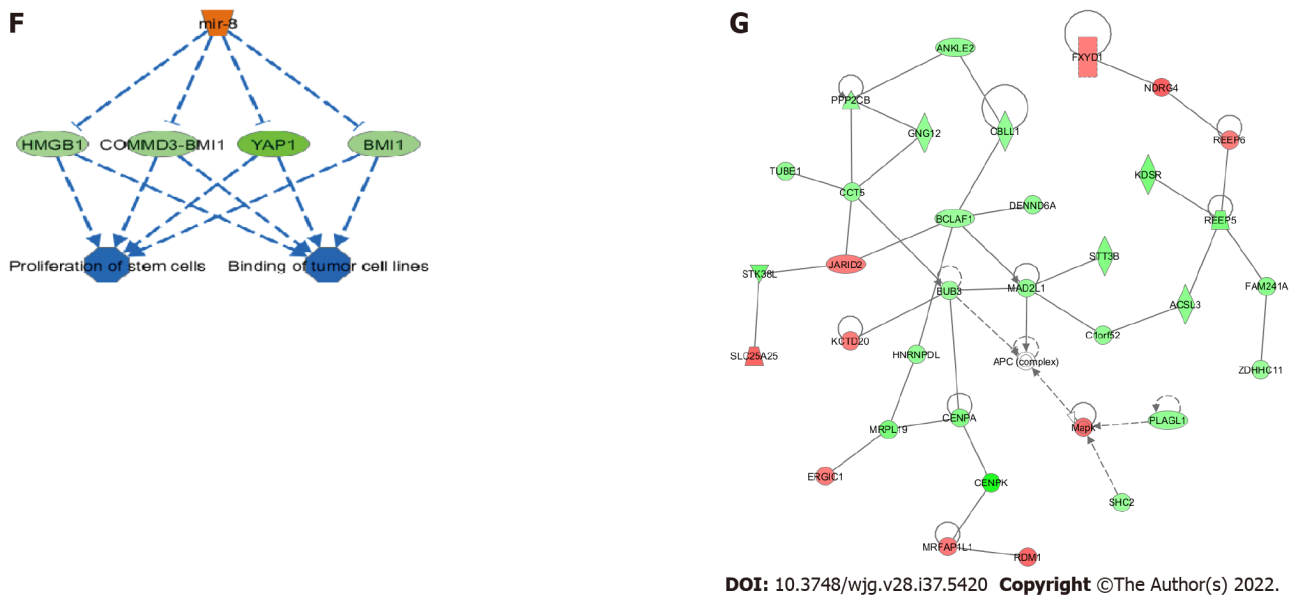


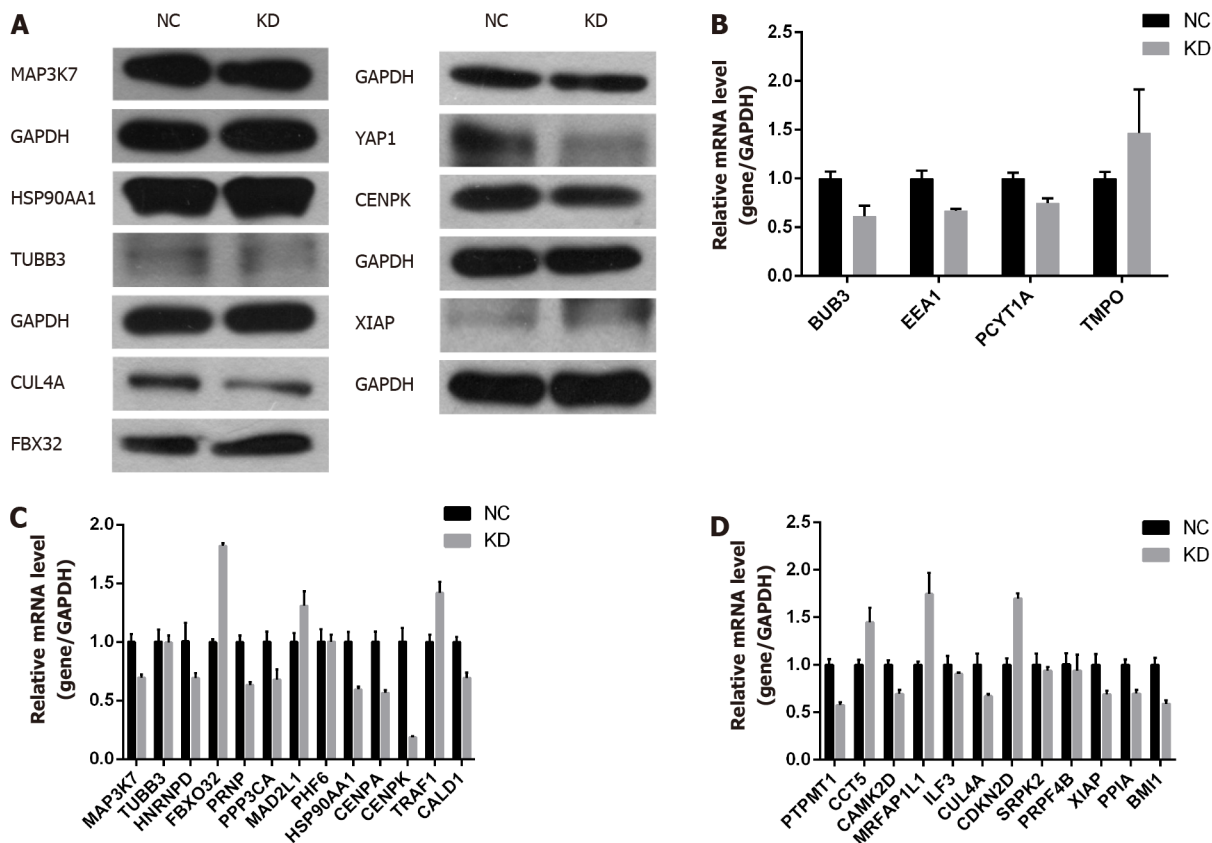
**Figure 3 Centromere protein K functions in colon cancer by regulating the expression of related genes.** A: Trend of molecules in the experimental results in the classical pathway; B: Upstream regulator network diagram (the orange line indicates consistent activation of upstream regulators and genes, the blue line indicates consistent upstream regulators and gene inhibition, the yellow line indicates inconsistent expression trends between upstream regulators and genes, and the gray line indicates that there is no prediction information related to the expression state in the dataset); C: Analysis and statistics of disease and functional enrichment (the transverse coordinate is the path name and the longitudinal coordinate is significance level of enrichment (negative logarithmic transformation in the bottom 10)); D: Disease and functional heatmap of the effect of disease and functional changes at gene expression levels; E: Activation and inhibition relationship between genes and disease or function; F: Interplay between genes and regulators and function in the dataset; G: Network of interaction relationships between molecules of a disease or function-related relationship. TGF- $\beta$ : Transforming growth factor beta; FOXO: Forkhead box O; SMAD: Suppressor of mothers against decapentaplegic; MDM: Mouse double minute; ATM: Ataxia telangiectasia mutated; ATR: Ataxia telangiectasia and Rad3 related; PAK: p21 activated kinases; NS: Non-structural; MAX: MYC associated factor X; c-MYC: Cellular myelocytomatosis oncogene; SCF: Stem cell factor; INK: CDKN2A, cyclin dependent kinase inhibitor 2A; BMI 1: BMI1 proto-oncogene; GSK: Guanosine kinase; CDK: Cyclin-dependent kinase; NRG: Neuregulin; EBP1: ErbB3-binding protein 1; SIN3A: Suppressor interacting 3a; SUV39H1: SUV39H1 histone lysine methyltransferase; DP-1: Dodeca-satellite-binding protein 1; E2F: Early region 2 binding factor; RB: Retinoblastoma; HDAC: Histone deacetylase; CD44: Cluster of differentiation-44; DDX18: DEAD-box helicase 18; HMGA: High mobility group A; MAD2L1: Mitotic arrest deficient 2 like 1; MCM: Mei-mini-chromosome maintenance; PLAGL: Pleiomorphic adenoma gene-like; SOX: SRY-box transcription factor; SSR: Signal sequence receptor subunit; YAP1: Yes1 associated transcriptional regulator; CCNE2: Cyclin E2; COMMD3: COMM domain containing 3.

group (Figure 6H). Tumor weight and volume were significantly decreased in the KD group compared to the NC group ( $P < 0.05$ ) (Figures 6F and 6G). Therefore, lentiviral infection of RKO cells inhibited the growth of tumor cells *in vivo*.

#### Effect of CENPK on proliferation of RKO cells

Expression of CENPK gene in CRC cells is shown in Figure 7A, and the target gene expression abundance was relatively low. Based on the mRNA level, the CENPK gene reduction efficiency was examined using qPCR. Expression of the CENPK gene in RKO and HCT116 cells in the experimental group was inhibited after 3 d of shRNA lentivirus infection (Figures 7B and 7C). Target reduction of foreign proteins due to CENPK gene expression was detected using western blot, which showed that shCENPK had a significant knockdown effect on the exogenous expression of CENPK gene at the protein level in 293T cells (Figure 7D). Endogenous protein expression of CENPK showed that shCENPK had a significant knockdown effect on endogenous CENPK expression at the protein level in RKO cells (Figure 7D). Endogenous expression of CENPK was knocked down at the protein level in HCT116 cells (Figure 7D).

After 3 d of shRNA lentivirus infection, 1500 cells were seeded in 96-well plates. The effect of CENPK on cell proliferation *via* Celigo detection showed that proliferation of RKO cells was significantly inhibited in the experimental group. Celigo continuous detection for 5 d suggested that the CENPK gene was significantly associated with RKO and HCT116 cell proliferation (Figures 7E-H). To examine the effects of gene reduction on cell proliferation after 3 d of shRNA lentivirus infection, the cells were seeded in 96-well plates. After 5 d, the proliferation rate of RKO and HCT116 cells in the experimental group was significantly inhibited, which suggests a significant correlation between CENPK gene and RKO and HCT116 cell proliferation (Figure 7G). Detection of the effect of CENPK gene reduction on apoptosis using FACS showed that after 5 d of shRNA lentivirus infection, RKO and HCT116 cells in the experimental group increased significantly, which suggested that the CENPK gene was significantly related to apoptosis of RKO and HCT116 cells (Figure 7J, Supplementary Figures 1 and 2). Based on the detection of CENPK for apoptosis, caspase 3/7 activity was increased after 3 d of shRNA lentivirus infection in the experimental group, which suggested that CENPK gene was significantly related to



DOI: 10.3748/wjg.v28.i37.5420 Copyright ©The Author(s) 2022.

**Figure 4 Centromere protein K plays a role by regulating F-box protein 32, Cullin 4A, Yes-associated protein isoform 1, and other genes in RKO cells.** A: Downstream gene (Yes-associated protein isoform 1, centromere protein K, Cullin 4A, F-box protein 32, X chromosome-linked inhibitor of apoptosis, heat shock protein 90 alpha family class A member 1, class III-tubulin, and mitogen-activated protein kinase kinase kinase 7) testing using western blot analysis in NC and KD groups; B-D: Relative gene expression detected using quantitative polymerase chain reaction in NC and KD groups. F-box protein 32 was upregulated, while Cullin 4A and Yes-associated protein isoform 1 were downregulated. FBX32: F-box protein 32; YAP1: Yes-associated protein isoform 1; CENPK: Centromere protein K; CUL4A: Cullin 4A; XIAP: X chromosome-linked inhibitor of apoptosis; HSP90AA1: Heat shock protein 90 alpha family class A member 1; TUBB3: Class III-tubulin; MAP3K7: Mitogen-activated protein kinase kinase kinase 7; BUB3: BUB3 mitotic checkpoint protein; EEA1: Early endosomal antigen 1; PCYT1A: Phosphate cytidyltransferase 1A; TMPO: Thymopoietin; HNRNP: Heterogeneous nuclear ribonucleoprotein D; PRNP: Prion protein; PPP3CA: Protein phosphatase 3 catalytic subunit alpha; MAD2L1: Mitotic arrest deficient 2 like 1; PHF6: PHD finger protein 6; CENPA: Centromere protein A; TRAF1: TNF receptor associated factor 1; CALD1: Caldesmon 1; PTPMT1: Protein tyrosine phosphatase mitochondrial 1; CCT5: Chaperonin containing TCP1 subunit 5; CAMK2D: Calcium/calmodulin dependent protein kinase II delta; MRFAP1L1: Morf4 family associated protein 1 like 1; ILF3: Interleukin enhancer binding factor 3; CDKN2D: Cyclin dependent kinase inhibitor 2D; SRPK2: SRSF protein kinase 2; PRPF4B: Pre-mRNA processing factor 4B; PPIA: Peptidylprolyl isomerase A; BMI1: BMI1 proto-oncogene; GAPDH: Glyceraldehyde-3-phosphate dehydrogenase. NC: RKO cells infected with CENPK negative control virus; KD: RKO cells with lentivirus-mediated short hairpin RNA interference of CENPK.

apoptosis of RKO and HCT116 cells (Figure 7I). Therefore, CENPK gene inhibited proliferation of RKO cells. After RNAi of the CENPK gene in RKO cells, associated genes in the signaling pathway were detected using PathScan. The protein expression levels in the p-ERK1/2, p-Stat1, p-Stat3, p-Akt (Ser473), p-HSP27, p-p70 S6 kinase, p-PRAS40, and p-p38 signaling pathways were significantly different ( $P < 0.05$ ) (Figure 7K).

**Inhibition of RKO and HCT116 cells by abrogation of CENPK and overexpression of CUL4A**

Lentivirus-mediated shRNA interference of CENPK in HCT116 cells and RKO cells was observed (Figure 8). The control and target lentivirus-infected cells (HCT116 cells and RKO cells) were observed after 72 h under a microscope, and cell infection efficiency reached > 80%, and the cell state was normal. The effects of CENPK gene reduction and CUL4A gene overexpression on HCT 116 and RKO cell proliferation using Celigo detection are shown in Figures 9A-D. At 3 d after lentiviral infection, the number of HCT 116 cells was 1000, and the number of RKO cells was 2000. After 5 d, the KD group exhibited slower cell proliferation compared to the NC (KD) group. Cell proliferation increased rapidly in the KD + OE and NC (OE) groups compared to the KD + NC (OE) and OE groups in HCT 116 cells (Figures 8A and 8B, Supplementary Figures 3 and 4) and RKO cells (Figures 6C and 6D). HCT 116 and RKO cell proliferation was measured using the MTT assay (Figures 9E-H). Cell proliferation increased slowly in the KD group compared to the NC (KD) group, but it increased rapidly in the OE group compared to the NC (OE) group. However, RKO cell proliferation was not consistently increased in the KD + OE

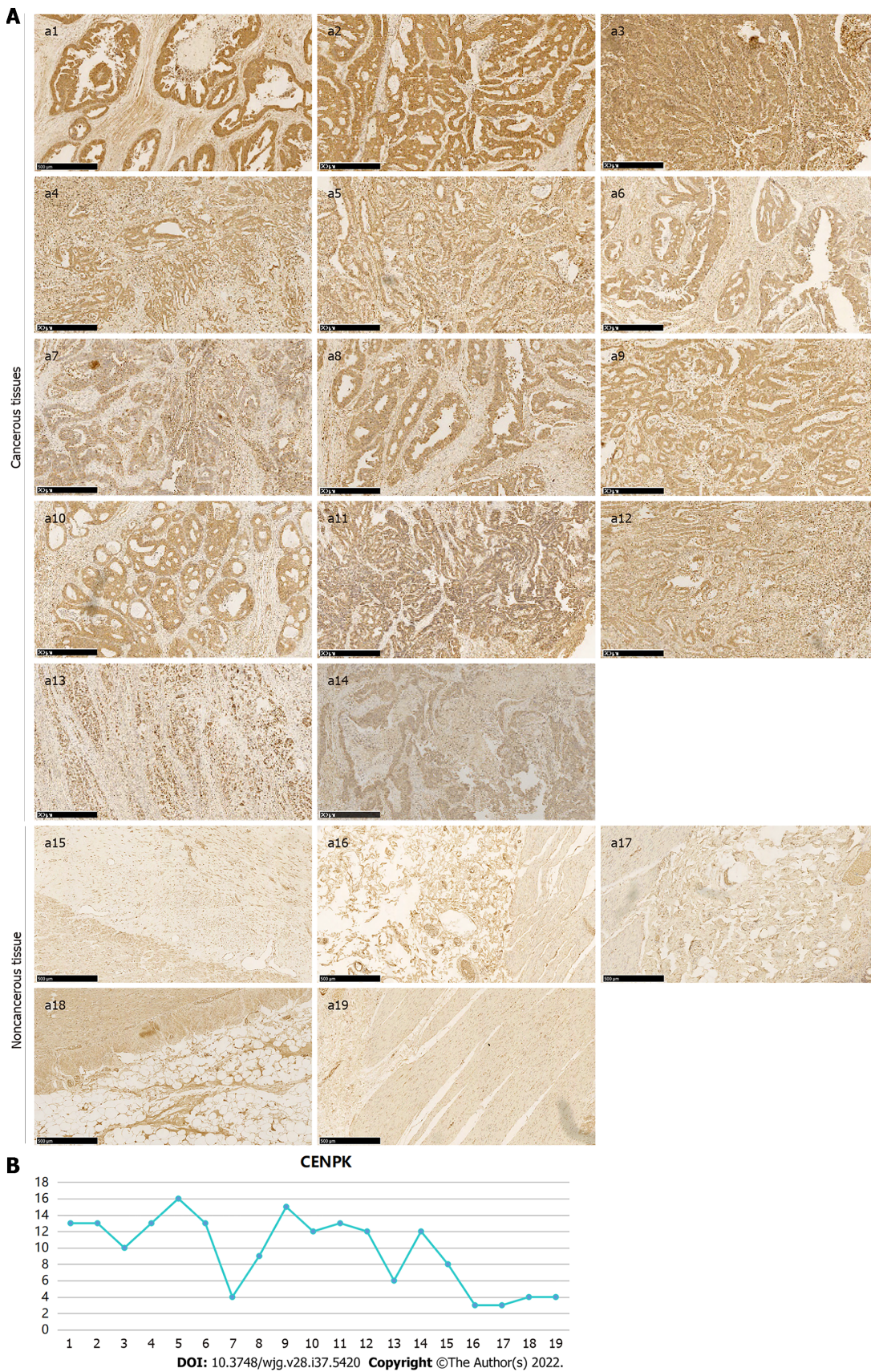


**Figure 5** Expression of centromere protein K in colon cancer tissue and noncancerous tissue detected using immunohistochemistry. A: Centromere protein K (CENPK) expression in cancerous (a1-a14) and noncancerous tissue (a15-a19) using immunohistochemistry (Scale bar: 500 μm) with VULCAN FAST RED CHROMOGEN kit 2; B: Positive expression of CENPK in cancerous and noncancerous tissues. CENPK: Centromere protein K.

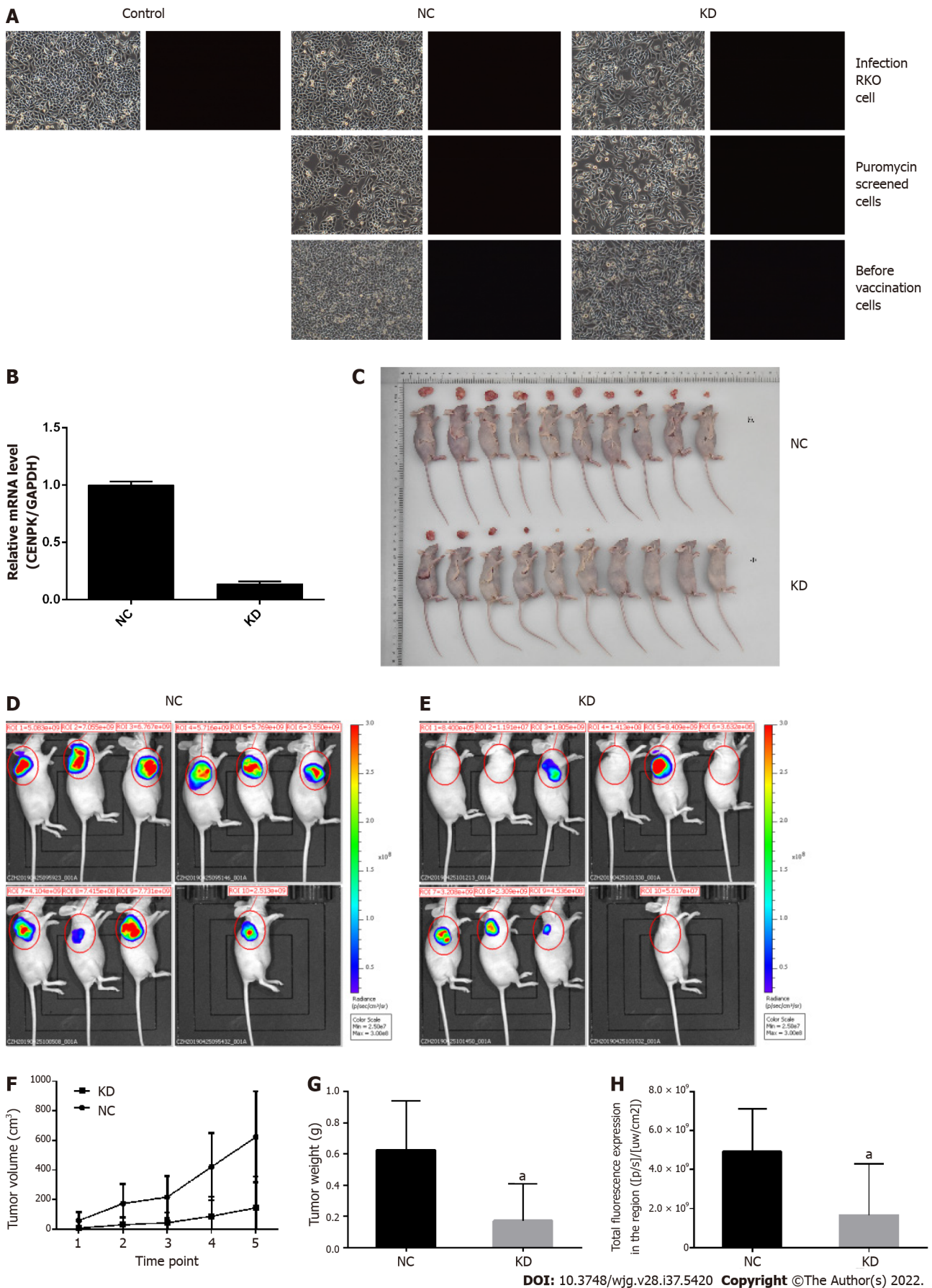


**Figure 6** Analysis of tumor growth in nude mice subcutaneously injected with lentivirus-infected RKO cells. A: Control lentivirus-infected RKO cells, RKO cells infected with centromere protein K (CENPK) negative control virus (NC), and RKO cells with CENPK gene short hairpin RNA virus infection (KD); puromycin-screened cells in the NC and KD groups; and RKO cells in the NC and KD groups before inoculation are shown ( $\times 100$  magnification). On the left and right

are bright field and fluorescence images, respectively; B: Real-time polymerase chain reaction detection of CENPK mRNA expression in RKO cells; C: Tumor status in nude mice subcutaneously injected with lentivirus-infected RKO cells in the NC and KD groups. D: Isoflurane gas anesthesia was applied for live imaging under a live imager in the NC group; E: Isoflurane gas anesthesia was applied for live imaging under a live imager in the KD group; F: Tumor volume of lentivirus-infected RKO cells examined in nude mice in the NC and KD groups; G: Tumor weight of lentivirus-infected RKO cells were examined in nude mice in the NC and KD groups; H: Regional total fluorescence expression in the NC and KD groups. \* $P < 0.05$ , compared with RKO cells infected with centromere protein K negative control virus. CENPK: Centromere protein K; NC: RKO cells infected with centromere protein K negative control virus; KD: RKO cells with lentivirus-mediated short hairpin RNA interference of centromere protein K.

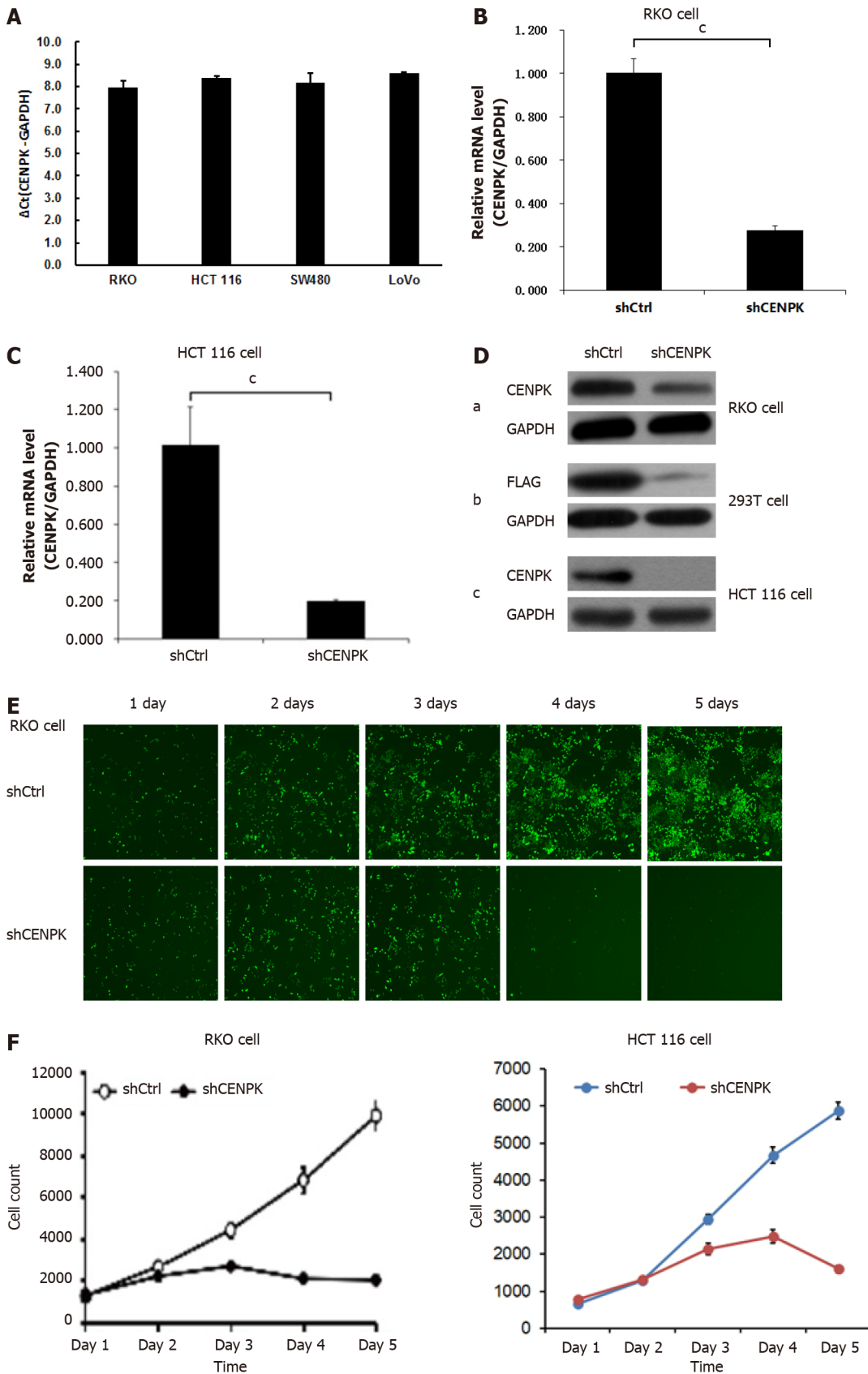
group compared with the KD + NC (OE) group, and HCT 116 cell proliferation was obviously increased in the KD + OE group. HCT 116 and RKO cell apoptosis was induced by CENPK gene reduction and CUL4A gene overexpression; therefore, caspase 3/7 activity and apoptotic cells were measured after lentiviral infection for 5 d. Based on the findings for HCT 116 and RKO cells shown in Figure 9I, caspase 3/7 activity and apoptotic cells were increased in the KD group compared to the NC (KD) group. Caspase 3/7 activity did not change significantly in the OE group, and apoptotic cells did not change significantly compared with the NC (OE) group. Similar to the KD + NC (OE) group, the KD + OE groups exhibited decreased caspase 3/7 activity and apoptosis. HCT 116 and RKO cell apoptosis *via* CENPK gene reduction and CUL4A gene overexpression was detected using FACS (Figure 9K, Supplementary Figures 5 and 6). HCT 116 and RKO cell apoptosis was increased significantly in the KD group ( $P < 0.01$ ) compared to the NC (KD) group. Apoptosis was decreased significantly in the KD + OE group ( $P < 0.01$ ) compared to the KD + NC (OE) group. However, no significant change in apoptosis occurred in the OE group. The FLAG protein level after CUL4A overexpression was detected using western blot (Figure 9J). The proliferation rate in the OE group compared to the NC group after CUL4A overexpression in HCT116 and RKO cells was detected by FLAG. These results suggested that lentivirus-mediated shRNA interference of CENPK inhibited the proliferation of RKO and HCT116 cells, and overexpression of the CUL4A gene reversed this effect in RKO and HCT 116 cells with CENPK gene knockdown.

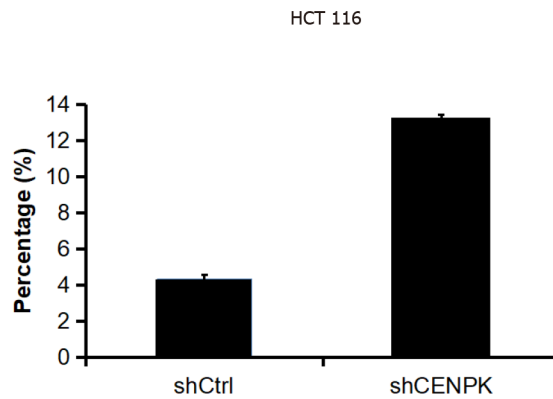
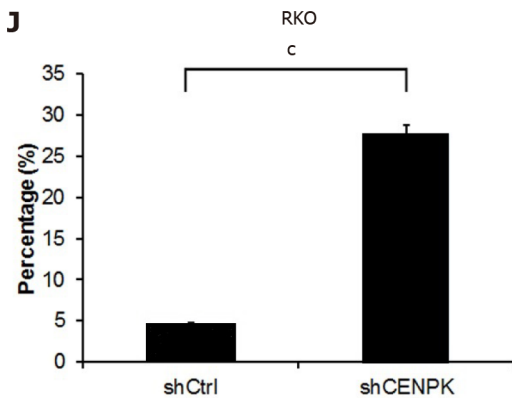
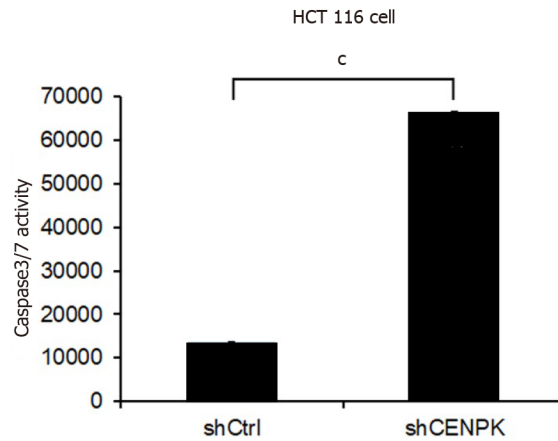
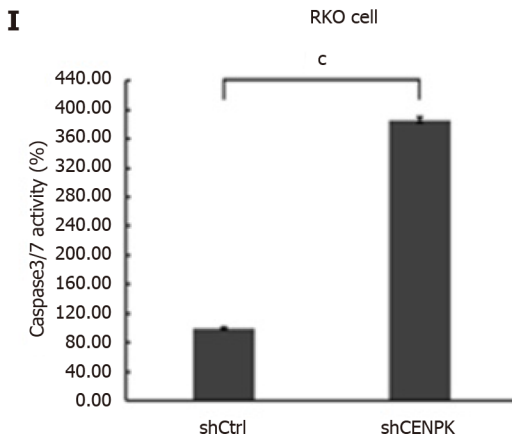
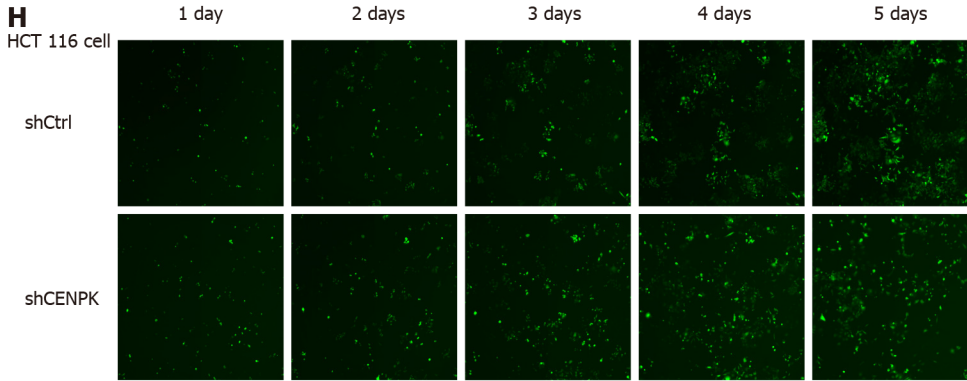
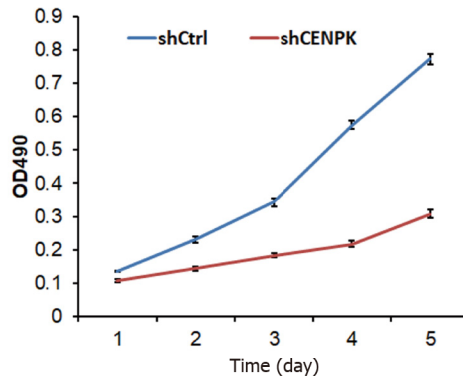
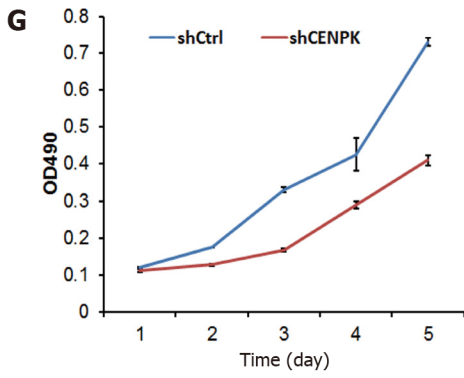
## DISCUSSION

CRC is one of the most common malignant tumors. Increasing evidence suggests that CENPK plays a key role in promoting carcinogenesis[14]. To the best of our knowledge, this study is the first to clarify the clinical value of CENPK in human CRC tissues. However, the underlying mechanism is largely unknown. The expression of CENPK in CRC tissues was quantified using western blot and quantitative real-time PCR. CENPK was highly expressed in CRC tissue and positively correlated with large tumor size and advanced tumor stage. CENPK was found to be frequently downregulated in CRC primary tumor samples compared to adjacent normal tissues, using bioinformatics analysis and experiments *in vivo*. Expression of the CENPK gene was significantly different in cancerous and noncancerous tissues, which supports the use of CENPK for diagnosis of CRC and patient selection for therapy. Tissue chip detection showed that CENPK expression was associated with pathological indicators, such as T stage, N stage, and clinical stage. This confirmed the low level of CENPK expression in early cancer and increasing expression during the course of the disease. We used *in vitro* and *in vivo* models to demonstrate that lentivirus-mediated shRNA interference of CENPK regulated the proliferation of CRC cells. The CENPK gene may affect the expression of a series of downstream genes by acting on YWHAZ and BMI1, which affect cell proliferation and invasion. Therefore, CENPK gene functions in the progression of CRC by altering the expression of CUL4A, CENPK, XIAP, FBX32, YAP1, MAP3K7, TUBB3, and HSP90AA1. Western blot analysis showed that FBX32 was upregulated and CUL4A and YAP1 were downregulated.

YAP1 is an effector of the Hippo pathway, which is critical for regulating organ size, cell proliferation, and tumor growth in mammals[15]. Research on YAP1 expression in CRC tissues showed the effect of silencing expression of the YAP1 gene on the proliferation and invasion of SW620 CRC cells [16]. Another study showed that FBX32 and the mRNA levels of several proteasome-related genes were significantly upregulated by methionine limitation[17]. Moreover, CUL4A is highly expressed in colon cancer and promotes the proliferation and inhibits the apoptosis of colon cancer cells by regulating the Hippo pathway[10]. Therefore, the mechanism of the effect of CUL4A expression on cell proliferation and apoptosis in CRC by regulating the CENPK pathway was further investigated.

Lentivirus-mediated shRNA interference of CENPK was successfully and stably induced in RKO cells, which lays a foundation for further study of the role of the CENPK gene in the carcinogenesis and progression of CRC. With regard to therapeutic options for CRC, increased CENPK expression inhibited CRC cell proliferation and induced apoptosis of RKO cells with lentiviral infection, which suggests that CENPK inhibits CRC progression. A xenograft mouse model also confirmed the tumor-suppressive function of CENPK. We used RKO cells with lentiviral infection to control these processes and inhibit tumor growth. Specifically, we found that the CENPK gene regulated tumor growth, and the total





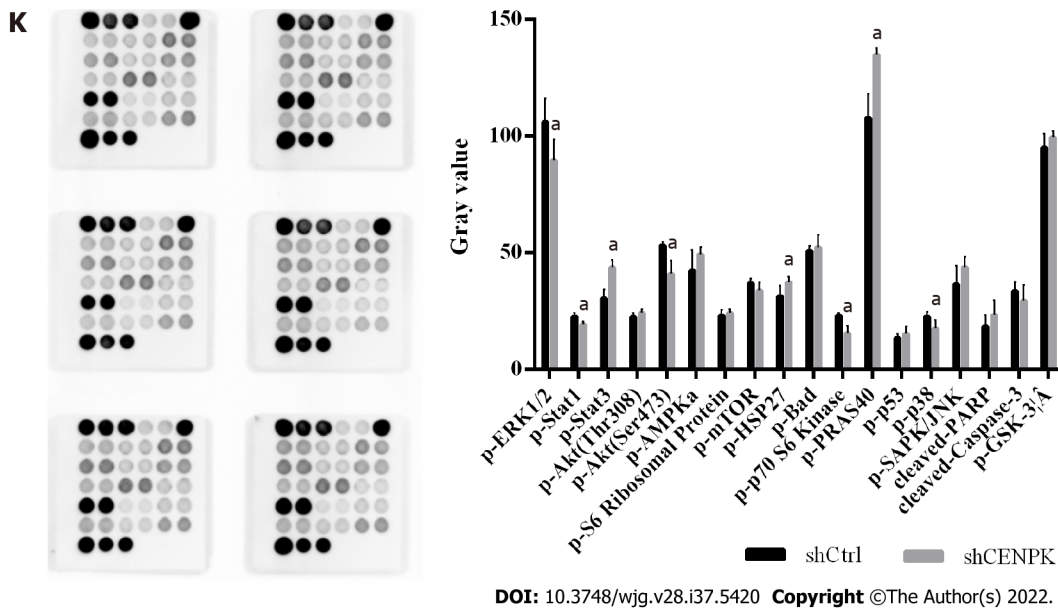


**Figure 7** Effects of centromere protein K on proliferation of RKO cells. A: Expression of the centromere protein K (CENPK) gene in colon cancer cells; B and C: CENPK mRNA level reduction in RKO and HCT116 cells; D: Exogenous expression of CENPK protein in RKO cells (a), 293T cells (b), and HCT116 cells (c); E and F: Effects of CENPK gene reduction on RKO cell proliferation by Celigo detection; G: Effects of CENPK gene reduction on RKO and HCT116 cell proliferation detected by MTT assay; H: Effects of CENPK gene reduction on HCT116 cell proliferation by Celigo detection; I: Effects of CENPK gene reduction on RKO and HCT116 cell apoptosis by caspases 3/7 detection; J: Effects of CENPK gene reduction on RKO and HCT116 cell apoptosis by FACS detection; K: Chemiluminescence analysis in the shCtrl and shCENPK groups. <sup>a</sup>*P* < 0.01, compared with shCtrl; <sup>b</sup>*P* < 0.05, shCtrl compared to the short hairpin RNA lentivirus treatment group; <sup>c</sup>*P* < 0.01, shCtrl compared to the short hairpin RNA lentivirus treatment group. CENPK: Centromere protein K.

fluorescence in the tumor was significantly decreased compared to the controls. We analyzed whether lentivirus-mediated shRNA interference of CENPK was involved in cell proliferation and apoptosis. The results indicated that interference with the CENPK gene inhibited RKO cell proliferation. Taken together, these findings support the hypothesis that lentivirus-mediated shRNA suppresses CENPK expression *via* lentivirus epigenetically. Overexpression of CENPK has been observed in various tumor types[8,18,19].

CUL4A plays a critical role in cellular proliferation and tumor invasion[20,21]. *In vitro* experiments were performed to verify the function of the CUL4A gene. To investigate whether CUL4A gene was involved in CENPK-induced CRC cell proliferation, we performed rescue experiments, which indicated that knockdown of CENPK and overexpression of CUL4A partially rescued proliferation in RKO and HCT116 cells. These findings support the hypothesis that interference with the CENPK gene inhibits RKO and HCT116 cell proliferation. Overexpression of CUL4A had a response effect on RKO and HCT116 cells.

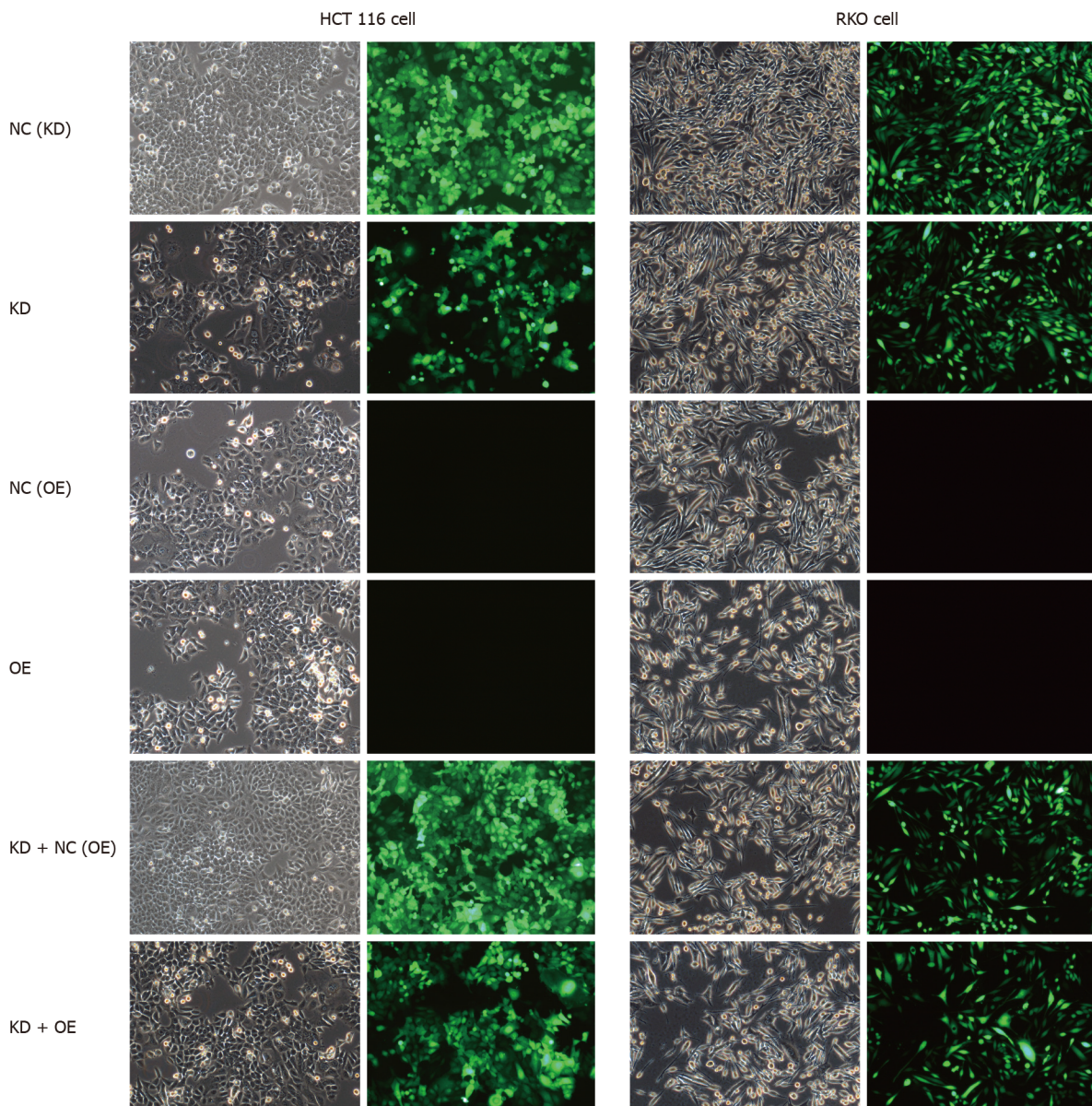
The functional effects of CUL4A proteins on their targets have been well characterized and are involved in the proliferation of cancer cells[22]. CUL4A may be a prognostic marker of precancerous lesions and a potential therapeutic target in cancer[23]. Consistent with these reports, overexpression of CUL4A was observed in 20 pairs of CRC tissues, and knockdown of CUL4A inhibited cell proliferation. A previous study showed that CUL4A was highly expressed in CRC and promoted proliferation and inhibited apoptosis of CRC cells by regulating the Hippo pathway[10]. Our study demonstrated that restoration of CUL4A expression suppressed CRC cell proliferation. These results indicate that CUL4A acts as a tumor suppressor in CRC. It has been found that high CUL4A protein expression is an independent prognostic marker in CRC[12].

## CONCLUSION

Our study demonstrated that overexpression of CUL4A led to CRC tumorigenesis, and knockdown of the CENPK gene affected CRC progression and development in target cells. To the best of our knowledge, this study is the first to investigate CUL4A protein expression and its potential interference with CENPK gene interactions in CRC. We demonstrated the critical role of the CUL4A gene in the progression of CRC. However, due to the complexity of shRNA biological function, further analysis is required to achieve a more comprehensive understanding of CRC diagnosis and therapy.

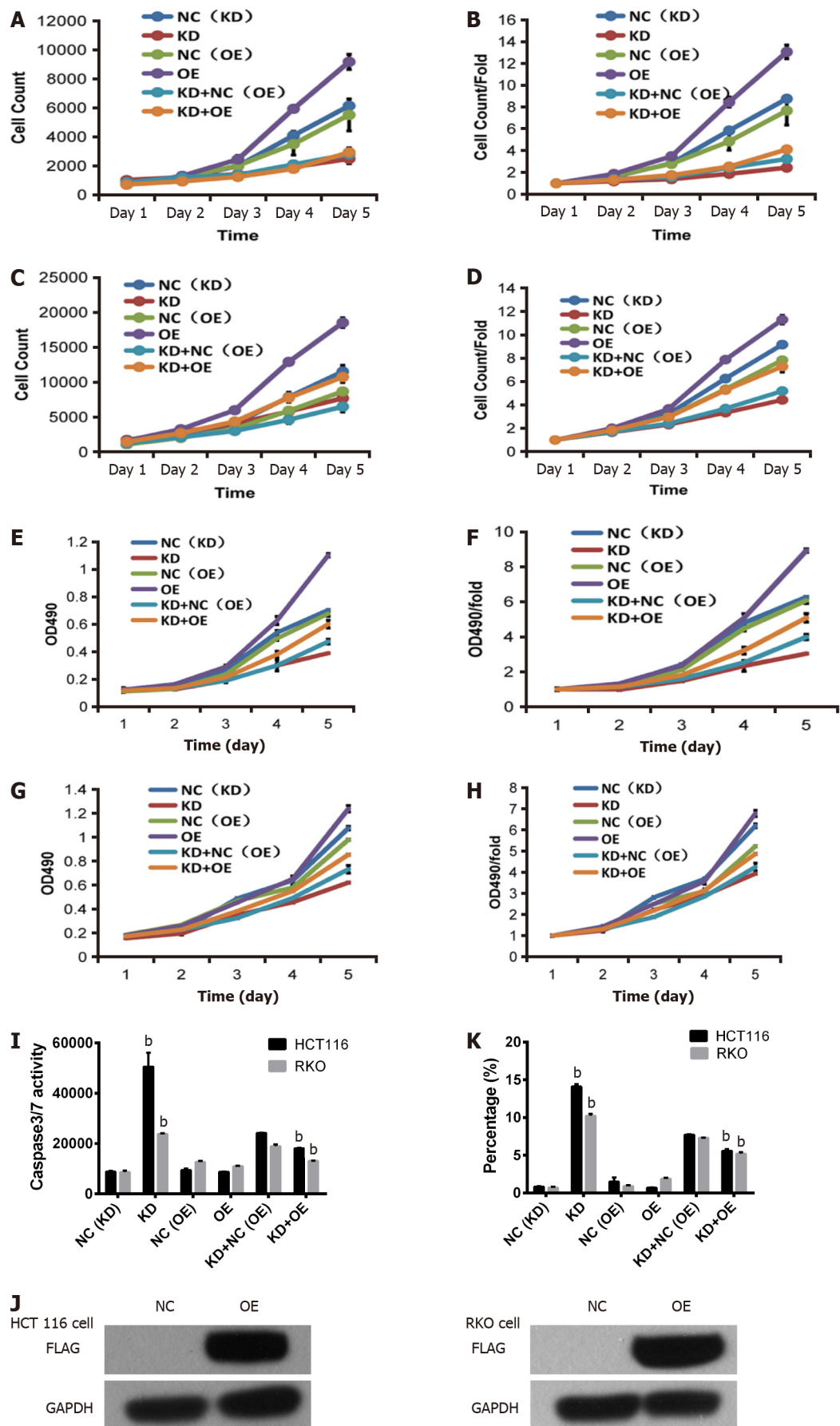
**Table 7 Correlation between centromere protein K gene expression and clinical data in cancerous tissues**

		Gene expression	T stage	N metastasis	Pathological grade
Gene expression	Correlation coefficient	1.000	0.135	0.143	0.135
	Significance (two-tailed)	0.000	0.018	0.012	0.018
T stage	Correlation coefficient	0.135	1.000	0.000	0.000
	Significance (two-tailed)	0.018	0.000	0.000	0.000
N metastasis	Correlation coefficient	0.143	0.000	1.000	0.000
	Significance (two-tailed)	0.012	0.000	0.000	0.000
Pathological grade	Correlation coefficient	0.135	0.000	0.000	1.000
	Significance (two-tailed)	0.018	0.000	0.000	0.000



DOI: 10.3748/wjg.v28.i37.5420 Copyright ©The Author(s) 2022.

**Figure 8** Lentivirus-mediated short hairpin RNA interference of centromere protein K in HCT116 and RKO cells. Bright field (left) and fluorescence images (right) are shown. NC: RKO or HCT 116 cells infected with centromere protein K negative control virus; KD: RKO or HCT 116 cells with centromere protein K gene short hairpin RNA virus infection; OE: RKO or HCT 116 cells virally infected with Cullin 4A.



DOI: 10.3748/wjg.v28.i37.5420 Copyright ©The Author(s) 2022.

**Figure 9** Inhibition of RKO and HCT116 colon cancer cells by abrogation of centromere protein K and overexpression of Cullin 4A. A and B: Effects of centromere protein K (CENPK) knockdown and Cullin 4A (CUL4A) overexpression on HCT116 cell proliferation detected by Celigo assay; C and D:

Effects of CENPK knockdown and CUL4A overexpression on RKO cell proliferation detected by Celigo assay; E and F: Effects of CENPK knockdown and CUL4A overexpression on HCT116 cell proliferation detected by MTT assay; G and H: Effects of CENPK knockdown and CUL4A overexpression on RKO cell proliferation detected by MTT assay; I: HCT116 and RKO cell apoptosis after CENPK knockdown and CUL4A overexpression detected by caspases 3/7; J: FLAG protein expression levels after CUL4A overexpression detected using western blot; K: HCT116 and RKO cell apoptosis. <sup>b</sup>*P* < 0.01, shCtrl compared to short hairpin RNA lentivirus treatment group. NC: RKO or HCT 116 cells infected with centromere protein K negative control virus; KD: RKO or HCT 116 cells with centromere protein K gene short hairpin RNA virus infection; OE: RKO or HCT 116 cells virally infected with Cullin 4A.

## ARTICLE HIGHLIGHTS

### Research background

Colorectal cancer (CRC) is one of the most common malignant tumors worldwide. Immunohistochemistry has found high expression of centromere protein (CENPK) in CRC. However, the role of CENPK in the progression of CRC is not well characterized.

### Research motivation

To explore the role of Cullin (CUL)4A expression and lentivirus-mediated transfection with short hairpin RNA (shRNA) for CENPK in CRC.

### Research objectives

We performed a series of *in vitro* experiments, such as quantitative polymerase chain reaction (qPCR), western blot, MTT assay, and flow cytometry, to evaluate the knockdown behavior of CENPK and overexpression of CUL4A in RKO and HCT 116 CRC cells.

### Research methods

We identified CENPK as a potential new oncogene for CRC based on bioinformatics analysis. *In vitro* experiments verified the function of this gene. We investigated the expression of CENPK in RKO and HCT 116 cells using virus infection and analyzed datasets from qPCR, western blot, and flow cytometry. The effect of RKO cells infected with virus on tumor growth was evaluated *in vivo* using quantitative analysis of fluorescence imaging.

### Research results

The downstream genes FBX32, CUL4A, and YAP1 were examined to evaluate the regulatory action of CENPK in RKO cells. Significantly delayed xenograft emergence, slower growth, and lower final tumor weight and volume were observed in the RKO and HCT 116 with lentivirus-mediated shRNA interference of CENPK. Interference of CENPK inhibited the proliferation rate of RKO cells *in vitro* and *in vivo*. The shRNA interference of CENPK inhibited the proliferation of RKO and HCT 116 cells, and overexpression of CUL4A gene responded to RKO and HCT 116 cells with CENPK silencing.

### Research conclusions

Our findings indicate a potential role of CENPK in promoting tumor proliferation, and it may serve as a novel diagnostic and prognostic biomarker in patients with CRC.

### Research perspectives

An investigation for lentivirus-mediated transfection with shRNA for CENPK and overexpression of CUL4A demonstrated major regulatory roles in CRC. Further analysis is required to achieve a more comprehensive understanding of CRC diagnosis and therapy.

## FOOTNOTES

**Author contributions:** Wu XL analyzed and interpreted the patient data; Han YR, XueFeng X, Ma YX, Xing GS, Yang ZW, Zhang Z, and Shi L did the experiments; Li X was a major contributor in writing the manuscript. All the authors read and approved the final manuscript.

**Supported by** the National Natural Science Foundation of China, No. 81860416 and No. 22168028; Inner Mongolia Autonomous Region Grassland Talent Innovation Talent Team Fund, No. 2019; and Inner Mongolia Natural Science Fund, No. 2021MS02005.

**Institutional review board statement:** The study was reviewed and approved by the Ethics Committee of The Affiliated Hospital of Inner Mongolia Medical University Institutional Review Board (Approval No. WZ 2021045).

**Conflict-of-interest statement:** All the authors report no relevant conflicts of interest for this article.

**Data sharing statement:** No additional data are available.

**Open-Access:** This article is an open-access article that was selected by an in-house editor and fully peer-reviewed by external reviewers. It is distributed in accordance with the Creative Commons Attribution NonCommercial (CC BY-NC 4.0) license, which permits others to distribute, remix, adapt, build upon this work non-commercially, and license their derivative works on different terms, provided the original work is properly cited and the use is non-commercial. See: <https://creativecommons.org/licenses/by-nc/4.0/>

**Country/Territory of origin:** China

**ORCID number:** Xian Li 0000-0002-9107-5096; Yi-Ru Han 0000-0001-8245-9533; Xuefeng Xuefeng 0000-0002-5058-5735; Yong-Xiang Ma 0000-0002-1027-0093; Guo-Sheng Xing 0000-0002-5183-7607; Zhi-Wen Yang 0000-0001-6502-3850; Zhen Zhang 0000-0002-5281-7067; Lin Shi 0000-0001-6543-8650; Xin-Lin Wu 0000-0002-2860-4477.

**S-Editor:** Wang JJ

**L-Editor:** Wang TQ

**P-Editor:** Wang JJ

## REFERENCES

- 1 **Matsushita N**, Matsushita S, Hirakawa S, Higashiyama S. Doxycycline-dependent inducible and reversible RNA interference mediated by a single lentivirus vector. *Biosci Biotechnol Biochem* 2013; **77**: 776-781 [PMID: 23563548 DOI: 10.1271/bbb.120917]
- 2 **Uppada SB**, Gowrikumar S, Ahmad R, Kumar B, Szeglin B, Chen X, Smith JJ, Batra SK, Singh AB, Dhawan P. MASTL induces Colon Cancer progression and Chemoresistance by promoting Wnt/ $\beta$ -catenin signaling. *Mol Cancer* 2018; **17**: 111 [PMID: 30068336 DOI: 10.1186/s12943-018-0848-3]
- 3 **Li Y**, Yang Z, Wu N, Xu L and Leng Z. Effects and Mechanism of shRNA Interfering with KLF4 Expression on the Migration and Invasion of Lgr5 + Colorectal Cancer Stem Cells. *Med J Wuhan University* 2018; **39**: 899-904 [DOI: 10.14188/j.1671-8852.2018.0509]
- 4 **Sacca R**, Engle SJ, Qin W, Stock JL, McNeish JD. Genetically engineered mouse models in drug discovery research. *Methods Mol Biol* 2010; **602**: 37-54 [PMID: 20012391 DOI: 10.1007/978-1-60761-058-8\_3]
- 5 **Zhao B**, Yang C, Yang S, Gao Y, Wang J. Construction of conditional lentivirus-mediated shRNA vector targeting the human Mirk gene and identification of RNAi efficiency in rhabdomyosarcoma RD cells. *Int J Oncol* 2013; **43**: 1253-1259 [PMID: 23913162 DOI: 10.3892/ijo.2013.2048]
- 6 **Wang J**, Li H, Xia C, Yang X, Dai B, Tao K, Dou K. Downregulation of CENPK suppresses hepatocellular carcinoma malignant progression through regulating YAP1. *Onco Targets Ther* 2019; **12**: 869-882 [PMID: 30774374 DOI: 10.2147/OTT.S190061]
- 7 **Li Q**, Liang J, Zhang S, An N, Xu L, Ye C. Overexpression of centromere protein K (CENPK) gene in Differentiated Thyroid Carcinoma promote cell Proliferation and Migration. *Bioengineered* 2021; **12**: 1299-1310 [PMID: 33904381 DOI: 10.1080/21655979.2021.1911533]
- 8 **Lee YC**, Huang CC, Lin DY, Chang WC, Lee KH. Overexpression of centromere protein K (CENPK) in ovarian cancer is correlated with poor patient survival and associated with predictive and prognostic relevance. *PeerJ* 2015; **3**: e1386 [PMID: 26587348 DOI: 10.7717/peerj.1386]
- 9 **Jia B**, Dao J, Han J, Huang Z, Sun X, Zheng X, Xiang S, Zhou H, Liu S. LINC00958 promotes the proliferation of TSCC via miR-211-5p/CENPK axis and activating the JAK/STAT3 signaling pathway. *Cancer Cell Int* 2021; **21**: 147 [PMID: 33658048 DOI: 10.1186/s12935-021-01808-z]
- 10 **Yi LJ**, Yi LJ, Ding N, Ren J. CUL4A promotes proliferation and inhibits apoptosis of colon cancer cells via regulating Hippo pathway. *Eur Rev Med Pharmacol Sci* 2020; **24**: 10518-10525 [PMID: 33155207 DOI: 10.26355/eurrev\_202010\_23404]
- 11 **Sui X**, Zhou H, Zhu L, Wang D, Fan S, Zhao W. CUL4A promotes proliferation and metastasis of colorectal cancer cells by regulating H3K4 trimethylation in epithelial-mesenchymal transition. *Onco Targets Ther* 2017; **10**: 735-743 [PMID: 28223829 DOI: 10.2147/OTT.S118897]
- 12 **Li C**, Bu J, Liao Y, Zhang J, Han J, Zhang H, Xing H, Li Z, Wu H, Liang L, Wang M, Qin W, Yang T. High Expressions of CUL4A and TP53 in Colorectal Cancer Predict Poor Survival. *Cell Physiol Biochem* 2018; **51**: 2829-2842 [PMID: 30562757 DOI: 10.1159/000496013]
- 13 **Wu XL**, Yang ZW, He L, Dong PD, Hou MX, Meng XK, Zhao HP, Wang ZY, Wang F, Baoluri, Wurenqimuge, Agudamu, Jia YF, Shi L. RRS1 silencing suppresses colorectal cancer cell proliferation and tumorigenesis by inhibiting G2/M progression and angiogenesis. *Oncotarget* 2017; **8**: 82968-82980 [PMID: 29137316 DOI: 10.18632/oncotarget.20897]
- 14 **Wang Y**, Wang Y, Ren C, Wang H, Zhang Y, Xiu Y. Upregulation of centromere protein K is crucial for lung adenocarcinoma cell viability and invasion. *Adv Clin Exp Med* 2021; **30**: 691-699 [PMID: 34118147 DOI: 10.17219/acem/133820]
- 15 **Ou C**, Sun Z, Li X, Ren W, Qin Z, Zhang X, Yuan W, Wang J, Yu W, Zhang S, Peng Q, Yan Q, Xiong W, Li G, Ma J. Corrigendum to "MiR-590-5p, a density-sensitive microRNA, inhibits tumorigenesis by targeting YAP1 in colorectal cancer". [Canc. Lett. 399 (2017) 53-63]. *Cancer Lett* 2018; **420**: 260 [PMID: 29429755 DOI: 10.1016/j.canlet.2018.01.073]
- 16 **Zhao YP**, Han ZW, Xie Y. Expression and significance of YAP1 in colorectal cancer tissues. *Chin J Curr Advan Gene Sur*

- 2019 [DOI: [10.11569/wejd.v22.i2.273](https://doi.org/10.11569/wejd.v22.i2.273)]
- 17 **Belghit I**, Skiba-Cassy S, Geurden I, Dias K, Surget A, Kaushik S, Panserat S, Seiliez I. Dietary methionine availability affects the main factors involved in muscle protein turnover in rainbow trout (*Oncorhynchus mykiss*). *Br J Nutr* 2014; **112**: 493-503 [PMID: [24877663](https://pubmed.ncbi.nlm.nih.gov/24877663/) DOI: [10.1017/S0007114514001226](https://doi.org/10.1017/S0007114514001226)]
  - 18 **Huang H**, Cheng S, Ding M, Wen Y, Ma M, Zhang L, Li P, Cheng B, Liang X, Liu L, Du Y, Zhao Y, Kafle OP, Han B, Zhang F. Integrative analysis of transcriptome-wide association study and mRNA expression profiles identifies candidate genes associated with autism spectrum disorders. *Autism Res* 2019; **12**: 33-38 [PMID: [30561910](https://pubmed.ncbi.nlm.nih.gov/30561910/) DOI: [10.1002/aur.2048](https://doi.org/10.1002/aur.2048)]
  - 19 **Parolin C**, Corso AD, Alberghina L, Porro D, Branduardi P. Heterologous production of five Hepatitis C virus-derived antigens in three *Saccharomyces cerevisiae* host strains. *J Biotechnol* 2005; **120**: 46-58 [PMID: [16039743](https://pubmed.ncbi.nlm.nih.gov/16039743/) DOI: [10.1016/j.jbiotec.2005.05.025](https://doi.org/10.1016/j.jbiotec.2005.05.025)]
  - 20 **Wang Y**, Wen M, Kwon Y, Xu Y, Liu Y, Zhang P, He X, Wang Q, Huang Y, Jen KY, LaBarge MA, You L, Kogan SC, Gray JW, Mao JH, Wei G. CUL4A induces epithelial-mesenchymal transition and promotes cancer metastasis by regulating ZEB1 expression. *Cancer Res* 2014; **74**: 520-531 [PMID: [24305877](https://pubmed.ncbi.nlm.nih.gov/24305877/) DOI: [10.1158/0008-5472.CAN-13-2182](https://doi.org/10.1158/0008-5472.CAN-13-2182)]
  - 21 **Pan Y**, Wang B, Yang X, Bai F, Xu Q, Li X, Gao L, Ma C, Liang X. CUL4A facilitates hepatocarcinogenesis by promoting cell cycle progression and epithelial-mesenchymal transition. *Sci Rep* 2015; **5**: 17006 [PMID: [26593394](https://pubmed.ncbi.nlm.nih.gov/26593394/) DOI: [10.1038/srep17006](https://doi.org/10.1038/srep17006)]
  - 22 **Ashok C**, Owais S, Sriyothi L, Selvam M, Ponne S, Baluchamy S. A feedback regulation of CREB activation through the CUL4A and ERK signaling. *Med Oncol* 2019; **36**: 20 [PMID: [30666499](https://pubmed.ncbi.nlm.nih.gov/30666499/) DOI: [10.1007/s12032-018-1240-2](https://doi.org/10.1007/s12032-018-1240-2)]
  - 23 **Feng M**, Wang Y, Bi L, Zhang P, Wang H, Zhao Z, Mao JH, Wei G. CUL4A<sup>DTL</sup> degrades DNA-PKcs to modulate NHEJ repair and induce genomic instability and subsequent malignant transformation. *Oncogene* 2021; **40**: 2096-2111 [PMID: [33627782](https://pubmed.ncbi.nlm.nih.gov/33627782/) DOI: [10.1038/s41388-021-01690-z](https://doi.org/10.1038/s41388-021-01690-z)]

## Retrospective Cohort Study

## Prognostic performance of an index based on lactic dehydrogenase and transaminases for patients with liver steatosis and COVID-19

Ricardo Ulises Macías-Rodríguez, Alberto Adrián Solís-Ortega, Victoria J Ornelas-Arroyo, Astrid Ruiz-Margáin, María Sarai González-Huezo, Nestor A Urdiales-Morán, Berenice M Román-Calleja, Juan M Mayorquín-Aguilar, José A González-Regueiro, Alejandro Campos-Murguía, Israel Vicente Toledo-Coronado, Mónica Chapa-Ibargüengoitia, Bernardo Valencia-Peña, Carlos Fernando Martínez-Cabrera, Nayelli C Flores-García

**Specialty type:** Gastroenterology and hepatology

**Provenance and peer review:** Invited article; Externally peer reviewed.

**Peer-review model:** Single blind

**Peer-review report's scientific quality classification**

Grade A (Excellent): 0  
Grade B (Very good): B, B  
Grade C (Good): 0  
Grade D (Fair): 0  
Grade E (Poor): 0

**P-Reviewer:** Hasabo EA, Sudan; Mamom J, Thailand

**Received:** June 22, 2022

**Peer-review started:** June 22, 2022

**First decision:** August 1, 2022

**Revised:** August 16, 2022

**Accepted:** September 13, 2022

**Article in press:** September 13, 2022

**Published online:** October 7, 2022



**Ricardo Ulises Macías-Rodríguez, Alberto Adrián Solís-Ortega, Victoria J Ornelas-Arroyo, Astrid Ruiz-Margáin, Berenice M Román-Calleja, Juan M Mayorquín-Aguilar, José A González-Regueiro, Alejandro Campos-Murguía, Bernardo Valencia-Peña, Carlos Fernando Martínez-Cabrera, Nayelli C Flores-García,** Department of Gastroenterology, Instituto Nacional de Ciencias Médicas y Nutrición Salvador Zubirán, Mexico City 14080, Mexico

**María Sarai González-Huezo, Nestor A Urdiales-Morán,** Department of Gastroenterology, Centro Médico ISSEMYM, Toluca 52140, Mexico

**Israel Vicente Toledo-Coronado, Mónica Chapa-Ibargüengoitia,** Department of Radiology, Instituto Nacional de Ciencias Médicas y Nutrición Salvador Zubirán, Mexico City 14080, Mexico

**Corresponding author:** Ricardo Ulises Macías-Rodríguez, MD, MSc, PhD, Assistant Professor, Department of Gastroenterology, Instituto Nacional de Ciencias Médicas y Nutrición Salvador Zubirán, Vasco de Quiroga 15, Col. Belisario Domínguez Sección XVI, Liver Fibrosis and Nutrition Lab, MICTLÁN Network: Mechanisms of Liver Injury, Cell Death and Translational Nutrition in Liver Diseases-Research Network, Mexico City 14080, Mexico.

[ricardomacro@yahoo.com.mx](mailto:ricardomacro@yahoo.com.mx)

## Abstract

### BACKGROUND

Metabolic associated fatty liver disease (MAFLD) is associated with complications and mortality in patients with coronavirus disease 2019 (COVID-19). However, there are no prognostic scores aimed to evaluate the risk of severe disease specifically in patients with MAFLD, despite its high prevalence. Lactate dehydrogenase, aspartate aminotransferase and alanine aminotransferase have been used as markers of liver damage. Therefore, we propose an index based on lactate dehydrogenase, aspartate aminotransferase and alanine aminotransferase for the prediction of complications and mortality in patients with MAFLD and COVID-19.

### AIM

To evaluate the prognostic performance of an index based on lactate dehydro-

genase and transaminases (aspartate aminotransferase/alanine aminotransferase) in patients with COVID-19 and MAFLD [liver fibrosis and nutrition (LNF)-COVID-19 index].

## METHODS

In this retrospective cohort study, two cohorts from two different tertiary centers were included. The first was the derivation cohort to obtain the score cutoffs, and the second was the validation cohort. We included hospitalized patients with severe COVID-19 and MAFLD. Liver steatosis was evaluated by computed tomography scan. Area under the receiver operating characteristic (ROC) curve analysis and survival analysis were used.

## RESULTS

In the derivation cohort, 44.6% had MAFLD; ROC curve analysis yielded a LFN-COVID-19 index > 1.67 as the best cutoff, with a sensitivity of 78%, specificity of 63%, negative predictive value of 91% and an area under the ROC curve of 0.77. In the multivariate analysis, the LFN-COVID-19 index > 1.67 was independently associated with the development of acute kidney injury (odds ratio: 1.8, 95% confidence interval: 1.3-2.5,  $P < 0.001$ ), orotracheal intubation (odds ratio: 1.9, 95% confidence interval: 1.4-2.4,  $P < 0.001$ ), and death (odds ratio: 2.86, 95% confidence interval: 1.6-4.5,  $P < 0.001$ ) in both cohorts.

## CONCLUSION

LFN-COVID-19 index has a good performance to predict prognosis in patients with MAFLD and COVID-19, which could be useful for the MAFLD population.

**Key Words:** COVID-19; Metabolic associated fatty liver disease; Lactate dehydrogenase; Transaminases; Prognosis; Nonalcoholic fatty liver disease

©The Author(s) 2022. Published by Baishideng Publishing Group Inc. All rights reserved.

**Core Tip:** The liver fibrosis and nutrition-coronavirus disease 2019 (LFN-COVID-19) index that includes lactate dehydrogenase and transaminases is a new prognostic index for patients with metabolic associated fatty liver disease and COVID-19; it was developed to specifically predict adverse clinical outcomes, including mortality, in this population with both conditions. The variables included in this index allow an easy, quick and reliable risk assessment in this population with simple markers, allowing for broad implementation.

**Citation:** Macías-Rodríguez RU, Solís-Ortega AA, Ornelas-Arroyo VJ, Ruiz-Margáin A, González-Huezo MS, Urdiales-Morán NA, Román-Calleja BM, Mayorquín-Aguilar JM, González-Regueiro JA, Campos-Murguía A, Toledo-Coronado IV, Chapa-Ibargüengoitia M, Valencia-Peña B, Martínez-Cabrera CF, Flores-García NC. Prognostic performance of an index based on lactic dehydrogenase and transaminases for patients with liver steatosis and COVID-19. *World J Gastroenterol* 2022; 28(37): 5444-5456

**URL:** <https://www.wjgnet.com/1007-9327/full/v28/i37/5444.htm>

**DOI:** <https://dx.doi.org/10.3748/wjg.v28.i37.5444>

## INTRODUCTION

The severe acute respiratory syndrome coronavirus 2 (SARS-CoV-2) pandemic (coronavirus disease 2019, COVID-19) still affects the entire world. As of June 15, 2022, 536720870 people have been infected, of whom 6312601 have died[1].

Different risk factors associated with the development of complications and mortality in patients with COVID-19 have been identified, including age > 60 years, the presence of cirrhosis, diabetes, immunodeficiencies, obesity, cardiovascular disease, chronic kidney disease and chronic obstructive pulmonary disease, among others[2-4]. Metabolic dysfunction associated fatty liver disease (MAFLD), regarded as the hepatic manifestation of metabolic syndrome, has a controversial role in the prognosis of patients with COVID-19. Some studies have reported a poor prognosis in patients with MAFLD, while others have only showed this finding when fibrosis was present. This could be explained by a more pronounced baseline systemic inflammatory profile and activation of the immune response in patients with liver fibrosis, which contributes to increased inflammation when SARS-CoV-2 infection is added[5, 6].

Acute respiratory distress syndrome is the major complication in patients with severe COVID-19; other complications such as cardiac or cardiovascular, renal and secondary infections may occur[7]. These patients, mainly those admitted to the intensive care unit, may present with laboratory abnormalities, such as leukopenia, lymphopenia (< 800 mm<sup>3</sup> at admission), elevated prothrombin time, elevated serum levels of D-dimer (> 1000 ng/mL), elevated inflammatory markers (ferritin > 300 µg/L), elevated lactate dehydrogenase (LDH), elevated liver enzymes, elevated creatine phosphokinase (twice the upper limit of normal) and elevated troponin I[7-9].

In patients with pneumonia associated with SARS-CoV-2 infection, high LDH levels correlate with lung damage, severe disease and mortality at day 30[10-13]. In the study by Yan *et al*[14], LDH (> 365 U/L), lymphocyte count (< 14.7%) and C-reactive protein (> 41.2 mg/L) were identified as the three laboratory abnormalities that predicted mortality risk with 90% accuracy, which represented a simple way to promptly recognize severe illness.

Likewise, in patients with acute liver injury (non-COVID-19 related), an increase in LDH levels has been reported, secondary to endothelial damage induced by macrophages during acute inflammation, conditioning microcirculation alterations and hypoxia. Thus, it has been suggested that LDH may have a discriminatory role in identifying the etiology of liver damage. As a marker of damage due to liver ischemia, it must be taken into account that LDH has a shorter half-life. Therefore, a faster fall occurs when the damage disappears, and it has been suggested as a parameter to monitor the evolution of patients with acute liver injury. The ubiquitous nature of LDH in the human body makes it a nonspecific but sensitive biomarker, which in the context of organ damage can provide information with diagnostic and prognostic potential. In the same way, increase in alanine aminotransferase (ALT), aspartate aminotransferase (AST) and the AST/ALT ratio has been associated to adverse clinical outcomes including mortality in patients with COVID-19[10-13,15].

Identifying factors associated with poor prognosis that may be related to a pathophysiological mechanism is ideal in patients with COVID-19 since those patients at risk of progressing to a severe illness could be identified promptly. Therefore, measures could be taken to influence the outcomes of those patients. In this sense, having a prognostic index specific for patients with MAFLD who develop COVID-19 may be useful to identify individuals at risk of developing adverse clinical outcomes.

Therefore, the aim of this study was to evaluate the performance of a prognostic index based on LDH, AST and ALT in patients with MAFLD and COVID-19 and its association with the development of adverse clinical outcomes and mortality.

## MATERIALS AND METHODS

This was a retrospective cohort study performed at two third-level hospitals in Mexico, (INCMNSZ and ISSEMYM) from March 2020 to July 2020, during the first phase of the COVID-19 pandemic and before steroids became a standard of care for severe COVID-19. The study was carried out according to the Declaration of Helsinki and was approved by the institutional Ethics Committee, ref. No. 3777).

### Validation process

This study consisted of two phases. Phase 1, a derivation/training cohort, (its methods are described below) used to create and evaluate the newly proposed prognostic index. This cohort was derived from a tertiary care center hospital in Mexico City (INCMNSZ). Phase 2, the validation cohort aimed to evaluate the diagnostic performance of the proposed index in patients with COVID-19 and liver steatosis at a different center. This cohort was derived from a tertiary care center hospital in Toluca, in the center of Mexico (ISSEMYM).

### Patients

All patients admitted during the period of study, > 18 years of age, either sex and with a confirmed diagnosis of SARS-CoV-2 infection by RT-PCR and with severe disease (pneumonia + respiratory rate > 30/respiratory distress/SaO<sub>2</sub> < 90%), were included in the study[19]. Patients without an adequate follow-up were excluded from the analysis (*e.g.*, those requiring referral to another hospital, those with insufficient information in the clinical records, *etc*). Follow-up and evaluation of the clinical outcomes were conducted through revision of electronic clinical records.

### Biochemical tests

Upon admission, a blood sample was drawn for determination of the following tests: complete blood count, glucose, creatinine, electrolytes, ferritin, C-reactive protein, LDH, liver chemistry, creatine phosphokinase, arterial blood gases, D-dimer, troponin I and fibrinogen. HIV (human Immunodeficiency virus) and viral hepatitis panel (HCV and HBV) were performed in all participants. All the tests met the quality standards from our central laboratory, accredited by the College of American Pathologists.

### Computed tomography scan

In order to evaluate the severity of pulmonary involvement, all patients underwent a pulmonary computed tomography scan, where a portion of the liver was also evaluated for the presence of steatosis. The methodology was previously described from our group[16]. Briefly, an expert radiologist blinded to the patient's clinical status evaluated computed tomography scans to detect liver steatosis, according to the following criteria: (1) Attenuation coefficient  $\leq 40$  Hounsfield units in the liver (segments VII and VIII); and (2) Attenuation coefficient  $\geq 10$  Hounsfield units between the splenic and liver parenchyma.

### Estimation of the LFN-COVID-19 index

The liver fibrosis and nutrition (LNF)-COVID-19 index was calculated according to the following formula:

$$\text{LFN-COVID-19 index} = (\text{AST}/\text{ALT}) \times (\text{LDH}/\text{LDH}_{\text{ULN}}).$$

Where AST/ALT ratio included transaminase levels expressed in U/L and was multiplied by the times above the upper limit of normal value for LDH (U/L). The final value was included in the statistical analysis for characterization of clinical outcomes.

### Statistical analysis

Sample size estimation considered a hypothetical area under the receiver operating characteristic curve (AUROC) of 0.8 for LFN-COVID-19 index and 0.7 as null hypothesis. Considering an alpha error of 0.05 and beta 0.20 and a negative/positive ratio of 1/1, estimation yielded 81 negative/positive cases (162 patients in total).

Normality of the data was evaluated with Kolmogorov-Smirnov test. Data was presented as mean  $\pm$  standard deviation, median (P25-P75) or absolute frequencies. Comparisons between the groups were made through Mann-Whitney *U* or Student's *t* test. ROC curve analysis was performed to obtain the best cutoff from the LFN-COVID-19 index for mortality, through the Youden index as well as sensitivity, specificity, positive and negative predictive values and likelihood ratios.

Clinical outcomes were evaluated by logistic regression and a time-dependent survival analysis, including Kaplan-Meier and Cox regression (Cox proportional-hazards model) for 28-d mortality and general mortality. Statistical analysis was carried out with the statistics software SPSS version 20.0 (IBM, Armonk, NY, United States) and ROC analysis with MedCalc Statistical Software version 19.4.1 (MedCalc Software Ltd, Ostend, Belgium).

## RESULTS

In the validation cohort a total of 457 patients were included in the final analysis (Figure 1), after excluding those without an adequate follow-up, those with computed tomography scan issues (artifacts, unable to evaluate liver or spleen tissue, post-surgical changes) or those with known autoimmune liver diseases, HIV, hepatitis C or B chronic infection or cancer.

### Participant's characteristics

General characteristics of the study population, with and without MAFLD are presented in Table 1. Mean age in the total population was  $50.4 \pm 13.3$  years, most of the patients were male (65.2%), and the mean body mass index (BMI) was  $30.1 \pm 5.6$  kg/m<sup>2</sup>. In general, in the group of patients with MAFLD there was a higher prevalence of overweight and obese patients, they were younger than those without MAFLD, and they had a higher prevalence of diabetes and metabolic syndrome.

### Biochemical tests

Biochemical tests related to proinflammatory status, such as LDH, creatine phosphokinase, lymphocytes and neutrophil/lymphocyte ratio, were higher in the MAFLD group, as well as liver chemistry abnormalities, glucose, triglycerides and prognostic scores (SOFA: sequential organ failure assessment).

### Index diagnostic performance

In the group of patients with MAFLD, diagnostic yield of the LFN-COVID-19 index [(AST/ALT)  $\times$  (LDH/LDH<sub>ULN</sub>)] was investigated through the AUROC analysis to determine the prognostic value of the index as a prognostic marker in patients with COVID-19. Characteristics related to diagnostic yield of the LFN-COVID-19 index are shown in Table 2. According to Youden's index, the best cutoff value of the LFN-COVID-19 index for mortality in patients with MAFLD was  $> 1.67$ . This cutoff value showed an AUROC of 0.77 [95% confidence interval (CI): 0.709-0.823,  $P < 0.0001$ ], with a sensitivity of 78.7% and specificity of 63.8% (Figure 2A). In general, the AUROC in this group of patients was better than in patients without MAFLD (AUROC: 0.703, 95%CI: 0.647-0.755,  $P < 0.0001$ ) (Figure 2B).

Table 3 shows the characteristics of patients with MAFLD according to the LFN-COVID-19 index. Similarities in both groups regarding metabolic syndrome and BMI were observed, while other

**Table 1** Baseline characteristics of the total population and according to metabolic associated fatty liver disease presence

Characteristics	All, n = 457	No MAFLD, n = 253	MAFLD, n = 204	P value
Demographic features				
Sex as male/female, %	65.2/34.8	63.6/36.4	67.2/32.8	0.432
Age in yr	50.4 ± 13.3	52.4 ± 14.0	47.8 ± 11.8	< 0.0001
BMI in kg/m <sup>2</sup>	30.1 ± 5.6	28.7 ± 4.9	31.8 ± 5.8	< 0.0001
Comorbidities, n (%)				
Malnutrition	10 (2.8)	7 (3.4)	3 (1.9)	< 0.0001
Normal weight	49 (13.6)	43 (21.0)	6 (3.9)	
Overweight	136 (37.9)	82 (40.0)	54 (35.1)	
Obesity G1	110 (30.6)	51 (24.9)	59 (38.3)	
Obesity G2	36 (10.0)	16 (7.8)	20 (13.0)	
Obesity G3	18 (5.0)	6 (2.9)	12 (7.8)	
T2DM	107 (23.5)	47 (18.7)	60 (29.6)	0.006
Hypertension	122 (26.8)	60 (23.8)	62 (30.5)	0.107
Chronic kidney disease	8 (1.8)	6 (2.4)	2 (1.0)	0.225
Pulmonary obstructive disease	4 (0.9)	1 (0.4)	3 (1.5)	0.235
Autoimmune disease	6 (1.3)	3 (1.2)	3 (1.5)	0.551
Immunosuppression	3 (0.7)	3 (1.2)	0 (0)	0.169
Metabolic syndrome	155 (36.0)	61 (25.5)	94 (49.0)	< 0.0001
Prognostic scores				
qSOFA	1 (0-1)	1 (0-1)	1 (0-1)	0.800
SOFA	2 (1-2)	2 (1-2)	2 (1-2)	0.034
NEWS	6.7 ± 2.3	6.6 ± 2.3	6.8 ± 2.2	0.190
PSI/PORT	62 (50-80)	62 (50-82)	61 (49-77)	0.316
SMART COP	3 (2-4)	3 (2-4)	3 (2-4)	0.091
Biochemical values				
CRP, ref: 0-1 mg/dL	13.2 (6.6-20.7)	13.1 (6.6-20.0)	13.7 (6.2-21.5)	0.286
Ferritin, ref: 11.0-306.8 ng/mL	747.8 ± 665.0	717.2 ± 662.0	784.0 ± 668.0	0.290
D-dimer, ref: 0-500 ng/mL	707 (426-1146)	699 (413-1138)	721 (451-1182)	0.418
LDH, ref: 120-246 U/L	388 ± 160	374 ± 149	406 ± 173	0.032
Troponin, ref: < 15 pg/mL	4.7 (3.2-8.2)	4.7 (3.1-10.4)	4.6 (3.2-7.1)	0.525
CPK, ref: 30-233 U/L	110 (59-242)	98 (55-210)	133 (66-311)	0.006
Bilirubin, ref: 0/3-1 mg/dL	0.68 ± 0.49	0.66 ± 0.54	0.69 ± 0.43	0.593
ALT, ref: 7-52 U/L	37.5 (25.0-56.0)	33.0 (23.8-54.7)	41.0 (28.0-59.0)	0.004
AST, ref: 13-39 U/L	42.0 (30.0-62.0)	40.0 (29.0-58.0)	43.9 (32.9-64.3)	0.051
Globulins, ref: 1.9-3.7 g/dL	3.2 ± 0.4	3.2 ± 0.4	3.2 ± 0.4	0.560
Albumin, ref: 3.5-5.7 g/dL	3.7 ± 0.4	3.6 ± 0.4	3.7 ± 0.4	0.051
ALP, ref: 34-104 U/L	86 (70-111)	86 (70-113)	85 (69-109)	0.505
Creatinine, ref: 0.6-1.2 mg/dL	0.9 (0.8-1.1)	0.9 (0.8-1.1)	0.9 (0.7-1.1)	0.877
Glucose, ref: 70-99 mg/dL	116 (102-144)	110 (99-131)	124 (105-184)	< 0.0001
Leukocytes, ref: 4-12 × 10 <sup>3</sup> /μL	7.6 (5.6-10.0)	7.2 (5.4-9.8)	7.9 (5.7-10.3)	0.191
Lymphocytes, ref: 1-3.9 × 10 <sup>3</sup> /μL	881.6 ± 509.0	835.0 ± 352.0	938.0 ± 649.0	0.043

Platelets, ref: 150-450 K/ $\mu$ L	239 $\pm$ 88	248 $\pm$ 95	227 $\pm$ 78	0.012
25 (HO) vitamin D, ref: 30-100 ng/mL	21.5 $\pm$ 8.0	21.6 $\pm$ 8.1	21.5 $\pm$ 8.0	0.917
Triglycerides, ref: < 150 mg/dL	159 $\pm$ 85	155 $\pm$ 60	165 $\pm$ 110	0.264
CT scan results, pulmonary involvement				
Mild, < 20%	91 (20.0)	51 (20.3)	40 (19.6)	0.281
Moderate, 20%-50%	172 (37.8)	102 (40.6)	70 (34.3)	
Severe, > 50%	192 (42.2)	98 (39.0)	94 (46.1)	
Treatment, n (%)				
Antibiotics	402 (88.4)	228 (90.8)	174 (85.3)	0.096
Antimalarials	132 (28.9)	72 (28.5)	60 (29.4)	0.823
Tocilizumab	51 (11.2)	26 (10.3)	25 (12.3)	0.504
Remdesivir	9 (2.0)	7 (2.8)	2 (1.0)	0.152
PaO <sub>2</sub> /FiO <sub>2</sub> ratio	233.9 $\pm$ 109.9	239.0 $\pm$ 91.0	227.0 $\pm$ 130.0	0.011
Neutrophil/lymphocyte ratio	7.0 (4.4-11.6)	7.2 (4.5-12.0)	6.7 (4.0-10.8)	0.860
Days between the beginning of symptoms and hospitalization	8.2 $\pm$ 4.4	8.6 $\pm$ 4.6	7.8 $\pm$ 4.0	0.110

BMI: Body mass index; T2DM: Type 2 diabetes mellitus; q-SOFA: Quick sequential organ failure assessment; SOFA: Sequential organ failure assessment; NEWS: National early warning score; PSI/PORT: Pneumonia severity index; CRP: C-reactive protein; LDH: Lactate dehydrogenase; CPK: Creatine phosphokinase; ALT: Alanine aminotransferase; AST: Aspartate aminotransferase; ALP: Alkaline phosphatase; CT: Computed tomography; MAFLD: Metabolic associated fatty liver disease; PaO<sub>2</sub>/FiO<sub>2</sub> ratio: Ratio of arterial oxygen partial pressure to fractional inspired oxygen.

**Table 2 Diagnostic yield of the LFN-COVID-19 index in patients with metabolic associated fatty liver disease**

Diagnostic yield	
Sensitivity	0.787 (0.643-0.893)
Specificity	0.638 (0.563-0.709)
Positive predictive value, %	0.360 (0.273-0.468)
Negative predictive value, %	0.910 (0.855-0.960)
+ Likelihood ratio	2.18 (1.70-2.80)
- Likelihood ratio	0.33 (0.20-0.60)
AUROC	0.770 (0.709-0.823), $P < 0.0001$
Youden index	0.4257

AUROC: Area under the receiver operating characteristic.

variables including age, prognostic scores, and biomarkers related to proinflammatory and prothrombotic status, severe COVID-19 (PaO<sub>2</sub>/FiO<sub>2</sub> < 100 mmHg), orotracheal intubation and other clinical outcomes, including mortality, were higher in the > 1.67 group.

### Prognostic performance

In order to determine if the LFN-COVID-19 index was independently associated with the presence of acute kidney injury or orotracheal intubation during hospitalization, a logistic regression was performed, observing that a value of > 1.67 was associated to adverse clinical outcomes, independently of metabolic factors, severity scores and demographic variables (Table 4).

A marker of mortality was studied by a 28-d Kaplan-Meier survival analysis (Figure 3), observing that patients with a value > 1.67 have a lower survival than those with a value < 1.67 ( $P < 0.001$ ). The influence of other variables on mortality was evaluated through univariate and multivariate Cox proportional hazard analysis. Table 5 summarized the variables that were significant in the univariate analysis, with the results subjected to the multivariate analysis where the variables that were independently associated with mortality were the LFN-COVID-19 index, the neutrophil/lymphocyte

**Table 3 Characteristics and outcomes in patients with metabolic associated fatty liver disease according to the LFN-COVID-19 index**

	< 1.67, n = 115	> 1.67, n = 89	P value
Demographic features			
Sex as male/female, %	63.5/36.5	71.9/28.1	0.203
Age in yr	46 ± 10	50 ± 12	0.011
BMI in kg/m <sup>2</sup>	31.1 ± 4.8	32.5 ± 6.9	0.111
Prognostic scores			
qSOFA	1 (0-1)	1 (1-1)	0.007
SOFA	2 (1-2)	2 (2-3)	0.004
NEWS	7 (5-8)	7 (6-9)	0.035
PSI/PORT	56 (47-69)	66 (53-85)	< 0.0001
SMART COP	3 (2-4)	4 (3-4)	0.012
Biochemical values			
CRP, ref: 0-1 mg/dL	8.5 (4.2-18.1)	17.2 (11.6-23.8)	< 0.0001
Ferritin, ref: 11.0-306.8 ng/mL	503 (266-970)	795 (412-1114)	0.003
D-dimer, ref: 0-500 ng/mL	587 (399-962)	967 (606-1549)	< 0.0001
LDH, ref: 120-246 µ/L	312 ± 86	529 ± 180	< 0.0001
Troponin, ref: < 15 pg/mL	3.7 (2.9-5.7)	6.1 (3.8-10.9)	< 0.0001
CPK, ref: 30-223 µ/L	107 (58-222)	190 (78-414)	0.001
Bilirubin, ref: 0/3-1 mg/dL	0.62 ± 0.30	0.78 ± 0.54	0.017
ALT, ref: 7-52 U/L	43.2 (31.0-61.2)	37.0 (26.3-52.8)	0.026
AST, ref: 13-39 U/L	38.3 (27.8-52.2)	52.4 (42.0-73.7)	< 0.0001
Globulins, ref: 1.9-3.7 g/dL	3.22 ± 0.39	3.29 ± 0.43	0.259
Albumin, ref: 3.5-5.7 g/dL	3.90 ± 0.42	3.50 ± 0.40	< 0.0001
ALP, ref: 34-104 µ/L	85 (70-109)	85 (67-110.5)	0.786
Creatinine, ref: 0.6-1.2 mg/dL	0.85 (0.69-1.00)	0.95 (0.79-1.16)	0.005
Glucose, ref: 70-99 mg/dL	118 (102-180)	135 (114-187)	0.03
Leukocytes, ref: 4-12 × 10 <sup>3</sup> /µL	7.6 (5.6-9.9)	8.3 (6.3-10.8)	0.089
Lymphocytes, ref: 1-3.9 × 10 <sup>3</sup> /µL	937 (693-1210)	715 (510-967)	< 0.0001
Platelets, ref: 150-450 K/µL	228 ± 78	226 ± 79	0.827
25 (HO) vitamin D, ref: 30-100 ng/mL	21.9 ± 7.8	20.9 ± 8.3	0.488
Triglycerides, ref: < 150 mg/dL	151 (118-187)	137 (111-184)	0.13
PaO <sub>2</sub> /FiO <sub>2</sub> ratio	240 (161-287)	159 (96-245)	< 0.0001
Neutrophil/lymphocyte ratio	5.9 (3.5-9.9)	9.6 (6.4-13.7)	< 0.0001
Other, n (%)			
Metabolic syndrome	49.0 (46.2)	45.0 (52.3)	0.401
Severe COVID-19, PaO <sub>2</sub> /FiO <sub>2</sub> < 100 mmHg	9 (8.2)	23 (26.7)	< 0.0001
Orotracheal intubation	13 (11.3)	36 (40.9)	< 0.0001
Acute kidney injury	11 (11)	26 (34.7)	< 0.0001
Thrombotic event	1 (1.0)	2 (2.7)	0.576
Death	6 (5.3)	25 (29.8)	< 0.0001
Days between the beginning of symptoms and hospitalization	7.2 ± 3.4	8.6 ± 4.9	0.027

Length of hospital stay in days	7 (4-10)	8 (6-10)	0.131
Days in ICU	7 (5-12)	12 (6-13)	0.395
Days between ICU requirement and death	7 (6-7)	5 (3-7)	0.203

BMI: Body mass index; q-SOFA: Quick-sequential organ failure assessment; SOFA: Sequential organ failure assessment; NEWS: National early warning score; PSI/PORT: Pneumonia severity index; CRP: C-reactive protein; LDH: Lactate dehydrogenase; CPK: Creatine phosphokinase; ALT: Alanine aminotransferase; AST: Aspartate aminotransferase; ALP: Alkaline phosphatase; COVID-19: Coronavirus disease 2019; ICU: Intensive care unit; PaO<sub>2</sub>/FiO<sub>2</sub> ratio: Ratio of arterial oxygen partial pressure to fractional inspired oxygen.

**Table 4 Logistic regression analysis to evaluate the association between LFN-COVID-19 index and clinical outcomes**

	Orotracheal intubation				Acute kidney injury			
	OR	95%CI	B coefficient	P value	OR	95%CI	B coefficient	P value
LFN-COVID-19 index	1.900	1.481-2.437	0.642	0.000	1.849	1.366-2.504	0.615	0.000
Sex	0.605	0.288-1.271	-0.502	0.185	0.280	0.103-0.765	-1.272	0.013
Age	0.966	0.939-0.993	-0.035	0.015	1.021	0.988-1.054	0.021	0.209
BMI	1.054	0.997-1.114	0.053	0.061	1.085	1.011-1.164	0.081	0.023

OR: Odds ratio; CI: Confidence interval; BMI: Body mass index; COVID-19: Coronavirus disease 2019.

**Table 5 Cox proportional hazard multivariate analysis for mortality in patients with metabolic associated fatty liver disease according to the LFN-COVID-19 index**

	OR	B coefficient	P value	95%CI
LFN-COVID-19 index	0.241	-1.422	0.013	0.079-0.741
PaO <sub>2</sub> /FiO <sub>2</sub> ratio	1.000	0.000	0.877	0.996-1.004
Neutrophil/lymphocyte ratio	1.043	0.042	0.030	1.004-1.083
Creatine phosphokinase	1.001	0.001	0.340	0.999-1.002
Body mass index in kg/m <sup>2</sup>	1.093	0.089	0.002	1.033-1.157

OR: Odds ratio; CI: Confidence interval; COVID-19: Coronavirus disease 2019; PaO<sub>2</sub>/FiO<sub>2</sub> ratio: Ratio of arterial oxygen partial pressure to fractional inspired oxygen.

ratio and BMI.

In this analysis, a LFN-COVID-19 index > 1.67 was associated independently to other variables of mortality, including severity markers, prognostic scores and general characteristics (Figure 4).

### Validation cohort

From the 697 patients included in the validation cohort, 104 had MAFLD (15.0%). In general, patients with MAFLD were younger and had higher degrees of obesity and mild abnormalities in liver chemistry (Supplementary Table 1). The MAFLD group was further analyzed according to the LFN-COVID-19 index, finding higher levels of C-reactive protein and D-dimer in the group > 1.67, with little changes in the rest of the variables (Supplementary Table 2). Interestingly, mechanical intubation and clinical outcomes including mortality, were more frequent in the > 1.67 group, as was found in the initial cohort (Supplementary Table 3). These same findings in another cohort and in a different hospital highlight the validity of the LFN-COVID-19 index.

## DISCUSSION

MAFLD is currently the main etiology of chronic liver disease in the world. The main associated risk factors are obesity, type 2 diabetes, dyslipidemia and metabolic syndrome, all factors with a growing incidence. Both risk factors for MAFLD and MAFLD itself have also been shown to have prognostic value in COVID-19, associating their presence with higher severity and mortality. However, it remains

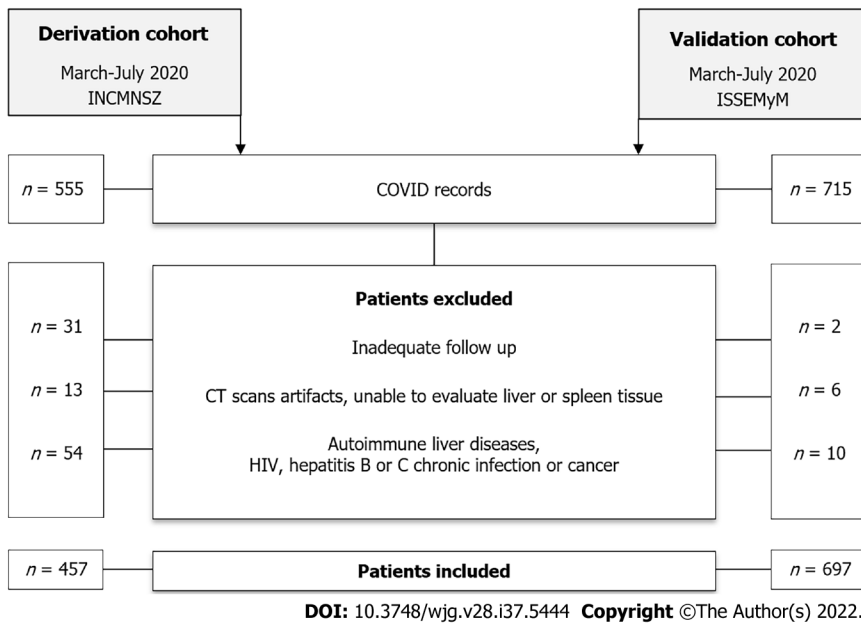


**Figure 1** Flowchart of participants in both cohorts. COVID: Coronavirus disease 2019; CT: Computed tomography; HIV: Human Immunodeficiency virus.

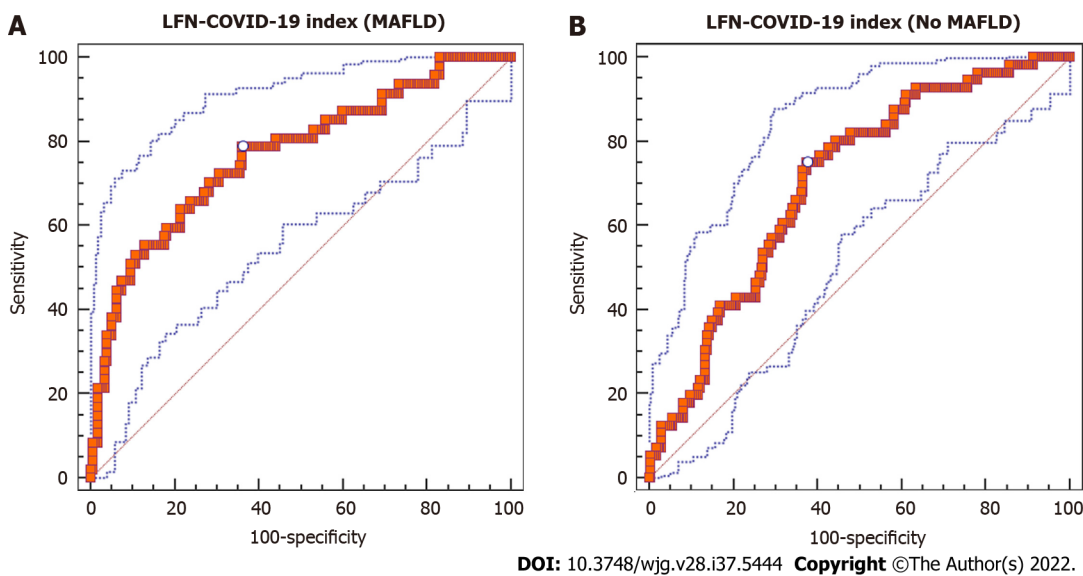


**Figure 2** Area under the receiver operating characteristic curve for the LFN-coronavirus disease 2019 index to predict mortality. A: Patients with metabolic associated fatty liver disease and coronavirus disease 2019; B: Patients without metabolic associated fatty liver disease and coronavirus disease 2019. MAFLD: Metabolic associated fatty liver disease; COVID-19: Coronavirus disease 2019; LFN: Liver fibrosis and nutrition.

controversial whether all patients within the spectrum of MAFLD have a worse prognosis or only those who, in addition to steatosis, have fibrosis[16].

Evidence pointing to MAFLD as a prognostic factor emerged from different studies around the world. A retrospective study in patients with COVID-19 found an association of MAFLD with higher intensive care unit admittance (OR: 2.3, 95%CI: 1.27-4.17), mechanical ventilation (2.08, 95%CI: 1.2-3.6) and in patients with cirrhosis with higher mortality (12.5, 95%CI: 2.16-72.5)[6]. In a cohort study in patients with COVID-19 and chronic liver disease (42% MAFLD), the authors observed a relative risk of 2.8 (95%CI: 1.9-4.0) for death in this group of patients, regardless of age, race, BMI, presence of hypertension or diabetes[12]. Another study conducted in Zhejiang, China found that hospitalized COVID-19 patients who had MAFLD with fibrosis (evaluated through FIB-4 and NFS - nonalcoholic fatty liver disease fibrosis score) were at increased risk of severe disease, regardless of other comorbidities[5]. Lastly, a study conducted by Lucifora *et al*[17] showed that patients with COVID-19 and MAFLD had a higher prevalence of alterations in the liver biochemistry test as well as a longer viral clearance time compared with patients without MAFLD.

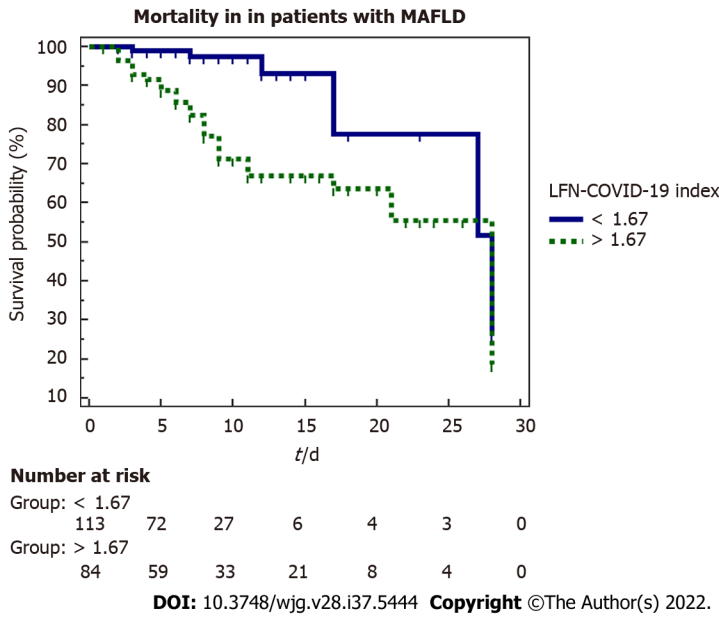


**Figure 3** Kaplan-Meier curve for 28-d mortality according to the LFN-coronavirus disease 2019 index. MAFLD: Metabolic associated fatty liver disease; COVID-19: Coronavirus disease 2019; LFN: Liver fibrosis and nutrition.

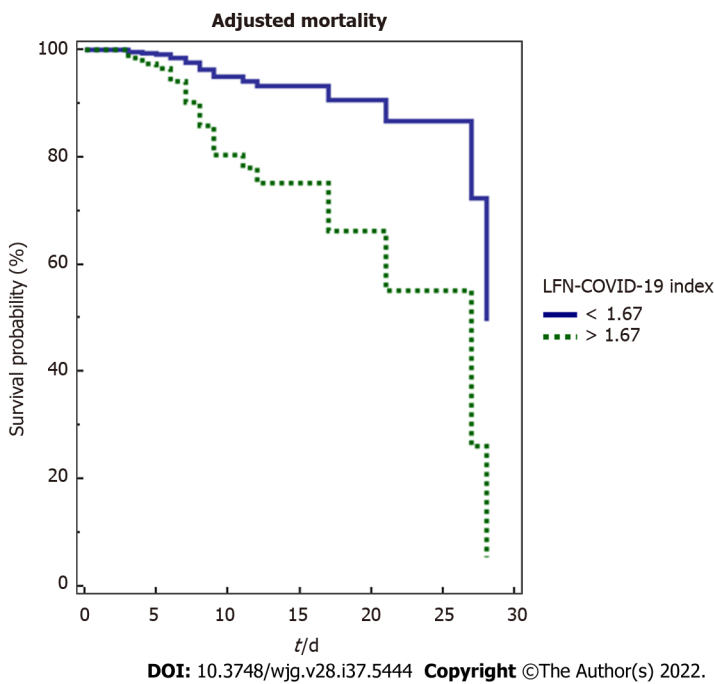


**Figure 4** Adjusted mortality analysis (Cox regression) for 28-d mortality according to LFN-coronavirus disease 2019 index. COVID-19: Coronavirus disease 2019; LFN: Liver fibrosis and nutrition.

Considering the evidence mentioned above, it is possible that the synergism between the baseline proinflammatory state of patients with MAFLD together with the body’s inflammatory response to COVID-19 could be the pathophysiological support that explains greater severity and worse prognosis in these patients. Another important component in multiorgan damage in COVID-19, is the state of hypoxemia, cell death and hypoperfusion reflected by biomarkers such as LDH, which correlates positively with worse clinical outcomes (including mortality). Although it is not specific for liver damage, it can be a sensitive and dynamic marker of hypoxic tissue damage due to its short half-life, together with other well-known markers of liver damage, such as AST, ALT and the AST/ALT ratio[10].

Due to the link between MAFLD and COVID-19 and the higher risk of mortality and adverse clinical outcomes, we conceived a prognostic index intended to be used in patients with MAFLD, including variables reflecting the pathophysiology of liver damage, mainly hepatocyte cell death induced by the factors previously mentioned, and associating it with hard clinical outcomes, including mortality[18].

The LFN-COVID-19 index includes the AST/ALT ratio as well as LDH levels normalized by the laboratory's upper limit of normal, facilitating the implementation of the index by non-restricting its usefulness to a specific cutoff value (AST, ALT or LDH). This overcomes the problem of regional variations in laboratory values. The use of this index has potential implications in clinical practice establishing a prognosis of patients. On the other hand, the simplicity of the index allows easy calculation and includes widely available, cheap and reliable laboratory tests.

In the present study, we found a good diagnostic performance of the LFN-COVID-19 index in hospitalized patients with MAFLD and COVID-19. In the ROC curve analysis, a cutoff value of  $> 1.67$  was associated with adverse clinical outcomes including the need for mechanical ventilation, acute kidney injury and higher mortality. This was reproduced in the validation cohort performed at a different center finding this cutoff point as the best for predicting these outcomes[19].

An interesting finding was that there were no differences in the days of stay in the intensive care unit based on this cutoff point. The same length of stay in the intensive care unit could be explained by the severity of the disease, where those with an index below 1.67 were discharged from the critical care area earlier and those with an index above 1.67 present earlier mortality.

Among the weaknesses of this study was the fact that the diagnosis of hepatic steatosis was made with computed tomography. However, given the high risk of transmission of SARS-CoV-2 to healthcare workers, this safer approach was chosen in order to reduce the exposure involved in carrying out a study such as transient hepatic elastography or magnetic resonance imaging requiring more time to perform it. Another aspect to highlight is that patients with COVID-19 usually present with elevated transaminases and LDH from multifactorial causes. Nevertheless, both biomarkers have been widely used as markers of hepatocyte cell death and may reflect liver damage occurring during SARS-CoV-2 infection and exacerbated in patients with MAFLD.

This study has several strengths. The sample size was adequate and sufficient due to the fact that the study was carried out in a center fully converted for the care of COVID-19 patients and included the general population in a country with a highest prevalence of MAFLD and a genetic profile that predisposes the population to the development of metabolic diseases such as type 2 diabetes mellitus, obesity and metabolic syndrome. In addition, we included an external validation cohort, where the results were replicated, enhancing the validity of the LFN-COVID-19 index.

---

## CONCLUSION

---

Based on the findings of this study, we propose a new prognostic index based on markers of liver damage and severity in patients with MAFLD and COVID-19, which can be used in clinical practice to stratify the risk of adverse outcomes in MAFLD patients. Timely actions to reduce the associated morbidity and mortality in this population could be achieved through the implementation of this index.

## ARTICLE HIGHLIGHTS

### **Research background**

This article was conceived considering the high prevalence of metabolic associated fatty liver disease (MAFLD) in the general population amid the coronavirus disease 2019 (COVID-19) pandemic and the risk of these patients in clinical settings with limited resources.

### **Research motivation**

The growing evidence showing worse clinical outcomes in patients with metabolic diseases and COVID-19, including those with fatty liver disease, and the lack of a specific index to specifically stratify patients with both conditions motivated the creation of an index capable of discriminating those patients with an unfavorable outcome.

### **Research objectives**

To evaluate the diagnostic yield of the liver fibrosis and nutrition (LNF)-COVID-19 index (includes lactate dehydrogenase, aspartate aminotransferase and alanine aminotransferase values), to predict adverse clinical outcomes, including mortality, in patients with both COVID-19 and MAFLD.

### **Research methods**

Data from a derivation cohort, including patients admitted with a diagnosis of severe COVID-19 and meeting the MAFLD criteria identified the best LFN-COVID-19 index cutoff value for risk stratification. The results were evaluated using a validation cohort.

**Research results**

The LFN-COVID-19 index with a cutoff point > 1.67 was associated with higher mortality ( $P < 0.001$ ) with an area under the curve of 0.77 (95% confidence interval: 0.709-0.823), sensitivity of 78.7% and specificity of 63.8%. It was independently associated with worse outcomes such as higher mortality, intubation rate and acute kidney injury in both cohorts.

**Research conclusions**

The LFN-COVID-19 index with a cutoff point > 1.67 showed good discrimination capability in patients with severe COVID-19 and MAFLD, identifying patients with an unfavorable prognosis associated with the need for mechanical ventilation, acute kidney injury and higher mortality.

**Research perspectives**

The use of this prognostic index will allow timely identification of patients with MAFLD and COVID-19 at higher risk of adverse clinical outcomes, leading to better therapeutic decision-making and resource allocation.

**FOOTNOTES**

**Author contributions:** Macías-Rodríguez RU contributed to conception and design of the study; Macías-Rodríguez RU, Solís-Ortega AA and Ornelas-Arroyo VJ contributed with data extraction, literature review and writing; Macías-Rodríguez RU, Ruiz-Margáin A and Román-Calleja BM contributed with writing and analysis of data; Macías-Rodríguez RU, Solís-Ortega AA, Ornelas-Arroyo VJ, Ruiz-Margáin A, Román-Calleja BM, González-Huezo MS, Urdiales-Morán NA, Mayorquín-Aguilar JM, González-Regueiro JA, Campos-Murguía A, Toledo-Coronado IV, Chapa-Ibargüengoitia M, Valencia-Peña B, Martínez-Cabrera CF and Flores-García NC contributed to drafting, critical revision, supervision and editing of the content of the manuscript.

**Institutional review board statement:** The study was reviewed and approved by the Instituto Nacional de Ciencias Médicas y Nutrición Salvador Zubirán Institutional Review Board (approval No. 3777).

**Informed consent statement:** Due to the retrospective nature of the study, no informed consent was needed.

**Conflict-of-interest statement:** All the authors report no relevant conflicts of interest for this article.

**Data sharing statement:** No additional data are available.

**STROBE statement:** The authors have read the STROBE Statement-checklist of items, and the manuscript was prepared and revised according to the STROBE Statement-checklist of items.

**Open-Access:** This article is an open-access article that was selected by an in-house editor and fully peer-reviewed by external reviewers. It is distributed in accordance with the Creative Commons Attribution NonCommercial (CC BY-NC 4.0) license, which permits others to distribute, remix, adapt, build upon this work non-commercially, and license their derivative works on different terms, provided the original work is properly cited and the use is non-commercial. See: <https://creativecommons.org/licenses/by-nc/4.0/>

**Country/Territory of origin:** Mexico

**ORCID number:** Ricardo Ulises Macías-Rodríguez 0000-0002-7637-4477; Alberto Adrián Solís-Ortega 0000-0003-2715-503X; Berenice M Román-Calleja 0000-0001-7624-9679; Juan M Mayorquín-Aguilar 0000-0002-5805-1455; José A González-Regueiro 0000-0001-5211-4710; Alejandro Campos-Murguía 0000-0002-2178-302X; Israel Vicente Toledo-Coronado 0000-0002-5479-3953; Mónica Chapa-Ibargüengoitia 0000-0001-7178-0073; Carlos Fernando Martínez-Cabrera 0000-0002-5549-5763; Nayelli C Flores-García 0000-0003-3930-2682.

**S-Editor:** Gao CC

**L-Editor:** Filipodia

**P-Editor:** Li X

**REFERENCES**

- 1 **Johns Hopkins University.** COVID-19 Dashboard by the Center for Systems Science and Engineering (CSSE) at Johns Hopkins University (JHU). *JHU* 2022; 1-2 [DOI: [10.21203/rs.3.rs-15447/v1](https://doi.org/10.21203/rs.3.rs-15447/v1)]
- 2 **Guan WJ, Ni ZY, Hu Y, Liang WH, Ou CQ, He JX, Liu L, Shan H, Lei CL, Hui DSC, Du B, Li LJ, Zeng G, Yuen KY, Chen RC, Tang CL, Wang T, Chen PY, Xiang J, Li SY, Wang JL, Liang ZJ, Peng YX, Wei L, Liu Y, Hu YH, Peng P, Wang JM, Liu JY, Chen Z, Li G, Zheng ZJ, Qiu SQ, Luo J, Ye CJ, Zhu SY, Zhong NS; China Medical Treatment Expert Group for Covid-19.** Clinical Characteristics of Coronavirus Disease 2019 in China. *N Engl J Med* 2020; **382**: 1708-1720

- [PMID: [32109013](#) DOI: [10.1056/NEJMoa2002032](#)]
- 3 **Santoso A**, Pranata R, Wibowo A, Al-Farabi MJ, Huang I, Antariksa B. Cardiac injury is associated with mortality and critically ill pneumonia in COVID-19: A meta-analysis. *Am J Emerg Med* 2021; **44**: 352-357 [PMID: [32331955](#) DOI: [10.1016/j.ajem.2020.04.052](#)]
  - 4 **Shi S**, Qin M, Shen B, Cai Y, Liu T, Yang F, Gong W, Liu X, Liang J, Zhao Q, Huang H, Yang B, Huang C. Association of Cardiac Injury With Mortality in Hospitalized Patients With COVID-19 in Wuhan, China. *JAMA Cardiol* 2020; **5**: 802-810 [PMID: [32211816](#) DOI: [10.1001/jamacardio.2020.0950](#)]
  - 5 **Targher G**, Mantovani A, Byrne CD, Wang XB, Yan HD, Sun QF, Pan KH, Zheng KI, Chen YP, Eslam M, George J, Zheng MH. Risk of severe illness from COVID-19 in patients with metabolic dysfunction-associated fatty liver disease and increased fibrosis scores. *Gut* 2020; **69**: 1545-1547 [PMID: [32414813](#) DOI: [10.1136/gutjnl-2020-321611](#)]
  - 6 **Hashemi N**, Viveiros K, Redd WD, Zhou JC, McCarty TR, Bazarbashi AN, Hathorn KE, Wong D, Njie C, Shen L, Chan WW. Impact of chronic liver disease on outcomes of hospitalized patients with COVID-19: A multicentre United States experience. *Liver Int* 2020; **40**: 2515-2521 [PMID: [32585065](#) DOI: [10.1111/liv.14583](#)]
  - 7 **Zhang G**, Hu C, Luo L, Fang F, Chen Y, Li J, Peng Z, Pan H. Clinical features and short-term outcomes of 221 patients with COVID-19 in Wuhan, China. *J Clin Virol* 2020; **127**: 104364 [PMID: [32311650](#) DOI: [10.1016/j.jcv.2020.104364](#)]
  - 8 **Huang C**, Wang Y, Li X, Ren L, Zhao J, Hu Y, Zhang L, Fan G, Xu J, Gu X, Cheng Z, Yu T, Xia J, Wei Y, Wu W, Xie X, Yin W, Li H, Liu M, Xiao Y, Gao H, Guo L, Xie J, Wang G, Jiang R, Gao Z, Jin Q, Wang J, Cao B. Clinical features of patients infected with 2019 novel coronavirus in Wuhan, China. *Lancet* 2020; **395**: 497-506 [PMID: [31986264](#) DOI: [10.1016/S0140-6736\(20\)30183-5](#)]
  - 9 **Siordia JA Jr**. Epidemiology and clinical features of COVID-19: A review of current literature. *J Clin Virol* 2020; **127**: 104357 [PMID: [32305884](#) DOI: [10.1016/j.jcv.2020.104357](#)]
  - 10 **Chaudhary A**, Chauhan V. Lactate dehydrogenase as an indicator of liver diseases. *J Adv Med Dental Sci Res* 2015; **3** [DOI: [10.12980/jclm.3.2015j5-54](#)]
  - 11 **Kotoh K**, Enjoji M, Kato M, Kohjima M, Nakamuta M, Takayanagi R. A new parameter using serum lactate dehydrogenase and alanine aminotransferase level is useful for predicting the prognosis of patients at an early stage of acute liver injury: a retrospective study. *Comp Hepatol* 2008; **7**: 6 [PMID: [18700988](#) DOI: [10.1186/1476-5926-7-6](#)]
  - 12 **Singh S**, Khan A. Clinical Characteristics and Outcomes of Coronavirus Disease 2019 Among Patients With Preexisting Liver Disease in the United States: A Multicenter Research Network Study. *Gastroenterology* 2020; **159**: 768-771.e3 [PMID: [32376408](#) DOI: [10.1053/j.gastro.2020.04.064](#)]
  - 13 **Cassidy WM**, Reynolds TB. Serum lactic dehydrogenase in the differential diagnosis of acute hepatocellular injury. *J Clin Gastroenterol* 1994; **19**: 118-121 [PMID: [7963356](#) DOI: [10.1097/00004836-199409000-00008](#)]
  - 14 **Yan L**, Zhang HT, Xiao Y, Wang M, Guo Y, Sun C, Liang J, Li S, Zhang M, Tang X, Cao H, Tan X, Huang NN, Jiao B, Luo A, Cao Z, Xu H, Yuan Y. Prediction of criticality in patients with severe Covid-19 infection using three clinical features: a machine learning-based prognostic model with clinical data in Wuhan. 2020 Preprint. Available from: medRxiv:20028027 [DOI: [10.1101/2020.02.27.20028027](#)]
  - 15 **Li X**, Xu S, Yu M, Wang K, Tao Y, Zhou Y, Shi J, Zhou M, Wu B, Yang Z, Zhang C, Yue J, Zhang Z, Renz H, Liu X, Xie J, Xie M, Zhao J. Risk factors for severity and mortality in adult COVID-19 inpatients in Wuhan. *J Allergy Clin Immunol* 2020; **146**: 110-118 [PMID: [32294485](#) DOI: [10.1016/j.jaci.2020.04.006](#)]
  - 16 **Ruiz-Margáin A**, Campos-Murguía A, González-Regueiro JA, Román-Calleja BM, Delint DK, Macías-Rodríguez RU. Reply to: "Liver fibrosis and adverse outcomes in COVID-19". *Dig Liver Dis* 2021; **53**: 800 [PMID: [33947641](#) DOI: [10.1016/j.dld.2021.04.001](#)]
  - 17 **Lucifora J**, Michelet M, Rivoire M, Protzer U, Durantel D, Zoulim F. Two-dimensional-cultures of primary human hepatocytes allow efficient HBV infection: Old tricks still work! *J Hepatol* 2020; **73**: 449-451 [PMID: [32423632](#) DOI: [10.1016/j.jhep.2020.03.042](#)]
  - 18 **Wynants L**, Van Calster B, Collins GS, Riley RD, Heinze G, Schuit E, Bonten MMJ, Dahly DL, Damen JAA, Debray TPA, de Jong VMT, De Vos M, Dhiman P, Haller MC, Harhay MO, Henckaerts L, Heus P, Kammer M, Kreuzberger N, Lohmann A, Luijken K, Ma J, Martin GP, McLernon DJ, Andaur Navarro CL, Reitsma JB, Sergeant JC, Shi C, Skoetz N, Smits LJM, Snell KIE, Sperrin M, Spijker R, Steyerberg EW, Takada T, Tzoulaki I, van Kuijk SMJ, van Bussel B, van der Horst ICC, van Royen FS, Verbakel JY, Wallisch C, Wilkinson J, Wolff R, Hooft L, Moons KGM, van Smeden M. Prediction models for diagnosis and prognosis of covid-19: systematic review and critical appraisal. *BMJ* 2020; **369**: m1328 [PMID: [32265220](#) DOI: [10.1136/bmj.m1328](#)]
  - 19 **World Health Organization**. Clinical management of COVID-19: evolutionary guidelines, January 25, 2021. [cited 16 Jun 2022]. In: World Health Organization [Internet]. Available from: <https://apps.who.int/iris/handle/10665/338882>

## Retrospective Study

## Efficacy of endoscopic ultrasound in the evaluation of small gastrointestinal stromal tumors

Qi-Chao Ge, Yu-Fan Wu, Zi-Ming Liu, Zhe Wang, Sheng Wang, Xiang Liu, Nan Ge, Jin-Tao Guo, Si-Yu Sun

**Specialty type:** Gastroenterology and hepatology**Provenance and peer review:** Unsolicited article; Externally peer reviewed.**Peer-review model:** Single blind**Peer-review report's scientific quality classification**

Grade A (Excellent): A, A

Grade B (Very good): B

Grade C (Good): 0

Grade D (Fair): 0

Grade E (Poor): 0

**P-Reviewer:** Kim HJ, South Korea; Sundaram S, India; Villa E, United States**Received:** June 22, 2022**Peer-review started:** June 22, 2022**First decision:** September 2, 2022**Revised:** September 14, 2022**Accepted:** September 20, 2022**Article in press:** September 20, 2022**Published online:** October 7, 2022**Qi-Chao Ge, Yu-Fan Wu, Zi-Ming Liu, Sheng Wang, Xiang Liu, Nan Ge, Jin-Tao Guo, Si-Yu Sun,** Department of Gastroenterology, Shengjing Hospital of China Medical University, Shenyang 110004, Liaoning Province, China**Zhe Wang,** Department of Pathology, Shengjing Hospital of China Medical University, Shenyang 110004, Liaoning Province, China**Corresponding author:** Jin-Tao Guo, MD, PhD, Professor, Department of Gastroenterology, Shengjing Hospital of China Medical University, No. 36 Sanhao Street, Shenyang 110004, Liaoning Province, China. [guojt@sj-hospital.org](mailto:guojt@sj-hospital.org)**Abstract****BACKGROUND**

Gastrointestinal stromal tumors (GISTs) with a diameter of < 2 cm are called small GISTs. Currently, endoscopic ultrasound (EUS) is widely used as a regular follow-up method for GISTs, which can also provide a preliminary basis for judging the malignancy potential of lesions. However, there are no studies on the accuracy of EUS to assess the malignant potential of small GISTs.

**AIM**

To evaluate the efficacy of EUS in the diagnosis and risk assessment of small GISTs.

**METHODS**

We collected data from patients with small GISTs who were admitted to Shengjing Hospital of China Medical University between October 2014 and July 2019. The accurate diagnosis and risk classifications of patients were based on the pathological assessment according to the modified National Institute of Health criteria after endoscopic resection or laparoscopic surgery. Preoperative EUS features (marginal irregularity, cystic changes, homogeneity, ulceration, and strong echogenic foci) were retrospectively analyzed. The assessment results based on EUS features were compared with the pathological features.

**RESULTS**

A total of 256 patients (69 men and 187 women) were enrolled. Pathological results included 232, 16, 7, and 1 very low-, low-, intermediate-, and high-risk cases, respectively. The most frequent tumor location was the gastric fundus (78.1%), and mitoses were calculated as > 5/50 high power field in 8 (3.1%)

patients. Marginal irregularity, ulceration, strong echo foci, and heterogeneity were detected in 1 (0.4%), 2 (0.8%), 22 (8.6%), and 67 (65.1%) patients, respectively. However, cystic changes were not detected. Tumor size was positively correlated with the mitotic index ( $P < 0.001$ ). Receiver operating curve analysis identified 1.48 cm as the best cut-off value to predict malignant potential (95% confidence interval: 0.824–0.956). EUS heterogeneity with tumor diameters  $> 1.48$  cm was associated with higher risk classification ( $P < 0.05$ ).

### CONCLUSION

Small GISTs (diameters  $> 1.48$  cm) with positive EUS features should receive intensive surveillance or undergo endoscopic surgery. EUS and dissection are efficient diagnostic and therapeutic approaches for small GISTs.

**Key Words:** Gastrointestinal stromal tumors; Endoscopic ultrasound; Diagnosis; Risk classification

©The Author(s) 2022. Published by Baishideng Publishing Group Inc. All rights reserved.

**Core Tip:** Endoscopic ultrasound (EUS) has been the recommended follow-up method for small gastrointestinal stromal tumors (GISTs); however, it is not clear whether positive EUS features can predict the malignant potential of small GISTs. Besides, undergoing close follow-up is an economic and mental burden on patients with small GISTs. This study illustrates an optimal cut-off value for the tumor size (1.48 cm) of small GISTs and uses heterogeneity to evaluate risk prediction. Overall, small GISTs with diameters  $> 1.48$  cm with positive EUS features should receive more intensive follow-up or undergo endoscopic surgery.

**Citation:** Ge QC, Wu YF, Liu ZM, Wang Z, Wang S, Liu X, Ge N, Guo JT, Sun SY. Efficacy of endoscopic ultrasound in the evaluation of small gastrointestinal stromal tumors. *World J Gastroenterol* 2022; 28(37): 5457-5468

**URL:** <https://www.wjgnet.com/1007-9327/full/v28/i37/5457.htm>

**DOI:** <https://dx.doi.org/10.3748/wjg.v28.i37.5457>

## INTRODUCTION

Gastrointestinal stromal tumors (GISTs) are the most common mesenchy-derived tumors of the gastrointestinal tract[1,2]. They occur most frequently in the stomach, accounting for approximately 60% of all cases[3,4]. Most GISTs contain mutations that activate the c-kit or platelet-derived growth factor receptor  $\alpha$  gene[5,6]. The golden standard for the diagnosis of GISTs relies on pathological features assessed by methods, such as hematoxylin and eosin (H&E) and immunohistochemical staining. Currently, the risk classification of GISTs is mainly based on the National Institute of Health (NIH) 2008 (modified) or Fletcher criteria[7,8], which include tumor size (2, 5, and 10 cm), mitotic index, primary tumor sites, and tumor rupture.

GISTs with a diameter of  $< 2$  cm are called small GISTs[9]. Currently, the management of small GISTs is controversial. There is no consensus on the treatment of GIST with a diameter of  $< 2$  cm in the latest guidelines of the National Comprehensive Cancer Network (NCCN) (United States), European Society for Medical Oncology (ESMO), and Chinese Society of Clinical Oncology (CSCO)[10-12]. Most small GISTs are discovered incidentally during regular endoscopic scanning, and they are now easier to be detected than before using endoscopic ultrasound (EUS). EUS has been the widely recommended surveillance method for small GISTs. In addition, EUS elastography, contrast-enhanced EUS, and EUS-guided fine needle aspiration and biopsy (EUS-FNA/FNB) have further improved their diagnostic accuracy[13-16]. Furthermore, EUS features have been used in some studies to predict the risk degree of GISTs[17-19]. However, the management of small GISTs remains controversial, and endoscopic resection *via* endoscopic submucosal dissection (ESD) or endoscopic full-thickness resection (EFTR) is not recommended as a routine treatment. Conversely, no study has focused on the positive EUS features for determining the degree of risk for small GISTs. Therefore, in this study, we aimed to identify the efficiency of EUS in the risk assessment and safety of endoscopic dissection for small GISTs.

## MATERIALS AND METHODS

### Patients

Data on consecutive patients with pathologically confirmed GISTs who were admitted to Shengjing Hospital of China Medical University between September 2014 and July 2019 were collected. The study included patients who underwent endoscopic resection and were pathologically or genotypically diagnosed with GISTs with a diameter of  $\leq 2$  cm. All the patients underwent preoperative EUS examination. Patients with other sarcomatous malignancies and/or with incomplete data were excluded. This study was approved by the Institutional Review Board and the Ethics Committee of China Medical University (No. 2022PS009K), and all the patients provided informed consent to participate in the study.

### EUS examination

Linear EUS (EG3870UT; Pentax, Tokyo, Japan) was used for the examination. Two experienced endoscopists, who were blinded to the pathological results of these lesions, retrospectively evaluated the characteristics of the EUS images to determine whether there were positive features, including irregular borders, cystic changes, ulcerations, strong echogenic foci, heterogeneity, and the presence of an exogenous type of development (Figures 1 and 2). According to the NCCN guidelines, one or more positive EUS features indicate the malignant potential of small GISTs.

### Endoscopic resection procedure

The equipment and accessories used during the endoscopic procedure included a standard single-channel gastroscope (EG29-i10, Pentax, Tokyo, Japan) and a transparent cap. Triangle- (IT knife, Olympus Corporation, Tokyo, Japan) and insulation- tipped knives (IT knife, Olympus Corporation, Tokyo, Japan) were used for the dissection and resection of tumors. During the procedure, hot biopsy forceps (FD-410LR, Olympus Corporation, Tokyo, Japan) were used for hemostasis. Metal clips (Boston Resolution™, Boston, United States) and an over-the-scope clips (OTSC) (Ovesco Endoscopy GmbH, Tuebingen, Germany) were used for the closure of defects.

All endoscopic resections were performed by skilled gastroenterologists, following the standard endoscopic treatment regimen. All procedures were performed using propofol sedation under continuous cardiorespiratory monitoring. Ligation-assisted endoscopic resection, ESD, and EFTR were performed to resect gastric GISTs.

### Pathological examination

All resected GIST specimens were routinely processed using a standard surgical pathology protocol after overnight fixation in 10% neutral buffered formalin solution. The details of the tumor site, size, shape, surface color, and consistency were documented by a surgical pathologist. Conventional immunohistochemistry with a panel of antibodies, such as CD117 (c-kit), CD34, Dog-1, S-100, and smooth muscle actin, was used to support the histopathological diagnosis of GIST. Based on the modified NIH criteria, patients with GISTs were divided into very low-, low-, intermediate-, and high-risk groups (Table 1).

### Follow-up strategy

All the patients were routinely followed-up with conventional endoscopic surveillance at 1, 3, 6, and 12 mo after resection. This was followed by annual abdominal computed tomography (CT) for 3 years to rule out recurrence and metastasis. If no residual tumor or tumor recurrence was observed, endoscopic examinations were performed once every 2 years. The follow-up period was up to October 2020. If residual tumor or tumor recurrence was detected, endoscopic resection or surgery could be performed.

### Statistical analysis

Data processing was performed using the SPSS statistical software (SPSS 23.0, Chicago, IL, United States). Continuous data are expressed as the mean  $\pm$  SD, and categorical data are displayed as number (*n*) or percentage (%). The accuracy of the diagnostic test was evaluated by sensitivity, specificity, false negative and positive rates, positive and negative likelihood ratios, and Youden's index. The Chi-square test was applied for intergroup comparisons. A receiver operating characteristic (ROC) curve was performed to determine the optimal tumor diameter for predicting malignant potential. Lesions with positive EUS features or mitoses more than 5/50 high power field (HPF) were defined as true positives. *P* value  $< 0.05$  was considered statistically significant.

## RESULTS

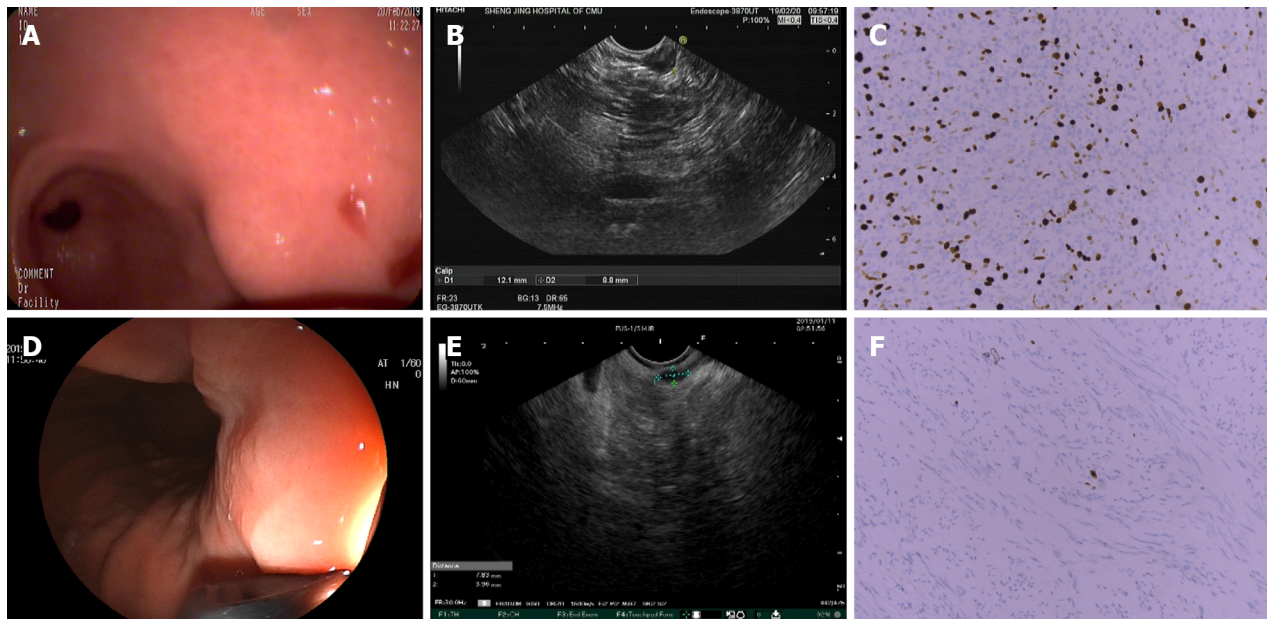
### Clinical and pathological features of small gastric GISTs

A total of 256 patients, including 69 men (27%) and 187 women (73%), were enrolled in the study

**Table 1** The modified National Institute of Health risk classification of small Gastrointestinal stromal tumors

Risk classification	Tumor diameter (d/cm)	Mitotic count (number/50 HPF)
Very-low	$D \leq 2$	Mitotic $\leq 5$
Intermediate	$D \leq 2$	$5 < \text{mitotic} \leq 10$
High	$D \leq 2$	Mitotic $> 10$

HPF: High power field.



DOI: 10.3748/wjg.v28.i37.5457 Copyright ©The Author(s) 2022.

**Figure 1** Endoscopic ultrasound imaging features were consistent with the postoperative pathological results. A: A lesion with a diameter of approximately 1.2 cm was observed in the gastric antrum using an endoscope; B: Heterogeneity was observed as a characteristic of endoscopic ultrasound (EUS) imaging; C: Gastric stromal tumor (intermediate risk). The spindle of the tumor cells is arranged in sheets and bundles with nuclear division of approximately 8-9/50 high power field. Immunohistochemistry: CD117 (+); CD34 (-); Desmin (-); Dog1 (+); Ki-67 (35%+); smooth muscle actin (+); and S-100 (-); D: A lesion with a diameter of approximately 0.6 cm was observed in the gastric fundus using an endoscope; E: EUS images were characterized by a hypoechoic mass in the muscularis propria; F: Gastric stromal tumor (very low risk). The spindle of the tumor cells is arranged in spindle and bundles without obvious nuclear division. Immunohistochemistry: CD117 (+); CD34 (-); Desmin (-); Dog1 (+); Ki-67 (< 1%+); smooth muscle actin (-); and S-100 (-).

(Table 2), with an average age of  $57.4 \pm 8.6$  years. The most frequent locations of the tumors were the gastric fundus (78.1%) and body (17.2%), and the average diameter of all lesions was 1.05 cm (range, 0.30–2.00 cm). These patients were eventually diagnosed with GISTs mainly based on pathological standards, such as H&E and immunohistochemistry staining. According to the modified NIH criterion, mitoses were calculated as  $> 5/50$  HPF and  $\leq 5/50$  HPF in 8 (3.1%) and 248 (96.9%) patients, respectively. The patients' features in the EUS images are shown in Table 2, illustrating that 67 (65.1%) and 22 (8.6%) cases were identified with heterogenous and hyperechoic foci, respectively. However, a lobular border and ulceration were detected in only 3 cases (1.2%).

### ROC curve analysis

To determine a suitable cut-off value for predicting the higher risk potential of small GISTs, aggressive biological behaviors were expanded to mitoses more than 5/50 HPF. Lesions with mitoses more than 5/50 HPF were defined as true positives. A tumor diameter of 1.48 cm was finally identified as the optimal cut-off value, with the area under the curve (AUC) being 0.89 (95% confidence interval: 0.824–0.956;  $P < 0.001$ ) (Figure 3A), a sensitivity of 0.875, and a specificity of 0.828 (Figure 3B). Subsequently, 208 and 48 patients were classified into groups with tumor size  $\leq 1.48$  cm and  $> 1.48$  cm, respectively. The comparison of the clinicopathological characteristics between the two groups is presented in Table 3. In the  $> 1.48$  cm group, a higher percentage of patients had more than 5 mitotic indexes/50 HPFs compared to those in the  $\leq 1.48$  cm group (14.58% vs 0.48%,  $P < 0.001$ ). Moreover, patients with larger tumor diameter tended to display positive EUS features (56.25% vs 31.25%,  $P = 0.002$ ).

Table 2 Clinicopathological characteristics of the patients

Characteristics	Cases (n = 256)
Age (year)	57.4 ± 8.6
Sex, n (%)	
Male	69 (27.0)
Female	187 (73.0)
Tumor location, n (%)	
Cardia	6 (2.3)
Fundus	200 (78.1)
Body	44 (17.2)
Antrum	6 (2.4)
Endoscopic resection, n (%)	
ESD	136 (53.1)
EFTR	120 (46.9)
Tumor size (cm), n (%)	
≤ 1.48	208 (81.3)
>1.48	48 (18.7)
Mitotic index (/50HPF), n (%)	
≤ 5	248 (96.9)
> 5	8 (3.1)
Modified NIH classification, n (%)	
Very-low	232 (90.6)
Low	16 (6.3)
Intermediate	7 (2.7)
High	1 (0.4)
Positive EUS features, n (%)	
Heterogenous	67 (65.1)
Hyperechoic foci	22 (8.6)
Lobular border	1 (0.4)
Ulceration	2 (0.8)

ESD: Endoscopic submucosal dissection; EFTR: Endoscopic full-thickness resection; EUS: Endoscopic ultrasound; HPF: High power field; NIH: National Institute of Health.

### Comparison of non-low-risk and low-risk GISTs in terms of EUS features

We compared the consistency of positive EUS features and pathological risk classification of small GISTs, and found that intermediate- and very low-risk cases presented with heterogeneous (Figure 1A-C) and hypoechoic (Figure 1D-F) EUS findings, respectively. This suggests that EUS imaging features were consistent with the postoperative pathological results. However, some cases showed that EUS imaging features were inconsistent with the postoperative pathological results [intermediate-risk case with hypoechoic mass (Figure 2A-C) and very-low-risk case with strong echogenic foci (Figure 2D-F)]. To further identify the efficiency of positive EUS features in the risk assessment of small GISTs, we divided these patients into non-low-risk and low-risk groups (Table 4). Five of eight patients with non-low-risk GISTs (62.5%) and 62 of 248 patients with low-risk GISTs (25%) had heterogeneous features. There was a significant difference ( $P = 0.031$ ) in the heterogeneous features between low- and high-grade risk GISTs. However, there was no statistical difference in hyperechoic foci and ulceration between low- and high-grade risk GISTs. Hyperechoic foci were found in 0 of 8 (0%) and 22 of 248 (8.87%) non-low- and low-risk groups, respectively. The ulcerative appearance was found in 0 of 8 (0%) and 2 of 248 (0.8%) non-low- and low-risk groups, respectively. Furthermore, other positive EUS

**Table 3 Comparisons of clinicopathological and endoscopic ultrasonographic features between  $\leq 1.48$  cm and  $> 1.48$  cm groups**

Characteristic	Tumor size		P value
	$\leq 1.48$ cm group	$> 1.48$ cm group	
Age (year)	57.3 $\pm$ 8.6	58.2 $\pm$ 8.4	0.49
Sex			0.368
Men	59	10	
Women	149	38	
Tumor location			0.01
Fundus	168	32	
Body	34	10	
Antrum	4	2	
Cardia	2	4	
Mitotic index (/50 HPFs)			< 0.001
$\leq 5$	207	41	
$> 5$	1	7	
Positive EUS features <sup>1</sup>			0.002
Yes	65	25	
No	143	23	

<sup>1</sup>Marginal irregularity, cystic changes, ulcers, strong echo foci, and heterogeneity. EUS: Endoscopic ultrasound; HPF: High power field.

**Table 4 Comparisons of positive endoscopic ultrasonographic features between the pathologically non-low-risk group and low-risk group**

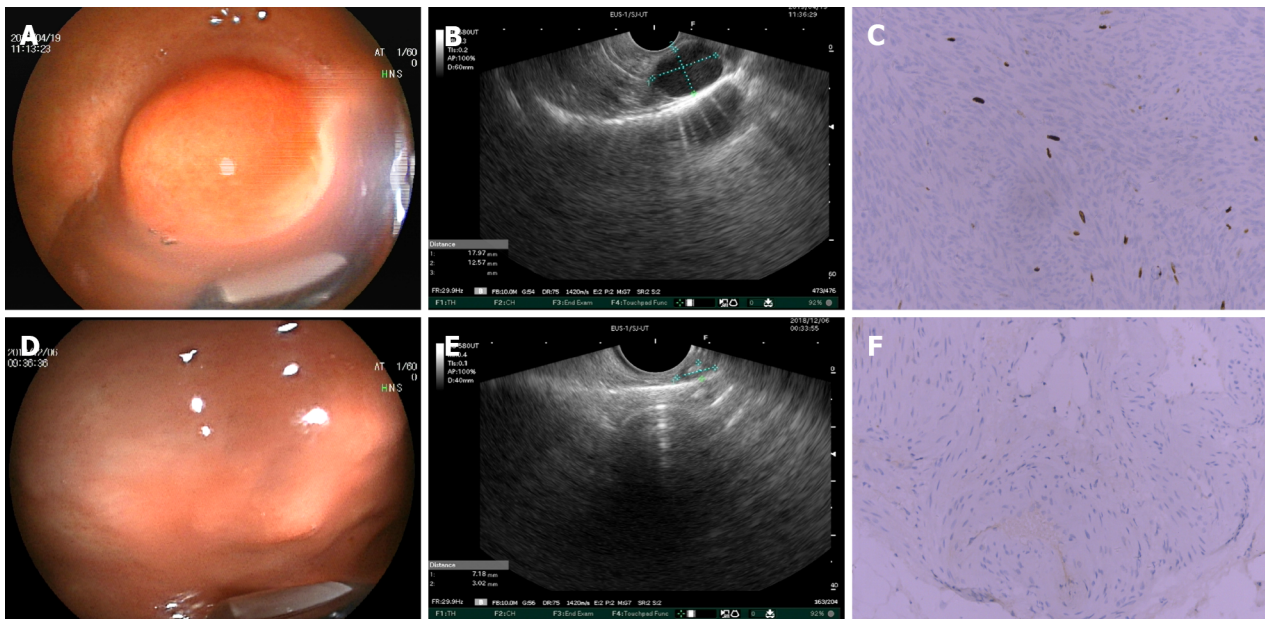
Positive EUS features	Risk classification		P value
	Intermediate/high	Very low/low	
Heterogeneous			0.031
Yes	5	62	
No	3	186	
Hyperechoic foci			NS
Yes	0	22	
No	8	226	
Ulcers			NS
Yes	0	2	
No	8	246	

EUS: Endoscopic ultrasound; NS: No significant.

features, such as marginal irregularity and cystic changes, were not detected in small GISTs.

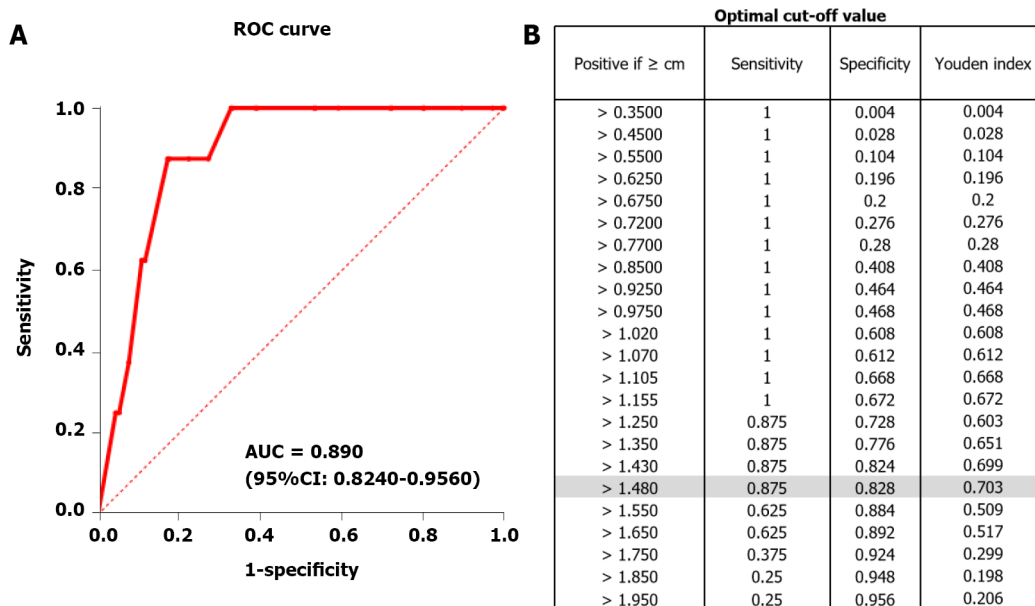
## DISCUSSION

The incidence of GIST ranges from 6 to 22 cases *per* 10<sup>6</sup> individuals *per* year[20,21], while that of small GISTs might be higher as more cases of asymptomatic small GISTs have been detected clinically due to the growing popularity of endoscopy in the recent years. Currently, there is no consensus on whether small GISTs ( $\leq 2$  cm) require resection or yearly surveillance in the latest guidelines, including NCCN, ESMO, and CSCO[10-12,22]. However, the ESMO recommends that resection should be the standard



DOI: 10.3748/wjg.v28.i37.5457 Copyright ©The Author(s) 2022.

**Figure 2 Endoscopic ultrasound imaging features were inconsistent with the postoperative pathological results.** A: A lesion with a diameter of approximately 2 cm was observed in the gastric fundus using an endoscope; B: Endoscopic ultrasound (EUS) images were characterized by a hypoechoic mass in the muscularis propria; C: Gastric stromal tumor (intermediate risk). The spindle of the tumor cells is arranged in a spindle and braided pattern with nuclear division of approximately 8/50 high power field. Immunohistochemistry: CD117 (+); CD34 (-); Desmin (-); Dog1 (+); Ki-67 (10%+); smooth muscle actin (-); and S-100 (-); D: A lesion with a diameter of approximately 0.6 cm was observed in the gastric fundus using an endoscope; E: Strong echogenic foci and heterogeneity were observed as characteristics of EUS imaging; F: Gastric stromal tumor (very low risk). The spindle of the tumor cells is arranged in spindle and bundles without obvious nuclear division. Some tissues calcify. Immunohistochemistry: CD117 (+); CD34 (+); Desmin (-); Ki-67 (1%+); smooth muscle actin (+); and S-100 (-).



DOI: 10.3748/wjg.v28.i37.5457 Copyright ©The Author(s) 2022.

**Figure 3 Receiver operating characteristic curve.** A: The receiver operating characteristic curve of the cut-off (1.48 cm); B: The optimal cut-off (1.48 cm) with a sensitivity of 0.875 and a specificity of 0.828. ROC: Receiver operating characteristic; AUC: Area under the curve.

treatment for histologically confirmed small GISTs[21]. Small GISTs are generally considered to have a low malignant potential, and few of them may progress to clinically relevant tumors. However, a population-based study reviewed 378 patients with small GISTs found that approximately 11.4% of small GISTs were accompanied by local progression or even distant metastasis when first diagnosed and claimed that small GISTs might progress and become life-threatening, with a mortality of 12% at 5 years[23]. Additionally, some scholars believe that the conservative observational methods for small GISTs can only evaluate whether the tumor diameter has increased, which will cause psychological

burden and risk to patients as clinicians would only passively wait for the tumor size to increase before performing surgical resection[24]. Therefore, it is critical to choose optimal approaches for accurately evaluating the clinical features and providing risk suggestions for small GISTs before their progression.

EUS has been recommended as an optimal method for the diagnosis and follow-up of small GISTs, while its efficacy in risk assessment of small GISTs is still not clear. The NCCN guidelines recommend that conservative follow-up should be performed in small GISTs lacking high-risk EUS features (marginal irregularity, cystic changes, ulcers, strong echo foci, and heterogeneity)[10]. Moreover, in recent years, many studies have shown that EUS can provide a preliminary basis for assessing the malignant potential of lesions. Palazzo *et al*[25] showed that EUS was reliable in predicting the malignant potential of GISTs, including three most predictive EUS features (one or more of the following: Irregular border, cystic changes, and lymph nodes with a malignant pattern) with a sensitivity of 91% and a specificity of 88%[25]. Jeon *et al*[26] found that the best predictor of high-risk GISTs was the combination of endoscopic and EUS features, including a tumor diameter > 3 cm, irregular border, mucosal ulceration, and a non-oval shape[26]. Concerning small GISTs, Gao *et al*[18] studied 69 patients suspected to have GISTs as indicated by EUS and concluded that the tumor size of > 9.5 mm was significantly correlated with tumor progression, which was of great value in predicting the malignant potential of the GISTs[18]. Wang *et al*[27] examined 648 cases of small GISTs and concluded that GISTs with a diameter of < 1.45 cm had an overall good prognosis; however, those with a diameter > 1.45 cm required intensive monitoring or had to undergo endoscopic surgery[27,28].

Our study enrolled a total of 256 patients who underwent ESD or EFTR during 2014–2019 in Shengjing Hospital including 248 very low- or low-risk cases and 8 intermediate/high-risk cases based on the modified NIH classification. We generated a ROC curve based on the potential malignancy predictor (mitoses more than 5/50 HPF) to determine the optimal cut-off value of tumor size. A tumor diameter of 1.48 cm was identified as the optimal cutoff value, with a sensitivity of 87.5%, a specificity of 82.8%, and an AUC of 0.89. Of all the 256 patients with small gastric GISTs included in our study, EUS features for malignancy prediction were studied retrospectively. Heterogeneous, hyperechoic foci, lobular border, and ulceration were detected in 67 (65.1%), 22 (8.6%), 1 (0.4%) and 2 (0.8%) patients, respectively. According to the optimal cut-off value, patients were subsequently divided into two groups:  $\leq 1.48$  cm and  $> 1.48$  cm. We identified that tumors with a diameter  $> 1.48$  cm were more likely to present positive EUS features ( $P = 0.002$ ). To further identify whether positive EUS features can predict the malignant potential of small GISTs, we compared EUS features between the non-low- and low-risk groups. The results showed that there was a significant difference between the two groups regarding the heterogeneity, which might suggest that patients with GISTs experiencing this EUS feature should be followed-up more frequently while considering endoscopic surgery when regular follow-up is not feasible or EUS-guided tissue acquisition for pathological assessment. However, there was no statistical difference in hyperechoic foci and ulceration features between the two groups. We believed that limited cases with these two EUS features might have resulted in a partial evaluation. Therefore, a larger scale study is needed to further comprehensively evaluate the efficacy of EUS for the risk prediction of small GISTs.

Other studies have shown that contrast-enhanced harmonic EUS and EUS-elastography can distinguish GISTs from other submucosal tumors, but the risk grade of GISTs cannot be evaluated[14, 29]. Moreover, another study suggests that EUS-FNA/FNB can be used to obtain tissue for assessing the malignancy risk of tumors[30]. However, for small GISTs, the diagnostic rate of EUS-FNA is low, and due to the small size of the lesion and certain mobility limitations, puncturing the tumor is difficult and the possibility of obtaining sufficient samples is low[31,32]. A study of 53 patients[33] showed that the successful diagnostic rate of an adequate specimen was related to the lesion size: Only 71% of lesions measuring  $< 20$  mm had complications led by repeated needle puncture[34,35]. In contrast, with the advance of endoscopic techniques, complete treatment has become possible *via* endoscopic surgery, such as ESD and EFTR. ESD is currently the most widely used endoscopic treatment for resecting GISTs. Studies have shown that ESD is safe and effective for treating GISTs that originate from the muscularis propria layer, with a diameter  $\leq 3$  cm and without extra-gastrointestinal invasion or abdominal metastasis[36–38]. The main adverse events of this technique are bleeding and perforation[39,40]. EFTR is mainly suitable for patients whose lesions are located in the deep muscularis propria layer and are closely connected to the serosal layer, in which metal clips, OTSCs, and other methods are used for rapid closure of defects to prevent pneumoperitoneum and peritonitis. In this study, only one patient treated with endoscopy developed delayed bleeding; however, the patient recovered well after endoscopic hemostasis was performed. Furthermore, all patients who underwent endoscopic resection had no recurrence or metastasis during a mean follow-up period of 40 mo (range, 15–72 mo), suggesting that endoscopic surgery is feasible and safe for small GISTs.

This study had a few limitations. First, the results of this retrospective study may be affected by selection bias. Second, the follow-up period was relatively short, which may result in missing cases of recurrence. Third, limited samples may affect the comprehensive evaluation of positive EUS features for risk classification. Therefore, multicenter randomized controlled trials should be conducted in the future to enhance the robustness of these conclusions.

## CONCLUSION

In conclusion, partial EUS features, such as heterogeneity, can be applied to predict higher-risk small GISTs with a diameter > 1.48 cm. These tumors with diameters > 1.48 cm should undergo more intensive surveillance. Endoscopic surgery should be strongly recommended for small GISTs if regular follow-up is infeasible for low recurrence rate and metastatic rate.

## ARTICLE HIGHLIGHTS

### **Research background**

Small gastrointestinal stromal tumors (GISTs) have a high incidence, and their prognosis and treatment remain controversial.

### **Research motivation**

Endoscopic ultrasound (EUS) plays a pivotal role in the diagnosis of GISTs, but its ability to assess the prognosis of small GISTs remains to be explored.

### **Research objectives**

To evaluate the efficacy of EUS in the diagnosis and risk assessment of small GISTs.

### **Research methods**

We collected data from patients with small GISTs, the diagnosis and risk classifications of which were based on the pathological assessment according to the modified National Institute of Health criteria after endoscopic resection or laparoscopic surgery. The assessment results based on EUS features (marginal irregularity, cystic changes, homogeneity, ulceration, and strong echogenic foci) were compared with the pathological features.

### **Research results**

A total of 256 patients (69 men and 187 women) were enrolled. Tumor size was positively correlated with the mitotic index ( $P < 0.001$ ). Receiver operating curve analysis identified 1.48 cm as the best cut-off value to predict malignant potential (95% confidence interval: 0.824–0.956). EUS heterogeneity with tumor diameters > 1.48 cm was associated with higher risk classification ( $P < 0.05$ ).

### **Research conclusions**

Small GISTs (diameters, > 1.48 cm) with positive EUS features should receive intensive surveillance or undergo endoscopic surgery. EUS and dissection are efficient diagnostic and therapeutic approaches for small GISTs.

### **Research perspectives**

EUS provides reference evidence for the precise assessment and early risk assessment of small GISTs.

## ACKNOWLEDGEMENTS

We thank Professor Si-Yu Sun, for his support and guidance during this study. We also thank all other doctors who participated in this study.

## FOOTNOTES

**Author contributions:** Ge QC wrote a majority portion of manuscript, prepared the figures and tables, and performed statistical analysis; Wu YF collected the data of patients; Liu ZM helped with the statistical analysis and manuscript writing; Wang Z provided and confirmed the pathological data of all the patients; Wang S, Liu X, and Ge N took part in the design of the study outline and performed tumor dissection; Guo JT and Sun SY were responsible for the revision of the manuscript for important intellectual content and supervised the study; all the authors read and gave their final approval for the manuscript to be submitted.

**Supported by** National Natural Science Foundation of China, No. 81900601; The University Innovation Team and Innovative Talent Support Program of Liaoning Province, No. LR2019073; and Shenyang Young and Middle-aged Science and Technology Innovation Talent Support Program, No. RC200438.

**Institutional review board statement:** This study was approved by the Ethics Review Committee of Shengjing

Hospital of China Medical University, No. 2022PS009K.

**Informed consent statement:** All the individual involved gave their informed consent prior to study inclusion.

**Conflict-of-interest statement:** All the authors report no relevant conflicts of interest for this article.

**Data sharing statement:** No additional data are available.

**Open-Access:** This article is an open-access article that was selected by an in-house editor and fully peer-reviewed by external reviewers. It is distributed in accordance with the Creative Commons Attribution NonCommercial (CC BY-NC 4.0) license, which permits others to distribute, remix, adapt, build upon this work non-commercially, and license their derivative works on different terms, provided the original work is properly cited and the use is non-commercial. See: <https://creativecommons.org/licenses/by-nc/4.0/>

**Country/Territory of origin:** China

**ORCID number:** Qi-Chao Ge 0000-0003-3412-2033; Yu-Fan Wu 0000-0003-4290-8263; Zi-Ming Liu 0000-0001-6123-4466; Zhe Wang 0000-0003-1877-826X; Sheng Wang 0000-0002-1531-7655; Nan Ge 0000-0002-5764-7054; Jin-Tao Guo 0000-0001-5722-6359; Si-Yu Sun 0000-0002-7308-0473.

**S-Editor:** Fan JR

**L-Editor:** A

**P-Editor:** Fan JR

## REFERENCES

- 1 **Di Vita M**, Zanghi A, Cavallaro A, Cardi F, Uhlig M, Ursi P, Lo Menzo E, Panebianco V, Cappellani A. Gastric GIST and prognostic models. Which is the best to predict survival after surgery? *Ann Ital Chir* 2019; **90**: 31-40 [PMID: 30942768]
- 2 **Xu C**, Han H, Wang J, Zhang B, Shao Y, Zhang L, Wang H, Wu Y, Li X, Li R, Tian Y. Diagnosis value of CD117 and PDGFRA, alone or in combination DOG1, as biomarkers for gastrointestinal stromal tumors. *Ann Transl Med* 2015; **3**: 308 [PMID: 26697468 DOI: 10.3978/j.issn.2305-5839.2015.10.07]
- 3 **Soreide K**, Sandvik OM, Soreide JA, Giljaca V, Jureckova A, Bulusu VR. Global epidemiology of gastrointestinal stromal tumours (GIST): A systematic review of population-based cohort studies. *Cancer Epidemiol* 2016; **40**: 39-46 [PMID: 26618334 DOI: 10.1016/j.canep.2015.10.031]
- 4 **Wang M**, Xu J, Zhang Y, Tu L, Qiu WQ, Wang CJ, Shen YY, Liu Q, Cao H. Gastrointestinal stromal tumor: 15-years' experience in a single center. *BMC Surg* 2014; **14**: 93 [PMID: 25403624 DOI: 10.1186/1471-2482-14-93]
- 5 **Corless CL**, Barnett CM, Heinrich MC. Gastrointestinal stromal tumours: origin and molecular oncology. *Nat Rev Cancer* 2011; **11**: 865-878 [PMID: 22089421 DOI: 10.1038/nrc3143]
- 6 **Hirota S**, Isozaki K, Moriyama Y, Hashimoto K, Nishida T, Ishiguro S, Kawano K, Hanada M, Kurata A, Takeda M, Muhammad Tunio G, Matsuzawa Y, Kanakura Y, Shinomura Y, Kitamura Y. Gain-of-function mutations of c-kit in human gastrointestinal stromal tumors. *Science* 1998; **279**: 577-580 [PMID: 9438854 DOI: 10.1126/science.279.5350.577]
- 7 **Murphey MD**. World Health Organization classification of bone and soft tissue tumors: modifications and implications for radiologists. *Semin Musculoskelet Radiol* 2007; **11**: 201-214 [PMID: 18260031 DOI: 10.1055/s-2008-1038310]
- 8 **Fletcher CD**, Berman JJ, Corless C, Gorstein F, Lasota J, Longley BJ, Miettinen M, O'Leary TJ, Remotti H, Rubin BP, Shmookler B, Sobin LH, Weiss SW. Diagnosis of gastrointestinal stromal tumors: A consensus approach. *Hum Pathol* 2002; **33**: 459-465 [PMID: 12094370 DOI: 10.1053/hupa.2002.123545]
- 9 **Demetri GD**, von Mehren M, Antonescu CR, DeMatteo RP, Ganjoo KN, Maki RG, Pisters PW, Raut CP, Riedel RF, Schuetze S, Sundar HM, Trent JC, Wayne JD. NCCN Task Force report: update on the management of patients with gastrointestinal stromal tumors. *J Natl Compr Canc Netw* 2010; **8** Suppl 2: S1-41; quiz S42 [PMID: 20457867 DOI: 10.6004/jnccn.2010.0116]
- 10 **von Mehren M**, Randall RL, Benjamin RS, Boles S, Bui MM, Ganjoo KN, George S, Gonzalez RJ, Heslin MJ, Kane JM, Keedy V, Kim E, Koon H, Mayerson J, McCarter M, McGarry SV, Meyer C, Morris ZS, O'Donnell RJ, Pappo AS, Paz IB, Petersen IA, Pfeifer JD, Riedel RF, Ruo B, Schuetze S, Tap WD, Wayne JD, Bergman MA, Scavone JL. Soft Tissue Sarcoma, Version 2.2018, NCCN Clinical Practice Guidelines in Oncology. *J Natl Compr Canc Netw* 2018; **16**: 536-563 [PMID: 29752328 DOI: 10.6004/jnccn.2018.0025]
- 11 **ESMO/European Sarcoma Network Working Group**. Gastrointestinal stromal tumours: ESMO Clinical Practice Guidelines for diagnosis, treatment and follow-up. *Ann Oncol* 2014; **25** Suppl 3: iii21-iii26 [PMID: 25210085 DOI: 10.1093/annonc/mdu255]
- 12 **Li J**, Ye Y, Wang J, Zhang B, Qin S, Shi Y, He Y, Liang X, Liu X, Zhou Y, Wu X, Zhang X, Wang M, Gao Z, Lin T, Cao H, Shen L; Chinese Society Of Clinical Oncology CSCO Expert Committee On Gastrointestinal Stromal Tumor. Chinese consensus guidelines for diagnosis and management of gastrointestinal stromal tumor. *Chin J Cancer Res* 2017; **29**: 281-293 [PMID: 28947860 DOI: 10.21147/j.issn.1000-9604.2017.04.01]
- 13 **Hu J**, Ge N, Wang S, Liu X, Guo J, Wang G, Sun S. The Role of Endoscopic Ultrasound and Endoscopic Resection for Gastric Glomus: A Case Series and Literature Review. *J Transl Int Med* 2019; **7**: 149-154 [PMID: 32010601 DOI: 10.2478/jtim-2019-0030]
- 14 **Kovacevic B**, Vilmann P. EUS tissue acquisition: From A to B. *Endosc Ultrasound* 2020; **9**: 225-231 [PMID: 32655082]

- DOI: [10.4103/eus.eus\\_21\\_20](https://doi.org/10.4103/eus.eus_21_20)
- 15 **Fabbri C**, Fornelli A, Fuccio L, Giovanelli S, Tarantino I, Antonini F, Liotta R, Frazzoni L, Gusella P, La Marca M, Barresi L, Macarri G, Traina M, De Biase D, Fiorino S, Jovine E, Larghi A, Cennamo V. High diagnostic adequacy and accuracy of the new 20G procure needle for EUS-guided tissue acquisition: Results of a large multicentre retrospective study. *Endosc Ultrasound* 2019; **8**: 261-268 [PMID: [31115386](https://pubmed.ncbi.nlm.nih.gov/31115386/) DOI: [10.4103/eus.eus\\_14\\_19](https://doi.org/10.4103/eus.eus_14_19)]
  - 16 **Ang TL**, Li JW, Kwek ABE, Thurairajah PH, Wang LM. The difference in histological yield between 19G EUS-FNA and EUS-fine-needle biopsy needles. *Endosc Ultrasound* 2019; **8**: 255-260 [PMID: [31115385](https://pubmed.ncbi.nlm.nih.gov/31115385/) DOI: [10.4103/eus.eus\\_12\\_19](https://doi.org/10.4103/eus.eus_12_19)]
  - 17 **Săftoiu A**, Vilmann P, Ciurea T. Utility of endoscopic ultrasound for the diagnosis and treatment of submucosal tumors of the upper gastrointestinal tract. *Rom J Gastroenterol* 2003; **12**: 215-229 [PMID: [14502323](https://pubmed.ncbi.nlm.nih.gov/14502323/)]
  - 18 **Gao Z**, Wang C, Xue Q, Wang J, Shen Z, Jiang K, Shen K, Liang B, Yang X, Xie Q, Wang S, Ye Y. The cut-off value of tumor size and appropriate timing of follow-up for management of minimal EUS-suspected gastric gastrointestinal stromal tumors. *BMC Gastroenterol* 2017; **17**: 8 [PMID: [28077094](https://pubmed.ncbi.nlm.nih.gov/28077094/) DOI: [10.1186/s12876-016-0567-4](https://doi.org/10.1186/s12876-016-0567-4)]
  - 19 **Kim GH**, Kim KB, Lee SH, Jeon HK, Park DY, Jeon TY, Kim DH, Song GA. Digital image analysis of endoscopic ultrasonography is helpful in diagnosing gastric mesenchymal tumors. *BMC Gastroenterol* 2014; **14**: 7 [PMID: [24400772](https://pubmed.ncbi.nlm.nih.gov/24400772/) DOI: [10.1186/1471-230X-14-7](https://doi.org/10.1186/1471-230X-14-7)]
  - 20 **Kim HJ**, Lim SJ, Park K, Yuh YJ, Jang SJ, Choi J. Multiple gastrointestinal stromal tumors with a germline c-kit mutation. *Pathol Int* 2005; **55**: 655-659 [PMID: [16185297](https://pubmed.ncbi.nlm.nih.gov/16185297/) DOI: [10.1111/j.1440-1827.2005.01885.x](https://doi.org/10.1111/j.1440-1827.2005.01885.x)]
  - 21 **Sanborn RE**, Blanke CD. Gastrointestinal stromal tumors and the evolution of targeted therapy. *Clin Adv Hematol Oncol* 2005; **3**: 647-657 [PMID: [16167051](https://pubmed.ncbi.nlm.nih.gov/16167051/)]
  - 22 **Casali PG**, Abecassis N, Aro HT, Bauer S, Biagini R, Bielack S, Bonvalot S, Boukovinas I, Bovee JVMG, Brodowicz T, Broto JM, Buonadonna A, De Álava E, Dei Tos AP, Del Muro XG, Dileo P, Eriksson M, Fedenko A, Ferraresi V, Ferrari A, Ferrari S, Frezza AM, Gasperoni S, Gelderblom H, Gil T, Grignani G, Gronchi A, Haas RL, Hassan B, Hohenberger P, Issels R, Joensuu H, Jones RL, Judson I, Jutte P, Kaal S, Kasper B, Kopeckova K, Krákorová DA, Le Cesne A, Lugowska I, Merimsky O, Montemurro M, Pantaleo MA, Piana R, Picci P, Piperno-Neumann S, Pousa AL, Reichardt P, Robinson MH, Rutkowski P, Safwat AA, Schöffski P, Sleijfer S, Stacchiotti S, Sundby Hall K, Unk M, Van Coevorden F, van der Graaf WTA, Whelan J, Wardelmann E, Zaikova O, Blay JY; ESMO Guidelines Committee and EURACAN. Gastrointestinal stromal tumours: ESMO-EURACAN Clinical Practice Guidelines for diagnosis, treatment and follow-up. *Ann Oncol* 2018; **29**: iv68-iv78 [PMID: [29846513](https://pubmed.ncbi.nlm.nih.gov/29846513/) DOI: [10.1093/annonc/mdy095](https://doi.org/10.1093/annonc/mdy095)]
  - 23 **Coe TM**, Fero KE, Fanta PT, Mallory RJ, Tang CM, Murphy JD, Sicklick JK. Population-Based Epidemiology and Mortality of Small Malignant Gastrointestinal Stromal Tumors in the USA. *J Gastrointest Surg* 2016; **20**: 1132-1140 [PMID: [27025710](https://pubmed.ncbi.nlm.nih.gov/27025710/) DOI: [10.1007/s11605-016-3134-y](https://doi.org/10.1007/s11605-016-3134-y)]
  - 24 **Fang YJ**, Cheng TY, Sun MS, Yang CS, Chen JH, Liao WC, Wang HP. Suggested cutoff tumor size for management of small EUS-suspected gastric gastrointestinal stromal tumors. *J Formos Med Assoc* 2012; **111**: 88-93 [PMID: [22370287](https://pubmed.ncbi.nlm.nih.gov/22370287/) DOI: [10.1016/j.jfma.2011.01.002](https://doi.org/10.1016/j.jfma.2011.01.002)]
  - 25 **Palazzo L**, Landi B, Cellier C, Cuillier E, Roseau G, Barbier JP. Endosonographic features predictive of benign and malignant gastrointestinal stromal cell tumours. *Gut* 2000; **46**: 88-92 [PMID: [10601061](https://pubmed.ncbi.nlm.nih.gov/10601061/) DOI: [10.1136/gut.46.1.88](https://doi.org/10.1136/gut.46.1.88)]
  - 26 **Jeon SW**, Park YD, Chung YJ, Cho CM, Tak WY, Kweon YO, Kim SK, Choi YH. Gastrointestinal stromal tumors of the stomach: endosonographic differentiation in relation to histological risk. *J Gastroenterol Hepatol* 2007; **22**: 2069-2075 [PMID: [18031362](https://pubmed.ncbi.nlm.nih.gov/18031362/) DOI: [10.1111/j.1440-1746.2006.04767.x](https://doi.org/10.1111/j.1440-1746.2006.04767.x)]
  - 27 **Wang M**, Xue A, Yuan W, Gao X, Fu M, Fang Y, Wang L, Shu P, Li H, Hou Y, Shen K, Sun Y, Qin X. Clinicopathological Features and Prognosis of Small Gastric Gastrointestinal Stromal Tumors (GISTs). *J Gastrointest Surg* 2019; **23**: 2136-2143 [PMID: [31012047](https://pubmed.ncbi.nlm.nih.gov/31012047/) DOI: [10.1007/s11605-018-04070-3](https://doi.org/10.1007/s11605-018-04070-3)]
  - 28 **Tsuji Y**, Kusano C, Gotoda T, Itokawa F, Fukuzawa M, Sofuni A, Matsubayashi J, Nagao T, Itoi T, Moriyasu F. Diagnostic potential of endoscopic ultrasonography-elasticity for gastric submucosal tumors: A pilot study. *Dig Endosc* 2016; **28**: 173-178 [PMID: [26530730](https://pubmed.ncbi.nlm.nih.gov/26530730/) DOI: [10.1111/den.12569](https://doi.org/10.1111/den.12569)]
  - 29 **Pesenti C**, Bories E, Caillol F, Ratone JP, Godat S, Monges G, Poizat F, Raoul JL, Ries P, Giovannini M. Characterization of subepithelial lesions of the stomach and esophagus by contrast-enhanced EUS: A retrospective study. *Endosc Ultrasound* 2019; **8**: 43-49 [PMID: [30264741](https://pubmed.ncbi.nlm.nih.gov/30264741/) DOI: [10.4103/eus.eus\\_89\\_17](https://doi.org/10.4103/eus.eus_89_17)]
  - 30 **Kuwatani M**, Sakamoto N. Evolution and a promising role of EUS-FNA in gene and future analyses. *Endosc Ultrasound* 2020; **9**: 151-153 [PMID: [32584309](https://pubmed.ncbi.nlm.nih.gov/32584309/) DOI: [10.4103/eus.eus\\_29\\_20](https://doi.org/10.4103/eus.eus_29_20)]
  - 31 **Okubo K**, Yamao K, Nakamura T, Tajika M, Sawaki A, Hara K, Kawai H, Yamamura Y, Mochizuki Y, Koshikawa T, Inada K. Endoscopic ultrasound-guided fine-needle aspiration biopsy for the diagnosis of gastrointestinal stromal tumors in the stomach. *J Gastroenterol* 2004; **39**: 747-753 [PMID: [15338368](https://pubmed.ncbi.nlm.nih.gov/15338368/) DOI: [10.1007/s00535-004-1383-0](https://doi.org/10.1007/s00535-004-1383-0)]
  - 32 **Attila T**, Aydın Ö. Lesion size determines diagnostic yield of EUS-FNA with onsite cytopathologic evaluation for upper gastrointestinal subepithelial lesions. *Turk J Gastroenterol* 2018; **29**: 436-441 [PMID: [30249558](https://pubmed.ncbi.nlm.nih.gov/30249558/) DOI: [10.5152/tjg.2018.17876](https://doi.org/10.5152/tjg.2018.17876)]
  - 33 **Akahoshi K**, Sumida Y, Matsui N, Oya M, Akinaga R, Kubokawa M, Motomura Y, Honda K, Watanabe M, Nagaie T. Preoperative diagnosis of gastrointestinal stromal tumor by endoscopic ultrasound-guided fine needle aspiration. *World J Gastroenterol* 2007; **13**: 2077-2082 [PMID: [17465451](https://pubmed.ncbi.nlm.nih.gov/17465451/) DOI: [10.3748/wjg.v13.i14.2077](https://doi.org/10.3748/wjg.v13.i14.2077)]
  - 34 **Hunt GC**, Smith PP, Faigel DO. Yield of tissue sampling for submucosal lesions evaluated by EUS. *Gastrointest Endosc* 2003; **57**: 68-72 [PMID: [12518134](https://pubmed.ncbi.nlm.nih.gov/12518134/) DOI: [10.1067/mge.2003.34](https://doi.org/10.1067/mge.2003.34)]
  - 35 **Sepe PS**, Moparty B, Pitman MB, Saltzman JR, Brugge WR. EUS-guided FNA for the diagnosis of GI stromal cell tumors: sensitivity and cytologic yield. *Gastrointest Endosc* 2009; **70**: 254-261 [PMID: [19482280](https://pubmed.ncbi.nlm.nih.gov/19482280/) DOI: [10.1016/j.gie.2008.11.038](https://doi.org/10.1016/j.gie.2008.11.038)]
  - 36 **Levy MJ**, Jondal ML, Clain J, Wiersma MJ. Preliminary experience with an EUS-guided trucut biopsy needle compared with EUS-guided FNA. *Gastrointest Endosc* 2003; **57**: 101-106 [PMID: [12518144](https://pubmed.ncbi.nlm.nih.gov/12518144/) DOI: [10.1067/mge.2003.49](https://doi.org/10.1067/mge.2003.49)]
  - 37 **Bai J**, Wang Y, Guo H, Zhang P, Ling X, Zhao X. Endoscopic resection of small gastrointestinal stromal tumors. *Dig Dis Sci* 2010; **55**: 1950-1954 [PMID: [20204697](https://pubmed.ncbi.nlm.nih.gov/20204697/) DOI: [10.1007/s10620-010-1168-7](https://doi.org/10.1007/s10620-010-1168-7)]
  - 38 **Yu C**, Liao G, Fan C, Yu J, Nie X, Yang S, Bai J. Long-term outcomes of endoscopic resection of gastric GISTs. *Surg*

*Endosc* 2017; **31**: 4799-4804 [PMID: 28424911 DOI: 10.1007/s00464-017-5557-2]

- 39 **Li B**, Chen T, Qi ZP, Yao LQ, Xu MD, Shi Q, Cai SL, Sun D, Zhou PH, Zhong YS. Efficacy and safety of endoscopic resection for small submucosal tumors originating from the muscularis propria layer in the gastric fundus. *Surg Endosc* 2019; **33**: 2553-2561 [PMID: 30478693 DOI: 10.1007/s00464-018-6549-6]
- 40 **An W**, Sun PB, Gao J, Jiang F, Liu F, Chen J, Wang D, Li ZS, Shi XG. Endoscopic submucosal dissection for gastric gastrointestinal stromal tumors: a retrospective cohort study. *Surg Endosc* 2017; **31**: 4522-4531 [PMID: 28374257 DOI: 10.1007/s00464-017-5511-3]

## Retrospective Study

# Online calculator for predicting the risk of malignancy in patients with pancreatic cystic neoplasms: A multicenter, retrospective study

Dong Jiang, Zi-Xiang Chen, Fu-Xiao Ma, Yu-Yong Gong, Tian Pu, Jiang-Ming Chen, Xue-Qian Liu, Yi-Jun Zhao, Kun Xie, Hui Hou, Cheng Wang, Xiao-Ping Geng, Fu-Bao Liu

**Specialty type:** Gastroenterology and hepatology

**Provenance and peer review:**

Unsolicited article; Externally peer reviewed.

**Peer-review model:** Single blind

**Peer-review report's scientific quality classification**

Grade A (Excellent): 0  
Grade B (Very good): B, B, B  
Grade C (Good): C  
Grade D (Fair): D  
Grade E (Poor): 0

**P-Reviewer:** Cheng H, China; Ghareeb WM, China; Luo J, China; Tsujinaka S, Japan

**Received:** June 16, 2022

**Peer-review started:** June 16, 2022

**First decision:** July 12, 2022

**Revised:** July 25, 2022

**Accepted:** September 8, 2022

**Article in press:** September 8, 2022

**Published online:** October 7, 2022



**Dong Jiang, Zi-Xiang Chen, Fu-Xiao Ma, Yu-Yong Gong, Tian Pu, Jiang-Ming Chen, Xue-Qian Liu, Yi-Jun Zhao, Kun Xie, Xiao-Ping Geng, Fu-Bao Liu,** Department of General Surgery, The First Affiliated Hospital of Anhui Medical University, Hefei 230000, Anhui Province, China

**Hui Hou,** Department of General Surgery, The Second Affiliated Hospital of Anhui Medical University, Hefei 230000, Anhui Province, China

**Cheng Wang,** Department of General Surgery, The First Affiliated Hospital of University of Science and Technology of China, Hefei 230000, Anhui Province, China

**Corresponding author:** Fu-Bao Liu, MD, PhD, Chief Doctor, Professor, Department of General Surgery, The First Affiliated Hospital of Anhui Medical University, No. 81 Meishan Road, Hefei 230000, Anhui Province, China. [lancetfb@126.com](mailto:lancetfb@126.com)

## Abstract

### BACKGROUND

Efficient and practical methods for predicting the risk of malignancy in patients with pancreatic cystic neoplasms (PCNs) are lacking.

### AIM

To establish a nomogram-based online calculator for predicting the risk of malignancy in patients with PCNs.

### METHODS

In this study, the clinicopathological data of target patients in three medical centers were analyzed. The independent sample t-test, Mann-Whitney U test or chi-squared test were used as appropriate for statistical analysis. After univariable and multivariable logistic regression analysis, five independent factors were screened and incorporated to develop a calculator for predicting the risk of malignancy. Finally, the concordance index (C-index), calibration, area under the curve, decision curve analysis and clinical impact curves were used to evaluate the performance of the calculator.

### RESULTS

Enhanced mural nodules [odds ratio (OR): 4.314; 95% confidence interval (CI): 1.618–11.503,  $P = 0.003$ ], tumor diameter  $\geq 40$  mm (OR: 3.514; 95% CI: 1.138–10.849,  $P = 0.029$ ), main pancreatic duct dilatation (OR: 3.267; 95% CI: 1.230–8.678,  $P =$

0.018), preoperative neutrophil-to-lymphocyte ratio  $\geq 2.288$  (OR: 2.702; 95%CI: 1.008–7.244,  $P = 0.048$ ), and preoperative serum CA19-9 concentration  $\geq 34$  U/mL (OR: 3.267; 95%CI: 1.274–13.007,  $P = 0.018$ ) were independent risk factors for a high risk of malignancy in patients with PCNs. In the training cohort, the nomogram achieved a C-index of 0.824 for predicting the risk of malignancy. The predictive ability of the model was then validated in an external cohort (C-index: 0.893). Compared with the risk factors identified in the relevant guidelines, the current model showed better predictive performance and clinical utility.

### CONCLUSION

The calculator demonstrates optimal predictive performance for identifying the risk of malignancy, potentially yielding a personalized method for patient selection and decision-making in clinical practice.

**Key Words:** Pancreatic cystic neoplasms; Risk of malignancy; Nomogram; Model; Prediction; Calculator

©The Author(s) 2022. Published by Baishideng Publishing Group Inc. All rights reserved.

**Core Tip:** A nomogram-based online calculator for predicting the risk of malignancy in patients with pancreatic cystic neoplasms was developed. The calculator demonstrates optimal predictive performance for identifying the risk of malignancy, potentially yielding a personalized method for patient selection and decision-making in clinical practice.

**Citation:** Jiang D, Chen ZX, Ma FX, Gong YY, Pu T, Chen JM, Liu XQ, Zhao YJ, Xie K, Hou H, Wang C, Geng XP, Liu FB. Online calculator for predicting the risk of malignancy in patients with pancreatic cystic neoplasms: A multicenter, retrospective study. *World J Gastroenterol* 2022; 28(37): 5469-5482

**URL:** <https://www.wjgnet.com/1007-9327/full/v28/i37/5469.htm>

**DOI:** <https://dx.doi.org/10.3748/wjg.v28.i37.5469>

## INTRODUCTION

Pancreatic cystic neoplasms (PCNs) are estimated to be present in 2%–45% of the general population[1–3]. With rapid advancements in medical examination technologies over the past decades, the use of these technologies in the identification of PCNs has dramatically increased. Moreover, PCNs are frequently discovered in asymptomatic patients[4]. Consequently, centers with high volumes of patients undergoing pancreatic surgery are evaluating an increasing number of PCNs cases annually. Nevertheless, how to properly manage patients with PCNs remains a topic of debate.

PCNs are usually divided into serous cystic neoplasms (SCNs), mucinous cystic neoplasms (MCNs), intraductal papillary mucinous neoplasms (IPMNs) and other rare cystic lesions, such as solid pseudo-papillary tumors (SPTs) and cystic neuroendocrine tumors (cNET) which show biological behavior ranging from benign to malignant[5,6]. Moreover, the main controversy regarding the treatment of PCNs is related to the inability to precisely determine their histopathological diagnosis without surgical resection[7,8], thereby precluding the accurate identification of different subtypes of PCNs. Consequently, clinicians are challenged to maintain a difficult balance between avoiding excessive surgical treatment and keeping a malignant lesion under surveillance.

Although previous studies have focused on the identification of different types of PCNs[9–11], only a few of these studies have emphasized the judgment or prediction of malignancy risk in PCNs. Thus, identifying a method that can accurately and preoperatively predict the risk of malignancy in PCNs is of great significance. Nomograms are effective statistical tools that enable the simultaneous consideration of various factors for clinicians to visualize the malignant probability of a neoplasm, allowing the formulation of an optimal therapeutic schedule. Nomogram possess other advantages including ease of comprehension, user-friendliness and personalized evaluation[12]. Therefore, this study aimed to establish a novel clinical online nomogram-based calculator to predict the risk of malignancy in PCNs.

## MATERIALS AND METHODS

The clinical and pathological data of patients with PCNs who underwent surgery at the Department of General Surgery in three medical centers between January 2015 and December 2021 were collected and analyzed. Patients from the First Affiliated Hospital of Anhui Medical University and Second Affiliated

Hospital of Anhui Medical University were set as the training cohort, while those from the First Affiliated Hospital of the University of Science and Technology of China were set as the validation cohort. All hospitals were high-volume surgical centers that employed similar therapeutic approaches for PCNs. Pathological diagnosis was confirmed by postoperative specimen examinations by two experienced pathologists. According to the histological classification of PCNs proposed by the World Health Organization (2019) and the Baltimore consensus meeting, PCNs are classified as those with low- or intermediate-grade dysplasia and those with high-grade dysplasia or invasive carcinoma[13,14]. Patients from the three centers who met the following criteria were included: (1) Patients who underwent surgical treatment and were confirmed as showing SCNs, IPMNs or MCNs in postoperative pathological examinations; (2) Patients with complete clinical data, including medical history and laboratory test data; and (3) Patients who underwent preoperative imaging examinations. The following patients were excluded: (1) Patients who were pathologically confirmed as having other rare cystic lesions such as SPTs and cNET; (2) Patients who were pathologically confirmed as having other uncommon and undefined cystic tumors of the pancreas; and (3) Patients with a history of pancreatic surgery, radiotherapy or chemotherapy. All clinical data were screened and collected in a computerized database by a professional research assistant. In this study, patients were categorized as showing low-risk (low- or intermediate-grade dysplasia) or high-risk (high-grade dysplasia or invasive carcinoma) disease based on the pathological diagnosis. The appearance of high-risk disease was characterized as a study endpoint. **Figure 1** depicts a flowchart of patient enrollment and the inclusion process. This study was conducted in accordance with the Declaration of Helsinki and was approved by the institutional ethics committee (Quick-PJ2022-06-26). All included patients or their relatives provided written informed consent before their data were analyzed.

### Perioperative management

In accordance with the similar preoperative evaluation protocol at all centers, all patients were routinely examined using blood tests, including routine blood counts and analysis of blood biochemistry, hemostatic function, immunological markers and tumor markers. Moreover, all patients underwent at least two preoperative imaging examinations through ultrasound (US), computed tomography (CT), magnetic resonance imaging or 2-<sup>18</sup>F-fluoro-2-deoxy-d-glucose positron emission tomography-CT, which provided information about the size, number, location and internal condition of the lesions. Definitive planning of the procedure was performed according to the examination results and the patient's age, comorbidities and preferences.

Surgical procedures, including pancreatoduodenectomy, total pancreatectomy, partial pancreatectomy and distal pancreatectomy with or without splenic preservation, were performed depending on the tumor location and characteristics. Experienced pancreatic surgeons performed all surgical procedures. Meanwhile, the balance between the benefits of oncological clearance and the risks of inadequate parenchymal preservation was carefully considered.

Normative and meticulous postoperative care including monitoring of vital signs, maintenance of moderate tissue perfusion and support for nutritional needs was implemented for every patient at the initial stage.

### Statistical analysis

All data, including demographic data, preoperative imaging data and clinical and pathological data were recorded in detail using a special recorder. Continuous variables were expressed as mean  $\pm$  SD for normally distributed variables or median (interquartile range) for non-normally distributed variables and statistical tests were used as appropriate (the independent sample t-test or the Mann-Whitney U test). Categorical variables were expressed as numbers (*n*) and proportions (%) and compared appropriately *via* Fisher's exact test or the chi-squared test. The cutoff values of continuous parameters were derived from the Youden index[15]. Univariable logistic regression analysis was performed on the training cohort to screen for risk factors associated with malignancy. On the basis of the univariable analysis, multivariable logistic regression analysis was conducted using variables that had statistical significance. A nomogram for the prediction of malignancy in patients with PCNs was developed based on the multivariable logistic regression model. The performance of the nomogram was evaluated using a concordance index (C-index) and calibration plots based on bootstrap validation method (*n* = 1000) to reduce overfitting bias. The area under the curve (AUC) of the receiver operating characteristic (ROC) curves and the quality indices such as sensitivity, specificity, accuracy, positive predictive value and negative predictive value with the associated 95% confidence intervals (CIs) of the model applied to the training and external validation cohorts were obtained. This allowed assessment of the predictive efficiency of the model in comparison with those of the risk factors identified in the relevant guidelines. The clinical usefulness of the nomogram was examined by determining the net benefit using decision curve analysis (DCA)[16]. DCA can assess the utility of models for decision making by plotting net benefit at a range of clinically reasonable risk thresholds. The predictive accuracy and clinical usefulness of the nomogram were demonstrated by clinical impact curves. Based on the sensitivity, specificity and predictive values, the optimal cutoff value was evaluated for accuracy. An online calculator for public use was created through shinyapps.io by RStudio to facilitate the use of the model in clinical practice. Statistical analyses were performed using R version 4.0.5 (<http://www.r-project.org/>), R Development

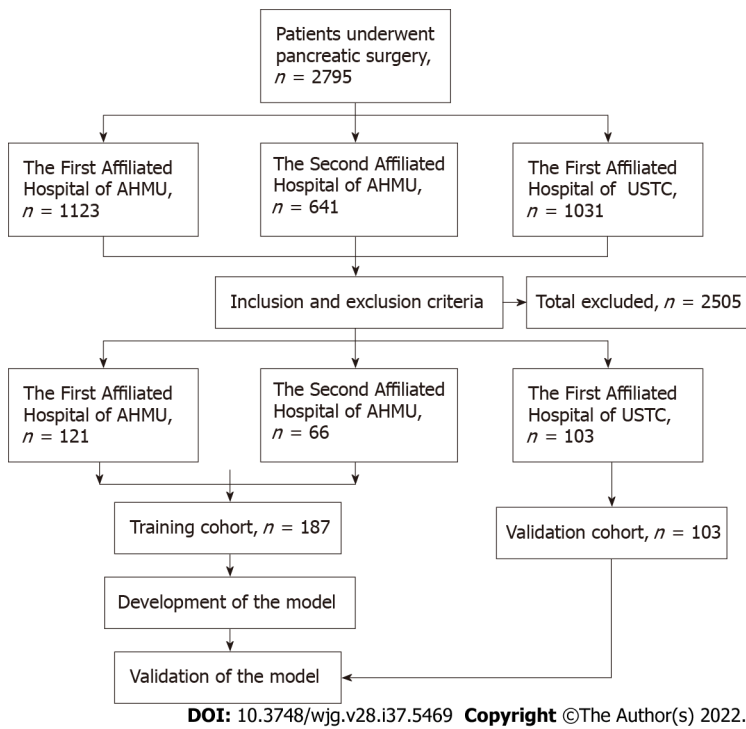


**Figure 1** Flowchart of patient recruitment and diagnosis. AHMU: Anhui Medical University; USTC: University of Science and Technology of China.

Core Team) and SPSS version 23.0 (SPSS Inc, Armonk, NY, United States. In this study, the packages rms, nomogramFormula, DynNom and rmda were utilized for statistical analysis and figure drawing. A two-tailed *P* value < 0.05 was considered significant.

## RESULTS

### *Patient cohorts and clinicopathologic features*

The clinicopathologic data of 1764 consecutive patients who underwent pancreatic surgery at the First Affiliated Hospital of Anhui Medical University and the Second Affiliated Hospital of Anhui Medical University between January 2015 and December 2021 were collected. Among them, 246 patients (13.9%) who were pathologically confirmed as having IPMNs, MCNs or SCNs were classified as the initial target population. Of these 246 patients, 59 (24.0%) who did not fulfill the inclusion criteria were excluded, including 19 patients with incomplete clinical or imaging data, nine with a history of pancreatic surgery, 25 with mixed pathological characteristics and 6 with a history of radiotherapy or chemotherapy. Ultimately, 187 patients (76.0%) were included in the training cohort. Based on the same criteria, an independent group consisting of 103 patients from the First Affiliated Hospital of University of Science and Technology of China who were eligible for inclusion in the same period was included in the present study and served as an external validation cohort. The two cohorts showed no significant differences in baseline characteristics (*P* > 0.05; Tables 1 and 2).

### *Univariable and multivariable analysis in the training cohort*

The results of the univariable and multivariable analyses of variables concerning malignancy in the training cohort were listed in Table 3. The optimal cutoff values of the neutrophil-to-lymphocyte ratio (NLR) was 2.288. Factors that significantly affected the risk of malignancy in the univariable analysis were then included in the multivariable analysis, which demonstrated that the presence of enhanced mural nodules [odds ratio (OR): 4.314; 95%CI: 1.618–11.503, *P* = 0.003], tumor diameter ≥ 40 mm (OR: 3.514; 95%CI: 1.138–10.849, *P* = 0.029), main pancreatic duct dilatation (OR: 3.267; 95%CI: 1.230–8.678, *P* = 0.018), preoperative NLR ≥ 2.288 (OR: 2.702; 95%CI: 1.008–7.244, *P* = 0.048) and preoperative serum CA19-9 concentration ≥ 34 U/mL (OR: 3.267; 95%CI: 1.274–13.007, *P* = 0.018) were independent risk factors for a high risk of malignancy in patients with PCNs.

### *Development and evaluation of the predictive model*

The factors that were proven to be related to a high risk of malignancy were utilized to establish a nomogram for evaluating the probability of malignancy (Figure 2). The model obtained using this approach showed good predictive capacity for estimating the risk of malignancy in patients with PCNs

Table 1 Preoperative clinical characteristics of patients with pancreatic cystic neoplasms

Characteristics	Training cohort	Validation cohort	P value
	n = 187 (64.5%)	n = 103 (35.5%)	
Sex			0.190
Male	126 (67.4)	77 (74.8)	
Female	61 (32.6)	26 (25.2)	
Age in yr			0.344
< 60	123 (65.8)	62 (60.2)	
≥ 60	64 (34.2)	41 (39.8)	
BMI	23.25 ± 3.37	23.00 ± 3.53	0.561
Weight loss			0.830
No	165 (88.2)	90 (87.4)	
Yes	22 (11.8)	13 (12.6)	
Alcohol			0.378
No	168 (89.8)	89 (86.4)	
Yes	19 (10.2)	14 (13.6)	
Symptomatic			0.602
No	74 (39.6)	44 (42.7)	
Yes	113 (60.4)	59 (57.3)	
NLR			0.510
< 2.288	134 (71.7)	70 (68.0)	
≥ 2.288	53 (28.3)	33 (32.0)	
TB in μmol/L			0.763
< 34.2	181 (96.8)	99 (96.1)	
≥ 34.2	6 (3.2)	4 (3.9)	
CEA in ng/mL			0.901
< 5	175 (93.6%)	96 (96.0%)	
≥ 5	12 (6.4)	7 (7.0)	
CA19-9 in U/mL			0.135
< 34	163 (87.2)	83 (80.6)	
≥ 34	24 (12.8)	20 (19.4)	
GGT in IU/L			0.287
< 150	174 (93.0)	99 (96.1)	
≥ 150	13 (7.0)	4 (3.9)	
ALP in IU/L			0.556
< 200	179 (95.7)	97 (94.2)	
≥ 200	8 (4.3)	6 (5.8)	

ALP: Alkaline phosphatase; BMI: Body mass index; CA19-9: Carbohydrate antigen 19-9; CEA: Carcinoembryonic antigen; GGT:  $\gamma$ -glutamyl transpeptidase; NLR: Neutrophil-to-lymphocyte; TB: Total bilirubin.

(training cohort: C-index, 0.824; 95%CI: 0.735–0.914, *vs* validation cohort: C-index, 0.893; 95%CI: 0.823–0.963). The calibration plots demonstrated good consistency between the observed and predicted probabilities in both the internal and external validations. Both predicted and reference curves were approximately aligned which indicates good performance of the nomogram (Figure 3). Overall performance was scored at 0.091 using Brier's score which measured the difference between observed

**Table 2 Preoperative imaging characteristics of patients with pancreatic cystic neoplasms**

Characteristic	Training cohort	Validation cohort	P value
	n = 187 (64.5%)	n = 103 (35.5%)	
Tumor involve the head of pancreas			0.239
Yes	65 (34.8)	43 (41.7)	
No	122 (65.2)	60 (58.3)	
Bile duct dilation			0.106
No	174 (93.0)	90 (87.4)	
Yes	13 (7.0)	13 (12.6)	
Tumor size in mm			0.254
< 40	158 (84.5)	92 (89.3)	
≥ 40	29 (15.5)	11 (10.7)	
Intratumoral septum			0.264
No	76 (40.6)	35 (34.0)	
Yes	111 (59.4)	68 (66.0)	
Cyst wall enhancement			0.244
No	118 (63.1)	72 (69.9)	
Yes	69 (36.9)	31 (30.1)	
Cyst wall thickening			0.709
No	178 (95.2)	97 (94.2)	
Yes	9 (4.8)	6 (5.8)	
Enhanced mural nodules			0.126
No	148 (79.1)	89 (86.4)	
Yes	39 (20.9)	14 (13.6)	
Intracapsular calcification			0.117
No	162 (86.6)	82 (79.6)	
Yes	25 (13.4)	21 (20.4)	
Main pancreatic duct dilatation			0.419
No	122 (65.2)	72 (69.9)	
Yes	65 (34.8)	31 (30.1)	

and predicted values (values closer to 0 indicate better predictive ability). A calibration slope of 1.0 was obtained to assess the agreement between observed and predicted values (values closer to 1.0 indicate better performance)[17]. An online calculator for predicting the risk of malignancy was created and was freely available at <https://ahmuptt.shinyapps.io/JDYX/>.

**Comparison of the performance of the nomogram and the risk factors identified in the relevant guidelines**

Using ROC analyses, the diagnostic performance of the nomogram established in this study was compared with those of the risk factors identified in the relevant guidelines[6,18], including tumor diameter ≥ 40 mm, enhanced mural nodules and main pancreatic duct dilatation (Figure 4). In the training cohort, the AUC values and 95% CIs of the nomogram and the three factors (tumor diameter ≥ 40 mm, enhanced mural nodules and main pancreatic duct dilatation) were 0.824 (0.735–0.914), 0.619 (0.496–0.742), 0.692 (0.575–0.810) and 0.653 (0.540–0.766), respectively. In the validation cohort, these values were 0.893 (0.823–0.963), 0.718 (0.560–0.876), 0.665 (0.506–0.824) and 0.672 (0.524–0.820), respectively. In both cohorts, significant statistical differences were found between the nomogram and the three factors (*P* < 0.05). The training cohort had an accuracy, sensitivity, specificity, positive predictive value and negative predictive value of 0.829, 0.643, 0.862, 0.451 and 0.932, respectively. In the validation cohort, these values were 0.925, 0.882, 0.826, 0.501 and 0.973, respectively. Thus, the

**Table 3 Univariable and multivariable logistic regression analyses of the risk factors for high risk of malignancy in patients with pancreatic cystic neoplasms**

Variable	OR comparisons	Univariable analysis		Multivariable analysis	
		OR (95%CI)	P value	OR (95%CI)	P value
Sex	Female <i>vs</i> Male	2.383 (1.054-5.386)	0.037 <sup>a</sup>	0.716 (0.232-2.213)	0.562
Age in yr	≥ 60 <i>vs</i> < 60	2.180 (0.967-4.915)	0.060		
BMI		0.986 (0.874-1.111)	0.816		
Weight loss	Yes <i>vs</i> No	2.437 (0.861-6.897)	0.093		
Alcohol	Yes <i>vs</i> No	2.252 (0.741-6.845)	0.153		
Symptomatic	Yes <i>vs</i> No	1.774 (0.737-4.271)	0.201		
Tumor involve the head of pancreas	Yes <i>vs</i> No	1.148 (0.487-2.705)	0.753		
Bile duct dilation	Yes <i>vs</i> No	1.788 (0.460-6.952)	0.402		
Tumor diameter in mm	≥ 40 <i>vs</i> < 40	4.094 (1.649-10.165)	0.002 <sup>a</sup>	3.514 (1.138-10.849)	0.029 <sup>a</sup>
Intratumoral septum	Yes <i>vs</i> No	0.539 (0.240-1.211)	0.135		
Cyst wall enhancement	Yes <i>vs</i> No	1.127 (0.494-2.569)	0.777		
Cyst wall thickening	Yes <i>vs</i> No	1.670 (0.329-8.488)	0.536		
Enhanced mural nodules	Yes <i>vs</i> No	6.490 (2.746-15.342)	< 0.001 <sup>a</sup>	4.314 (1.618-11.503)	0.003 <sup>a</sup>
Intracapsular calcification	Yes <i>vs</i> No	0.208 (0.027-1.606)	0.132		
Main pancreatic duct dilatation	Yes <i>vs</i> No	3.574 (1.558-8.201)	0.003 <sup>a</sup>	3.267 (1.230-8.678)	0.018 <sup>a</sup>
NLR	≥ 2.288 <i>vs</i> < 2.288	3.077 (1.350-7.015)	0.008 <sup>a</sup>	2.702 (1.008-7.244)	0.048 <sup>a</sup>
TB in μmol/L	≥ 34.2 <i>vs</i> < 34.2	6.240 (1.192-32.657)	0.030 <sup>a</sup>	0.870 (0.050-15.020)	0.924
ALP in IU/L	≥ 200 <i>vs</i> < 200	9.420 (1.499-59.213)	0.017 <sup>a</sup>	0.632 (0.064-6.285)	0.695
GGT in IU/L	≥ 150 <i>vs</i> < 150	2.925 (0.931-9.189)	0.066		
CEA in ng/mL	≥ 5 <i>vs</i> < 5	6.955 (2.060-23.477)	0.002 <sup>a</sup>	3.798 (0.825-17.482)	0.087
CA199 in U/mL	≥ 34 <i>vs</i> < 34	4.547 (1.750-11.816)	0.002 <sup>a</sup>	3.267 (1.274-13.007)	0.018 <sup>a</sup>

<sup>a</sup>*P* < 0.05.

ALP: Alkaline phosphatase; BMI: Body mass index; CA19-9: Carbohydrate antigen 19-9; CEA: Carcinoembryonic antigen; CI: Confidence interval; GGT: γ-glutamyl transpeptidase; NLR: Neutrophil-to-lymphocyte; OR: Odds ratio; TB: Total bilirubin.

nomogram showed high accuracy in predicting the risk of malignancy in patients with PCNs. When considering the maximum Youden index value, the optimal cutoff value of the nomogram was 160.8 in the ROC curve and the sensitivity and specificity for differentiating between high and low risk were 64.3% and 86.2%, respectively. This cut off value is used to categorize patients with total nomogram score of < 160.8 points or ≥ 160.8 points as either low- or high-risk group, respectively. In the training cohort, DCA showed that using the nomogram to predict the risk of malignancy had a greater net benefit than the other three factors when the threshold probability ranged from 0.2 to 1.0. In the validation cohort, DCA showed that the nomogram had a greater net benefit when the threshold probability ranged from 0.0 to 0.4 (Figure 5). Figure 6 depicts the number of high-risk patients (solid red line) and the number of high-risk patients with the outcome (black dotted line) at different threshold probabilities within a given population. In both the training and validation cohorts, the solid red and black dotted lines show a great fit indicating that the model has remarkable predictive ability.

## DISCUSSION

The increasing use of high-resolution cross-sectional imaging techniques has resulted in more frequent detection of PCNs in recent years[19]. However, accurate prediction of the risk of malignancy of PCNs as early as possible is of great value in developing more appropriate individualized treatment strategies. In the current study, we developed and validated a preoperative clinical model that strongly predicted the risk of high-grade dysplasia or invasive cancer in patients with PCNs.

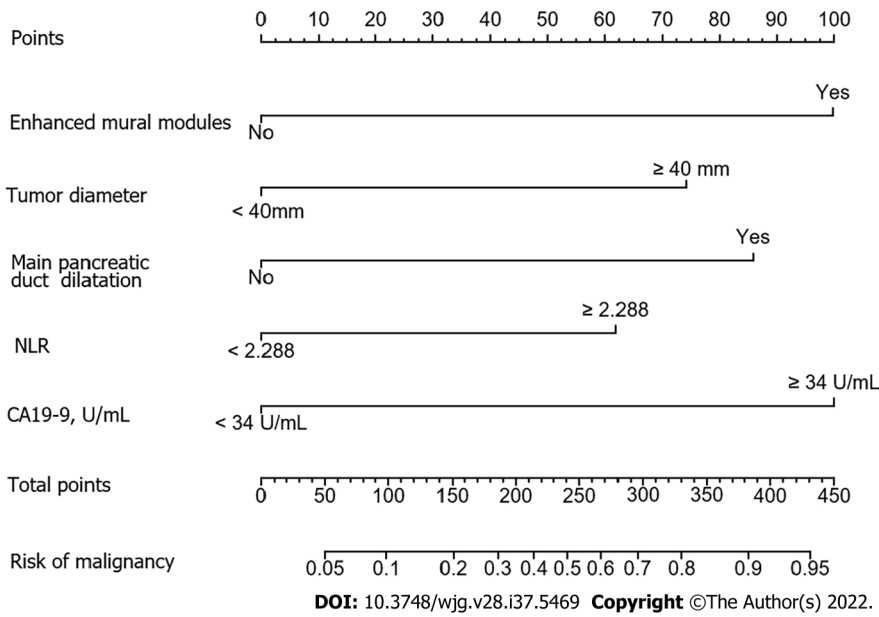


**Figure 2** Nomogram for predicting risk of malignancy in the training cohort. NLR: Neutrophil-to-lymphocyte ratio.

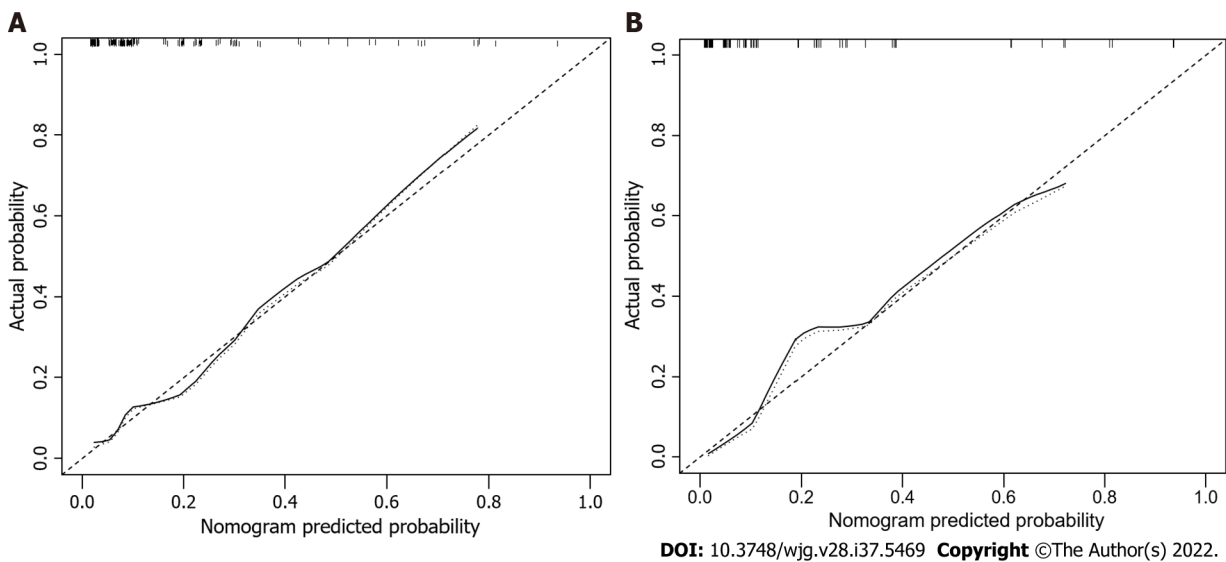


**Figure 3** Calibration curves for predicting the risk of malignancy. The nomogram had concordance index values of 0.824 and 0.893 in the training and validation cohort, respectively. A: Training cohort; B: Validation cohort.

As shown in Tables 1 and 2, our study analyzed dozens of objective factors, and the findings indicated that for patients with PCNs, lesions with enhanced mural nodules, tumor diameter  $\geq 40$  mm, main pancreatic duct dilatation, preoperative NLR  $\geq 2.288$  and preoperative serum CA19-9 levels  $\geq 34$  U/mL were significant independent predictors. These factors were combined with patients' preoperative imaging and serological data to quantify the risk of malignancy concisely and spontaneously. The sufficient statistical power of the model for predicting the risk of malignancy was verified based on multiple validation methods. The C-index of the model in the validation cohort was 0.893 (0.823–0.963), highlighting the ability of the model to distinguish low-risk disease from high-risk disease in a large group of patients. In addition, we used an independent validation dataset that effectively decreased the risk of overfitting the model to an individual dataset. The similarity between the C-index of the training [0.824 (0.735–0.914)] and validation [0.893 (0.823–0.963)] cohorts suggested that this model was widely applicable. In addition, a mobile-friendly online version of the nomogram was programmed to eliminate the inconvenience of traditional nomograms in clinical use.

The latest guidelines, including the European evidence-based guidelines on PCNs and the International Association of Pancreatology guidelines of 2017, have described the management strategies for different subtypes of PCNs in detail[6,18]. In addition, many published nomogram models for predicting malignancy in patients with a specific subtype of PCNs, such as IPMNs, have been

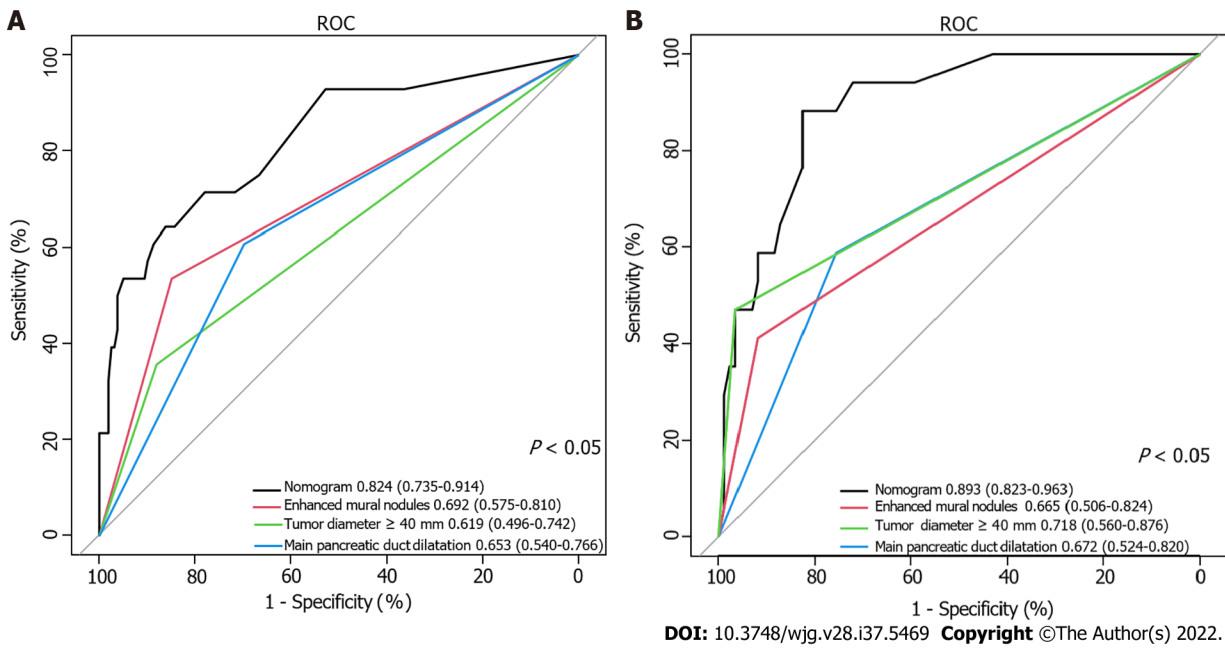


**Figure 4** Receiver operating characteristic curve of the nomogram and other three risk factors identified in guidelines. A: Training cohort; B: Validation cohort. AUC: Area under the curve.

established to facilitate the preoperative prediction of malignant lesions[20-22]. Nevertheless, real-world preoperative diagnosis of the different PCN subtypes remains difficult due to their similarities in both clinical and imaging features. In particular, accurate diagnosis of pathological neoplasms and preoperative assessments of the benign or malignant status of some lesions with atypical manifestations are even more difficult[23]. Previous studies have reported differing probabilities for the accurate preoperative identification of each subtype. Salvia *et al*[24] found that in 476 patients with PCNs, 78% showed postoperative pathological examination results consistent with the preoperative diagnosis[24]. Furthermore, a multicenter study of 2251 patients in China showed that the preoperative diagnosis was not always accurate for a specific subtype with a correct diagnosis rate of only 33% [25]. Meanwhile, the risk factors proposed to be associated with malignant lesions in the guidelines lack universality, efficiency and accuracy in clinical applications to a certain extent. In this study, a model with strong practicability and high predictive efficiency was constructed by analyzing PCNs showing similar clinical and imaging manifestations across subtypes. Therefore, this model can help clinicians predict the risk of lesion malignancy when they are unable to accurately determine the PCN subtype or have difficulties in confirming the nature of the tumor.

NLR was also included as a laboratory indicator in the nomogram. Researches have shown that inflammation contributes to the occurrence and progression of tumors by releasing cytokines and other inflammatory mediators[26,27]. NLR measurement can serve as a simple and convenient way to assess the systemic inflammatory response and many recent studies have confirmed that inflammatory markers play an important role in predicting benign and malignant PCNs[28-30]. In the current study, a significant correlation was found between NLR and high-risk groups by multivariable analysis and the cutoff value of NLR was calculated as 2.43 which was rarely studied and reported in previous studies. We believe that neutrophils can recruit and activate inflammatory cells by producing cytokines and chemokines thus acting on the tumor microenvironment. In addition, reactive oxygen species and proteases produced by neutrophils can regulate tumor cell proliferation, angiogenesis and metastasis [31]. Thus, an increase in NLR may indicate a macroscopic withdrawal of inflammatory and immune responses in the local tumor microenvironment.

The nomogram was chosen to establish the model mainly because of its ability to assign risk probabilities on a continuous scale as an individualized risk score, rather than simply dividing patients into malignant and benign groups. This allows for additional risk stratification and may help patients and doctors tailor treatment decisions based on patients' individual risks. In addition, as shown in Figure 2, the nomogram showed that the model score for cases with serum CA19-9 levels  $\geq$  34 U/mL (100 points) was significantly higher than that for cases with an NLR of  $\geq$  2.288 (61 points), suggesting that serum CA19-9 levels  $\geq$  34 U/mL increase the possibility of a malignant lesion significantly. Moreover, the additive effect of several risk factors is important clinically. In this context, the patient-specific quantitative estimation of risk is valuable. Therefore, in cases where benign and malignant PCNs cannot be easily distinguished, clinicians can calculate the total nomogram scores using this predictive model. We propose that surgical treatment should be considered as the first choice for patients with a total nomogram score  $\geq$  160.

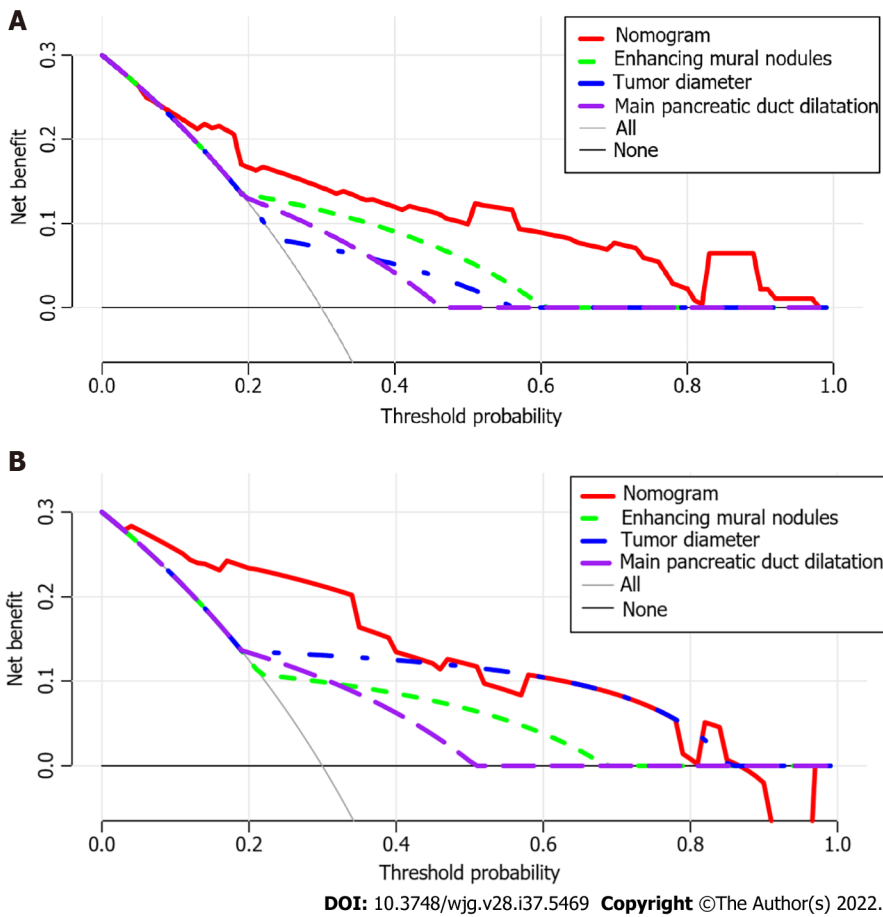


**Figure 5 Decision curve analysis of the nomogram and other three risk factors identified in guidelines.** The x-axis represents the threshold probability and the y-axis represents the net benefit. In the training cohort, the nomogram adds more net benefit than the other three factors when the threshold probability ranged from 0.2 to 1.0. In the validation cohort, the nomogram adds more net benefit than the other three factors when the threshold probability ranged from 0.0 to 0.4. A: In the training cohort; B: In the validation cohort.

In recent years, machine learning has rapidly developed as a tool with promising results and improved usability[32]. Machine learning addresses many preexisting and novel medical challenges and is widely discussed by researchers and practitioners alike. Machine learning algorithms have many advantages, such as improved flexibility and scalability when compared with traditional statistical methods. This makes machine learning advantageous for many tasks, including risk stratification, diagnosis, classification and survival predictions. Another advantage of machine learning is the ability to analyze diverse data types (*e.g.*, demographic data, laboratory findings, imaging data and doctors' free-text notes) and to incorporate them into predictions for disease risk, diagnosis, prognosis and appropriate treatment[33]. Despite these advantages, the application of machine learning in healthcare delivery also presents unique challenges, including the need for data pre-processing, model training and refinement of the system with respect to the actual clinical problem. Also crucial are ethical considerations which include medico-legal implications, doctors' understanding of machine learning tools, and data privacy and security[34]. In summary, attempts can be made to refine the model further using advanced machine learning in the future.

The present study had several limitations that merit discussion. First, endoscopic US (EUS) helps identify PCNs with features that may indicate the need for surgical resection[6]. However, in our study, only less than 10% of the patients underwent EUS. This may be attributable to the considerable interobserver variation in EUS-based diagnoses. On the other hand, data on EUS-based differentiation between benign and malignant PCNs are inconsistent[35,36]. Moreover, economic affordability is an important consideration, especially for most patients from rural areas. Second, heterogeneity in pathological diagnosis to determine the grade of dysplasia or malignancy and heterogeneity between different imaging examinations may exist. Third, this was a retrospective study considering only patients who underwent surgery which meant that it had inherent limitations resulting from potential selection biases; prospective validation is therefore required to confirm the value of the findings.

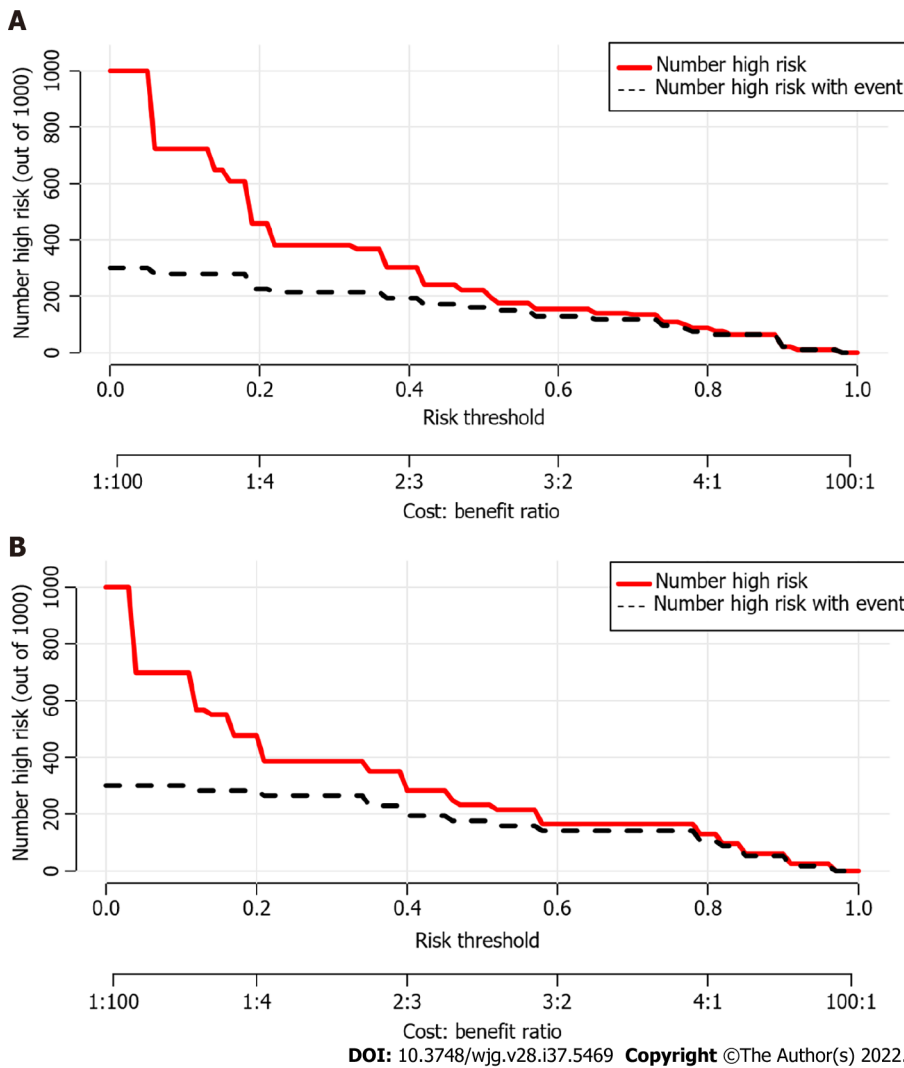


**Figure 6 Clinical impact curves of the nomogram.** At different threshold probabilities within a given population, the number of high-risk patients (solid red line) and the number of high-risk patients with the outcome (black dotted line) are shown. In both training and validation cohort, the solid red line and black dotted line show a great fit. A: In the training cohort; B: In the validation cohort.

## CONCLUSION

In conclusion, we developed and validated a novel online calculator using a nomogram based on widely available data to predict the risk of malignancy in patients with PCNs dynamically. The calculator is user-friendly, highly accurate and well validated. Clinicians can use it to alert patients at high risk of malignancy at early stages and to design individual therapy for them.

## ARTICLE HIGHLIGHTS

### Research background

Efficient and practical methods for predicting the risk of malignancy in patients with pancreatic cystic neoplasms (PCNs) are currently lacking.

### Research motivation

Currently, there is no effective clinical prediction model for patients with PCNs and no large study has been conducted to predict malignant risk.

### Research objectives

The aim of this study was to identify the risk factors influencing the malignant risk of PCNs and develop a prediction model that is useful for clinical surgeons when making decisions regarding surgical interventions.

### Research methods

Data collected in three major medical centers were analyzed to identify independent risk parameters and propose a calculator for patients with PCNs. A number of statistical indices, such as concordance index, calibration curves, area under the curve, decision curve analysis, CIC and others were used to evaluate the performance of the nomogram.

### Research results

Five factors, including enhanced mural nodules, tumor diameter  $\geq 40$  mm, main pancreatic duct dilatation, preoperative neutrophil-to-lymphocyte ratio  $\geq 2.288$  and preoperative serum CA19-9 concentration  $\geq 34$  U/mL were found to independently influencing the risk of malignancy. As a result, the model we constructed has a greater predictive value than the factors identified in relevant guidelines.

### Research conclusions

For the first time, a model was developed to predict the malignant risk of PCNs and an online calculator was further established to guide decision-making.

### Research perspectives

More medical centers included, more data collection and application of "Artificial Intelligence".

---

## ACKNOWLEDGEMENTS

We would like to thank Prof. Faming Pan (Department of Epidemiology and Biostatistics, School of Public Health, Anhui Medical University), who has made valuable support to the data quality and data analysis which ensured the reliability of the study.

---

## FOOTNOTES

**Author contributions:** Jiang D, Chen JM, Chen ZX and Ma FX contributed to the data analysis and participated in drafting the article; Liu XQ, Gong YY, and Pu T extracted the clinical data and calculated the clinical correlations; Xie K and Zhao YJ interpreted the results and revised the manuscript; Liu FB, Hou H, Wang C and Geng XP gave final approval of the version to be published; All authors contributed to the design and interpretation of the study and to further drafts and approved the final version to be published.

**Supported by** University Natural Science Research Project of Anhui Province, No. KJ2021ZD0021.

**Institutional review board statement:** The study was reviewed and approved by the Institutional ethics committees of the First Affiliated Hospital of Anhui Medical University (Approval Quick-PJ2022-06-26).

**Informed consent statement:** All study participants or their legal guardian provided informed written consent prior to study enrollment.

**Conflict-of-interest statement:** All the authors report no relevant conflicts of interest for this article.

**Data sharing statement:** No additional data are available.

**Open-Access:** This article is an open-access article that was selected by an in-house editor and fully peer-reviewed by external reviewers. It is distributed in accordance with the Creative Commons Attribution NonCommercial (CC BY-NC 4.0) license, which permits others to distribute, remix, adapt, build upon this work non-commercially, and license their derivative works on different terms, provided the original work is properly cited and the use is non-commercial. See: <https://creativecommons.org/licenses/by-nc/4.0/>

**Country/Territory of origin:** China

**ORCID number:** Dong Jiang 0000-0003-3372-6062; Tian Pu 0000-0002-6961-0814; Jiang-Ming Chen 0000-0003-4683-5866; Yi-Jun Zhao 0000-0001-9082-8861; Kun Xie 0000-0002-2491-4988; Hui Hou 0000-0002-5997-1229; Cheng Wang 0000-0001-7899-2079; Xiao-Ping Geng 0000-0002-6219-6366; Fu-Bao Liu 0000-0003-3431-2187.

**S-Editor:** Fan JR

**L-Editor:** Filipodia

**P-Editor:** Yu HG

## REFERENCES

- 1 **de Jong K**, Nio CY, Hermans JJ, Dijkgraaf MG, Gouma DJ, van Eijck CH, van Heel E, Klass G, Fockens P, Bruno MJ. High prevalence of pancreatic cysts detected by screening magnetic resonance imaging examinations. *Clin Gastroenterol Hepatol* 2010; **8**: 806-811 [PMID: 20621679 DOI: 10.1016/j.cgh.2010.05.017]
- 2 **Girometti R**, Intini S, Brondani G, Como G, Londero F, Bresadola F, Zuiani C, Bazzocchi M. Incidental pancreatic cysts on 3D turbo spin echo magnetic resonance cholangiopancreatography: prevalence and relation with clinical and imaging features. *Abdom Imaging* 2011; **36**: 196-205 [PMID: 20473669 DOI: 10.1007/s00261-010-9618-4]
- 3 **Ip IK**, Mortele KJ, Prevedello LM, Khorasani R. Focal cystic pancreatic lesions: assessing variation in radiologists' management recommendations. *Radiology* 2011; **259**: 136-141 [PMID: 21292867 DOI: 10.1148/radiol.10100970]
- 4 **Laffan TA**, Horton KM, Klein AP, Berlanstein B, Siegelman SS, Kawamoto S, Johnson PT, Fishman EK, Hruban RH. Prevalence of unsuspected pancreatic cysts on MDCT. *AJR Am J Roentgenol* 2008; **191**: 802-807 [PMID: 18716113 DOI: 10.2214/AJR.07.3340]
- 5 **Kern SE**, Hruban RH, Hidalgo M, Yeo CJ. An introduction to pancreatic adenocarcinoma genetics, pathology and therapy. *Cancer Biol Ther* 2002; **1**: 607-613 [PMID: 12642681 DOI: 10.4161/cbt.307]
- 6 **European Study Group on Cystic Tumours of the Pancreas**. European evidence-based guidelines on pancreatic cystic neoplasms. *Gut* 2018; **67**: 789-804 [PMID: 29574408 DOI: 10.1136/gutjnl-2018-316027]
- 7 **Kim SY**, Lee JM, Kim SH, Shin KS, Kim YJ, An SK, Han CJ, Han JK, Choi BI. Macrocystic neoplasms of the pancreas: CT differentiation of serous oligocystic adenoma from mucinous cystadenoma and intraductal papillary mucinous tumor. *AJR Am J Roentgenol* 2006; **187**: 1192-1198 [PMID: 17056905 DOI: 10.2214/AJR.05.0337]
- 8 **Wang GX**, Wang ZP, Chen HL, Zhang D, Wen L. Discrimination of serous cystadenoma from mucinous cystic neoplasm and branch duct intraductal papillary mucinous neoplasm in the pancreas with CT. *Abdom Radiol (NY)* 2020; **45**: 2772-2778 [PMID: 32705313 DOI: 10.1007/s00261-020-02664-7]
- 9 **Chen S**, Ren S, Guo K, Daniels MJ, Wang Z, Chen R. Preoperative differentiation of serous cystic neoplasms from mucin-producing pancreatic cystic neoplasms using a CT-based radiomics nomogram. *Abdom Radiol (NY)* 2021; **46**: 2637-2646 [PMID: 33558952 DOI: 10.1007/s00261-021-02954-8]
- 10 **Yang J**, Guo X, Ou X, Zhang W, Ma X. Discrimination of Pancreatic Serous Cystadenomas From Mucinous Cystadenomas With CT Textural Features: Based on Machine Learning. *Front Oncol* 2019; **9**: 494 [PMID: 31245294 DOI: 10.3389/fonc.2019.00494]
- 11 **Dmitriev K**, Kaufman AE, Javed AA, Hruban RH, Fishman EK, Lennon AM, Saltz JH. Classification of Pancreatic Cysts in Computed Tomography Images Using a Random Forest and Convolutional Neural Network Ensemble. *Med Image Comput Comput Assist Interv* 2017; **10435**: 150-158 [PMID: 29881827 DOI: 10.1007/978-3-319-66179-7\_18]
- 12 **Balachandran VP**, Gonen M, Smith JJ, DeMatteo RP. Nomograms in oncology: more than meets the eye. *Lancet Oncol* 2015; **16**: e173-e180 [PMID: 25846097 DOI: 10.1016/S1470-2045(14)71116-7]
- 13 **Nagtegaal ID**, Odze RD, Klimstra D, Paradis V, Rugge M, Schirmacher P, Washington KM, Carneiro F, Cree IA; WHO Classification of Tumours Editorial Board. The 2019 WHO classification of tumours of the digestive system. *Histopathology* 2020; **76**: 182-188 [PMID: 31433515 DOI: 10.1111/his.13975]
- 14 **Basturk O**, Hong SM, Wood LD, Adsay NV, Albores-Saavedra J, Biankin AV, Brosens LA, Fukushima N, Goggins M, Hruban RH, Kato Y, Klimstra DS, Klöppel G, Krasinskas A, Longnecker DS, Matthaei H, Offerhaus GJ, Shimizu M, Takaori K, Terris B, Yachida S, Esposito I, Furukawa T; Baltimore Consensus Meeting. A Revised Classification System and Recommendations From the Baltimore Consensus Meeting for Neoplastic Precursor Lesions in the Pancreas. *Am J Surg Pathol* 2015; **39**: 1730-1741 [PMID: 26559377 DOI: 10.1097/PAS.0000000000000533]
- 15 **Youden WJ**. Index for rating diagnostic tests. *Cancer* 1950; **3**: 32-35 [PMID: 15405679 DOI: 10.1002/1097-0142(1950)3:1<32::aid-encr2820030106>3.0.co;2-3]
- 16 **Vickers AJ**, Cronin AM, Elkin EB, Gonen M. Extensions to decision curve analysis, a novel method for evaluating diagnostic tests, prediction models and molecular markers. *BMC Med Inform Decis Mak* 2008; **8**: 53 [PMID: 19036144 DOI: 10.1186/1472-6947-8-53]
- 17 **Semenkovich TR**, Yan Y, Subramanian M, Meyers BF, Kozower BD, Nava R, Patterson GA, Kreisel D, Puri V. A Clinical Nomogram for Predicting Node-positive Disease in Esophageal Cancer. *Ann Surg* 2021; **273**: e214-e221 [PMID: 31274650 DOI: 10.1097/SLA.0000000000003450]
- 18 **Tanaka M**, Fernández-Del Castillo C, Kamisawa T, Jang JY, Levy P, Ohtsuka T, Salvia R, Shimizu Y, Tada M, Wolfgang CL. Revisions of international consensus Fukuoka guidelines for the management of IPMN of the pancreas. *Pancreatol* 2017; **17**: 738-753 [PMID: 28735806 DOI: 10.1016/j.pan.2017.07.007]
- 19 **Gaujoux S**, Brennan MF, Gonen M, D'Angelica MI, DeMatteo R, Fong Y, Schattner M, DiMaio C, Janakos M, Jarnagin WR, Allen PJ. Cystic lesions of the pancreas: changes in the presentation and management of 1,424 patients at a single institution over a 15-year time period. *J Am Coll Surg* 2011; **212**: 590-600; discussion 600 [PMID: 21463795 DOI: 10.1016/j.jamcollsurg.2011.01.016]
- 20 **Attiyeh MA**, Fernández-Del Castillo C, Al Efishat M, Eaton AA, Gönen M, Batts R, Pergolini I, Rezaee N, Lillemoe KD, Ferrone CR, Mino-Kenudson M, Weiss MJ, Cameron JL, Hruban RH, D'Angelica MI, DeMatteo RP, Kingham TP, Jarnagin WR, Wolfgang CL, Allen PJ. Development and Validation of a Multi-institutional Preoperative Nomogram for Predicting Grade of Dysplasia in Intraductal Papillary Mucinous Neoplasms (IPMNs) of the Pancreas: A Report from The Pancreatic Surgery Consortium. *Ann Surg* 2018; **267**: 157-163 [PMID: 28079542 DOI: 10.1097/SLA.0000000000002015]
- 21 **Jang JY**, Park T, Lee S, Kim Y, Lee SY, Kim SW, Kim SC, Song KB, Yamamoto M, Hatori T, Hirono S, Satoi S, Fujii T, Hirano S, Hashimoto Y, Shimizu Y, Choi DW, Choi SH, Heo JS, Motoi F, Matsumoto I, Lee WJ, Kang CM, Han HS, Yoon YS, Sho M, Nagano H, Honda G, Kim SG, Yu HC, Chung JC, Nagakawa Y, Seo HI, Yamaue H. Proposed Nomogram Predicting the Individual Risk of Malignancy in the Patients With Branch Duct Type Intraductal Papillary Mucinous Neoplasms of the Pancreas. *Ann Surg* 2017; **266**: 1062-1068 [PMID: 27607098 DOI: 10.1097/SLA.0000000000001985]
- 22 **Shimizu Y**, Hijioka S, Hirono S, Kin T, Ohtsuka T, Kanno A, Koshita S, Hanada K, Kitano M, Inoue H, Itoi T, Ueki T,

- Matsuo K, Yanagisawa A, Yamaue H, Sugiyama M, Okazaki K. New Model for Predicting Malignancy in Patients With Intraductal Papillary Mucinous Neoplasm. *Ann Surg* 2020; **272**: 155-162 [PMID: 30499803 DOI: 10.1097/SLA.0000000000003108]
- 23 **Sahani DV**, Kadavigere R, Saokar A, Fernandez-del Castillo C, Brugge WR, Hahn PF. Cystic pancreatic lesions: a simple imaging-based classification system for guiding management. *Radiographics* 2005; **25**: 1471-1484 [PMID: 16284129 DOI: 10.1148/rg.256045161]
- 24 **Salvia R**, Malleo G, Marchegiani G, Pennacchio S, Paiella S, Paimi M, Pea A, Butturini G, Pederzoli P, Bassi C. Pancreatic resections for cystic neoplasms: from the surgeon's presumption to the pathologist's reality. *Surgery* 2012; **152**: S135-S142 [PMID: 22766364 DOI: 10.1016/j.surg.2012.05.019]
- 25 **Pancreatic Surgery of Chinese Academic Society of Young Surgeons**. [The current status of diagnosis and treatment of pancreatic cystic neoplasm in China: a report of 2 251 cases]. *Zhonghua Wai Ke Za Zhi* 2018; **56**: 24-29 [PMID: 29325350 DOI: 10.3760/cma.j.issn.0529-5815.2018.01.007]
- 26 **Bausch D**, Pausch T, Krauss T, Hopt UT, Fernandez-del-Castillo C, Warshaw AL, Thayer SP, Keck T. Neutrophil granulocyte derived MMP-9 is a VEGF independent functional component of the angiogenic switch in pancreatic ductal adenocarcinoma. *Angiogenesis* 2011; **14**: 235-243 [PMID: 21442180 DOI: 10.1007/s10456-011-9207-3]
- 27 **Gong L**, Cumpian AM, Caetano MS, Ochoa CE, De la Garza MM, Lapid DJ, Mirabolfathinejad SG, Dickey BF, Zhou Q, Moghaddam SJ. Promoting effect of neutrophils on lung tumorigenesis is mediated by CXCR2 and neutrophil elastase. *Mol Cancer* 2013; **12**: 154 [PMID: 24321240 DOI: 10.1186/1476-4598-12-154]
- 28 **Zhou W**, Rong Y, Kuang T, Xu Y, Shen X, Ji Y, Lou W, Wang D. The value of systemic inflammatory markers in identifying malignancy in mucinous pancreatic cystic neoplasms. *Oncotarget* 2017; **8**: 115561-115569 [PMID: 29383181 DOI: 10.18632/oncotarget.23310]
- 29 **Gemenetzis G**, Bagante F, Griffin JF, Rezaee N, Javed AA, Manos LL, Lennon AM, Wood LD, Hruban RH, Zheng L, Zaheer A, Fishman EK, Ahuja N, Cameron JL, Weiss MJ, He J, Wolfgang CL. Neutrophil-to-lymphocyte Ratio is a Predictive Marker for Invasive Malignancy in Intraductal Papillary Mucinous Neoplasms of the Pancreas. *Ann Surg* 2017; **266**: 339-345 [PMID: 27631774 DOI: 10.1097/SLA.0000000000001988]
- 30 **Goh BK**, Tan DM, Chan CY, Lee SY, Lee VT, Thng CH, Low AS, Tai DW, Cheow PC, Chow PK, Ooi LL, Chung AY. Are preoperative blood neutrophil-to-lymphocyte and platelet-to-lymphocyte ratios useful in predicting malignancy in surgically-treated mucin-producing pancreatic cystic neoplasms? *J Surg Oncol* 2015; **112**: 366-371 [PMID: 26280242 DOI: 10.1002/jso.23997]
- 31 **Gregory AD**, Houghton AM. Tumor-associated neutrophils: new targets for cancer therapy. *Cancer Res* 2011; **71**: 2411-2416 [PMID: 21427354 DOI: 10.1158/0008-5472.CAN-10-2583]
- 32 **Harish KB**, Price WN, Aphinyanaphongs Y. Open-Source Clinical Machine Learning Models: Critical Appraisal of Feasibility, Advantages, and Challenges. *JMIR Form Res* 2022; **6**: e33970 [PMID: 35404258 DOI: 10.2196/33970]
- 33 **Sendak M**, Gao M, Nichols M, Lin A, Balu S. Machine Learning in Health Care: A Critical Appraisal of Challenges and Opportunities. *EGEMS (Wash DC)* 2019; **7**: 1 [PMID: 30705919 DOI: 10.5334/egems.287]
- 34 **Decherchi S**, Pedrini E, Mordenti M, Cavalli A, Sangiorgi L. Opportunities and Challenges for Machine Learning in Rare Diseases. *Front Med (Lausanne)* 2021; **8**: 747612 [PMID: 34676229 DOI: 10.3389/fmed.2021.747612]
- 35 **Donahue TR**, Hines OJ, Farrell JJ, Tomlinson JS, Eibl G, Reber HA. Cystic neoplasms of the pancreas: results of 114 cases. *Pancreas* 2010; **39**: 1271-1276 [PMID: 20717069 DOI: 10.1097/MPA.0b013e3181e1d6f4]
- 36 **Kim JH**, Eun HW, Park HJ, Hong SS, Kim YJ. Diagnostic performance of MRI and EUS in the differentiation of benign from malignant pancreatic cyst and cyst communication with the main duct. *Eur J Radiol* 2012; **81**: 2927-2935 [PMID: 22227264 DOI: 10.1016/j.ejrad.2011.12.019]

## Observational Study

## Application of an artificial intelligence system for endoscopic diagnosis of superficial esophageal squamous cell carcinoma

Qian-Qian Meng, Ye Gao, Han Lin, Tian-Jiao Wang, Yan-Rong Zhang, Jian Feng, Zhao-Shen Li, Lei Xin, Luo-Wei Wang

**Specialty type:** Gastroenterology and hepatology

**Provenance and peer review:**

Unsolicited article; Externally peer reviewed.

**Peer-review model:** Single blind

**Peer-review report's scientific quality classification**

Grade A (Excellent): A, A

Grade B (Very good): B

Grade C (Good): 0

Grade D (Fair): 0

Grade E (Poor): 0

**P-Reviewer:** Shiroma S, Japan;

Sudou K, Japan; Tsoulfas G, Greece

**Received:** June 2, 2022

**Peer-review started:** June 2, 2022

**First decision:** August 1, 2022

**Revised:** August 9, 2022

**Accepted:** September 20, 2022

**Article in press:** September 20, 2022

**Published online:** October 7, 2022



Qian-Qian Meng, Ye Gao, Han Lin, Tian-Jiao Wang, Yan-Rong Zhang, Zhao-Shen Li, Lei Xin, Luo-Wei Wang, Department of Gastroenterology, Changhai Hospital, Shanghai 200433, China

Jian Feng, Qingdao Medcare Digital Engineering Co. Ltd., Qingdao Medcare Digital Engineering Co. Ltd., Qingdao 26600, Shandong Province, China

**Corresponding author:** Luo-Wei Wang, MD, Chief Doctor, Department of Gastroenterology, Changhai Hospital, No. 168 Changhai Road, Yangpu District, Shanghai 200433, China. [wangluoweimd@126.com](mailto:wangluoweimd@126.com)

**Abstract****BACKGROUND**

Upper gastrointestinal endoscopy is critical for esophageal squamous cell carcinoma (ESCC) detection; however, endoscopists require long-term training to avoid missing superficial lesions.

**AIM**

To develop a deep learning computer-assisted diagnosis (CAD) system for endoscopic detection of superficial ESCC and investigate its application value.

**METHODS**

We configured the CAD system for white-light and narrow-band imaging modes based on the YOLO v5 algorithm. A total of 4447 images from 837 patients and 1695 images from 323 patients were included in the training and testing datasets, respectively. Two experts and two non-expert endoscopists reviewed the testing dataset independently and with computer assistance. The diagnostic performance was evaluated in terms of the area under the receiver operating characteristic curve, accuracy, sensitivity, and specificity.

**RESULTS**

The area under the receiver operating characteristics curve, accuracy, sensitivity, and specificity of the CAD system were 0.982 [95% confidence interval (CI): 0.969-0.994], 92.9% (95% CI: 89.5%-95.2%), 91.9% (95% CI: 87.4%-94.9%), and 94.7% (95% CI: 89.0%-97.6%), respectively. The accuracy of CAD was significantly higher than that of non-expert endoscopists (78.3%,  $P < 0.001$  compared with CAD) and comparable to that of expert endoscopists (91.0%,  $P = 0.129$  compared with CAD). After referring to the CAD results, the accuracy of the non-expert endoscopists

significantly improved (88.2% *vs* 78.3%,  $P < 0.001$ ). Lesions with Paris classification type 0-IIb were more likely to be inaccurately identified by the CAD system.

### CONCLUSION

The diagnostic performance of the CAD system is promising and may assist in improving detectability, particularly for inexperienced endoscopists.

**Key Words:** Computer-aided diagnosis; Artificial intelligence; Deep learning; Esophageal squamous cell carcinoma; Early detection of cancer; Upper gastrointestinal endoscopy

©The Author(s) 2022. Published by Baishideng Publishing Group Inc. All rights reserved.

**Core Tip:** Esophageal squamous cell carcinoma (ESCC) poses a heavy burden to high-risk areas, and screening using upper gastrointestinal endoscopy is an established strategy for early detection and prognosis improvement. However, endoscopic detection of superficial-ESCC can be challenging and depends greatly on operator experience. We developed and validated a novel computer-assisted diagnostic system with a deep neural network algorithm to detect superficial ESCC using upper endoscopy with white-light and narrow-band imaging. The system demonstrated high diagnostic accuracy, which is comparable to that of expert endoscopists. The diagnostic performance of non-expert endoscopists was significantly improved under the assistance of this system.

**Citation:** Meng QQ, Gao Y, Lin H, Wang TJ, Zhang YR, Feng J, Li ZS, Xin L, Wang LW. Application of an artificial intelligence system for endoscopic diagnosis of superficial esophageal squamous cell carcinoma. *World J Gastroenterol* 2022; 28(37): 5483-5493

**URL:** <https://www.wjgnet.com/1007-9327/full/v28/i37/5483.htm>

**DOI:** <https://dx.doi.org/10.3748/wjg.v28.i37.5483>

## INTRODUCTION

Esophageal cancer is the seventh most common and sixth most fatal malignancy[1], and esophageal squamous cell carcinoma (ESCC) is the most prevalent histological type[2]. Screening high-risk populations using upper gastrointestinal endoscopy may facilitate early detection and treatment[3], and markedly improve the prognosis of ESCC[4]. However, due to its subtlety and flat appearance under white light imaging (WLI) or image-enhanced endoscopy, identification of early stage ESCC may be especially difficult for inexperienced endoscopists[5-7]. A recent multicenter cohort study found that 6.4% of all esophageal cancers were missed during upper gastrointestinal endoscopy, which was associated with poor survival[8].

In recent years, artificial intelligence (AI)-aided endoscopy has garnered attention, and several studies have heralded this technique as a promising tool for improving the detection of early ESCC[9-12]. A systematic review showed that the pooled sensitivity and specificity of AI for ESCC diagnosis were 0.95 and 0.92, respectively, and AI performed better than endoscopists, although the differences were not statistically significant[13]. However, few computer-assisted diagnosis (CAD) systems for ESCC that support WLI and narrow-band imaging (NBI) have been applied in clinical practice. We developed and validated a novel CAD system with a deep neural network algorithm to detect superficial ESCC using upper endoscopy with WLI and NBI. Moreover, we assessed its value for endoscopists with differing experience levels of superficial ESCC detection and investigated the characteristics of lesions that were inaccurately identified by the CAD system.

## MATERIALS AND METHODS

### Preparation of datasets for training and testing

Static and non-magnified WLI or NBI images used for CAD system training and testing for superficial ESCC were retrospectively retrieved from endoscopic databases of four general hospitals in mainland China between January 2016 and April 2019. For the training dataset, 1503 WLI images and 2100 NBI images from 622 cases of superficial ESCC and high-grade intraepithelial neoplasia (HGIN), and 523 WLI images and 321 NBI images from 215 non-cancerous cases (including normal, esophagitis, submucosal lesion, and leukoplakia) were obtained from the First Affiliated Hospital of Zhengzhou University, Xingtai First Hospital, and Tangyin People's Hospital. For the independent testing dataset,

577 WLI images and 793 NBI images from 209 cases of superficial ESCC and HGIN, and 209 WLI images and 116 NBI images from 114 non-cancerous cases were obtained from Changhai Hospital. All images were captured using an Olympus gastroscope (GIF-H260, GIF-H260Z, GIF-H290, GIF-Q260J, or GIF-HQ290; Olympus, Tokyo, Japan). Poor-quality images, including blurred images, and those with mucus or foam that prevented adequate mucosal inspection were excluded from the study. The personal data of the patients in the images were hidden. This study was approved by the ethics committee of Shanghai Changhai Hospital (No. CHEC2019-002).

All superficial ESCC and HGIN images were obtained from patients who underwent subsequent endoscopic submucosal dissection. Additionally, histologic results including margin status and invasion depth of endoscopic submucosal dissection specimens were retrieved. Three experienced gastro-intestinal (GI) pathologists conducted histological assessments. Histological images were first reviewed by two independent pathologists who determined the final pathological result through diagnostic consensus. In case of disagreement, images were reviewed by a third pathologist, and the final decision was discussed. Non-cancerous images were confirmed by three experienced endoscopists (all with > 15 years of experience), before inclusion in training and testing datasets.

All images were annotated by the three endoscopists mentioned above. The first endoscopist reviewed and marked the WLI and NBI images (margins of the lesion) using specific frames. The second endoscopist reviewed the annotations of the first, and if in agreement, the annotation was completed. Alternately, the images were reviewed by a third endoscopist, and the final decision was made in unison. Paris classification subtypes of lesions were also recorded[14].

### **Development of the CAD system**

CAD system development was based on the YOLO v5 deep-learning algorithm. YOLO v5 employs cross stage partial network as the backbone for feature extraction and path aggregation network to generate a feature pyramid network to perform feature aggregation and pass it to the prediction mode. YOLO v5 demonstrated increased efficiency and efficacy compared to previous versions. To improve network accuracy, we modified the loss function of YOLO V5 and introduced the mapping distance of the aspect ratio. The input of this network was esophageal images, and the output was an indicator frame that captured the rectangular region of interest, together with the predicted quantitative level of confidence for ESCC above the frame (Figure 1).

### **Testing of the CAD system**

The diagnostic accuracy of the CAD system was validated using a previously established independent testing dataset. To compare the performance of the CAD system with that of endoscopists and investigate its added value, four endoscopists from Changhai Hospital were invited to review the images in the testing dataset, independently and with the assistance from the CAD system. Two experts (endoscopy experience  $\geq 10$  years) and two non-expert endoscopists (endoscopy experience > 1 year but < 5 years) participated. None were involved in the selection and annotation of images. All images in the testing dataset, including 598 WLI and 817 NBI cancerous and 209 WLI and 116 NBI non-cancerous images, were randomly sequenced, and all participating endoscopists independently reviewed the images and made diagnoses within one day. After a washout period of one month, the images were randomly re-sequenced, and endoscopists reviewed the images using the results of the CAD system as a reference. Throughout the study, participating endoscopists were unaware of the correct endoscopic and histologic diagnoses, their own performance, and the diagnostic accuracy of the CAD system.

### **Outcome measures**

Primary outcome measures included the area under the receiver operating characteristic curve (AUROC), accuracy, sensitivity, and specificity of the CAD system. Secondary outcome measures included positive predictive value (PPV) and negative predictive value (NPV) of the CAD system; diagnostic performance of participating endoscopists; and improvement in diagnostic accuracy, sensitivity, and specificity in the expert and non-expert groups, after referring to the CAD system results.

### **Statistical analysis**

AUROC, accuracy, sensitivity, specificity, PPV, and NPV were calculated, and the binomial 95% confidence intervals (CI) were estimated using the CAD-predicted confidence  $\geq 0.5$ , as the prespecified criteria for testing positive. The DeLong test was used to compare different AUROCs. A two-sided McNemar test was used to compare differences in accuracy, sensitivity, and specificity. Differences in more than three groups were compared using Cochran's *Q* test. Additionally, the McNemar test was used for post-hoc comparisons of *P* values adjusted using Bonferroni's method. Pearson's chi-squared test, *t* test, and Mann-Whitney *U* test were used wherever applicable. Superficial ESCC lesions with a CAD-predicted confidence < 0.5 and an intersection over union (IoU) value < 0.45 were defined as inaccurately identified. A *P* value < 0.05 was considered statistically significant. All statistical analyses were performed using SPSS 26.0 (SPSS Inc., Chicago, IL, United States). The statistical methods of this study were reviewed by XFY from Department of Health Statistics, Naval Medical University.

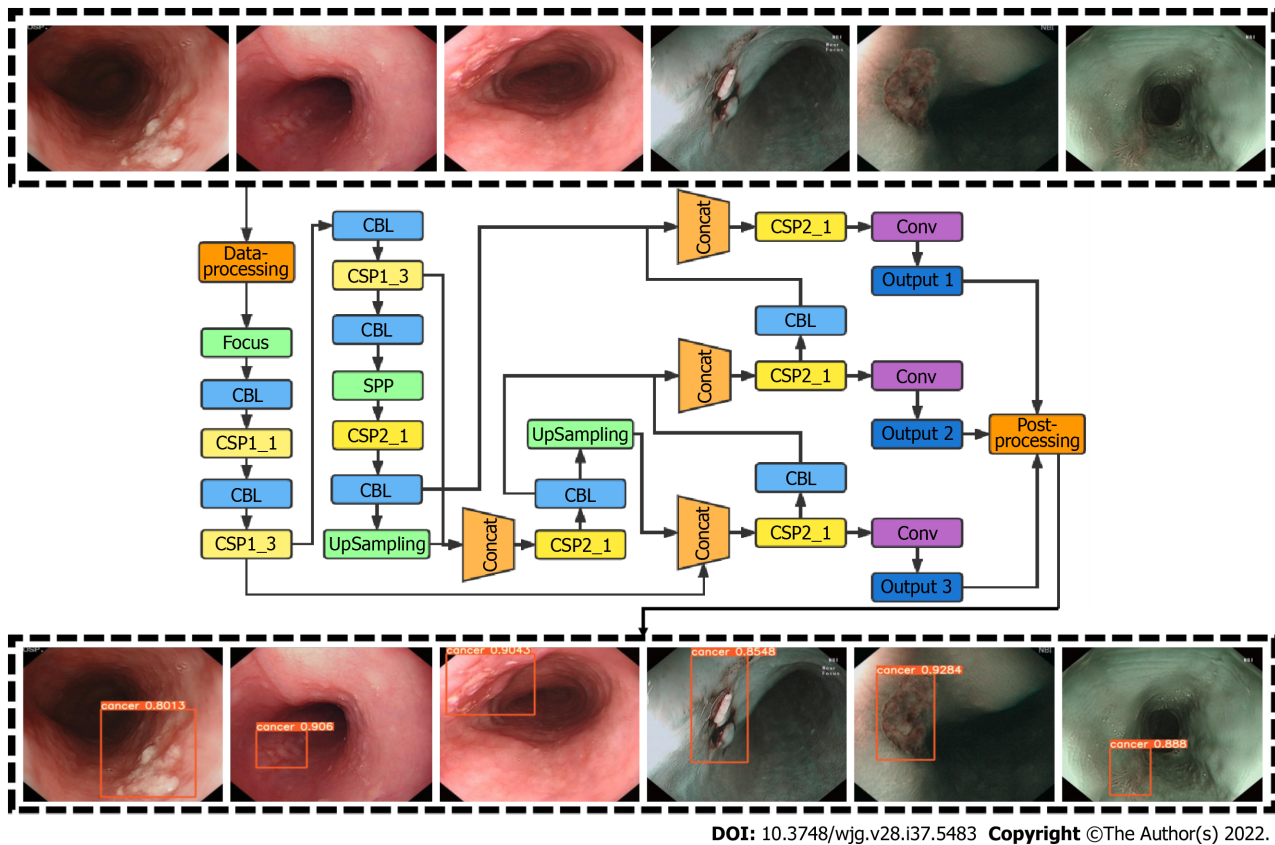


**Figure 1** The architecture of the computer-assisted diagnosis system. The input of this network was the esophageal images, and the output was an indicator frame that captured the interest region, together with the predicted quantitative level of confidence for esophageal squamous cell carcinoma.

## RESULTS

### Characteristics of subjects and lesions in test dataset

Table 1 summarizes the characteristics of the patients and lesions in the testing dataset. For 209 cases of superficial ESCC, the lesion size was 2.0 (1.2-4.0) cm and most (82.3%) were located in the middle thoracic esophagus. Flat-type (0-IIb) lesions accounted for 53.6%, and most lesions involved < 25% of the esophageal circumference. Regarding histologic depth of invasion, 165 Lesions (78.9%) were limited to the lamina propria (LPM), 38 (18.2%) invaded the muscularis mucosa or superficial submucosa, and 6 (2.9%) extended beyond the superficial submucosa. Of the 114 non-cancerous cases, 23 were diagnosed with gastroesophageal reflux disease, five were diagnosed with esophageal submucosal lesions, and 86 were judged to be normal on upper gastrointestinal endoscopy.

### Diagnostic performance of the CAD system

The receiver operating characteristic (ROC) curve of the CAD system is shown in Figure 2. The AUROC of the WLI, NBI, and combined modes were 0.970, 0.988, and 0.982, respectively. The AUROC of WLI, NBI, and the combined mode did not differ significantly. The diagnostic performance measures of the CAD system in the testing dataset are summarized in Table 2. In per-patient analysis, the accuracy, sensitivity, specificity, PPV, and NPV of the CAD system were 92.9%, 91.9%, 94.7%, 97.0%, and 86.4%, respectively. The accuracy ( $P < 0.001$ ), sensitivity ( $P < 0.001$ ), and specificity ( $P = 0.015$ ) of the CAD system were significantly different among the different imaging modes. In post-hoc comparisons, the accuracy of the NBI (adjusted  $P < 0.001$ ) and combined modes (adjusted  $P = 0.002$ ) was significantly higher than that of the WLI mode. Furthermore, the sensitivity of NBI (adjusted  $P < 0.001$ ) and combined modes (adjusted  $P = 0.014$ ) was significantly higher than that of the WLI mode. No statistically significant differences in specificity were found in post-hoc comparisons between the two imaging modes. The results of the per-imaging analysis are presented in Table 2.

### Comparison between the CAD system and endoscopists

Figure 3 compares the diagnostic performance of the CAD system under the combined WLI and NBI modes, among endoscopists with different experience levels. The accuracy (91.0% vs 78.3%,  $P < 0.001$ ), sensitivity (90.0% vs 76.1%,  $P < 0.001$ ), and specificity (93.0% vs 82.5%,  $P = 0.002$ ) were significantly higher for expert endoscopists than for non-expert endoscopists. The diagnostic performance of the

**Table 1 Characteristics of subjects and lesions involved in the testing dataset**

Characteristics	Values
<b>Cancerous cases (n = 209)</b>	
Age (yr), mean ± SD	62.0 ± 7.2
Sex, Male/Female	158/51
Lesion location, Ce/Ut/Mt/Lt/Ae	2/21/172/14/0
Lesion size (cm), median (Q1, Q3)	2.0 (1.2-4.0)
Paris classification, 0-I/IIa/IIb/IIc/IIa+IIc/III	6/43/112/26/20/2
Circumference, < 1/4, 1/4-1/2, 1/2-3/4, > 3/4	117/63/18/11
Depth of invasion, EP-LPM/MM-SM1/SM2	165/38/6
<b>Non-Cancerous cases (n = 114)</b>	
Age (yr), mean ± SD	63.2 ± 5.3
Sex, male/female	65/49
Endoscopic diagnosis, GERD/submucosal lesion/normal	23/5/86

SD: Standard deviation; Ce: Cervical esophagus; Ut: Upper thoracic esophagus; Mt: Middle thoracic esophagus; Lt: Lower thoracic esophagus; Ae, Abdominal esophagus; Q1: Lower quartile; Q3: Upper quartile; EP-LPM: Epithelium or lamina propria; MM-SM1: Muscularis mucosa or submucosal invasion < 200 µm; SM2: Submucosal invasion > 200 µm; GERD: Gastroesophageal reflux disease.

**Table 2 Diagnostic performance of the computer-assisted diagnosis system in the testing dataset**

	Per-patient analysis				Per-image analysis			
	Overall (%)	WLI (%)	NBI (%)	P value	Overall (%)	WLI (%)	NBI (%)	P value
Accuracy (95%CI)	92.9 (89.5-95.2)	89.2 (85.3-92.1)	94.7 (91.7-96.7)	< 0.001	87.5 (85.9-89.0)	85.9 (83.3-88.1)	89.0 (86.8-90.9)	0.156
Sensitivity (95%CI)	91.9 (87.4-94.9)	88.0 (82.9-91.8)	94.3 (90.2-96.7)	< 0.001	86.6 (84.7-88.3)	84.1 (80.8-86.8)	88.4 (86.0-90.4)	0.067
Specificity (95%CI)	94.7 (89.0-97.6)	91.2 (84.6-95.2)	95.6 (90.1-98.1)	0.015	91.7 (88.2-94.3)	90.9 (86.2-94.1)	93.4 (87.0-96.8)	0.750
PPV (95%CI)	97.0 (93.5-98.6)	94.8 (90.8-97.2)	97.7 (94.3-98.9)	0.316	97.9 (96.9-98.5)	96.2 (94.2-97.6)	99.0 (98.0-99.5)	0.004
NPV (95%CI)	86.4 (79.3-91.3)	80.6 (73.0-86.5)	90.1 (83.5-94.2)	0.099	61.1 (56.6-65.4)	67.4 (61.7-72.6)	51.8 (44.8-58.8)	0.003

WLI: White-light imaging; NBI: Narrow-band imaging; PPV: Positive predictive value; NPV: Negative predictive value.

CAD system was significantly higher than that of non-expert endoscopists ( $P < 0.001$ ) and similar to that of expert endoscopists.

### Improvement after referring to CAD

Figure 4 depicts improved diagnostic performance of endoscopists for superficial ESCC after referring to the results of the CAD system. The accuracy (88.2% vs 78.3%,  $P < 0.001$ ), sensitivity (87.6% vs 76.1%,  $P < 0.001$ ), and specificity (89.5% vs 82.5%,  $P = 0.039$ ) of the non-expert endoscopists were all significantly improved after using the CAD system, whereas the diagnostic performances of expert endoscopists did not differ significantly between the two stages. After referring to the CAD system, the accuracy (88.2% vs 93.2%,  $P < 0.001$ ) and sensitivity (87.6% vs 92.3%,  $P = 0.013$ ) of the non-experts were still significantly lower than those of the experts, while the disparities were markedly decreased. The specificity (89.5% vs 94.7%,  $P = 0.124$ ) was similar between experts and non-experts after referring to the CAD.

### Inaccurately identified lesions

Under the prespecified definition, 23 (11.0%) lesions were inaccurately identified. Table 3 compares the characteristics of lesions with accurate and inaccurate identifications. The proportion of type 0-IIb lesions was significantly higher in inaccurately identified lesions (73.9% vs 51.1%,  $P = 0.038$ ), and the proportion of lesions limited to the LPM was higher in the inaccurate identification group, although not significantly so (91.3% vs 77.4%,  $P = 0.123$ ).

**Table 3 Characteristics of lesions that were inaccurately identified by the computer-assisted diagnosis system**

Characteristics	Accurate identification (n = 186)	Inaccurate identification (n = 23)	P value
Lesion location, n (%)			1.000
Ce	2 (1.1)	0 (0)	
Ut	13 (7.0)	2 (8.7)	
Mt	152 (81.7)	20 (87.0)	
Lt	19 (10.2)	1 (4.3)	
Lesion size (cm), median (Q1, Q3)	2.0 (1.1-4.0)	3 (1.5-3.0)	0.476
Paris classification, n (%)			0.038
Type 0-IIb	95 (51.1)	17 (73.9)	
Other non-flat types	91 (48.9)	6 (26.1)	
Circumference, n (%)			0.591
< 1/4	107 (57.4)	10 (43.5)	
1/4-1/2	54 (29.0)	9 (39.1)	
1/2-3/4	16 (8.6)	2 (8.7)	
> 3/4	9 (4.8)	2 (8.7)	
Depth of invasion, n (%)			0.123
EP-LPM	144 (77.4)	21 (91.3)	
MM and deeper	42 (22.6)	2 (8.7)	

Ce: Cervical esophagus; Ut: Upper thoracic esophagus; Mt: Middle thoracic esophagus; Lt: Lower thoracic esophagus; Q1: Lower quantile; Q3: Upper quantile; EP-LPM: Epithelium or lamina propria; MM: Muscularis mucosa.

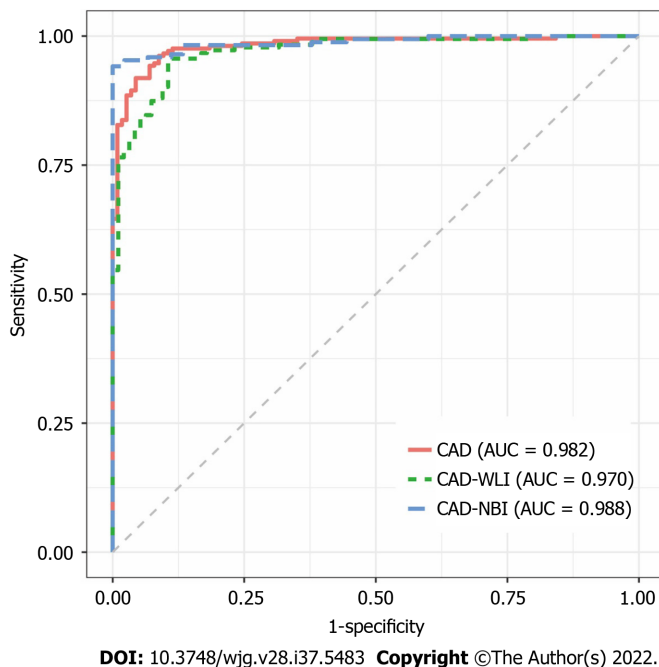


**Figure 2 Receiver operating characteristic curve for the computer-assisted diagnosis system in the testing dataset.** CAD: Computer-assisted diagnosis; AUC: Area under the curve; WLI: White light imaging; NBI: Narrow-band imaging.

## DISCUSSION

Upper gastrointestinal endoscopy is critical for screening and early diagnosis of ESCC. However, the subtle endoscopic appearance of most superficial ESCC types is challenging for early detection and

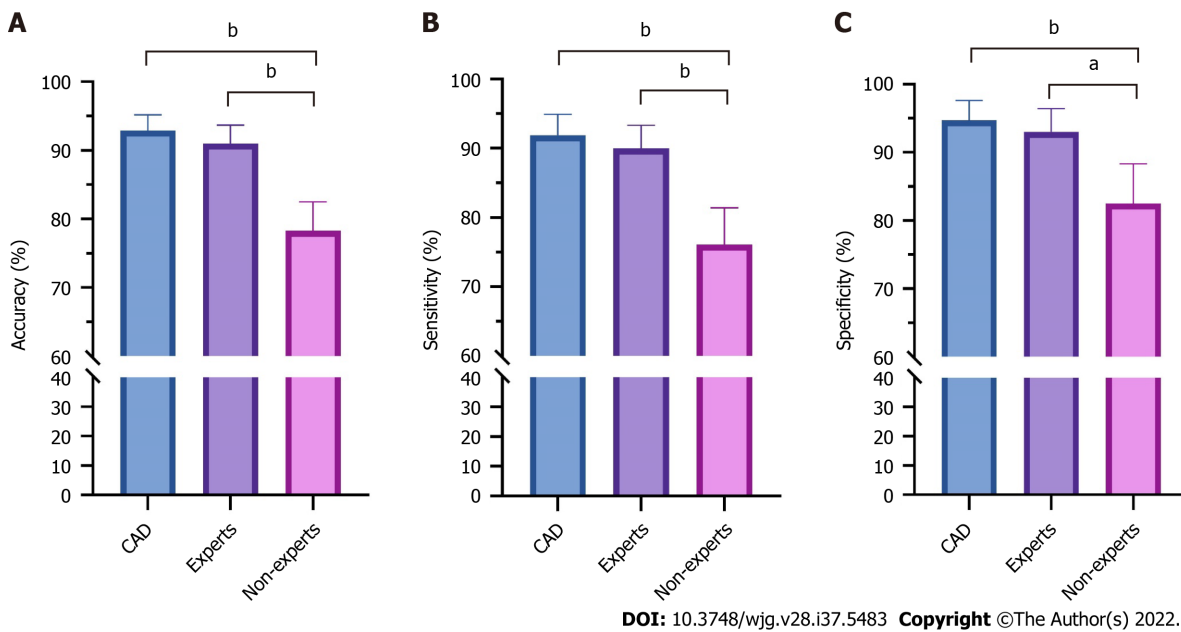


**Figure 3 Comparison of diagnostic performances between the computer-assisted diagnosis system and endoscopists for superficial esophageal squamous cell carcinoma.** A: Accuracy; B: Sensitivity; C: Specificity. <sup>a</sup> $P < 0.05$ ; <sup>b</sup> $P < 0.01$ . CAD: Computer-assisted diagnosis.

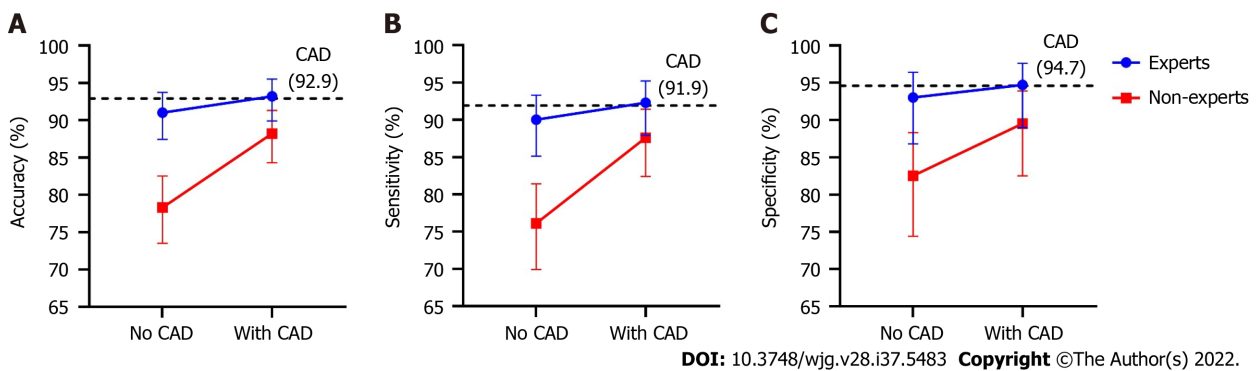


**Figure 4 The improvements in the diagnostic performance of endoscopists after referring to the results of computer-assisted diagnosis system.** A: Accuracy; B: Sensitivity; C: Specificity. CAD: Computer-assisted diagnosis.

relies greatly on the skills and experience of endoscopists. Herein, we developed and validated a novel deep-learning-based CAD system for the detection of superficial ESCC in the WLI and NBI modes of upper gastrointestinal endoscopy. The AUROC, accuracy, sensitivity, and specificity of the CAD system were 0.982, 92.9%, 91.9%, and 94.7%, respectively. The diagnostic performance was significantly superior to that of non-experts and comparable to that of expert endoscopists. After referring to the results of the CAD system, the detectability of non-expert endoscopists significantly improved, and disparities between experts and non-experts markedly decreased. This system may assist in improving the detectability of superficial ESCC, particularly for inexperienced endoscopists and in undeveloped areas with limited resources.

Horie *et al*[9] developed a deep learning-based CAD system for superficial ESCC, with a sensitivity of 98% and low PPV of 40%. Zhao *et al*[15] developed an AI-based model for magnifying NBI images for automated classification of intrapapillary capillary loops, with a mean diagnostic accuracy of 89.6%. In a recent study by Guo *et al*[16], the authors developed a CAD system for real-time automated diagnosis of precancerous lesions and ESCC based on endoscopic video datasets, which achieved a per-lesion sensitivity of 100%. A systematic review by Visaggi *et al*[13] reported that the AUROC, sensitivity, and specificity of AI in diagnosing ESCC were 0.97, 0.95, and 0.92, respectively. However, few existing systems can support WLI and NBI, both of which are indispensable to the diagnosis of superficial ESCC under the same algorithm framework. We developed the current system under the updated YOLO v5 algorithm network supporting WLI and NBI, and achieved an AUROC, accuracy, sensitivity, and specificity of 0.982, 92.9%, 91.9%, and 94.7%, respectively, which was comparable to the best performance reported in previous studies. Esophageal endoscopic imaging is affected by factors such as

esophageal peristalsis, contraction, and imaging quality. Therefore, to supplement data by mimicking the above influencing factors, we added undistorted imaging correction enhancement based on the original data enhancement method of YOLO v5.

Superficial ESCC is difficult to inspect under WLI; however, NBI may significantly improve detectability with similar sensitivity and higher specificity than Lugol chromoendoscopy[6]. This may explain the demonstrated decrease in the accuracy and sensitivity of the CAD system, without NBI. Cai *et al*[10] reported on a deep neural network (DNN)-based system that utilizes WLI with high accuracy and sensitivity, for early ESCC detection. They subsequently developed a CAD-NBI system and found that its accuracy (94.3% *vs* 89.5%,  $P = 0.028$ ) and specificity (96.7% *vs* 83.1%,  $P < 0.001$ ) were significantly better than those of the CAD-WLI system[12]. By using CAD-WLI and CAD-NBI, endoscopists can significantly improve their diagnostic efficacy. Taken together, we recommend the combined implementation of NBI with other image-enhancing techniques for the detection of superficial ESCC, even under the CAD system.

To assess the clinical application value of the CAD system, endoscopists of varying experience reviewed the entire testing dataset independently and after referring to the diagnostic results of the CAD system. During the independent review, non-expert endoscopists showed significantly lower accuracy, sensitivity, and specificity than the experts, which highlighted the difficulty of novices in detecting superficial ESCC and disparities in detectability among endoscopists. The diagnostic performance of the non-experts significantly improved after referring to the CAD system. This suggests that the results of the CAD system provide useful references for non-expert endoscopists and facilitate further inspection and evaluation of potentially malignant lesions. The improved diagnostic performance of non-experts remained unequal to that of the CAD system, suggesting that endoscopists had made independent decisions, rather than relying completely on CAD. Similar results were reported in previous studies[10,12,17]. In the current study, although the performance of non-experts was still inferior to that of the experts after referring to the CAD system, the disparity markedly decreased. This suggests that the CAD system can homogenize the performance of endoscopists by overcoming the differences among endoscopists with different experience levels. In clinical practice, the usefulness of high-definition and imaging-enhanced endoscopy may be jeopardized by the inadequate number of highly trained endoscopists. In contrast, the CAD system does not require additional training and has instead been found to improve the performance of non-expert endoscopists by approximating the level of expertise. Thus, the CAD system may be especially useful in resource-limited areas, to improve the quality of endoscopic services and patient outcomes.

To our knowledge, this is the first study to analyze the characteristics of inaccurately identified lesions. We defined cases of inaccurate identification based on the predicted confidence and accuracy of the location frame. Endoscopists should be aware that flat-type and earlier-stage lesions limited to the LPM may be associated with an increased risk of inaccurate identification. To avoid a missed diagnosis of superficial ESCC, we recommend the use of Lugol's staining or magnifying endoscopy for flat-type lesions that are difficult to distinguish even under CAD.

In clinical practice, the CAD system automatically captures images as endoscopists inspect the esophagus, once integrated into an endoscopy workstation. Additionally, images frozen by endoscopists were input into the CAD system for analysis and detection of potential lesions. The CAD system then address potential malignant lesions with an indicator frame and a predicted quantitative level of confidence. Lesions with a predicted confidence  $\geq 0.5$  are strongly suggested for further evaluation and endoscopic biopsy. Other lesions may also be further evaluated or biopsied based on endoscopists' discretion. The diagnostic accuracy for ESCC is significantly improved after referring to the CAD system, particularly for non-expert endoscopists. Moreover, an updated CAD system that can process real-time videos or images with suboptimal quality is in development and may further facilitate clinical practice. In future, both endoscopists and patients may benefit from the increasing application of AI in endoscopy.

Our study had several limitations. First, the number of included endoscopists was relatively small, and the representation might be inadequate. Second, only still and non-magnified images were included; thus, the identification of videos and types of intrapapillary capillary loops could not be achieved. Third, the numbers and angles of lesions in NBI and WLI images were not identical in the testing dataset, and biases may exist in the comparison of diagnostic performance among the different modes of the CAD system.

---

## CONCLUSION

We developed and validated a deep-learning CAD system, for the endoscopic detection of superficial ESCC, that achieved a high diagnostic accuracy comparable to that of expert endoscopists and could significantly improve the detecting ability of non-expert endoscopists.

## ARTICLE HIGHLIGHTS

### Research background

Esophageal squamous cell carcinoma (ESCC) is a leading cause of cancer-related morbidity and mortality worldwide. Upper gastrointestinal endoscopy is critical for ESCC detection; however, endoscopists require long-term training to avoid missing superficial lesions. Artificial intelligence (AI) has been increasingly investigated to assist endoscopic diagnosis.

### Research motivation

AI has shown promising results for endoscopic diagnosis of superficial ESCC. However, few AI-based computer-assisted diagnosis (CAD) systems for ESCC that support white-light and narrow-band imaging have been applied in clinical practice.

### Research objectives

We aimed to develop a CAD system for endoscopic detection of superficial ESCC and investigate its application value.

### Research methods

We configured the CAD system for white-light and narrow-band imaging modes based on the YOLO v5 algorithm. A total of 4447 images from 837 patients and 1695 images from 323 patients were included in the training and testing datasets, respectively. Two experts and two non-expert endoscopists reviewed the testing dataset independently and with computer assistance. The diagnostic performance was evaluated in terms of the area under the receiver operating characteristic curve, accuracy, sensitivity, and specificity.

### Research results

The area under the receiver operating characteristics curve, accuracy, sensitivity, and specificity of the CAD system were 0.982 [95% confidence interval (CI): 0.969-0.994], 92.9% (95%CI: 89.5%-95.2%), 91.9% (95%CI: 87.4%-94.9%), and 94.7% (95%CI: 89.0%-97.6%), respectively. The accuracy of CAD was significantly higher than that of non-expert endoscopists (78.3%,  $P < 0.001$  compared with CAD) and comparable to that of expert endoscopists (91.0%,  $P = 0.129$  compared with CAD). After referring to the CAD results, the accuracy of the non-expert endoscopists significantly improved (88.2% *vs* 78.3%,  $P < 0.001$ ).

### Research conclusions

The diagnostic performance of the CAD system is promising and may assist in improving detectability, particularly for inexperienced endoscopists.

### Research perspectives

An updated CAD system that can process real-time videos or images with suboptimal quality is in development. Randomized controlled trials are warranted to investigate the clinical pragmaticity.

## FOOTNOTES

**Author contributions:** Wang LW was the guarantor and designed the study; Lin H, Wang TJ, Zhang YR, Feng J participated in the acquisition, analysis, and interpretation of the data; Gao Y, Meng QQ drafted the initial manuscript; Xin L, Li ZS revised the article critically for important intellectual content; Meng QQ, Gao Y and Lin H contributed equally to this article.

**Supported by** Shanghai Science and Technology Innovation Action Program, No. 21Y31900100; and 234 Clinical Research Fund of Changhai Hospital, No. 2019YXK006.

**Institutional review board statement:** The study was reviewed and approved by the Shanghai Changhai Hospital Ethical Committee.

**Informed consent statement:** All study participants, or their legal guardian, provided informed written consent prior to study enrollment.

**Conflict-of-interest statement:** Dr. Wang reports grants from The Science and Technology Commission of Shanghai Municipality during the conduct of the study. Other authors report no relevant conflicts of interest for this article.

**Data sharing statement:** No additional data are available.

**STROBE statement:** The authors have read the STROBE Statement—checklist of items, and the manuscript was

prepared and revised according to the STROBE Statement – checklist of items.

**Open-Access:** This article is an open-access article that was selected by an in-house editor and fully peer-reviewed by external reviewers. It is distributed in accordance with the Creative Commons Attribution NonCommercial (CC BY-NC 4.0) license, which permits others to distribute, remix, adapt, build upon this work non-commercially, and license their derivative works on different terms, provided the original work is properly cited and the use is non-commercial. See: <https://creativecommons.org/licenses/by-nc/4.0/>

**Country/Territory of origin:** China

**ORCID number:** Qian-Qian Meng 0000-0003-4719-1425; Ye Gao 0000-0002-6338-9602; Han Lin 0000-0002-0137-5176; Tian-Jiao Wang 0000-0002-7537-8089; Yan-Rong Zhang 0000-0002-5779-3828; Jian Feng 0000-0001-9022-462X; Zhao-Shen Li 0000-0002-1650-4014; Lei Xin 0000-0002-0495-8780; Luo-Wei Wang 0000-0002-6588-0542.

**S-Editor:** Gong ZM

**L-Editor:** A

**P-Editor:** Gong ZM

## REFERENCES

- 1 **Bray F**, Ferlay J, Soerjomataram I, Siegel RL, Torre LA, Jemal A. Global cancer statistics 2018: GLOBOCAN estimates of incidence and mortality worldwide for 36 cancers in 185 countries. *CA Cancer J Clin* 2018; **68**: 394-424 [PMID: 30207593 DOI: 10.3322/caac.21492]
- 2 **Arnold M**, Ferlay J, van Berge Henegouwen MI, Soerjomataram I. Global burden of oesophageal and gastric cancer by histology and subsite in 2018. *Gut* 2020; **69**: 1564-1571 [PMID: 32606208 DOI: 10.1136/gutjnl-2020-321600]
- 3 **Chen R**, Liu Y, Song G, Li B, Zhao D, Hua Z, Wang X, Li J, Hao C, Zhang L, Liu S, Wang J, Zhou J, Zhang Y, Li Y, Feng X, Li L, Dong Z, Wei W, Wang G. Effectiveness of one-time endoscopic screening programme in prevention of upper gastrointestinal cancer in China: a multicentre population-based cohort study. *Gut* 2021; **70**: 251-260 [PMID: 32241902 DOI: 10.1136/gutjnl-2019-320200]
- 4 **Hölscher AH**, Bollschweiler E, Schröder W, Metzger R, Gutschow C, Drebbler U. Prognostic impact of upper, middle, and lower third mucosal or submucosal infiltration in early esophageal cancer. *Ann Surg* 2011; **254**: 802-7; discussion 807 [PMID: 22042472 DOI: 10.1097/SLA.0b013e3182369128]
- 5 **Lee YC**, Wang CP, Chen CC, Chiu HM, Ko JY, Lou PJ, Yang TL, Huang HY, Wu MS, Lin JT, Hsiu-Hsi Chen T, Wang HP. Transnasal endoscopy with narrow-band imaging and Lugol staining to screen patients with head and neck cancer whose condition limits oral intubation with standard endoscope (with video). *Gastrointest Endosc* 2009; **69**: 408-417 [PMID: 19019362 DOI: 10.1016/j.gie.2008.05.033]
- 6 **Morita FH**, Bernardo WM, Ide E, Rocha RS, Aquino JC, Minata MK, Yamazaki K, Marques SB, Sakai P, de Moura EG. Narrow band imaging versus lugol chromoendoscopy to diagnose squamous cell carcinoma of the esophagus: a systematic review and meta-analysis. *BMC Cancer* 2017; **17**: 54 [PMID: 28086818 DOI: 10.1186/s12885-016-3011-9]
- 7 **Ishihara R**, Takeuchi Y, Chatani R, Kidu T, Inoue T, Hanaoka N, Yamamoto S, Higashino K, Uedo N, Iishi H, Tatsuta M, Tomita Y, Ishiguro S. Prospective evaluation of narrow-band imaging endoscopy for screening of esophageal squamous mucosal high-grade neoplasia in experienced and less experienced endoscopists. *Dis Esophagus* 2010; **23**: 480-486 [PMID: 20095991 DOI: 10.1111/j.1442-2050.2009.01039.x]
- 8 **Rodríguez de Santiago E**, Hernanz N, Marcos-Prieto HM, De-Jorge-Turrión MÁ, Barreiro-Alonso E, Rodríguez-Escaja C, Jiménez-Jurado A, Sierra-Morales M, Pérez-Valle I, Machado-Volpato N, García-Prada M, Núñez-Gómez L, Castaño-García A, García García de Paredes A, Peñas B, Vázquez-Sequeiros E, Albillos A. Rate of missed oesophageal cancer at routine endoscopy and survival outcomes: A multicentric cohort study. *United European Gastroenterol J* 2019; **7**: 189-198 [PMID: 31080603 DOI: 10.1177/2050640618811477]
- 9 **Horie Y**, Yoshio T, Aoyama K, Yoshimizu S, Horiuchi Y, Ishiyama A, Hirasawa T, Tsuchida T, Ozawa T, Ishihara S, Kumagai Y, Fujishiro M, Maetani I, Fujisaki J, Tada T. Diagnostic outcomes of esophageal cancer by artificial intelligence using convolutional neural networks. *Gastrointest Endosc* 2019; **89**: 25-32 [PMID: 30120958 DOI: 10.1016/j.gie.2018.07.037]
- 10 **Cai SL**, Li B, Tan WM, Niu XJ, Yu HH, Yao LQ, Zhou PH, Yan B, Zhong YS. Using a deep learning system in endoscopy for screening of early esophageal squamous cell carcinoma (with video). *Gastrointest Endosc* 2019; **90**: 745-753.e2 [PMID: 31302091 DOI: 10.1016/j.gie.2019.06.044]
- 11 **Luo H**, Xu G, Li C, He L, Luo L, Wang Z, Jing B, Deng Y, Jin Y, Li Y, Li B, Tan W, He C, Seeruttun SR, Wu Q, Huang J, Huang DW, Chen B, Lin SB, Chen QM, Yuan CM, Chen HX, Pu HY, Zhou F, He Y, Xu RH. Real-time artificial intelligence for detection of upper gastrointestinal cancer by endoscopy: a multicentre, case-control, diagnostic study. *Lancet Oncol* 2019; **20**: 1645-1654 [PMID: 31591062 DOI: 10.1016/S1470-2045(19)30637-0]
- 12 **Li B**, Cai SL, Tan WM, Li JC, Yalikong A, Feng XS, Yu HH, Lu PX, Feng Z, Yao LQ, Zhou PH, Yan B, Zhong YS. Comparative study on artificial intelligence systems for detecting early esophageal squamous cell carcinoma between narrow-band and white-light imaging. *World J Gastroenterol* 2021; **27**: 281-293 [PMID: 33519142 DOI: 10.3748/wjg.v27.i3.281]
- 13 **Visaggi P**, Barberio B, Gregori D, Azzolina D, Martinato M, Hassan C, Sharma P, Savarino E, de Bortoli N. Systematic review with meta-analysis: artificial intelligence in the diagnosis of oesophageal diseases. *Aliment Pharmacol Ther* 2022; **55**: 528-540 [PMID: 35098562 DOI: 10.1111/apt.16778]

- 14 **Endoscopic Classification Review Group.** Update on the paris classification of superficial neoplastic lesions in the digestive tract. *Endoscopy* 2005; **37**: 570-578 [PMID: 15933932 DOI: 10.1055/s-2005-861352]
- 15 **Zhao YY, Xue DX, Wang YL, Zhang R, Sun B, Cai YP, Feng H, Cai Y, Xu JM.** Computer-assisted diagnosis of early esophageal squamous cell carcinoma using narrow-band imaging magnifying endoscopy. *Endoscopy* 2019; **51**: 333-341 [PMID: 30469155 DOI: 10.1055/a-0756-8754]
- 16 **Guo L, Xiao X, Wu C, Zeng X, Zhang Y, Du J, Bai S, Xie J, Zhang Z, Li Y, Wang X, Cheung O, Sharma M, Liu J, Hu B.** Real-time automated diagnosis of precancerous lesions and early esophageal squamous cell carcinoma using a deep learning model (with videos). *Gastrointest Endosc* 2020; **91**: 41-51 [PMID: 31445040 DOI: 10.1016/j.gie.2019.08.018]
- 17 **Yang XX, Li Z, Shao XJ, Ji R, Qu JY, Zheng MQ, Sun YN, Zhou RC, You H, Li LX, Feng J, Yang XY, Li YQ, Zuo XL.** Real-time artificial intelligence for endoscopic diagnosis of early esophageal squamous cell cancer (with video). *Dig Endosc* 2021; **33**: 1075-1084 [PMID: 33275789 DOI: 10.1111/den.13908]

## Observational Study

## Insights into hepatitis E virus epidemiology in Croatia

Pavle Jelacic, Thomas Ferenc, Anna Mrzljak, Lorena Jemersic, Natasa Janev-Holcer, Milan Milosevic, Maja Bogdanic, Ljubo Barbic, Branko Kolaric, Vladimir Stevanovic, Mateja Vujica, Zeljka Jurekovic, Jadranka Pavicic Saric, Maja Vilibic, Tatjana Vilibic-Cavlek

**Specialty type:** Gastroenterology and hepatology

**Provenance and peer review:**

Invited article; Externally peer reviewed.

**Peer-review model:** Single blind

**Peer-review report's scientific quality classification**

Grade A (Excellent): 0  
Grade B (Very good): 0  
Grade C (Good): C, C  
Grade D (Fair): 0  
Grade E (Poor): 0

**P-Reviewer:** Jackson K, Australia; Zhou C, China

**Received:** July 16, 2022

**Peer-review started:** July 16, 2022

**First decision:** August 6, 2022

**Revised:** August 15, 2022

**Accepted:** September 16, 2022

**Article in press:** September 16, 2022

**Published online:** October 7, 2022



**Pavle Jelacic, Natasa Janev-Holcer**, Department of Environmental Health, Croatian Institute of Public Health, Zagreb 10000, Croatia

**Thomas Ferenc**, Department of Radiology, Merkur University Hospital, Zagreb 10000, Croatia

**Anna Mrzljak**, Department of Gastroenterology and Hepatology, University Hospital Center Zagreb, Zagreb 10000, Croatia

**Anna Mrzljak, Tatjana Vilibic-Cavlek**, School of Medicine, University of Zagreb, Zagreb 10000, Croatia

**Lorena Jemersic**, Department of Virology, Croatian Veterinary Institute, Zagreb 10000, Croatia

**Natasa Janev-Holcer**, Department of Social Medicine and Epidemiology, Faculty of Medicine University of Rijeka, Rijeka 51000, Croatia

**Milan Milosevic**, Department of Occupational and Environmental Health, Andrija Stampar School of Public Health, Zagreb 10000, Croatia

**Maja Bogdanic, Tatjana Vilibic-Cavlek**, Department of Virology, Croatian Institute of Public Health, Zagreb 10000, Croatia

**Ljubo Barbic, Vladimir Stevanovic**, Department of Microbiology and Infectious Diseases with Clinic, Faculty of Veterinary Medicine University of Zagreb, Zagreb 10000, Croatia

**Branko Kolaric**, Department of Gerontology and Social Medicine, Andrija Stampar Teaching Institute of Public Health, Zagreb 10000, Croatia

**Mateja Vujica**, Institute of Emergency Medicine of Krapina-Zagorje County, Krapina 49000, Croatia

**Zeljka Jurekovic**, Department of Nephrology, Merkur University Hospital, Zagreb 10000, Croatia

**Jadranka Pavicic Saric**, Department of Anesthesiology, University Hospital Merkur, Zagreb 10000, Croatia

**Maja Vilibic**, Department for Social Psychiatry, Psychotherapy and Psychodiagnostics, University Clinical Hospital Center "Sestre Milosrdnice", Zagreb 10000, Croatia

**Corresponding author:** Anna Mrzljak, FEBG, PhD, Adjunct Professor, Associate Professor, Department of Gastroenterology and Hepatology, University Hospital Center Zagreb, Kispaticeva 12, Zagreb 10000, Croatia. [anna.mrzljak@gmail.com](mailto:anna.mrzljak@gmail.com)

## Abstract

### BACKGROUND

Hepatitis E virus (HEV) is an emerging virus of global health concern. The seroprevalence rates differ greatly according to geographic region and population group.

### AIM

To analyze the seroprevalence of HEV in exposed (animal-related professions) and nonexposed populations, as well as solid organ and hematopoietic stem cell transplant patients.

### METHODS

Forestry workers ( $n = 93$ ), hunters ( $n = 74$ ), and veterinarians ( $n = 151$ ) represented the exposed population. The general population ( $n = 126$ ) and pregnant women ( $n = 118$ ) constituted the control group. Transplant patients included liver transplant recipients (LTRs) ( $n = 83$ ), kidney transplant recipients (KTRs) ( $n = 43$ ), and hematopoietic stem cell transplant recipients (HSCRs) ( $n = 39$ ). HEV immunoglobulin G antibodies were detected using the enzyme-linked immunosorbent assay and confirmed by the immunoblot test.

### RESULTS

The HEV seroprevalence significantly differed between groups: Veterinarians 15.2%, hunters 14.9%, forestry workers 6.5%, general population 7.1%, and pregnant women 1.7%. In transplant patients, the seropositivity was highest in LTRs (19.3%), while in KTRs and HSCRs, the seroprevalence was similar to the general population (6.9% and 5.1%, respectively). A significant increase in seropositivity with age was observed from 2.9% in individuals less than 30 years to 23.5% in those older than 60 years. Sociodemographic characteristics (sex, educational level, area of residence, and number of household members), eating habits (game meat, offal, and pork products consumption), and environmental and housing conditions (drinking water supply, type of water drainage/sewer, waste disposal, domestic animals) were not associated with HEV seropositivity. However, individuals who reported a pet ownership were more often seropositive compared to those who did not have pet animals (12.5% *vs* 7.0%).

### CONCLUSION

The results of this study showed that individuals in professional contact with animals and LTRs are at higher risk for HEV infection. In addition, age is a significant risk factor for HEV seropositivity.

**Key Words:** Hepatitis E virus; Seroprevalence; Veterinarians; Hunters; Forestry workers; Transplant patients; Croatia

©The Author(s) 2022. Published by Baishideng Publishing Group Inc. All rights reserved.

**Core Tip:** Hepatitis E virus (HEV) is an emerging viral pathogen of public health concern. We analyzed the epidemiological characteristics of HEV infection in different groups in Croatia. The highest seroprevalence was reported in professionally exposed individuals such as veterinarians, hunters, and liver transplant recipients. Seropositivity was similar in the general population, forestry workers, kidney transplant patients, and hematopoietic stem cell transplant patients. The lowest seroprevalence was recorded in pregnant women. A significant increase in seroprevalence with age was observed. Pet ownership was also associated with HEV seropositivity. Sex, environmental and housing conditions, and eating habits were not associated with HEV seroprevalence.

**Citation:** Jelicic P, Ferenc T, Mrzljak A, Jemersic L, Janev-Holcer N, Milosevic M, Bogdanic M, Barbic L, Kolaric B, Stevanovic V, Vujica M, Jurekovic Z, Pavicic Saric J, Vilibic M, Vilibic-Cavlek T. Insights into hepatitis E virus epidemiology in Croatia. *World J Gastroenterol* 2022; 28(37): 5494-5505

**URL:** <https://www.wjgnet.com/1007-9327/full/v28/i37/5494.htm>

**DOI:** <https://dx.doi.org/10.3748/wjg.v28.i37.5494>

## INTRODUCTION

Hepatitis E virus (HEV) is an emerging viral pathogen of global health concern. It is a nonenveloped RNA virus, a member of the *Hepeviridae* family, genus *Orthohepevirus*[1]. Along with hepatitis B and hepatitis C virus (1.5 million new infections per year for each virus)[2,3], HEV is a major cause of viral hepatitis worldwide with approximately 20 million documented infections annually, over three million symptomatic cases, and 60-70000 fatal outcomes[4]. East and South Asia account for more than 60% of all reported cases[5]. There are eight known HEV genotypes. HEV-1 and HEV-2 are confined to humans and mainly cause infections in developing countries of tropical and subtropical regions[4-6]. HEV-3 and HEV-4 have been isolated from humans and different animal species (pigs, wild boars, deer, rabbits, goats, cows), primarily causing sporadic, autochthonous human infections in the developed world[5,7]. HEV-5 and HEV-6 have been restricted to wild boars only, while genotypes 7 and 8 have been isolated in dromedary and Bactrian camels[7,8]. In low-income countries, the main mode of HEV transmission is the fecal-oral route (contaminated drinking water, poor hygiene), whereas in more industrialized countries people are getting infected through zoonotic transmission (uncooked or undercooked animal products, mainly infected meat, and milk)[6,7]. Pigs are the main HEV animal reservoir. Almost 13% of domestic pigs and 9.5% of wild boars are actively infected by HEV with 10% of commercial pork products being HEV-RNA-positive[9]. Several other foods have also been proposed as a potential source of HEV infection in humans, *e.g.*, shellfish, mussels, and oysters[6]. One study found that HEV maintains infectivity for up to 21 d at 37 °C and up to 28 d at usual room temperature[8]. The virus can also be transmitted through blood transfusion, intravenous drug use, solid organ transplantation (SOT), hemodialysis, or maternal-fetal interaction[5,7]. In most cases, HEV presents as a self-limiting acute illness with low mortality rates (1%-2%) in immunocompetent individuals. However, genotypes 3, 4, and 7 may induce chronic infection and subsequent cirrhosis in immunocompromised patients, especially in SOT recipients, and human immunodeficiency virus-positive individuals[4]. Pregnant women are more susceptible to rapid disease progression such as fulminant hepatic and extrahepatic manifestations and obstetric complications leading to high mortality rates (15%-25%) compared to the non-pregnant population[4,5]. Professionally exposed individuals (*e.g.*, forestry workers, veterinarians, hunters, farmers) are also at increased risk of getting infected by HEV. Detected HEV seroprevalence rates in professionally exposed workers differ greatly between countries: Forestry workers (2.2%-31.0%) [10-13], hunters (3.81%-22.2%)[13-15], and veterinarians (10.2%-43.7%)[16,17]. In the transplant population, HEV seroprevalence rates were reportedly between 6.0% and 29.6%[18].

The seroepidemiological studies have shown that HEV is widespread in Croatia with seroprevalence rates ranging from 2.7% in healthcare professionals to 24.4% in liver transplant patients and up to 43.5% in hemodialysis patients[19,20]. However, only preliminary data are available on the HEV seroprevalence in animal-related professions. The aim of this study was to analyze the HEV epidemiology in different professionally exposed (animal-related) and nonexposed population groups in Croatia.

## MATERIALS AND METHODS

### Study participants

From October 2016 to September 2017, serum samples collected from Croatian residents were tested for the presence of HEV immunoglobulin G (IgG) antibodies. Samples were obtained from different exposed and nonexposed population groups. Forestry workers, hunters, and veterinarians represented the exposed population. The general population and pregnant women constituted the control group. In addition, from January 2021 to December 2021, a total of 165 serum samples were collected from SOT recipients [liver transplant recipients (LTRs) and kidney transplant recipients (KTRs)] and hematopoietic stem cell transplant recipients (HSCRs). None of the participants showed symptoms of acute hepatitis or reported a recent febrile disease. The distribution of study participants according to the population group is presented in [Table 1](#).

### Methods

HEV IgG antibodies were detected using a commercial enzyme-linked immunosorbent assay (ELISA) based on recombinant antigens of HEV genotypes 1 and 3 (anti-hepatitis E virus IgG ELISA; Euroimmun, Lübeck, Germany). Reactive samples were tested for the presence of HEV IgM antibodies (anti-hepatitis E virus IgM ELISA; Euroimmun). Additionally, ELISA IgG-positive samples were confirmed by a commercial immunoblot (IB) assay using highly purified recombinant HEV antigens: O2N genotype 1/3, O2C genotype 1/3, O2M genotype 1, O3 genotype 1/3 (HEV Recomline; Mikrogen, Neuried, Germany). IB-positive samples were further retested using a second assay (Euroline anti-hepatitis E virus IgG, Euroimmun, Lübeck, Germany) based on the recombinant HEV genotypes 1-4 antigens (ORF2). For the IB, the manufacturer states a diagnostic sensitivity of 96.6% and specificity of 97.1% (Mikrogen) and 100% (Euroimmun).

**Table 1 Exposed and nonexposed population groups included in the study**

Population	<i>n</i>	Median age, yr	IQR, yr
<b>Exposed group</b>			
Hunters	74	55	41-60
Veterinarians	151	46	36-55.5
Forestry workers	93	43	31-51
<b>Non-exposed group</b>			
General population	126	48	33-62
Pregnant women	118	31.5	29-35
<b>Transplant patients</b>			
Liver transplant recipients	83	60	49-65.5
Kidney transplant recipients	43	52.5	42-62
Hematopoietic stem cell recipients	39	55	51-64

IQR: Interquartile range.

**Table 2 Hepatitis E virus immunoglobulin G prevalence in exposed and nonexposed populations**

Population group	Tested, <i>n</i> (%)	HEV IgG, <i>n</i> (%)	95%CI	<i>P</i> value
Hunters	74	11 (14.9)	8.2-14.2	0.003
Veterinarians	151	23 (15.2)	10.2-21.6	
Forestry workers	93	6 (6.5)	2.7-12.8	
General population	126	9 (7.1)	3.3-13.1	
Pregnant women	118	2 (1.7)	0.2-5.9	
Liver transplant recipients	83	16 (19.3)	11.4-29.4	
Kidney transplant recipients	43	3 (6.9)	1.5-19.1	
Hematopoietic stem cell recipients	39	2 (5.1)	0.6-7.3	

CI: Confidence interval; HEV: Hepatitis E virus; IgG: Immunoglobulin G.

To identify potential risk factors that may be associated with HEV infection, for animal-related professions (exposed group) and nonexposed group, data on demographic characteristics and potential risk factors (eating habits, environmental and housing conditions, traveling history, and blood transfusion) were collected using a questionnaire. The modified Health-Environment-Life Style questionnaire created by the Andrija Stampar School of Public Health, School of Medicine, University of Zagreb was used in the study.

### Statistical analysis

The HEV IgG prevalence is presented as a percentage with 95% confidence intervals (CIs). Differences in categorical variables between HEV seropositive and seronegative participants were tested using the Fisher's exact or Fisher-Freeman-Halton test. Odds ratio (OR) and relative risk (RR) were also calculated. Variables with statistical significance in a bivariate analysis were analyzed in multivariate regression analysis (binary logistic regression).  $P < 0.05$  was considered statistically significant. Statistical analysis was performed using MedCalc® Statistical Software version 20.022 (MedCalc Software Ltd., Ostend, Belgium; <https://www.medcalc.org>; 2021).

## RESULTS

HEV IgG antibodies were detected in 72/727 (9.9%; 95%CI: 7.8-12.3) participants: 40/278 (12.6%; 95%CI: 9.3-16.6) in the exposed group, 11/244 (4.3%; 95%CI: 2.3-7.3) in the nonexposed group, and 12/165

**Table 3** Hepatitis E virus immunoglobulin G prevalence according to sociodemographic characteristics

Characteristic	Subjects <sup>1</sup> , n	HEV IgG, n (%)	95%CI	P value
Sex				0.065
Male	238	29 (10.9)	7.6-15.0	
Female	282	22 (7.2)	4.7-10.6	
Age group in yr				< 0.001
< 30	99	3 (2.9)	0.8-7.6	
30-39	147	11 (7.0)	3.8-11.7	
40-49	94	5 (5.1)	2.0-10.7	
50-59	90	11 (10.9)	5.9-18.1	
60 +	62	19 (23.5)	15.3-33.5	
Area of residence				0.144
Rural	151	16 (9.6)	5.8-14.7	
Suburban	54	11 (16.9)	9.3-27.4	
Urban	255	24 (8.6)	5.7-12.3	
Number of household members				0.301
≤ 3	258	22 (7.9)	5.1-11.4	
> 3	177	21 (10.6)	6.9-15.5	
Educational level				0.467
Primary school	58	5 (7.9)	3.1-16.5	
High school	254	25 (9.0)	6.0-12.7	

<sup>1</sup>Subjects who filled a questionnaire.

CI: Confidence interval; HEV: Hepatitis E virus; IgG: Immunoglobulin G.

(12.7%; 95% CI: 8.1-18.8) in transplant patients. None of the participants were HEV IgM-positive. There were significant differences in the IgG seroprevalence rates among population groups (Table 2). In animal-related professions, the seropositivity was higher (14.9% in hunters and 15.2% in veterinarians) than in pregnant women (1.7%) and the general population (7.1%). Seroprevalence in transplant populations was highest in LTR (19.3%), followed by KTR (6.9%) and HSCR (5.1%).

A significant increase in seroprevalence was observed according to age. Participants in the age group 60 + years and 50-59 years showed higher seropositivity rates (23.5% and 10.9%, respectively) compared to younger age groups (2.9%-7.0%). There was no difference in HEV seroprevalence according to sex, area of residence, number of household members, and educational level (Table 3). HEV seropositivity did not differ regarding to the frequency of game meat, offal, and pork products consumption. However, there was a difference in the seroprevalence rates according to the frequency of shellfish consumption (Table 4).

Analyzing the environmental and housing conditions of the study participants and HEV seropositivity (Table 5), no significant difference was found according to drinking water supply, type of water drainage/sewer, and waste disposal. However, participants who reported having pet animals had a higher seroprevalence rate compared to those who did not have pet animals (12.5% vs 7.0%). Travel history as well as previous blood transfusion, surgical procedure, and tattoo/piercing were not associated with HEV seroprevalence (Table 6).

Risk analysis showed that animal-related professions and liver transplant patients were more likely to be HEV seropositive than other tested groups: Hunters OR = 3.873, 95% CI: 1.605-9.341; RR = 3.445, 95% CI: 1.556-7.628; veterinarians OR = 3.985, 95% CI: 1.883-8.435; RR = 3.531, 95% CI: 1.771-7.038; LTRs OR = 5.058, 95% CI: 2.240-11.420; RR = 4.276, 95% CI: 2.068-8.839 (Table 7).

## DISCUSSION

The zoonotic risk of HEV transmission is well established, while exact transmission routes remain to be determined. The HEV seroprevalence rates vary greatly according to geographical region and study

Table 4 Hepatitis E virus immunoglobulin G prevalence according to eating habits

Eating habits	Subjects <sup>1</sup> , n	HEV IgG, n (%)	95%CI	P value
Shellfish consumption				0.004
Never	60	15 (25.0)	14.4-37.0	
Rarely	374	32 (8.6)	6.0-11.7	
Once a month	16	2 (12.5)	2.7-34.4	
Every week	2	0 (0)	0-84.1 <sup>2</sup>	
Game meat consumption				0.104
Never	20	1 (5.0)	0.5-21.1	
Rarely	324	30 (9.3)	6.5-12.8	
Once a month	89	14 (15.7)	9.3-24.3	
Every week	19	4 (21.1)	7.6-42.6	
Offal consumption (liver)				0.070
Never	25	0 (0)	0-13.7 <sup>2</sup>	
Rarely	296	29 (9.8)	6.8-13.6	
Once a month	120	18 (15.0)	9.5-22.2	
Every week	11	2 (18.2)	4-46.7	
Pork products consumption				0.216
No	204	18 (8.8)	5.5-13.3	
Yes	249	31 (12.4)	8.8-17.0	

<sup>1</sup>Subjects who filled a questionnaire.

<sup>2</sup>One-sided 97.5% confidence interval.

CI: Confidence interval; HEV: Hepatitis E virus; IgG: Immunoglobulin G.

cohorts. The proposed transmission routes linked to professional exposures include frequent contact with the zoonotic HEV reservoirs, such as pigs and other wildlife species (mainly wild boar)[12]. Forestry workers, hunters, and veterinarians represented risk populations in this study. The HEV seroprevalence was significantly higher in the exposed population (12.6%) compared to the nonexposed population (4.3%). In the exposed group, seroprevalence was similar in the veterinarians (15.2%) and hunters (14.9%), while it was lower in the forestry workers (6.5%).

HEV seropositivity in forestry workers included in this study was similar to the seroprevalence in the Croatian general population (7.1%). Seroepidemiological studies conducted among forestry workers in Europe showed seropositivity of 31% in France (2002-2003)[11] and 18% in Germany (Brandenburg, 2008)[21]. In more recent studies, HEV antibodies were detected in 2.2% of forest rangers from western Poland (Poznan, 2014)[10], 5% of forestry workers from eastern Poland (Lubelskie Voivodship, 2014-2015)[13], and 14% of forestry workers in Italy (Trentino-Alto Adige Region, 2014-2015)[12]. Although forestry workers have been identified as being at risk of HEV infection in several studies, the French study revealed for the first time that woodcutters are at a particularly high risk of infection. Among woodcutters, 37.2% were found to be seropositive compared to game and fishing keepers/rangers and silviculturists (20.0% and 24.8% seropositive, respectively)[11]. Close contact with wild boar stools in the forest environment could be an additional source of HEV infection in this risk population.

HEV seropositivity in the Croatian hunters included (14.9%) was two times higher than that in the general population. Two studies conducted among Polish hunters from 2010 to 2012 showed a HEV seropositivity of 25% [22] and 22.2%, respectively [14]. A similar seroprevalence rate (25%) was detected in Italian hunters from the Latium Region tested during the hunting season [23] and German hunters (21%) from Central Germany tested in 2013 [15]. By contrast, only 4.2% of hunters from nine Estonian counties were seropositive to HEV in 2013 [24] as well as 3.81% of Polish hunters from the Lubelskie Voivodship (eastern Poland) tested from 2014 to 2015 [13].

In 2009, serum samples were collected from participants of the National Veterinary Congress in Helsinki. Finnish veterinarians commonly have HEV antibodies with a seroprevalence of 10.2%. The highest seroprevalence rate of 17.8% was unexpectedly detected in small animal practitioners [17]. A study from Norway in 2013 found IgG seroprevalence of 14%. When stratifying by work experience, HEV seroprevalence in Norwegian veterinarians working with swine was more than two times higher

**Table 5** Hepatitis E virus immunoglobulin G prevalence according to environmental and housing conditions

Characteristics	Subjects <sup>1</sup> , n (%)	HEV IgG, n (%)	95%CI	P value
Drinking water supply				0.694
Public water supply	431	43 (10.0)	7.4-13.1	
Private water well	70	7 (10.0)	4.6-18.6	
Bottled water	4	0 (0)	0-60.2 <sup>2</sup>	
Others	4	1 (25.0)	2.8-71.6	
Type of water drainage/sewer				0.781
Public sewer	320	33 (10.3)	7.3-14	
Septic tank	185	18 (9.7)	6.1-14.6	
Others	4	0 (0)	0-60.2 <sup>2</sup>	
Waste disposal				1.000
Public	501	51 (10.2)	7.8-13.1	
Burning	5	0 (0)	0-52.2 <sup>2</sup>	
Slurry	2	0 (0)	0-84.1 <sup>2</sup>	
Having pet animals				0.039
Yes	265	33 (12.5)	8.9-16.8	
No	243	17 (7.0)	4.3-10.7	
Having domestic animals				0.629
Yes	140	16 (11.4)	7.0-17.5	
No	348	35 (10.1)	7.2-13.5	
Rodent control in the basement				0.670
Yes	264	28 (10.6)	7.3-14.7	
No	243	23 (9.5)	6.3-13.6	
Storing food in the basement				0.346
Yes	122	15 (12.3)	7.4-19.0	
No	385	36 (9.4)	6.7-12.6	

<sup>1</sup>Subjects who filled a questionnaire.

<sup>2</sup>One-sided 97.5% confidence interval.

CI: Confidence interval; HEV: Hepatitis E virus; IgG: Immunoglobulin G.

compared to those who did not work with swine (22% *vs* 9%)[25]. Chinese studies conducted from 2003 to 2017 demonstrated high IgG seropositivity in veterinarians ranging from 26.7% [16] to 43.7% [26]. In addition, a high seroprevalence rate of 23% was notified in swine veterinarians in the United States [27].

By contrast, a Thai study found no association between HEV seroprevalence and frequent direct occupational pig contact [28]. A very low HEV seropositivity (2.6%) was found in Estonian veterinarians. All antibody-positive veterinarians worked in small animal clinics and some of them were cat or dog owners [29]. The majority of veterinarians included in this study are small animal practitioners and showed seropositivity to HEV of 15.2%. In some countries, significant regional differences in the HEV seroprevalence were observed. In Polish hunters, seroprevalence varied from 10% to 42.4% [14].

A recent meta-analysis of 14626 transplant recipients showed that anti-HEV seroprevalence ranges from 6%-29.6% [18]. This wide HEV seroprevalence range reflects the differences in viral circulation within different geographical regions and the impact of assays used in the particular study. In our transplant cohort, LTRs showed the highest seroprevalence rate of 19.3%, and in the risk analysis for HEV IgG seropositivity exhibited the highest OR of 5.058 among tested groups. This supports the hypothesis that HEV in combination with other factors may promote chronic inflammation and even be a cofactor in hepatocellular carcinoma occurrence leading to liver transplant candidacy [30]. Chronicity of HEV infection is of emerging relevance in transplant recipients; however, there are still conflicting viewpoints on the overall anti-HEV seroprevalence and rate of chronic HEV infection in immunocompromised patients [31].

**Table 6** Hepatitis E virus immunoglobulin G prevalence according to other potential risk factors

Characteristics	Subjects <sup>1</sup> , n	HEV IgG, n (%)	95%CI	P value
Traveling abroad				0.621
Yes	119	11 (9.2)	5-15.4	
No	369	40 (10.8)	8-14.3	
Blood transfusion				0.120
Yes	44	8 (18.2)	9-31.4	
No	410	41 (10)	7.4-13.2	
Surgical procedure				0.570
Yes	230	23 (10)	6.6-14.4	
No	223	26 (11.7)	7.9-16.4	
Tattoo and piercing				0.540
Yes	72	6 (8.3)	3.6-16.4	
No	378	43 (11.4)	8.5-14.9	

<sup>1</sup>Subjects who filled a questionnaire.

CI: Confidence interval; HEV: Hepatitis E virus; IgG: Immunoglobulin G.

**Table 7** Risk analysis for hepatitis E virus immunoglobulin G seropositivity

Population group	OR	95%CI	P value	RR	95%CI	P value
General population	Ref			Ref		
Hunters	3.873	1.605-9.341	0.002	3.445	1.556-7.628	0.002
Veterinarians	3.985	1.883-8.435	< 0.001	3.531	1.771-7.038	< 0.001
Forestry workers	1.529	0.549-4.261	0.416	1.495	0.569-3.929	0.414
Liver transplant recipients	5.058	2.240-11.420	< 0.001	4.276	2.068-8.839	< 0.001
Kidney transplant recipients	1.588	0.424-5.946	0.491	1.547	0.450-5.320	0.488
Hematopoietic stem cell recipients	1.145	0.244-5.373	0.863	1.137	0.262-4.938	0.863

CI: Confidence interval; OR: Odds ratio; RR: Relative risk.

Several studies have found sex variations in HEV seropositivity, with males having higher seropositivity compared to women[14,32]. This study found no significant difference in the seropositivity between men (10.9%) and women (7.2%). Similarly, a German study found no sex differences in the HEV seropositivity[15]. An increase in HEV seroprevalence with age, which is likely to reflect cumulative exposure to HEV over time was observed in many studies[11,12,14,27]. In this study, the highest seropositivity (23.5%) was observed in the age group 60 + years compared to 2.9%-10.9% in other age groups. By contrast, one German study conducted in forestry workers did not find a statistically significant association between seropositivity and age[21]. Similarly, no association of HEV seroprevalence with age was observed in Norwegian veterinarians[25].

Working with a septic tank was identified as a strong risk factor for HEV infection in the Netherlands [33]. Additionally, using a stream or well as a source of water has been identified as a risk factor for HEV infection in some countries[34]. Similar to a previous Croatian study[35], in this study, we found no difference in the HEV seroprevalence regarding the type of drainage/sewer, type of water supply, and waste disposal.

Eating habits were associated with HEV seropositivity in some studies. Eating internal pig organs more than twice a week was linked to a higher seroprevalence of anti-HEV IgG in a rural community in Thailand[28]. In France, the presence of anti-HEV IgG was associated with the consumption of pork meat, pork liver sausages, game meat, offal, and oysters[36]. The association between HEV seroprevalence and consumption of stewed offal was also confirmed among Polish hunters[12]. In Italy, many seropositive individuals reported consumption of raw or undercooked food, particularly shellfish (mussels) and unbottled drinking water[37]. This study found no association between offal consumption

and HEV seropositivity. Although participants who reported eating pork liver every week showed a higher seroprevalence rate (18.2%) compared to those who did not eat or ate pork liver rarely (0%-15.0%), this difference was not significant. In addition, there was no difference in the seropositivity regarding pork meat and game meat consumption. Similar to our results, a German study showed that wild boar meat consumption was not associated with HEV seroprevalence. However, HEV RNA was detected in muscle specimens from wild boar, suggesting this is a possible HEV transmission route[15]. Surprisingly, there was a significant difference in the seroprevalence regarding shellfish consumption in our study, with the highest seroprevalence in participants who reported to never eat shellfish. However, due to a very small number in the tested subgroups regarding the frequency of shellfish consumption, this limitation should be considered when interpreting the results.

In this study, a pet ownership was associated with HEV seroprevalence with a seropositivity rate of 12.5% in individuals who reported having a cat/dog compared to 7.0% in those who did not have pet animals. Animal ownership, including both domestic and pet animals, was not found to be a risk factor for HEV infection in a Jordanian study[38]. The use of a self-reported questionnaire in the study is a limitation that should be addressed. In addition, data on the risk factors in the transplant patients were not available.

---

## CONCLUSION

---

The results of this study showed that individuals in professional contact with animals are at higher risk for HEV infection. Identification of people at risk for HEV infection is essential to implement preventive measures and educate these groups about modes of HEV transmission and prevention. Since immunocompromised populations such as SOT are at risk of chronic hepatitis E, such individuals should be counseled regarding the risk of HEV before and after transplantation.

## ARTICLE HIGHLIGHTS

### **Research background**

Hepatitis E virus (HEV) seroprevalence rates differ greatly according to the geographic region and population group.

### **Research motivation**

Only preliminary data are available on the HEV seroprevalence in some population groups in Croatia.

### **Research objectives**

To determine the HEV seroprevalence in different populations (animal-related professions, transplant patients, general population).

### **Research methods**

HEV immunoglobulin G antibodies were detected using an enzyme-linked immunosorbent assay. Initially, reactive samples were confirmed by immunoblot test.

### **Research results**

Significant differences in HEV seropositivity were observed among the population groups: Veterinarians 15.2%, hunters 14.9%, forestry workers 6.5%, general population 7.1%, pregnant women 1.7%, liver transplant recipients 19.3%, kidney transplant recipients 6.9%, and hematopoietic stem cell recipients 5.1%. Older age was a significant risk factor for HEV seropositivity. In addition, pet ownership was associated with HEV seroprevalence. Sociodemographic characteristics, eating habits, and environmental and housing conditions were not associated with the HEV seropositivity.

### **Research conclusions**

Professional contact with animals and older age are significant risk factors for HEV infection.

### **Research perspectives**

Further studies on a large sample of exposed and nonexposed population are needed to determine the HEV RNA prevalence/seroprevalence and clinical significance of HEV infection in the Croatian population.

## FOOTNOTES

**Author contributions:** Jelicic P and Vilibic-Cavlek T conceived the study and wrote the original draft; Ferenc T, Mrzljak A, and Vilibic-Cavlek T wrote the original draft; Janev-Holcer N, Bogdanic M, Mrzljak A, Barbic L, Stevanovic V, Vujica M, Jurekovic Z, Pavicic Saric J, and Vilibic M were involved in the data collection and analysis; Milosevic M and Kolaric B performed the statistical analyses; Jemersic L and Vilibic-Cavlek T revised the manuscript critically; and all authors approved the final version of the manuscript.

**Supported by** the Croatian Science Foundation (Emerging and Neglected Hepatotropic Viruses after Solid Organ and Hematopoietic Stem Cell Transplantation to Mrzljak A), No. IP-2020-02-7407.

**Institutional review board statement:** The study was approved by the Ethic Committee of the Croatian Institute of Public Health (protocol code 80327/1-16, approved on 12 February 2016) and School of Medicine University of Zagreb (protocol code 641-01/20-02/01, approved on 22 October 2020).

**Informed consent statement:** Written informed consent was obtained from all participants included in the study.

**Conflict-of-interest statement:** All the authors report no relevant conflicts of interest for this article.

**Data sharing statement:** Data sharing available upon request.

**STROBE statement:** The authors have read the STROBE Statement-checklist of items, and the manuscript was prepared and revised according to the STROBE Statement-checklist of items.

**Open-Access:** This article is an open-access article that was selected by an in-house editor and fully peer-reviewed by external reviewers. It is distributed in accordance with the Creative Commons Attribution NonCommercial (CC BY-NC 4.0) license, which permits others to distribute, remix, adapt, build upon this work non-commercially, and license their derivative works on different terms, provided the original work is properly cited and the use is non-commercial. See: <https://creativecommons.org/licenses/by-nc/4.0/>

**Country/Territory of origin:** Croatia

**ORCID number:** Pavle Jelicic 0000-0003-3200-1596; Thomas Ferenc 0000-0002-4917-9270; Anna Mrzljak 0000-0001-6270-2305; Lorena Jemersic 0000-0002-8379-4787; Natasa Janev-Holcer 0000-0002-2584-6681; Milan Milosevic 0000-0001-9008-7645; Maja Bogdanic 0000-0002-8236-3205; Ljubo Barbic 0000-0002-5170-947X; Branko Kolaric 0000-0002-0884-4043; Vladimir Stevanovic 0000-0002-9572-8760; Mateja Vujica 0000-0001-7766-5113; Zeljka Jurekovic 0000-0003-0690-2577; Jadranka Pavicic Saric 0000-0003-4124-8056; Maja Vilibic 0000-0002-5357-5890; Tatjana Vilibic-Cavlek 0000-0002-1877-5547.

**S-Editor:** Wang JJ

**L-Editor:** Filipodia

**P-Editor:** Wang JJ

## REFERENCES

- 1 **Webb GW**, Dalton HR. Hepatitis E: an underestimated emerging threat. *Ther Adv Infect Dis* 2019; **6**: 2049936119837162 [PMID: 30984394 DOI: 10.1177/2049936119837162]
- 2 **World Health Organization.** Hepatitis B. [cited 10 June 2022]. Available from: <https://www.who.int/news-room/fact-sheets/detail/hepatitis-b>
- 3 **World Health Organization.** Hepatitis C. [cited 10 June 2022]. Available from: <https://www.who.int/news-room/fact-sheets/detail/hepatitis-c>
- 4 **Nimgaonkar I**, Ding Q, Schwartz RE, Ploss A. Hepatitis E virus: advances and challenges. *Nat Rev Gastroenterol Hepatol* 2018; **15**: 96-110 [PMID: 29162935 DOI: 10.1038/nrgastro.2017.150]
- 5 **Raji YE**, Toung OP, Taib NM, Sekawi ZB. Hepatitis E Virus: An emerging enigmatic and underestimated pathogen. *Saudi J Biol Sci* 2022; **29**: 499-512 [PMID: 35002446 DOI: 10.1016/j.sjbs.2021.09.003]
- 6 **Doceul V**, Bagdassarian E, Demange A, Pavo N. Zoonotic Hepatitis E Virus: Classification, Animal Reservoirs and Transmission Routes. *Viruses* 2016; **8** [PMID: 27706110 DOI: 10.3390/v8100270]
- 7 **Primadharsini PP**, Nagashima S, Okamoto H. Mechanism of Cross-Species Transmission, Adaptive Evolution and Pathogenesis of Hepatitis E Virus. *Viruses* 2021; **13** [PMID: 34069006 DOI: 10.3390/v13050909]
- 8 **Ferri G**, Vergara A. Hepatitis E Virus in the Food of Animal Origin: A Review. *Foodborne Pathog Dis* 2021; **18**: 368-377 [PMID: 33784472 DOI: 10.1089/fpd.2020.2896]
- 9 **Li P**, Ji Y, Li Y, Ma Z, Pan Q. Estimating the global prevalence of hepatitis E virus in swine and pork products. *One Health* 2022; **14**: 100362 [PMID: 34977322 DOI: 10.1016/j.onehlt.2021.100362]
- 10 **Bura M**, Bukowska A, Michalak M, Bura A, Nawrocki MJ, Karczewski M, Mozer-Lisewska I. Exposure to hepatitis E virus, hepatitis A virus and *Borrelia* spp. infections in forest rangers from a single forest district in western Poland. *Adv Clin Exp Med* 2018; **27**: 351-355 [PMID: 29533542 DOI: 10.17219/acem/65787]

- 11 **Carpentier A**, Chaussade H, Rigaud E, Rodriguez J, Berthault C, Boué F, Tognon M, Touzé A, Garcia-Bonnet N, Choutet P, Coursaget P. High hepatitis E virus seroprevalence in forestry workers and in wild boars in France. *J Clin Microbiol* 2012; **50**: 2888-2893 [PMID: 22718947 DOI: 10.1128/JCM.00989-12]
- 12 **Monini M**, Ostanello F, Dominicis A, Tagliapietra V, Vaccari G, Rizzoli A, Trombetta CM, Montomoli E, Di Bartolo I. Seroprevalence of Hepatitis E Virus in Forestry Workers from Trentino-Alto Adige Region (Northern Italy). *Pathogens* 2020; **9** [PMID: 32674277 DOI: 10.3390/pathogens9070568]
- 13 **Weiner M**, Tokarska-Rodak M, Plewik D, Pańczuk A, Szepeluk A, Krajewska M. The Serological Surveillance of Hepatitis E virus among Hunters and Foresters in Eastern Poland. *Pol J Microbiol* 2017; **66**: 277-279 [PMID: 28735306 DOI: 10.5604/01.3001.0010.7882]
- 14 **Baumann-Popczyk A**, Popczyk B, Gołąb E, Rożej-Bielicka W, Sadkowska-Todys M. A cross-sectional study among Polish hunters: seroprevalence of hepatitis E and the analysis of factors contributing to HEV infections. *Med Microbiol Immunol* 2017; **206**: 367-378 [PMID: 28776194 DOI: 10.1007/s00430-017-0515-0]
- 15 **Schielke A**, Ibrahim V, Czogiel I, Faber M, Schrader C, Dremsek P, Ulrich RG, John R. Hepatitis E virus antibody prevalence in hunters from a district in Central Germany, 2013: a cross-sectional study providing evidence for the benefit of protective gloves during disembowelling of wild boars. *BMC Infect Dis* 2015; **15**: 440 [PMID: 26493830 DOI: 10.1186/s12879-015-1199-y]
- 16 **Kang YH**, Cong W, Zhang XY, Wang CF, Shan XF, Qian AD. Hepatitis E virus seroprevalence among farmers, veterinarians and control subjects in Jilin province, Shandong province and Inner Mongolia Autonomous Region, China. *J Med Virol* 2017; **89**: 872-877 [PMID: 27664799 DOI: 10.1002/jmv.24693]
- 17 **Kantala T**, Kinnunen PM, Oristo S, Jokelainen P, Vapalahti O, Maunula L. Hepatitis E Virus Antibodies in Finnish Veterinarians. *Zoonoses Public Health* 2017; **64**: 232-238 [PMID: 27621202 DOI: 10.1111/zph.12312]
- 18 **Buescher G**, Ozga AK, Lorenz E, Pischke S, May J, Addo MM, Horvatits T. Hepatitis E seroprevalence and viremia rate in immunocompromised patients: a systematic review and meta-analysis. *Liver Int* 2021; **41**: 449-455 [PMID: 33034121 DOI: 10.1111/liv.14695]
- 19 **Mrzljak A**, Dinjar-Kujundzic P, Vilibic-Cavlek T, Jemersic L, Prpic J, Dakovic-Rode O, Kolaric B, Vince A. Hepatitis E seroprevalence and associated risk factors in Croatian liver transplant recipients. *Rev Soc Bras Med Trop* 2019; **52**: e20190302 [PMID: 31618309 DOI: 10.1590/0037-8682-0302-2019]
- 20 **Mrzljak A**, Dinjar-Kujundzic P, Knotek M, Kudumija B, Ilic M, Gulin M, Zibar L, Hrstic I, Jurekovic Z, Kolaric B, Jemersic L, Prpic J, Tomljenovic M, Vilibic-Cavlek T. Seroprevalence of hepatitis E in patients on haemodialysis in Croatia. *Int Urol Nephrol* 2020; **52**: 371-378 [PMID: 31894559 DOI: 10.1007/s11255-019-02363-3]
- 21 **Dremsek P**, Wenzel JJ, John R, Ziller M, Hofmann J, Groschup MH, Werdermann S, Mohn U, Dorn S, Motz M, Mertens M, Jilg W, Ulrich RG. Seroprevalence study in forestry workers from eastern Germany using novel genotype 3- and rat hepatitis E virus-specific immunoglobulin G ELISAs. *Med Microbiol Immunol* 2012; **201**: 189-200 [PMID: 22179131 DOI: 10.1007/s00430-011-0221-2]
- 22 **Sadkowska-Todys M**, Baumann-Popczyk A, Wnukowska N, Popczyk B, Kucharczyk B, Gołąb E. Occurrence and prevalence of selected zoonotic agents: *Echinococcus multilocularis*, *Trichinella spiralis* and hepatitis E virus (HEV) in the population of Polish hunters--results of the study conducted in 2010-2012. *Przegl Epidemiol* 2015; **69**: 673-678, 823 [PMID: 27139343]
- 23 **Montagnaro S**, De Martinis C, Sasso S, Ciarcia R, Damiano S, Auletta L, Iovane V, Zottola T, Pagnini U. Viral and Antibody Prevalence of Hepatitis E in European Wild Boars (*Sus scrofa*) and Hunters at Zoonotic Risk in the Latium Region. *J Comp Pathol* 2015; **153**: 1-8 [PMID: 26025105 DOI: 10.1016/j.jcpa.2015.04.006]
- 24 **Ivanova A**, Tefanova V, Reshetnjak I, Kuznetsova T, Geller J, Lundkvist Å, Janson M, Neare K, Velström K, Jokelainen P, Lassen B, Hütt P, Saar T, Viltrop A, Golovljova I. Hepatitis E Virus in Domestic Pigs, Wild Boars, Pig Farm Workers, and Hunters in Estonia. *Food Environ Virol* 2015; **7**: 403-412 [PMID: 26141050 DOI: 10.1007/s12560-015-9210-8]
- 25 **Lange H**, Øverbø J, Borgen K, Dudman S, Hoddevik G, Urdahl AM, Vold L, Sjurseth SK. Hepatitis E in Norway: seroprevalence in humans and swine. *Epidemiol Infect* 2017; **145**: 181-186 [PMID: 27671461 DOI: 10.1017/S0950268816002144]
- 26 **Yue N**, Wang Q, Zheng M, Wang D, Duan C, Yu X, Zhang X, Bao C, Jin H. Prevalence of hepatitis E virus infection among people and swine in mainland China: A systematic review and meta-analysis. *Zoonoses Public Health* 2019; **66**: 265-275 [PMID: 30884147 DOI: 10.1111/zph.12555]
- 27 **Meng XJ**, Wiseman B, Elvinger F, Guenette DK, Toth TE, Engle RE, Emerson SU, Purcell RH. Prevalence of antibodies to hepatitis E virus in veterinarians working with swine and in normal blood donors in the United States and other countries. *J Clin Microbiol* 2002; **40**: 117-122 [PMID: 11773103 DOI: 10.1128/JCM.40.1.117-122.2002]
- 28 **Hinjoy S**, Nelson KE, Gibbons RV, Jarman RG, Mongkolsirichaikul D, Smithsuwan P, Fernandez S, Labrique AB, Patchanee P. A cross-sectional study of hepatitis E virus infection in healthy people directly exposed and unexposed to pigs in a rural community in northern Thailand. *Zoonoses Public Health* 2013; **60**: 555-562 [PMID: 23280251 DOI: 10.1111/zph.12030]
- 29 **Lassen B**, Janson M, Neare K, Tallo T, Reshetnjak I, Kuznetsova T, Viltrop A, Golovljova I, Jokelainen P. Prevalence of Antibodies Against Hepatitis E Virus in Veterinarians in Estonia. *Vector Borne Zoonotic Dis* 2017; **17**: 773-776 [PMID: 28933680 DOI: 10.1089/vbz.2017.2122]
- 30 **Colson P**, Borentain P, Gérolami R. Hepatitis E virus as an agent of hepatocellular carcinoma. *Int J Infect Dis* 2019; **80**: 62-63 [PMID: 30634042 DOI: 10.1016/j.ijid.2018.12.015]
- 31 **Kamar N**, Garrouste C, Haagsma EB, Garrigue V, Pischke S, Chauvet C, Dumortier J, Cannesson A, Cassuto-Viguiet E, Thervet E, Conti F, Lebray P, Dalton HR, Santella R, Kanaan N, Essig M, Mousson C, Radenne S, Roque-Afonso AM, Izopet J, Rostaing L. Factors associated with chronic hepatitis in patients with hepatitis E virus infection who have received solid organ transplants. *Gastroenterology* 2011; **140**: 1481-1489 [PMID: 21354150 DOI: 10.1053/j.gastro.2011.02.050]
- 32 **Joon A**, Rao P, Shenoy SM, Baliga S. Prevalence of Hepatitis A virus (HAV) and Hepatitis E virus (HEV) in the patients presenting with acute viral hepatitis. *Indian J Med Microbiol* 2015; **33** Suppl: 102-105 [PMID: 25657123 DOI: 10.4103/0255-0857.150908]

- 33 **Tulen AD**, Vennema H, van Pelt W, Franz E, Hofhuis A. A case-control study into risk factors for acute hepatitis E in the Netherlands, 2015-2017. *J Infect* 2019; **78**: 373-381 [PMID: [30738918](#) DOI: [10.1016/j.jinf.2019.02.001](#)]
- 34 **Meng QF**, You HL, Wang WL, Zhou N, Dong W, Cong W. Seroprevalence and risk factors of hepatitis E virus infection among children in China. *J Med Virol* 2015; **87**: 1573-1577 [PMID: [25940435](#) DOI: [10.1002/jmv.24203](#)]
- 35 **Vilibic-Cavlek T**, Vilibic M, Kolaric B, Jemersic L, Kucinar J, Barbic L, Bagaric A, Stevanovic V, Tabain I, Sviben M, Jukic V, Mlinaric-Galinovic G. Seroepidemiology of Hepatitis E in Selected Population Groups in Croatia: A Prospective Pilot Study. *Zoonoses Public Health* 2016; **63**: 494-502 [PMID: [26776465](#) DOI: [10.1111/zph.12254](#)]
- 36 **Mansuy JM**, Gallian P, Dimeglio C, Saune K, Arnaud C, Pelletier B, Morel P, Legrand D, Tiberghien P, Izopet J. A nationwide survey of hepatitis E viral infection in French blood donors. *Hepatology* 2016; **63**: 1145-1154 [PMID: [27008201](#) DOI: [10.1002/hep.28436](#)]
- 37 **La Fauci V**, Facciola A, Riso R, Calimeri S, Lo Giudice D, Squeri R. Seroprevalence of hev antibodies in a sample of pregnant women in the city of Messina. *Ann Ig* 2017; **29**: 232-238 [PMID: [28383615](#) DOI: [10.7416/ai.2017.2151](#)]
- 38 **Obaidat MM**, Roess AA. Seroprevalence and risk factors of Hepatitis E infection in Jordan's population: First report. *Int J Infect Dis* 2018; **66**: 121-125 [PMID: [29146513](#) DOI: [10.1016/j.ijid.2017.11.015](#)]

## Massive bleeding from gastric submucosal arterial collaterals secondary to splenic artery thrombosis: A case report

Alberto Martino, Marco Di Serafino, Francesco Paolo Zito, Franco Maglione, Raffaele Bennato, Luigi Orsini, Alessandro Iacobelli, Raffaella Niola, Luigia Romano, Giovanni Lombardi

**Specialty type:** Gastroenterology and hepatology

**Provenance and peer review:**

Unsolicited article; Externally peer reviewed.

**Peer-review model:** Single blind

**Peer-review report's scientific quality classification**

Grade A (Excellent): A  
Grade B (Very good): B  
Grade C (Good): 0  
Grade D (Fair): 0  
Grade E (Poor): 0

**P-Reviewer:** Chang A, Thailand;  
Tieranu CG, Romania

**Received:** June 18, 2022

**Peer-review started:** June 18, 2022

**First decision:** July 11, 2022

**Revised:** July 17, 2022

**Accepted:** September 8, 2022

**Article in press:** September 8, 2022

**Published online:** October 7, 2022



**Alberto Martino, Francesco Paolo Zito, Raffaele Bennato, Luigi Orsini, Giovanni Lombardi,** Department of Gastroenterology and Digestive Endoscopy, AORN “Antonio Cardarelli”, Napoli 80131, Italy

**Marco Di Serafino, Luigia Romano,** Department of General and Emergency Radiology, AORN “Antonio Cardarelli”, Napoli 80131, Italy

**Franco Maglione,** Department of Radiology, Sanatrix Clinic, Napoli 80127, Italy

**Alessandro Iacobelli,** Department of Pathology, AORN “Antonio Cardarelli”, Napoli 80131, Italy

**Raffaella Niola,** Department of Interventional Radiology, AORN “Antonio Cardarelli”, Napoli 80131, Italy

**Corresponding author:** Alberto Martino, MD, Staff Physician, Department of Gastroenterology and Digestive Endoscopy, AORN “Antonio Cardarelli”, Via Antonio Cardarelli 9, Napoli 80131, Italy. [albertomartinomd@gmail.com](mailto:albertomartinomd@gmail.com)

### Abstract

#### BACKGROUND

Gastric submucosal arterial collaterals (GSAC) secondary to splenic artery occlusion is an extraordinary rare and potentially life-threatening cause of acute upper gastrointestinal bleeding. Here, we report a case of massive bleeding from GSAC successfully treated by means of a multidisciplinary minimally invasive approach.

#### CASE SUMMARY

A 60-year-old non-cirrhotic gentleman with a history of arterial hypertension was admitted due to hematemesis. Emergent esophagogastroduodenoscopy revealed pulsating and tortuous varicose shaped submucosal vessels in the gastric fundus along with a small erosion overlying one of the vessels. In order to characterize the fundic lesion, pre-operative emergent computed tomography-angiography was performed showing splenic artery thrombosis (SAT) and tortuous arterial structures arising from the left gastric artery and the left gastroepiploic artery in the gastric fundus. GSAC was successfully treated by means of a minimally invasive step-up approach consisting in endoscopic clipping followed by transcatheter arterial embolization (TAE).

## CONCLUSION

This was a previously unreported case of bleeding GSAC secondary to SAT successfully managed by means of a multidisciplinary minimally invasive approach consisting in endoscopic clipping for the luminal bleeding control followed by elective TAE for the definitive treatment.

**Key Words:** Upper gastrointestinal bleeding; Non variceal upper gastrointestinal bleeding; Acute upper gastrointestinal bleeding; Gastric submucosal arterial collaterals; Splenic artery thrombosis; Case report

©The Author(s) 2022. Published by Baishideng Publishing Group Inc. All rights reserved.

**Core Tip:** Gastric submucosal arterial collaterals (GSAC) secondary to splenic artery occlusion is an extremely rare cause of severe non variceal upper gastrointestinal bleeding. Herein, we describe a previously unreported case of massive bleeding from GSAC secondary to splenic artery thrombosis effectively treated by endoscopic mechanical hemostasis followed by endovascular embolization.

**Citation:** Martino A, Di Serafino M, Zito FP, Maglione F, Bennato R, Orsini L, Iacobelli A, Niola R, Romano L, Lombardi G. Massive bleeding from gastric submucosal arterial collaterals secondary to splenic artery thrombosis: A case report. *World J Gastroenterol* 2022; 28(37): 5506-5514

**URL:** <https://www.wjgnet.com/1007-9327/full/v28/i37/5506.htm>

**DOI:** <https://dx.doi.org/10.3748/wjg.v28.i37.5506>

## INTRODUCTION

Acute upper gastrointestinal bleeding (UGIB) is a common gastroenterological emergency associated with significant morbidity and mortality. Reported hospitalization rate is 61-78 cases *per* 100,000 adults *per* year[1-3], whereas estimated overall mortality is around 10% [4,5]. Peptic ulcers are the most common cause of acute UGIB, followed by oesophageal varices, Mallory-Weiss syndrome and neoplasms[1,3,4]. Acute UGIB caused by gastric submucosal arterial collaterals (GSAC) secondary to splenic artery occlusion (SAO) is extremely rare, with only few cases reported worldwide up to date. Herein, we describe a previously unreported case of bleeding GSAC secondary to splenic artery thrombosis (SAT) successfully treated by means of endoscopic mechanical hemostasis followed by endovascular embolization.

## CASE PRESENTATION

### Chief complaints

A 60-year-old non-cirrhotic gentleman was admitted to our dedicated bleed unit for severe anemia (hemoglobin 4.8 g/dL on admission) and recent onset of hematemesis and melena with unstable hemodynamic parameters.

### History of present illness

One attack of hematemesis and two episodes of melena occurred two and 24 h prior to the hospital admission, respectively.

### History of past illness

The patient had a history of arterial hypertension. He denied any history of, or risk factors for, liver disease, pancreatitis, abdominal trauma and hypercoagulable states.

### Personal and family history

The patient denied personal and family history.

### Physical examination

At admission, the patient was hemodynamically unstable (pulse of 110 bpm, blood pressure of 100/50 mmHg). He was afebrile, with respiratory rate of 15 rpm and oxygen saturation of 98%. His physical examination was negative for any evidence of portal hypertension or other stigmata of chronic liver disease. Abdominal examination revealed non-distended, non-tender abdomen with normoactive bowel sounds. The digital rectal examination showed black terry feces.

### **Laboratory examinations**

Complete blood count revealed a hemoglobin level of 4.8 g/dL and hematocrit of 14.6%. All other laboratoristic exams, including coagulation, liver and renal function tests, were within normal values.

### **Imaging examinations**

Following high-dose intravenous proton pump inhibitor administration, blood transfusion and hemodynamic stabilization, emergent esophagogastroduodenoscopy (EGD) under monitored anaesthesia care was performed. A moderate amount of fresh blood within the stomach was noted and fully aspirated. The retroflexion maneuver revealed varicose shaped pulsating and tortuous submucosal vessels in the gastric fundus without active bleeding. A small erosion overlying one of the vessels consistent with an area of recent healed rupture was noted (Figure 1). Given the absence of clinical or laboratory signs of portal hypertension, we decided to perform emergent computed tomography-angiography (CTA) in order to further characterize the fundic lesion and to look for signs of portal hypertension. SAT and tortuous arterial structures emerging from the left gastric artery (LGA) and the left gastroepiploic artery (LGEA) in the gastric fundus were showed. No signs of active bleeding were observed (Figure 2).

### **Further hospital course**

Given the high-risk of massive early rebleeding due to the presence of a small erosion overlying one of the GSAC vessels, we decided to attempt therapeutic EGD in order to provide definitive treatment in a more stable non-emergent setting. The patient was informed that in case of luminal bleeding control failure, emergent transcatheter arterial embolization (TAE) would be performed by the pre-alerted interventional radiologist. Immediately after the first endoclip application downstream to the mucosal erosion, spurting bleeding started. Hemostasis was achieved by means of two endoclips placement upstream to the mucosal defect. Finally, two endoclips were further prophylactically positioned (Figure 3 and Video 1).

---

## **MULTIDISCIPLINARY EXPERT CONSULTATION**

---

No rebleeding was observed following the endoscopic treatment. However, the patient refused splenectomy for definitive treatment. Therefore, after multidisciplinary evaluation, involving GI endoscopist, surgeon, diagnostic and interventional radiologist, a minimally-invasive approach with elective TAE was planned.

---

## **FINAL DIAGNOSIS**

---

Non variceal acute UGIB from GSAC secondary to SAT.

---

## **TREATMENT**

---

Operative angiography showed SAT with multiple collateral arteries arising from the LGA and the LGEA and projecting in the gastric fundus (Figure 4). Selective TAE of the LGA collaterals with trisacryl gelatin microspheres (Embospheres, Guerbet Biomedical, Louvres, France) was effectively realized.

---

## **OUTCOME AND FOLLOW-UP**

---

Post-operative stay was complicated by splenic infarction, responsive to conservative treatment (Figure 5). The patient underwent hematology consultation and thrombophilic disorders were excluded. No rebleeding occurred. The patient was discharged with stable haemoglobin value (9.1 g/dL) on post-operative day 18. No rebleeding was observed at 12-mo follow-up.

---

## **DISCUSSION**

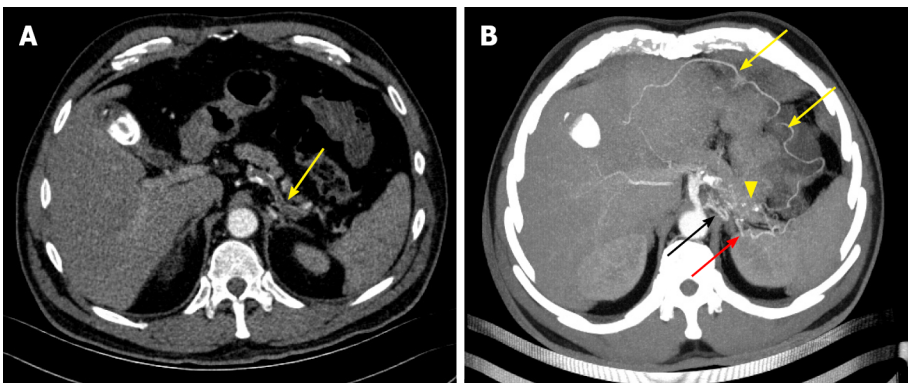
---

GSAC are an extraordinary rare cause of massive UGIB. They are not related to portal hypertension, resulting from either occlusion or congenital absence of the SA. SAO may be congenital, idiopathic, or secondary to various conditions such as surgery, endovascular procedure, trauma and extrinsic compression. In the case of SAO, in order to provide splenic blood supply, extensive collaterals may



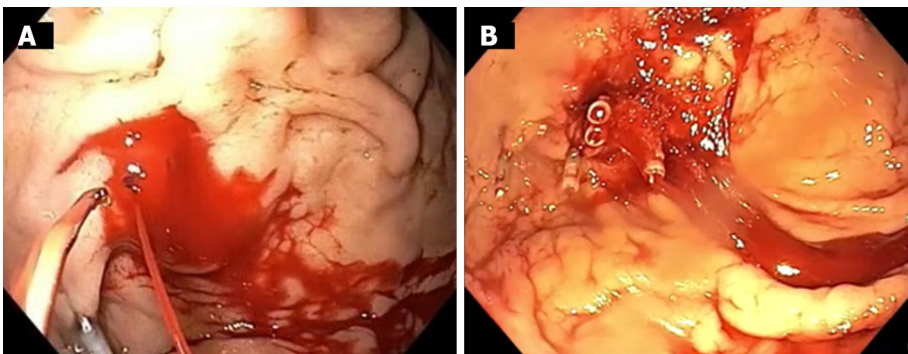
DOI: 10.3748/wjg.v28.i37.5506 Copyright ©The Author(s) 2022.

**Figure 1** Emergent esophagogastroduodenoscopy: Retroflexed view of the gastric fundus showing varicose-shaped submucosal vessels with a small erosion (arrow).



DOI: 10.3748/wjg.v28.i37.5506 Copyright ©The Author(s) 2022.

**Figure 2** Emergent computed tomography angiography: Axial view. A: Arterial phase showing complete splenic artery thrombosis (arrow); B: Arterial phase curved-multiplanar reconstruction showing splenic artery collateral vessels (yellow arrows) with an arterial cluster at the gastric fundus (arrowhead) arising from the left gastric artery (black arrow) and the left gastroepiploic artery (red arrow).



DOI: 10.3748/wjg.v28.i37.5506 Copyright ©The Author(s) 2022.

**Figure 3** Therapeutic esophagogastroduodenoscopy. A: Spurting active bleeding of the gastric submucosal arterial collaterals after first endoclip application; B: Successful mechanical hemostasis achievement.

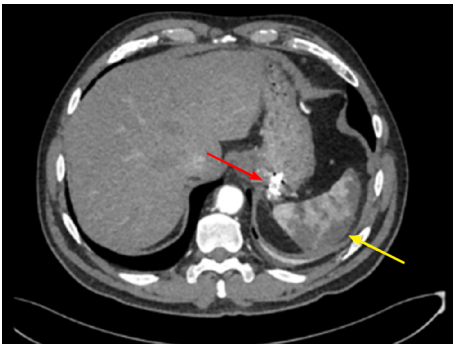
arise from adjacent proximal patent arteries, such as the pancreatic, left gastric, gastroepiploic, and short gastric arteries and pass through the gastric wall[6]. Collateral supply may be clinically asymptomatic or may less frequently present with massive UGIB from erosion of GSAC.

The differential diagnosis of GSAC includes mainly isolated gastric varices (IGV). Gastric vascular lesions due to collateralization of an occluded splenic artery may have a very similar endoscopic appearance to IGV and can be easily misinterpreted on EGD. However, they are, as opposed to GSAC, due to cirrhotic portal hypertension or splenic vein obstruction resulting in left-sided portal hypertension[7,8]. Therefore, an accurate differential diagnosis between these two entities is crucial. Indeed, endoscopic cyanoacrylate glue injection (ECGI), currently recommended as the first-line treatment for



DOI: 10.3748/wjg.v28.i37.5506 Copyright ©The Author(s) 2022.

**Figure 4** Operative angiography showing a cluster of collateral arterial vessels emerging from the left gastric artery (red arrow) and the left gastroepiploic artery (yellow arrow) projecting into the gastric fundus. It also shows previously placed endoclips on the submucosal collateral arteries of the gastric fundus without active contrast extravasation (arrowhead).



DOI: 10.3748/wjg.v28.i37.5506 Copyright ©The Author(s) 2022.

**Figure 5** Post-operative computed tomography angiography: Axial view showing collateral arteries of the gastric fundus treated by endoscopic clipping plus microspheres embolization (red arrow) and splenic infarction (yellow arrow).

bleeding IGV[9], is associated with a significant risk of systemic embolization and life-threatening adverse events in case of direct arterial injection of cyanoacrylate[10-12]. Finally, fatal arterial embolic complications in hepatolienogastric blood supply have been reported during ECGI to a non-variceal bleeding source[13-16]. A high level of diagnostic certainty is thus required before proceeding with ECGI.

We performed a comprehensive literature search of PubMed/MEDLINE and EMBASE electronic databases up to March 2022, identifying 10 case reports of GSAC secondary to SAO (Table 1).

In 1984, Spriggs[17] first reported a case of severe UGIB due to GSAC secondary to SA congenital absence[17]. The diagnosis was made by arteriography and the treatment consisted in splenectomy followed by partial gastrectomy due to rebleeding. Later on, a similar case was reported, effectively treated by means of splenectomy after ligation of the LGA[18].

In 2000, Baron *et al*[19] reported a case of bleeding GSAC secondary to post-traumatic SAO. It was diagnosed by operative angiography and successfully treated by splenectomy and partial gastric devascularization[19]. Subsequently, Worthley and colleagues described a case of UGIB secondary to SAO due to previous SA aneurysmectomy. As previously reported, it was managed by angiography followed by splenectomy with ligation of the splenic vein and artery together with the left gastric and short gastric arteries[20].

In 2004, Cyraný *et al*[21,22] illustrated the first case of massive UGIB from GSAC secondary to SAT successfully managed endoscopically. Of interest, pre-operative diagnosis was made by endoscopy only, and treatment consisted in ECGI alone. No rebleeding was observed. However, post-procedural stay was complicated by the occurrence of splenic infarction, treated conservatively[21,22].

Later on, the first case of bleeding GSAC successfully treated by endovascular embolization alone was reported by Mnatzakanian *et al*[23] Pre-operative accurate diagnosis was made by CTA followed by

**Table 1 Summary of case reports reporting acute upper gastrointestinal bleeding from gastric submucosal arterial collaterals secondary to occlusion or congenital absence of the splenic artery**

Case	Ref.	Age/sex	Presentation	SAO etiology	Diagnosis	Treatment	Major AEs	Outcome	Follow-up (months)
1	Spriggs[17], 1984	31/M	Hematemesis	SA congenital absence	Angiography	Splenectomy + partial gastrectomy (due to rebleeding)	Severe respiratory distress	Alive-no rebleeding	-
2	Durrans <i>et al</i> [18], 1985	13/M	Hematemesis	SA congenital absence	Angiography	LGA ligation + splenectomy	None	Alive-no rebleeding	-
3	Baron <i>et al</i> [19], 2000	36/M	Hematemesis	Blunt abdominal trauma	Angiography	Splenectomy + partial gastric devascularization	None	Alive-no rebleeding	18
4	Worthley <i>et al</i> [20], 2003	68/F	Melena	Iatrogenic(SA aneurysmectomy)	Angiography	Splenectomy + ligation of SV and SA with LGA and SGA	None	Alive-no rebleeding	-
5	Cyrany <i>et al</i> [21], 2004	59/M	Hematemesis and melena	SAT	CTA + angiography	ECGI	Splenic infarction	Alive-no rebleeding	9
6	Mnatzakanian <i>et al</i> [23], 2008	66/M	Melena	-	CTA + angiography	TAE (coils and pledgets)	None	Alive-no rebleeding	-
7	von Trotha <i>et al</i> [26], 2011	69/M	-	SAT	CTA + angiography + EUS	ECGI + endoscopic clipping + splenectomy and SGA collaterals dissection	Splenic infarction	Alive-no rebleeding	6
8	Saddekni <i>et al</i> [24], 2012	23/F	Hematemesis and melena	Iatrogenic (SA ligation)	CTA + angiography	TAE (coils)	None	Alive-no rebleeding	8
9	Arslan <i>et al</i> [27], 2017	52/M	Hematemesis	SAT	CTA	-	-	Death	-
10	Al-Balas <i>et al</i> [25], 2021	49/M	Hematemesis	SAT	CTA + angiography	TAE (coils) + splenectomy and bleeding gastric vessel ligation (due to rebleeding)	None	Alive-no rebleeding	18
11	Our case	60/M	Hematemesis and melena	SAT	CTA + angiography	Endoscopic clipping + TAE (microspheres)	Splenic infarction	Alive-no rebleeding	12

SAO: Splenic artery occlusion; AEs: Adverse events; SA: Splenic artery; LGA: Left gastric artery; SGA: Short gastric arteries; SAT: Splenic artery thrombosis; CTA: Computed tomography angiography; ECGI: Endoscopic cyanoacrylate glue injection; TAE: Transcatheter arterial embolization; EUS: Endoscopic ultrasound.

angiogram, in order to rule out IGV. No procedure-related major adverse events were observed[23]. Few years later, another case successfully managed in a very similar manner was described[24]. Conversely, Al-Balas *et al*[25] recently reported a case of bleeding GSAC initially managed *via* TEA and subsequently requiring emergency laparotomy with ligation of a bleeding gastric vessel and splenectomy due to severe rebleeding occurrence[25].

In 2011, von Trotha *et al*[26] reported a case of bleeding GSAC secondary to idiopathic SAT. GSAC was endoscopically misdiagnosed as type 1 IGV and ECGI with subsequent clipping was performed in order to control active bleeding. Of note, the authors did not clarify the choice for endoscopic clipping adoption in the setting of supposed IGV. Furthermore, as previously reported by Cyrany and colleagues, ECGI was complicated by splenic infarction. A proper diagnosis was subsequently made by CTA and conventional angiography. Interestingly, endoscopic color doppler ultrasonography was adopted to secure the diagnosis and laparoscopic splenectomy was finally provided for the definitive treatment[26].

Up to date, one case only of fatal UGIB due to GSAC has been reported. In this instance, urgent EGD failed to identify the source of bleeding. CTA examination was then performed showing GSAC due to SAT, in the absence of active bleeding. However, after diagnosis, no treatment was provided and death due to recurrent bleeding occurred[27].

Our case is the first report in which bleeding GSAC was effectively treated with endoscopic mechanical hemostasis alone for the luminal bleeding control and subsequent elective TAE for the definitive treatment. Given the absence of active bleeding and portal hypertension signs or history, emergent CTA was performed prior to endoscopic treatment in order to properly characterize the gastric vascular lesion. Following endoscopic treatment neither adverse events nor rebleeding signs

occurred. The patient refused splenectomy with or without partial gastrectomy for the definitive treatment. Thus, following multidisciplinary evaluation, elective TAE was planned and effectively realized. Post-operative stay was complicated by splenic ischemia, effectively treated by conservative medical treatment. In our case, the presumed etiology of GSAC was idiopathic SAT. Given the formation of an extensive collateral pathway preserving the splenic perfusion, complete SAO likely occurred gradually.

---

## CONCLUSION

Gastroenterologists should be aware of this potentially life-threatening, albeit extraordinary rare, source of massive upper gastrointestinal hemorrhage, in order to allow proper management. In our opinion, endoscopic mechanical hemostasis seems to be a safe and effective method for the luminal bleeding control across referral centers. Conversely, we may not recommend ECGI adoption given the potential occurrence of fatal adverse events due to arterial embolization. CTA appears to be the best modality for a prompt differential diagnosis, and should be performed in all UGIB patients with endoscopic evidence of gastric varicose shaped submucosal vessels and no signs or history of portal hypertension. For the definitive treatment of bleeding GSAC, either a minimally invasive approach with TAE or a standard approach with splenectomy may be provided, taking into account patient preference and status.

---

## ACKNOWLEDGEMENTS

We are grateful to Velia De Magistris for English editing.

---

## FOOTNOTES

**Author contributions:** Martino A was responsible for the conception of the paper, execution of the endoscopic procedures, drafting of the article, interpretation of the data and final approval of the article; Di Serafino M was responsible for conception of the paper, execution of the diagnostic radiological examinations, drafting of the article and final approval of the article; Zito FP was responsible for the conception of the paper, drafting of the article, interpretation of data and final approval of the article; Maglione F and Niola R were responsible for execution of the interventional radiological procedures, drafting of the article, interpretation of the data and final approval of the article; Bennato R, Orsini L and Iacobelli A were responsible for drafting of the article, interpretation of data and final approval of the article; Romano L and Lombardi G were responsible for the analysis and interpretation of data, revision of the manuscript for important intellectual content and final approval of the article.

**Informed consent statement:** Informed consent was obtained from the patient for the publication of this report and any accompanying images.

**Conflict-of-interest statement:** All the authors report no relevant conflicts of interest for this article.

**CARE Checklist (2016) statement:** The authors have read the CARE Checklist (2016), and the manuscript was prepared and revised according to the CARE Checklist (2016).

**Open-Access:** This article is an open-access article that was selected by an in-house editor and fully peer-reviewed by external reviewers. It is distributed in accordance with the Creative Commons Attribution NonCommercial (CC BY-NC 4.0) license, which permits others to distribute, remix, adapt, build upon this work non-commercially, and license their derivative works on different terms, provided the original work is properly cited and the use is non-commercial. See: <https://creativecommons.org/licenses/by-nc/4.0/>

**Country/Territory of origin:** Italy

**ORCID number:** Alberto Martino 0000-0002-8759-6518; Marco Di Serafino 0000-0001-6972-1859; Francesco Paolo Zito 0000-0002-1084-3373; Raffaele Bennato 0000-0002-8343-8205; Luigi Orsini 0000-0001-7029-3994; Raffaella Niola 0000-0002-6668-5669; Luigia Romano 0000-0002-5201-547X; Giovanni Lombardi 0000-0002-5957-3132.

**Corresponding Author's Membership in Professional Societies:** Società Italiana Di Gastroenterologia Ed Endoscopia Digestiva; Associazione Italiana Gastroenterologi Ed Endoscopisti Digestivi Ospedalieri; European Society of Gastrointestinal Endoscopy.

**S-Editor:** Fan JR

**L-Editor:** A

**P-Editor:** Fan JR

## REFERENCES

- 1 **Laine L**, Yang H, Chang SC, Datto C. Trends for incidence of hospitalization and death due to GI complications in the United States from 2001 to 2009. *Am J Gastroenterol* 2012; **107**: 1190-5; quiz 1196 [PMID: [22688850](#) DOI: [10.1038/ajg.2012.168](#)]
- 2 **Abougergi MS**, Travis AC, Saltzman JR. The in-hospital mortality rate for upper GI hemorrhage has decreased over 2 decades in the United States: a nationwide analysis. *Gastrointest Endosc* 2015; **81**: 882-8.e1 [PMID: [25484324](#) DOI: [10.1016/j.gie.2014.09.027](#)]
- 3 **Wuerth BA**, Rockey DC. Changing Epidemiology of Upper Gastrointestinal Hemorrhage in the Last Decade: A Nationwide Analysis. *Dig Dis Sci* 2018; **63**: 1286-1293 [PMID: [29282637](#) DOI: [10.1007/s10620-017-4882-6](#)]
- 4 **Hearnshaw SA**, Logan RF, Lowe D, Travis SP, Murphy MF, Palmer KR. Acute upper gastrointestinal bleeding in the UK: patient characteristics, diagnoses and outcomes in the 2007 UK audit. *Gut* 2011; **60**: 1327-1335 [PMID: [21490373](#) DOI: [10.1136/gut.2010.228437](#)]
- 5 **Nahon S**, Hagège H, Latrive JP, Rosa I, Nalet B, Bour B, Faroux R, Gower P, Arpurt JP, Denis J, Henrion J, Rémy AJ, Pariente A; Groupe des Hémorragies Digestives Hautes de l'ANGH. Epidemiological and prognostic factors involved in upper gastrointestinal bleeding: results of a French prospective multicenter study. *Endoscopy* 2012; **44**: 998-1008 [PMID: [23108771](#) DOI: [10.1055/s-0032-1310006](#)]
- 6 **Stolze T**, Wienbeck M. [The collateral circulation in the chronic occlusion of the splenic artery]. *Rofo* 1976; **124**: 386-387 [PMID: [131773](#) DOI: [10.1055/s-0029-1230356](#)]
- 7 **Sarin SK**, Jain AK, Lamba GS, Gupta R, Chowdhary A. Isolated gastric varices: prevalence, clinical relevance and natural history. *Dig Surg* 2003; **20**: 42-47 [PMID: [12637804](#) DOI: [10.1159/000068865](#)]
- 8 **Köklü S**, Coban S, Yüksel O, Arhan M. Left-sided portal hypertension. *Dig Dis Sci* 2007; **52**: 1141-1149 [PMID: [17385040](#) DOI: [10.1007/s10620-006-9307-x](#)]
- 9 **de Franchis R**, Bosch J, Garcia-Tsao G, Reiberger T, Ripoll C; Baveno VII Faculty. Baveno VII - Renewing consensus in portal hypertension. *J Hepatol* 2022; **76**: 959-974 [PMID: [35120736](#) DOI: [10.1016/j.jhep.2021.12.022](#)]
- 10 **Lee CW**, Liu KL, Wang HP, Chen SJ, Tsang YM, Liu HM. Transcatheter arterial embolization of acute upper gastrointestinal tract bleeding with N-butyl-2-cyanoacrylate. *J Vasc Interv Radiol* 2007; **18**: 209-216 [PMID: [17327553](#) DOI: [10.1016/j.jvir.2006.12.003](#)]
- 11 **Jaе HJ**, Chung JW, Jung AY, Lee W, Park JH. Transcatheter arterial embolization of nonvariceal upper gastrointestinal bleeding with N-butyl cyanoacrylate. *Korean J Radiol* 2007; **8**: 48-56 [PMID: [17277563](#) DOI: [10.3348/kjr.2007.8.1.48](#)]
- 12 **Kim BS**, Do HM, Razavi M. N-butyl cyanoacrylate glue embolization of splenic artery aneurysms. *J Vasc Interv Radiol* 2004; **15**: 91-94 [PMID: [14709694](#) DOI: [10.1097/01.rvi.0000099537.29957.13](#)]
- 13 **Lee GH**, Kim JH, Lee KJ, Yoo BM, Hahm KB, Cho SW, Park YS, Moon YS. Life-threatening intraabdominal arterial embolization after histoacryl injection for bleeding gastric ulcer. *Endoscopy* 2000; **32**: 422-424 [PMID: [10817185](#) DOI: [10.1055/s-2000-9002](#)]
- 14 **Lee KJ**, Kim JH, Hahm KB, Cho SW, Park YS. Randomized trial of N-butyl-2-cyanoacrylate compared with injection of hypertonic saline-epinephrine in the endoscopic treatment of bleeding peptic ulcers. *Endoscopy* 2000; **32**: 505-511 [PMID: [10917181](#) DOI: [10.1055/s-2000-3816](#)]
- 15 **Kobilica N**, Flis V, Sojar V. Major complication after Histoacryl injection for endoscopic treatment of bleeding peptic ulcer. *Endoscopy* 2012; **44** Suppl 2 UCTN: E204-E205 [PMID: [22622746](#) DOI: [10.1055/s-0032-1308923](#)]
- 16 **Vallieres E**, Jamieson C, Haber GB, Mackenzie RL. Pancreatoduodenal necrosis after endoscopic injection of cyanoacrylate to treat a bleeding duodenal ulcer: a case report. *Surgery* 1989; **106**: 901-903 [PMID: [2814823](#)]
- 17 **Spriggs DW**. Congenital absence of the splenic artery. *Cardiovasc Intervent Radiol* 1984; **7**: 303-305 [PMID: [6335674](#) DOI: [10.1007/BF02625116](#)]
- 18 **Durrans D**, Fawcitt RA, Taylor TV. Congenital absence of the splenic artery associated with major gastric bleeding in adolescence. *Br J Surg* 1985; **72**: 456-457 [PMID: [3874675](#) DOI: [10.1002/bjs.1800720618](#)]
- 19 **Baron PW**, Sindram D, Suhocki P, Webb DD, Clavien PA. Upper gastrointestinal bleeding from gastric submucosal arterial collaterals secondary to splenic artery occlusion: treatment by splenectomy and partial gastric devascularization. *Am J Gastroenterol* 2000; **95**: 3003-3004 [PMID: [11051401](#) DOI: [10.1111/j.1572-0241.2000.03228.x](#)]
- 20 **Worthley DL**, Rayner CK, Devitt PG, Fraser R. Gastric hemorrhage as a late complication of splenic artery aneurysm repair: a dramatic way to vent one's spleen. *J Gastroenterol Hepatol* 2003; **18**: 604-605 [PMID: [12702057](#) DOI: [10.1046/j.1440-1746.2003.03012.x](#)]
- 21 **Cyrany J**, Kopáčová M, Rejchrt S, Krajina A, Bureš J. Gastric arterial bleeding secondary to chronic occlusion of the splenic artery. *Folia Gastroenterol Hepatol* 2004; **2**: 92-98
- 22 **Cyrany J**, Kopacova M, Rejchrt S, Jirkovsky V, Al-Tashi M, Bures J. Gastric arterial bleeding secondary to chronic occlusion of the splenic artery (with video). *Gastrointest Endosc* 2010; **71**: 1335; author reply 1336 [PMID: [20598266](#) DOI: [10.1016/j.gie.2009.09.039](#)]
- 23 **Mnatzakanian G**, Smaggus A, Wang CS, Common AA, Jeejeebhoy KN. Splenic artery collaterals masquerading as gastric fundal varices on endoscopy: a sticky situation. *Gastrointest Endosc* 2008; **67**: 751-755 [PMID: [18206881](#) DOI: [10.1016/j.gie.2007.09.044](#)]
- 24 **Saddekni S**, Abdel-Aal AK, Oser RF, Underwood E, Bag A. Transcatheter embolization of extensive left gastric artery collaterals presenting with massive upper gastrointestinal bleed. *Vasc Endovascular Surg* 2012; **46**: 480-483 [PMID: [22669265](#) DOI: [10.1177/1538574412449908](#)]
- 25 **Al-Balas H**, Metwalli ZA, Sada DM. Chronic splenic artery occlusion with gastric wall arterial ectasia, an unusual cause of massive upper gastrointestinal hemorrhage. *BJR Case Rep* 2021; **7**: 20200194 [PMID: [34131504](#) DOI: [10.1259/bjrcr.20200194](#)]
- 26 **von Trotha KT**, Binnebösel M, Truong S, Behrendt FF, Wasmuth HE, Neumann UP, Jansen M. Severe gastric variceal haemorrhage due to splenic artery thrombosis and consecutive arterial bypass. *BMC Surg* 2011; **11**: 14 [PMID: [21711534](#) DOI: [10.1186/1471-2482-11-14](#)]

- 27 **Arslan S**, Onur MR, Akpınar E. A rare cause of upper gastrointestinal hemorrhage: chronic thrombosis of the splenic artery. *Turk J Gastroenterol* 2017; **28**: 221-222 [PMID: [28316323](#) DOI: [10.5152/tjg.2017.16745](#)]



Published by **Baishideng Publishing Group Inc**  
7041 Koll Center Parkway, Suite 160, Pleasanton, CA 94566, USA  
**Telephone:** +1-925-3991568  
**E-mail:** [bpgoffice@wjgnet.com](mailto:bpgoffice@wjgnet.com)  
**Help Desk:** <https://www.f6publishing.com/helpdesk>  
<https://www.wjgnet.com>

